Molecular and Functional Characterization of microRNA-137 in Oligodendroglial Tumors

YANG, Ling

A Thesis Submitted in Partial Fulfillment of
the Requirements for the Degree of
Master of Philosophy
in
Anatomical and Cellular Pathology

The Chinese University of Hong Kong
April 2011

ACKNOWLEDGEMENTS

I would like to take this opportunity to express my gratitude to my supervisor, Professor Ho-keung Ng for taking me as a research student in his research laboratory. His kind encouragement, constant support and invaluable guidance have been extremely important to me throughout my study for the degree of Master of Philosophy and in completing my project.

I am extremely grateful to my co-supervisor, Mr. Jesse Chung-sean Pang, for his technical assistance, inspiring advice and encouragement that help me so much in this study. Being a freshman in laboratory research, his thoughtful ideas and perceptive discussions throughout my graduate years have greatly taught me about science and approaches to research.

My sincere thanks are given to Miss Kay Ka Wai Li for sharing her knowledge on microRNA and glioma fields with me. Special thanks go to Ms. Nellie Yuk-Fei Chung for performing the FISH analysis and technical assistance. I am indebted to Dr. Hiu-Ming Li, for his countless efforts in sample and follow-up data collection and expert advice on immunohistochemical analysis, which are important in my study. Many thanks go to Dr. Kin-Mang Lau for providing the pMIR-REPORT vector and his suggestion on my project. I also would like to express my obliged thanks to my lab mates, Dr. Aden Chan and Miss Carina Luk for their encouragement and cooperation.

I would like to thank my friends and colleagues and all the staff in 5/F, Cancer Centre and Department of Anatomical and Cellular Pathology for their kind help and support.

Thanks are also given to all members of the thesis examination committee for their effort in examining this thesis.

Moreover, I would like to express my deepest appreciation to my family, especially my parents and Feng He for their care, patience, support and endless love. Last but not least, I thank my GOD for His mercy and grace every day. Without all these important ones, I might not be able to complete my Master of Philosophy. study.

AWARDS AND PRESENTATIONS

Awards

Best poster award. The fifteenth Annual Scientific Symposium of the Hong Kong Cancer Institute and the fifth Sino-US Conference - Personalized Medicine In Cancer Therapy, Hong Kong, 2010.

Presentations

1. Ling Yang, Jesse Chung-sean Pang, Kay Ka Wai Li, Wai Sang Poon, Liangfu Zhou and Ho-keung Ng. Molecular and functional characterization of microRNA-137 in oligodendroglial tumors. ***The eighth Asia Pacific multidisciplinary meeting for nervous system disease - Brain 2011***, Hong Kong. January 7-8, 2011. Poster presentation No.13.
2. Ling Yang, Jesse Chung-sean Pang, Kay Ka Wai Li, Wai Sang Poon, Liangfu Zhou and Ho-keung Ng. Molecular and functional characterization of microRNA-137 in oligodendroglial tumors. ***The fifteenth Annual Scientific Symposium of the Hong Kong Cancer Institute and the fifth Sino-US Conference - Personalized Medicine In Cancer Therapy***, Hong Kong. November 13-14, 2010. Poster presentation No.37.
3. Ling Yang, Jesse Chung-sean Pang, Kay Ka Wai Li, Liangfu Zhou and Ho-keung Ng. Molecular and functional characterization of microRNA-137 in oligodendroglial tumors. ***The seventh Asia Pacific multidisciplinary meeting for nervous system disease - Brain 2010***, Hong Kong. January 8-9, 2010. Poster presentation No.11.

ABSTRACT

Diffuse gliomas, comprising of oligodendroglial tumors (OTs), astrocytomas and glioblastoma multiforme (GBM), are the most common primary brain neoplasms in adults. Unlike other glioma subtypes, OTs show distinct clinical features of better outcome and sensitivity to chemotherapy. Concurrent deletion of chromosome arms 1p and 19q is the most frequent genetic alteration detected in 60%–80% of OTs. The 1p/19q codeletion or 1p loss alone has been associated with favorable prognosis and chemosensitivity in OT patients. It is believed that the 1p arm carries important OT-related genes, whose inactivation is involved in OT development. In an attempt to identify tumor suppressor genes located on the 1p arm, numerous research groups have reported the isolation of candidate genes. Although these genes were demonstrated to be downregulated in OTs, no conclusive evidence was provided with regard to their role in OT formation. The pathogenesis of OTs remains elusive. MicroRNAs (miRNAs) are an abundant class of small (19-25 nucleotides) non-protein-coding RNAs, which repress expression of their target genes at post-transcriptional level. Recent investigations have implicated a link between miRNA deregulation and development of various cancers, including gliomas. A better understanding of the biology of miRNAs and their targets may shed light on the molecular pathogenesis of gliomas and on the potential of these RNA molecules as therapeutic targets in treatment of this group of brain tumors.

A recent study reported that microRNA-137 (miR-137) expression was significantly decreased in astrocytomas of all grades with inhibitory role in GBM cell proliferation. In addition, miR-137 was able to induce neuronal-like differentiation in mouse neural stem cells and tumor stem cells derived from GBM

and mouse OT. MiR-137 is therefore suggested as a potential growth suppressive miRNA in gliomas. The objectives of this study are to investigate the potential involvement of miR-137 in pathogenesis of OTs and GBM, and to elucidate its biological function through identification and characterization of its targets.

A collection of 36 primary OTs (13 oligodendrogliomas, 7 anaplastic oligodendrogliomas, 13 oligoastrocytomas and 3 anaplastic oligoastrocytomas) were recruited for this study. Quantitative RT-PCR (qRT-PCR) revealed significant downregulation of miR-137 in 90% (18/20) of oligodendrogliomas ($p=0.016$) and 100% (16/16) of oligoastrocytomas ($p=0.009$) examined when compared to the mean expression level of 3 normal brain samples. Reduced miR-137 expression was observed in 3 OT and 7 GBM cell lines as well. Statistical analysis showed that reduced miR-137 expression was associated with tumor grade ($p=0.010$) and higher Ki-67 labeling index ($p=0.009$), but not with allelic deletion of chromosome 1p and of chromosomes 1p/19q, gender or age. Moreover, miR-137 expression was restored in OT cells after treatment with demethylating agent and histone deacetylase inhibitor ($p<0.001$). These findings suggested that miR-137 expression might be modulated by epigenetic modifications and its downregulation might contribute to the development and progression of OTs.

To determine the biological role of miR-137 in glioma, several functional assays were carried out. Ectopic expression of miR-137 suppressed cell growth in eight glioma cell lines (derived from two oligodendrogliomas, one oligoastrocytoma and five glioblastomas) examined by MTT assay and cell counts ($p<0.015$). Soft agar assay indicated that miR-137 inhibited cell anchorage-independent growth in OT and GBM cells ($p<0.001$). Suppression of DNA synthesis and enhanced apoptosis were

observed following miR-137 transfection in these cells as evaluated by BrdU incorporation and cleaved-PARP level. Matrigel invasion assay revealed that miR-137 significantly suppressed glioma cell motility ($p<0.001$). In addition, ectopic expression of miR-137 in GBM cells induced upregulation of β-tubulin III, a neuronal marker, suggesting that miR-137 was able to induce neuronal-like differentiation in GBM cells. Collectively, these results suggested that miR-137 might act as a potential tumor suppressive miRNA in OT and GBM.

To identify target genes of miR-137, a computational approach using four miRNA prediction algorithms (TargetScan, PicTar, miRanda and microCosm) was employed. Five predicted candidate genes (*CSE1L*, *ERBB4*, *NRP1*, *CDC42* and *AKT2*) that have been implicated in tumorigenesis were selected to further analysis. Dual-luciferase reporter assay demonstrated that luciferase activity was significantly reduced in cells cotransfected with miR-137 and reporter construct containing a putative miR-137 binding site in the 3'UTR of CSE1L or ERBB4 ($p<0.001$), but not of the other three candidate genes. No reduction of luciferase activity was observed in control cells cotransfected with miRNA negative control or with construct carrying mutant miR-137 recognition site. These findings indicated that miR-137 interacted specifically with the 3' untranslated regions of CSE1L and ERBB4 in glioma cells. Further study showed that miR-137 transfection reduced expression of CSE1L protein, but not mRNA, levels in glioma cells. Taken together, the results suggested that that miR-137 negatively regulated *CSE1L* through translational inhibition in glioma.

To investigate the role of CSE1L in glioma, qRT-PCR was performed to determine CSE1L expression. The results showed that the CSE1L mRNA level was

significantly elevated in 30% (6/20) of oligodendrogliomas (p=0.039) and 75% (12/16) of oligoastrocytomas (p=0.006) examined, compared to normal brain. Enhanced CSE1L transcript was also detected in 2 of 3 OT cells and 6 of 7 GBM cell lines studied (p=0.014). Immunohistochemistry study further demonstrated overexpression of CSE1L protein in both oligodendrogliomas and oligoastrocytomas compared with 13 non-neoplastic brain tissues (p<0.001). Although the abundance of CSE1L mRNA or protein did not correlate with miR-137 level in OTs (p=0.326 and p=0.300, respectively), these data have unveiled upregulation of CSE1L in OTs at both mRNA and protein levels, suggesting CSE1L may play a role in glioma development.

In the functional characterization of CSE1L, small interfering RNA-mediated knockdown of CSE1L resulted in suppressed proliferation, induced apoptosis and reduced invasiveness in glioma cells (p<0.001). These effects were similar but to a less extent to those induced by miR-137 overexpression, suggesting that miR-137 may exert its functional effects partially through CSE1L.

In summary, the results demonstrated frequent downregulation of miR-137 in OTs, whose restoration inhibits proliferation, invasion and induced apoptosis and differentiation in OT and GBM cells, suggesting that miR-137 may act as a growth suppressor and differentiation promoter in gliomagenesis. A nuclear transport factor, CSE1L is identified as a novel target of miR-137 and its overexpression is common in OTs. It was suggested that both miR-137 and its target, CSE1L may play important roles in the development of glioma. The therapeutic potential of miR-137-*CSE1L* pathway in glioma management was also highlighted.

摘要

瀰漫性神經膠質瘤是成人中最常見的原發性腦腫瘤，包括少突膠質細胞腫瘤（oligodendroglial tumors, OTs），星形細胞瘤和多形性膠質母細胞瘤（glioblastoma multiform, GBM）。不同於其他神經膠質瘤，OTs 具有更好的治療結果及對化療的敏感性這些臨床特點。高頻（60-80%）的染色體 1p 和 19q 同時丟失是 OTs 最常發生的遺傳變化。染色體 1p 和 19q 同時丟失或 1p 單獨丟失還和 OTs 病人更好的預後以及化療敏感性有關。據認為，染色體 1p 上有重要的 OTs 相關基因，其失活參與 OTs 發展。試圖確定位於 1p 上的腫瘤抑制基因，很多研究組已報告候選基因的確定。雖然這些基因被證明在 OTs 中下調，並沒有確鑿的證據提供關於它們在 OTs 形成中的作用。OTs 的發病機理仍然難以解釋。微型核糖核酸（microRNAs, miRNAs）是一類豐富的小分子（19-25 個核苷酸）非蛋白編碼核糖核酸，它在轉錄后水平抑制其靶基因的表達。最近的調查顯示 miRNA 異常牽涉各種癌癥包括神經膠質瘤的發展。對 miRNA 的生物學以及靶標的更好瞭解可能揭示出對神經膠質瘤的分子發病機制和這些核糖核酸分子作為這種腦腫瘤治療靶點的潛力。

最近的一項研究報告顯示，miRNA-137 在各級星形細胞瘤中的表達明顯減少，且對 GBM 細胞增殖有抑制作用。此外，miRNA-137 能夠誘導小鼠神經幹細胞，GBM 腫瘤幹細胞和小鼠 OT 腫瘤幹細胞的神經元樣分化。因此，miR-137 被建議為一個潛在的神經膠質瘤生長抑制 miRNA。本研究的目的是探討 miR-137 在 OT 和 GBM 發病機制中的可能參與，并通過鑒定和描述它的靶標來闡明其生物學作用。

共 36 例原發性 OTs（包括 13 例少突膠質細胞瘤，7 例間變性少突膠質細胞瘤 13 例少突星型細胞瘤和 3 例間變性少突星型細胞瘤）被用來進行本研究。定量逆轉錄聚合酶鏈式反應（qRT-PCR）檢測結果顯示，miR-137 的表達水平在 90%（18/20）的少突膠質細胞瘤（p=0.016）和 100%（16/16）的少突星型細胞瘤（p=0.009）中比 3 例正常腦組織中的平均表達顯著下調。MiR-137 的低表達也在 3 種 OT 細胞系和 7 種 GBM 細胞系種觀察到。統計分析表明，miR-137 的低表達與腫瘤分級（p=0.010）和較高的 Ki-67 標記指數（p=0.009）有關，

但與染色體 1p 等位缺失，染色體 1p/19q 丟失，性別或年齡無關。此外，經去甲基化和组蛋白去乙酰酶抑制剂處理后，OT 細胞系中的 miR-137 恢復表达（p<0.001）。這些結果表明，miR-137 的表達可能被表觀遺傳修飾所調控，其下調可能有助於 OT 的發生及進展。

爲了確定 miR-137 在神經膠質瘤中的生物學作用，我進行了一些功能性檢測。通過 MTT 檢測和細胞計數，異位 miR-137 表達抑制 8 種神經膠質瘤細胞系（从 2 例少突膠質細胞瘤，1 例少突星型細胞瘤和 5 例 GBM 產生）的生長（p<0.015）。軟瓊脂檢測表明，miR-137 抑制 OT 和 GBM 細胞的錨地獨立增長（p<0.001）。通過 5-溴-2-脫氧尿嘧啶（BrdU）結合和裂解 PARP 的水平檢測發現，經 miR-137 轉染后，OT 和 GBM 細胞中 DNA 合成被抑制，而細胞凋亡增强。基底膜侵襲實驗顯示，miR-137 顯著抑制神經膠質瘤細胞的運動性（p<0.001）。此外，miR-137 異位表達還能誘導 GBM 細胞中一種神經元標記 β-微管蛋白-III 的表達，顯示 miR-137 能夠誘導 GBM 細胞的神經元樣分化。總的來說，這些結果表明了 miR-137 可能是一個潛在的 OT 和 GBM 腫瘤抑制 miRNA。

爲了鑒定 miR-137 的靶基因，計算方法包括四種 miRNA 預測程序（TargetScan，PicTar，miRanda 和 microCosm）被採用。五個涉及腫瘤發生的被預測候選基因（CSE1L，ERBB4，NRP1，CDC42 和 AKT2）被選定進行進一步的分析。雙螢光素酶報告檢測表明，在共轉染了包含有位於 CSE1L 和 ERBB4 轉錄子 3'端非翻譯區域中假定的 miR-137 結合位點的報告載體與 miR-137 的神經膠質瘤細胞中，螢光素酶的活性明顯降低（p<0.001）。而對於其它三個候選基因，則沒有螢光素酶活性改變。當使用陰性對照 miRNA 或攜帶了突變后的 miR-137 識別位點的載體時，也沒有螢光素酶的活性下降。這些發現顯示了在神經膠質瘤細胞中，miR-137 能夠與 CSE1L 和 ERBB4 轉錄子的 3'端非翻譯區域相互作用。進一步的研究表明，miR-137 轉染降低了神經膠質瘤細胞中 CSE1L 蛋白，而非轉錄子水平的表達。總的來說，這些結果顯示在神經膠質瘤中，miR-137 通過抑制蛋白翻譯來負調控 CSE1L。

爲了探討 CSEIL 在神經膠質瘤中的作用，qRT-PCR 方法被用來確定

CSE1L 的表達水平。結果表明，CSE1L 信使 RNA 在 30%（6/20）的少突膠質細胞瘤（p=0.039）及 75%（12/16）的少突星形細胞瘤（p=0.006）中，比正常的腦組織中顯著表達升高。過表達的 CSE1L 轉錄子也在 3 種 OT 細胞系之中的 2 種以及 7 種 OT 細胞系之中的 6 種中檢測到（p=0.014）。免疫組織化學研究進一步證明 CSEIL 蛋白在少突膠質細胞瘤和少突星形細胞瘤中與 13 个非腫瘤腦組織相比都有过表達（p<0.001）。雖然 CSE1L 信使 RNA 和蛋白含量都與 miR-137 水平没有明顯的關聯（分別 p=0.326 和=0.300），這些數據已经顯示了在 OT 中 CSE1L 在信使 RNA 和蛋白水平上均有上調，暗示了 CSE1L 可能在神經膠質瘤的發展中起作用。

對於 CSE1L 的功能特性，在神經膠質瘤細胞中小分子干擾 RNA 介導的 CSE1L 表達抑制引起了細胞增殖抑制，細胞凋亡誘導以及細胞侵襲性降低（p<0.001）。這些效果與 miR-137 在神經膠質瘤細胞中過度表達後的效果相似，但程度較少，表明了 miR-137 很可能部份通過 CSE1L 發揮其作用。

綜上所述，本研究結果顯示，miR-137 在 OT 和 GBM 細胞中頻繁表達下調。恢復 miR-137 的表達能夠抑制 OT 和 GBM 細胞的增長，侵襲以及誘導細胞凋亡和分化，暗示了 miR-137 可能是一個神經膠質瘤形成過程中的生長抑制者和分化推動者。一種核運輸因子，CSE1L 被確定為一個新的 miR-137 靶標基因，它在 OT 中常見過表達。研究結果表明 miR-137 和它的靶標，CSE1L 可能在神經膠質瘤的發生中起重要的作用。miR-137-CSE1L 通路在神經膠質瘤治療中的潛力也同時被發現。

TABLE OF CONTENTS

LIST OF TABLES

LIST OF FIGURES

LIST OF ABBREVIATIONS

5-aza-dC	5-aza-2' deoxycytidine
AGO	Argonaute
AJAP1	Adherens junctions associated protein 1
AKT2	V-akt murine thymoma viral oncogene homolog 2
APAF1	Apoptotic peptidase activating factor 1
APS	Ammonium persulfate
ARP5	Angiopoietin-related protein 5
BAC	Bacterial artificial chromosome
BCL2	B-cell CLL/lymphoma 2
BMF	Bcl2 modifying factor
BMI1	B lymphoma Mo-MLV insertion region 1 homolog
bp	Base pair
BrdU	5-bromo-2'-deoxyuridine
BSA	Bovine serum albumin
°C	Degree Celsius
CAB39	Calcium binding protein 39
CAMTA1	Calmodulin binding transcription activator 1
CDC42	Cell division cycle 42
CDK	Cyclin dependent kinase
CDKN	Cyclin-dependent kinase inhibitor
cDNA	Complementary DNA
CGH	Comparative genomic hybridization
CITED4	Cbp/p300-interacting transactivator, with Glu/Asp-rich carboxy-terminal domain, 4
CLL	Chronic lymphocytic leukaemia
CpG	Cytosine.phosphate.guanine
CSE1L	CSE1 chromosome segregation 1-like (yeast)
C_T	Threshold cycle
CTGF	Connective tissue growth factor
DAB	3,3'-diaminobenzidine

DAPI	4,6-diamidino-2-phenylindole
dATP	Deoxyadenosine triphosphate
DAXX	Death-domain associated protein
dCTP	Deoxycytidine triphosphate
DEPC	Diethylpyrocarbonate
DFFB	DNA fragmentation factor beta polypeptide
DGCR8	Digeorge syndrome critical region gene 8
dGTP	Deoxyguanosine triphosphate
DIRAS3	DIRAS family, GTP-binding RAS-like 3
DMSO	Dimethyl sulfoxide
DNA	Deoxyribonucleic acid
DNase	Deoxyribonuclease
DNMT1	DNA (cytosine-5-)-methyltransferase 1
dNTP	Deoxyribonucleoside triphosphate
dTTP	Deoxythimidine triphosphate
dUTP	Deoxyuridine triphosphate
E2F3	E2F transcription factor 3
EDTA	Ethylenediaminetetraacetic acid
EGFR	Epidermal growth factor receptor
EGTA	Ethylene glycol tetraacetic acid
ERBB4	V-erb-a erythroblastic leukemia viral oncogene homolog 4 (avian)
ERK	Extracellular signal-regulated kinase
ESC	Embryonic stem cell
Ezh2	Enhancer of zeste homolog 2
FFPE	Formalin-fixed paraffin-embedded
FISH	Fluorescence in situ hybridization
FITC	Fluorescein isothiocyanate
GAPDH	Glyceraldehyde-3-phosphate dehydrogenase
GBM	Glioblastoma multiforme
GFAP	Glial fibrillary acidic protein
H&E	Haematoxylin and eosin
H_2O_2	Hydrogen peroxide

H3K4	H3 on lysine 4
H3K9	H3 on lysine 9
HGF	hepatocyte growth factor
HOXD10	Homeobox D10
HRP	Horseradish peroxidase,
IDH1	Isocitrate dehydrogenase 1
IHC	Immunohistochemistry
IRS	Immunoreactive score
IRS1	Insulin receptor substrate 1
IRS2	Insulin receptor substrate 2
Jarid1b, Kdm5b	Lysine (K)-specific demethylase 5B
kDa	Kilodalton
LB	Luria bertani
LI	Labeling index
LOH	Loss of heterozygosity
LRRFIP1	Leucine rich repeat interacting protein 1
LSD1, KDM1A	Lysine (K)-specific demethylase 1A
MCL1	Myeloid cell leukemia sequence 1
$MgCl_2$	Magnesium chloride
MGMT	O^6-Methylguanine-DNA methyltransferase
Mib1	Mindbomb homolog 1
miRISC	miRNA-induced silencing complex
miRNA	microRNA
miRNP	miRNA-ribonucleoprotein
MITF	Microphthalmia-associated transcription factor
MRE	miRNA recognition element
mRNA	Messenger RNA
MTT	3-(4,5-Dimethylthiazol-2-yl)-2,5-diphenyltetrazolium bromide
Na_2VO_4	Sodium orthovanadate
NaF	Sodium fluoride
NF1	Neurofibromin 1
NRP1	Neuropilin 1

NSC	Neuronal stem cell
OA	Oligoastrocytoma
OD	Oligodendroglioma
OD	Optical density
OT	Oligodendroglial tumor
PARP	Poly (ADP-ribose) polymerase
PBS	Phosphate buffered saline
PCR	Polymerase chain reaction
PCV	Procarbazine, lomustine, vincristine
PDCD4	Programmed cell death 4
PI3K	Phosphoinositide-3-kinase
PMSF	Phenylmethylsulfonyl fluoride
PP	Percentage of positive cells
pre-miRNA	Precursor miRNA
pri-miRNA	Primary miRNA
PTBT1	Polypyrimidine tract binding protein 1
PTEN	Phosphatase and tensin homology
PVDF	Polyvinylidene fluoride
qRT-PCR	Quantitative reverse transcription-polymerase chain reaction
RB1	Retinoblastoma 1
RECK	Reversion-inducing-cysteine-rich protein with kazal motifs
RIPA	Radio-immunoprecipitation assay
RNA	Ribonucleic acid
RNAi	RNA interference
Rnase	Ribonuclease
RHOC	RAS homolog gene family member C
RT	Reverse transcription
SCP1	Small C-terminal domain phosphatase 1
SDS	Sodium dodecyl sulfate
SDS-PAGE	Sodium dodecyl sulfate-polyacrylamide gel electrophoresis
SI	Staining intensity
siRNA	Short interfering RNA

SOX9	Sex determining region Y-box 9
SSC	Saline sodium citrate
STAT3	Signal transducer and activator of transcription 3
STMN1	Stathmin 1
TBST	Tris-buffered saline with Tween 20
TCGA	The Cancer Genome Atlas
TEMED	N,N,N',N'-tetramethylethylenediamine
TGFBR2	Transforming growth factor, beta receptor II
TIMP3	TIMP metallopeptidase inhibitor 3
TMZ	Temozolomide
TP53	Tumor protein 53
TP53INP1	TP53 inducible nuclear protein 1
TP63	Tumor protein p63
TP73	Tumor protein p73
TRBP	Transactivation-responsive RNA-binding protein
TSA	Trichostatin A
TSG	Tumor suppressor gene
Tuj1	β-tubulin III
U	Enzyme activity unit
UTR	Untranslated region
V	Volt
v/v	Volume per volume
VNTR	Variable nucleotide tandem repeat
w/v	Weight per volume
WHO	World Health Organization

CHAPTER 1 INTRODUCTION

1.1 Gliomas

Gliomas refer to a collection of most common intracranial neoplasms, which account for more than 70% of all tumors of central nervous system (Ohgaki *et al.*, 2005). According to current World Health Organization (WHO) classification of Tumors of the Central Nervous System, gliomas can be classified as astrocytic, oligodendroglial and ependymal tumors based on the tumor cell types and histological appearance (Louis *et al.*, 2007).

Gliomas are categorized into WHO grade I to IV based on the degree of malignancy evaluated by various histological characteristics, such as mitotic activity, necrosis and microvascular proliferation. High-grade (WHO grade III-IV) gliomas are more aggressive than low-grade (WHO grade I-II) gliomas. WHO grade I gliomas generally display benign behaviors, whereas WHO grade II-IV gliomas are malignant with diffuse infiltration throughout the surrounding brain tissues. As summarized in Table 1.1, astrocytic tumors are subsequently grouped as pilocytic astrocytoma (WHO grade I), diffuse astrocytoma (WHO grade II), anaplastic astrocytoma (WHO grade III) or glioblastoma (WHO grade IV). Oligodendroglial tumors (OTs) are classified as WHO grade II or anaplastic form, WHO grade III (Louis *et al.*, 2007).

Table 1.1 Grading of astrocytic and oligodendroglial tumors by WHO

WHO grade	Astrocytic tumors	Oligodendroglial tumors
I	Pilocytic astrocytoma	
II	Diffuse astrocytoma	Oligodendroglioma Oligoastrocytoma
III	Anaplastic astrocytoma	Anaplastic oligodendroglioma Anaplastic oligoastrocytoma
IV	Glioblastoma multiforme	

1.1.1 Oligodendroglial tumors (OTs)

OTs can be categorized histologically as oligodendrogliomas (ODs) or oligoastrocytomas (OAs). The latter displays morphological components of both oligodendroglial and astrocytic tumors. The incidence rate of OTs is 0.5 per 100,000 people annually in Europe, constituting approximately 10% of all gliomas. OTs arise mostly in adults with a peak incidence at 35-50 years of age and a slight male preference (Ohgaki *et al.*, 2005; Reifenberger *et al.*, 2007; Rodriguez *et al.*, 2010).

Pure oligodendrogliomas have a better prognosis than oligoastrocytomas and astrocytomas of the same grade. A favorable median survival time of OTs is associated with WHO grade II, combined chromosomes 1p and 9q loss and proliferative activity. Moreover, OTs are more sensitive to chemotherapy compared to other glioma types of the same grade. Treatments of OTs consist of surgical resection and subsequent chemotherapy and/or radiotherapy (Ohgaki *et al.*, 2005; Reifenberger *et al.*, 2007; Rodriguez *et al.*, 2010).

1.1.2 Glioblastoma multiforme (GBM)

GBM is the most aggressive (WHO grade IV) and the most common astrocytic tumor, comprising up to 70% of all gliomas. Generally, there are about 3-4 new cases diagnosed in 100,000 people per year in European and North American countries. GBM preferentially develops in adults, with peak incidence occurring between 45 to 70 years of age. Males are more susceptible than females to GBM with a male/female ratio of 1.26-1.28:1.(Kleihues *et al.*, 2007)

The vast majority (>90%) of GBM manifest rapidly *de novo* without any precursor lesion identified and arise typically in elder patients. These tumors are

termed primary GBM. In contrast, secondary GBM develops by progression from low-grade diffuse astrocytoma or anaplastic astrocytoma within 5-10 years and mostly diagnosed in mid-age patients. Primary and secondary GBMs share similar clinical features, including rapid proliferation, high invasion activity and resistance to therapeutic treatment. However, genetic studies have revealed that these tumors may originate from distinct pathways. Due to its infiltrative growth pattern and inherent property, GBM is refractory to complete resection and is generally recalcitrant to chemo/radiotherapy. Therefore GBM is regarded as a lethal tumor with a median patient survival of 4.7~7.8 months (Ohgaki *et al.*, 2005; Kleihues *et al.*, 2007; Ohgaki *et al.*, 2007).

1.1.3 Molecular pathology of gliomas

Intensive research in the past two decades has unveiled a variety of genetic alterations associated with the development of gliomas. These genetic aberrations provide clues to the process of tumor development (Figure 1.1) and more importantly, help diagnosis, prognosis and therapy design.

1.1.3.1 Genetic alterations in OTs

By comparative genomic hybridization (CGH) and microsatellite analysis, earlier investigations have uncovered chromosomal imbalances in OTs, including gains on chromosome 7, 8q and 11q, and losses on chromosomes 1p, 4, 9q, 10q, 14, 17p 19q and 22q. Losses of 9q and 10q are more frequent in anaplastic variants and are thought as progression-associated aberrations. (Reifenberger *et al.*, 1994; Zhu *et al.*, 1998; Bigner *et al.*, 1999; Reifenberger *et al.*, 2003; Jeuken *et al.*, 2004; Kitange *et al.*, 2005) Some gene abnormality have been identified in these chromosomal

regions, such as deletion of cyclin-dependent kinase inhibitor 2A (*CDKN2A*) in 9q and mutation of phosphatase and tensin homolog (*PTEN*), a negative regulator of the phosphoinositide-3-kinase (PI3K) pathway, in 10q. (Bigner *et al.*, 1999; Watanabe *et al.*, 2001; Reifenberger *et al.*, 2003; Jeuken *et al.*, 2004; Reifenberger *et al.*, 2007; Bromberg *et al.*, 2009)

Among these chromosomal instabilities, loss of heterozygosity (LOH) on chromosomal arms 1p and 19q is the predominant genetic alteration in OTs and is detected in 67-87% of tumors (Bello *et al.*, 1994; Reifenberger *et al.*, 1994; Bigner *et al.*, 1999; Husemann *et al.*, 1999; Smith *et al.*, 1999). The abnormality mostly affect the entire 1p and 19q arms (Felsberg *et al.*, 2004; Barbashina *et al.*, 2005), probably resulting from an unbalanced t(1;19)(q10;p10) translocation involving chromosomes 1 and 19 (Griffin *et al.*, 2006; Jenkins *et al.*, 2006) and the concomitant loss of one copy each of 1p and 19q. The high frequency of 1p/19q codeletion suggests the existence of OT-related genes on these chromosomes.

There has been extensive effort to identify the OT-related gene on chromosome 1p for understanding the molecular basis of OT development. It was postulated that alteration of the OT-related genes may attribute to gene rearrangement at the breakpoints of t(1;19)(q10;p10) translocation, haploinsufficiency of genes or potential epigenetic inactivation.

Located at the juxta-centromeric region of 1p is the *NOTCH2* gene, which has been implicated in oligodendrocyte differentiation (Hu *et al.*, 2003). Loss of *NOTCH2* was associated with a favorable prognosis in oligodendroglioma and GBM patients (Boulay *et al.*, 2007). However, there is no physical rearrangement or somatic mutation of *NOTCH2* detected in oligodendrogliomas carrying

t(1;19)(q10;p10) (Benetkiewicz *et al.*, 2009). Other candidate genes that have been associated with OTs, include *CDKN2C* (Husemann *et al.*, 1999), *TP73* (Dong *et al.*, 2002), *DFFB* (McDonald *et al.*, 2005), *AJAP1* (McDonald *et al.*, 2006), *CAMTA1* (Barbashina *et al.*, 2005), *STMN1* (Ngo *et al.*, 2007), *CITED4* (Tews *et al.*, 2007), *DIRAS3* (Riemenschneider *et al.*, 2008) and *KIAA0495/PDAM* (Pang *et al.*, 2010). These genes were inactivated due to mutation, chromosomal deletion, transcriptional silencing and/or epigenetic modification. More recently, numerous genes on 1p or 19q were found deregulated in 1p/19q codeleted oligodendrogliomas by high-throughput gene expression profiling analysis (Tews *et al.*, 2006). Whether any of these deregulated genes are involved in OT formation require further investigation.

Besides genes that are mapped to 1p or 19q, other altered genes have been discovered. Tumor protein p53 (*TP53*) gene encoded protein p53 is implicated in tumorigenesis as a tumor suppressor (Aylon *et al.*, 2007). Usually mutually exclusive with 1p/19q co-deletion, *TP53* mutation is rare (10~15%) in oligodendrogliomas, but more common (30~50%) in oligoastrocytomas (Reifenberger *et al.*, 2003; Jeuken *et al.*, 2004; Okamoto *et al.*, 2004; Reifenberger *et al.*, 2007; Watanabe *et al.*, 2009; Bourne *et al.*, 2010; Kim *et al.*, 2010). However, p53/MDM2/MDM4/p14^{ARF} pathway inactivation is present in 21% of oligodendrogliomas and 50% of anaplastic oligodendrogliomas (Watanabe *et al.*, 2001).

Another newly identified genetic alteration in gliomas is mutation of isocitrate dehydrogenase 1 (*IDH1*). The *IDH1* mutation is detected at a high incidence rate (>80%) in WHO grade II and III astrocytomas, secondary GBM and OTs but is rare in primary GBM (Balss *et al.*, 2008; Watanabe *et al.*, 2009; Yan *et al.*, 2009; Kim *et*

al., 2010). Such mutation is found in most gliomas (>60%) harboring either 1p/19q codeletion or *TP53* mutation, strongly suggesting that *IDH1* mutation is a very early event in the development of gliomas and subsequent 1p/19q loss or *TP53* mutation directs the progression to oligodendroglial or astrocytic phenotype, respectively (Ichimura *et al.*, 2009; Watanabe *et al.*, 2009).

Expression profiles of OTs with 1p/19q loss have unveiled a subset (proneural) of OT exhibiting differential gene expression signatures resembling those of normal brain. Moreover, the proneural OT patients benefit a favorable clinical outcome than the GBM-like subtype. (Huang *et al.*, 2004; Mukasa *et al.*, 2004; Ducray *et al.*, 2008; Ferrer-Luna *et al.*, 2009; Cooper *et al.*, 2010)

Taken together, a vast majority of OTs exhibited *IDH1* mutation at early stage of OT pathogenesis. Subsequent 1p/19q loss leads to development of oligodendroglioma, whereas oligoastrocytoma usually carries either 1p/19q deletion or *TP53* mutation.

Despite these rapidly increasing knowledge of molecular pathogenesis of OT, it remain largely elusive which genes are pivotal for OT development. Therefore, identification and characterization of the OT-related genes are essential for better understanding of these tumors and the development of molecular-based therapy.

1.1.3.2 Prognostic and predictive factors in OTs

Better prognosis of OT patients can be predicted by some clinical factors, such as younger patient age, lower tumor grade, frontal location, more complete tumor resection and pure oligodendroglial histology. (Okamoto *et al.*, 2004; Reifenberger *et al.*, 2007; van den Bent *et al.*, 2008)

The 1p/19 codeletion or 1p loss alone has been demonstrated to be a strong predictor of longer survival and sensitivity to radio/chemo treatment in 1988 (Cairncross *et al.*, 1998). Since then, numerous studies have confirmed the clinical relevance of 1p/19q codeletion in OT patients treated with radiotherapy (Bauman *et al.*, 2000) and adjuvant procarbazine, lomustine, and vincristine (PCV) (Cairncross *et al.*, 1998; Ino *et al.*, 2001; Cairncross *et al.*, 2006; Jenkins *et al.*, 2006; van den Bent *et al.*, 2006) or with temozolomide (TMZ) (Hoang-Xuan *et al.*, 2004; Brandes *et al.*, 2006; Kouwenhoven *et al.*, 2006). Notably, the results from large-scale clinical trials involving hundreds of anaplastic OT patients have strongly reinforced the prognostic relevance of concurrent loss of 1p and 19q (Cairncross *et al.*, 2006; van den Bent *et al.*, 2006). In addition, 1p/19q codeletion is also prognostic in OT patients without any radio/chemotherapy (Kanner *et al.*, 2006), raising the issue that 1p/19q loss represents a prognostic rather than predictive marker in OTs.

Other molecular alterations of prognostic significance include *IDH1* mutation and promoter methylation of O^6-Methylguanine-DNA methyltransferase (*MGMT*). MGMT is a DNA repair enzyme that removes promutagenic alkyl groups from O^6-methylguanine adducts in DNA, to prevent cells from G:C-->A:T mutations in DNA replication. Both *IDH1* mutation and *MGMT* methylation are observed to be prognostic for both overall and progression-free survival in anaplastic OT patients treated with radiotherapy or combined radiotherapy/PCV treatment in a clinical trial study OTs (van den Bent *et al.*, 2009; van den Bent *et al.*, 2010). It was also observed that 1p/19q codeletion, *IDH1* mutation and *MGMT* methylation correlated with each other in anaplastic OTs (van den Bent *et al.*, 2009; van den Bent *et al.*, 2010)

1.1.3.3 Genetic alterations in GBM

Genome-wide genetic investigations using cytogenetic, CGH and microsatellite analyses have identified multiple chromosomal aberrations in GBM. Most frequent aberrant regions include gain of chromosome 7, 8q and 20q, and losses of chromosomes 9p, 10q, 13q, 17p and 22q (Lang *et al.,* 1994; Kim *et al.,* 1995; Weber *et al.,* 1996; Mohapatra *et al.,* 1998; Hui *et al.,* 2001; Ohgaki *et al.,* 2004). Further molecular analysis, such as array-based CGH, fluorescent *in situ* hybridization (FISH) and gene sequencing, revealed minimal altered genomic segments and gene abnormality on the frequently unstable chromosomes. For instance, over 60% of both primary and secondary GBM show LOH 10q (Ohgaki *et al.,* 2004), where *PTEN* was mapped. Inactivating mutation of *PTEN* was present in 5-40% of GBM (Tohma *et al.,* 1998; Ohgaki *et al.,* 2004; Ohgaki *et al.,* 2009). Amplification of epidermal growth factor receptor (*EGFR*) in chromosome 7 (Ekstrand *et al.,* 1992; Watanabe *et al.,* 1996; Ohgaki *et al.,* 2004), *TP53* mutation in chromosome 17p (Watanabe *et al.,* 1996; Ohgaki *et al.,* 2004) are also representative molecular abnormalities in GBM with a predominance in primary and secondary GBM, respectively. There are numerous alterations on other oncogenic or tumor suppressor genes, including neurofibromin 1 (*NF1*) mutation, Mdm2 p53 binding protein homolog (mouse) (*MDM2),* Mdm4 p53 binding protein homolog (mouse) (*MDM4)* and cyclin-dependent kinase 4 (*CDK4)* amplification as well as *CDKN2A* deletion or promoter methylation (Ohgaki *et al.,* 2004; Ohgaki 2005; Kleihues *et al.,* 2007; Ohgaki *et al.,* 2007; Kanu *et al.,* 2009; Ohgaki *et al.,* 2009).

Collectively, several major signaling pathways involved in cell cycle progression and cell survival regulation are deregulated in GBM, including

EGFR/RAS/NF1/PTEN/PI3K, p53/MDM2/MDM4/$p14^{ARF}$ and $p16^{INK4a}$/CDK4/CDK6/RB1 (Ohgaki *et al.*, 2004; Ohgaki *et al.*, 2009).

New insight of identifying abnormal molecular pathways and glioma subtypes came from integrative genomic study. The Cancer Genome Atlas (TCGA) project determined changes of DNA copy number, somatic mutations of all known genes, expression profilings of mRNA and microRNA, and aberrant DNA methylation, and correlated the molecular findings with clinical information in a large series of GBM (The Cancer Genome Altas Research Network 2008). The integrated multidimensional genomic data have not only confirmed some established genetic alterations, such as *TP53, PTEN, EGFR, NF1* and *RB1* aberrations (The Cancer Genome Altas Research Network 2008), but also distinguished four GBM subtypes (classical, mesenchymal, proneural and neural) based on distinct genetic expression pattern. Patients with proneural subtype of GBM tended to have a longer survival than other subtypes (Verhaak *et al.*, 2010). As complex data have been generated by TCGA genomic project, the ongoing data analysis will provide more valuable hints for GBM (Wrensch *et al.*, 2009; Noushmehr *et al.*, 2010).

Knowledge of the genetic changes in GBM may lead to more targeted therapies, improved quality of life, and prolonged survival. Overall, although a lot of efforts have been made to understand the pathogenesis of glioma, the molecular mechanism has not yet been clearly elucidated.

1.1.3.4 Prognostic and predictive factors in GBM

Clinical prognostic factors for GBM include patient age, extent of tumor resection and presence of necrosis (Ohgaki *et al.*, 2004; Ohgaki *et al.*, 2005;

Houillier *et al.*, 2006; Kleihues *et al.*, 2007; Ohgaki *et al.*, 2007; Felsberg *et al.*, 2009).

Promoter methylation of *MGMT* is frequently detected in 40-45% of GBM, reducing the MGMT activity (Esteller *et al.*, 2000; Hegi *et al.*, 2005; Weller *et al.*, 2009; Zawlik *et al.*, 2009). A clinical relevance of *MGMT* methylation is uncovered by its association with better response to chemotherapy and favorable overall and progression-free survival in adjuvant TMZ-treated GBM patients, but not in patients who received radiotherapy only (Paz *et al.*, 2004; Hegi *et al.*, 2005; Criniere *et al.*, 2007; Felsberg *et al.*, 2009; Weller *et al.*, 2009).

As mentioned earlier in section 1.1.3.1, *IDH1* mutation at codon 132 is differentially detected in primary (<5%) and secondary GBM (>80%) (Balss *et al.*, 2008; Watanabe *et al.*, 2009; Yan *et al.*, 2009), *IDH1* mutation may predict a longer survival for GBM and anaplastic astrocytoma patients (Parsons *et al.*, 2008; Nobusawa *et al.*, 2009; Weller *et al.*, 2009; Yan *et al.*, 2009). In addition, although showing a low frequency (<15%) (Nakamura *et al.*, 2000), allelic loss of 1p has been associated with a longer survival in GBM (Homma *et al.*, 2006), but not in some other studies (Houillier *et al.*, 2006; Boulay *et al.*, 2007; Felsberg *et al.*, 2009; Weller *et al.*, 2009).

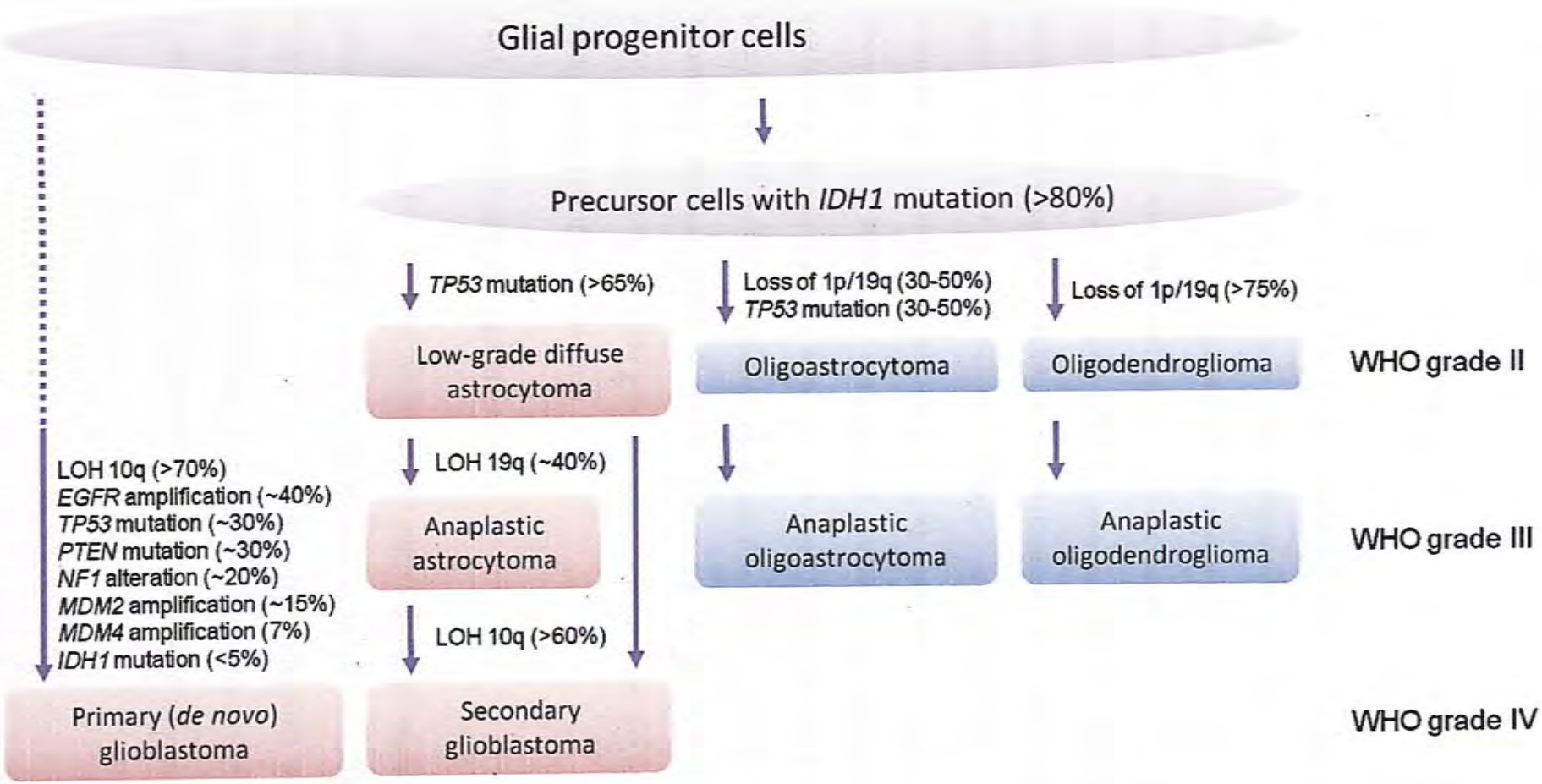

Figure 1.1 Overview of proposed genetic pathways to astrocytic and oligodendroglial gliomas. (Okamoto *et al.*, 2004; Reifenberger *et al.*, 2007; Ohgaki *et al.*, 2009; Watanabe *et al.*, 2009; Bourne *et al.*, 2010).

1.2 microRNA (miRNA)

MiRNAs are a class of endogenous short (19-25 nucleotides) non-coding RNAs that regulate gene expression post-transcriptionally. The first discovered miRNA was lin-4, which showed antisense RNA-RNA interaction with the 3' untranslated region (UTR) of lin-14 mRNA in *Caenorhabditis elegans,* suggesting a novel endogenous negative control mechanism for gene regulation (Lee *et al.*, 1993). Not until seven years later the second miRNA let-7 was identified. Let-7 functions as a modulator of multiple genes involved in *Caenorhabditis elegans* developmental timing via similar regulative mechanism as lin-4 (Reinhart *et al.*, 2000). It was then discovered that let-7 and lin-4 were evolutionarily conserved from flies to human, prompting the speculation that miRNAs might play a universal role across species (Pasquinelli *et al.*, 2000; Lagos-Quintana *et al.*, 2002). In the following decade, miRNA has become a hotspot in biology. To date, 17,341 miRNAs have been identified in 142 species including human, mouse, flies, worms, plants and viruses according to miRBase database (http://www.mirbase.org/; release 16.0, September 2010). Currently, there are 1,366 annotated human miRNAs, and the list is still rapidly growing (Griffiths-Jones 2010).

1.2.1 miRNA biogenesis and function

Genomic analysis indicated that mammalian miRNA genes are located mostly within defined transcription units (~70%), as well as in the intergenic areas, suggesting that transcription of miRNAs is either in parallel with their host transcripts or in autonomy (Rodriguez *et al.*, 2004). In some cases, miRNAs are organized in close conjunction as genomic clusters and expressed polycistronically

as single transcriptional units (Lee *et al.*, 2002), such as the miR-17-92 cluster on human chromosome 13q13 (He *et al.*, 2005).

Mammalian miRNA biogenesis begins with transcription generating a kilobases-long primary transcript (pri-miRNA) mediated by RNA polymerase II in nucleus. Containing a 5' methylguanylate cap structure and a 3' poly (A) tail, pri-miRNA folds into a hairpin structure with imperfect complementary stem-loop region. Pri-miRNA is sequentially cleaved into ~70-nucleotide precursor miRNA (pre-miRNA) by the ribonuclease (RNase) III enzyme Drosha and cofactor DiGeorge syndrome critical region gene 8 (DGCR8). The pre-miRNA is next translocated by Exportin-5/RanGTP complex to the cytoplasm, where it is cleaved to yield ~22-bp miRNA duplexes by another RNase III enzyme Dicer, assisted by a double-strand RNA binding protein, transactivation-responsive RNA-binding protein (TRBP). The single-strand mature miRNA is then released through unwinding of the duplex by helicase, whereas the other strand (miRNA*) is usually degraded. After maturation, miRNAs are assembled with the argonaute (AGO) family proteins to form the effector miRNA-induced silencing complex (miRISC) or ribonucleoprotein (miRNP) complex (Kim 2005; Liu *et al.*, 2008; Krol *et al.*, 2010).

Canonically, miRISC directs sequence-specific binding of miRNA to the miRNA recognition elements (MREs) located at 3'UTR of mRNAs. The target mRNA undergoes translational repression and/or transcript cleavage depending on the degree of complementarity between miRNA and the target mRNA. MiRNAs that show near perfectly base pairing triggers cleavage-dependent target mRNA cleavage, which resembles siRNA resultant inhibition. However, what occurs more often in animals is partial complementarity allowing mismatches and bulges that favors

translational repression of the target transcript (Filipowicz *et al.,* 2008). In that case, perfectly base- pairing between the 2^{nd}-8^{th} nucleotides (seed region) at the 5' end of miRNA with target mRNA is essential for miRNA target recognition (Bartel 2004; Lewis *et al.,* 2005; Bartel 2009). The process of miRNA biogenesis and its functional mechanisms are shown in Figure 1.2.

It has been estimated that miRNA could regulate more than 30% of the human genome (Lewis *et al.,* 2005). Both computational and microarray analyses indicated that a mammalian miRNA can have hundreds of targets (Lewis *et al.,* 2005; Lim *et al.,* 2005), whereas a single mRNA can be regulated by distinct miRNAs cooperatively (Krek *et al.,* 2005). As a result, a complicated regulatory network is formed by miRNAs and their target genes to control diverse biological processes, including cell proliferation, apoptosis, development, morphogenesis and metabolism.

Nowadays, investigation of the miRNA-mRNA regulation network focuses on identification of miRNA target genes through combined computational and experimental approaches. A series of algorithms have been developed to predict potential miRNA targets, followed by experimental validation (Dalmay 2008; Bartel 2009; Orom *et al.,* 2010; Thomas *et al.,* 2010).

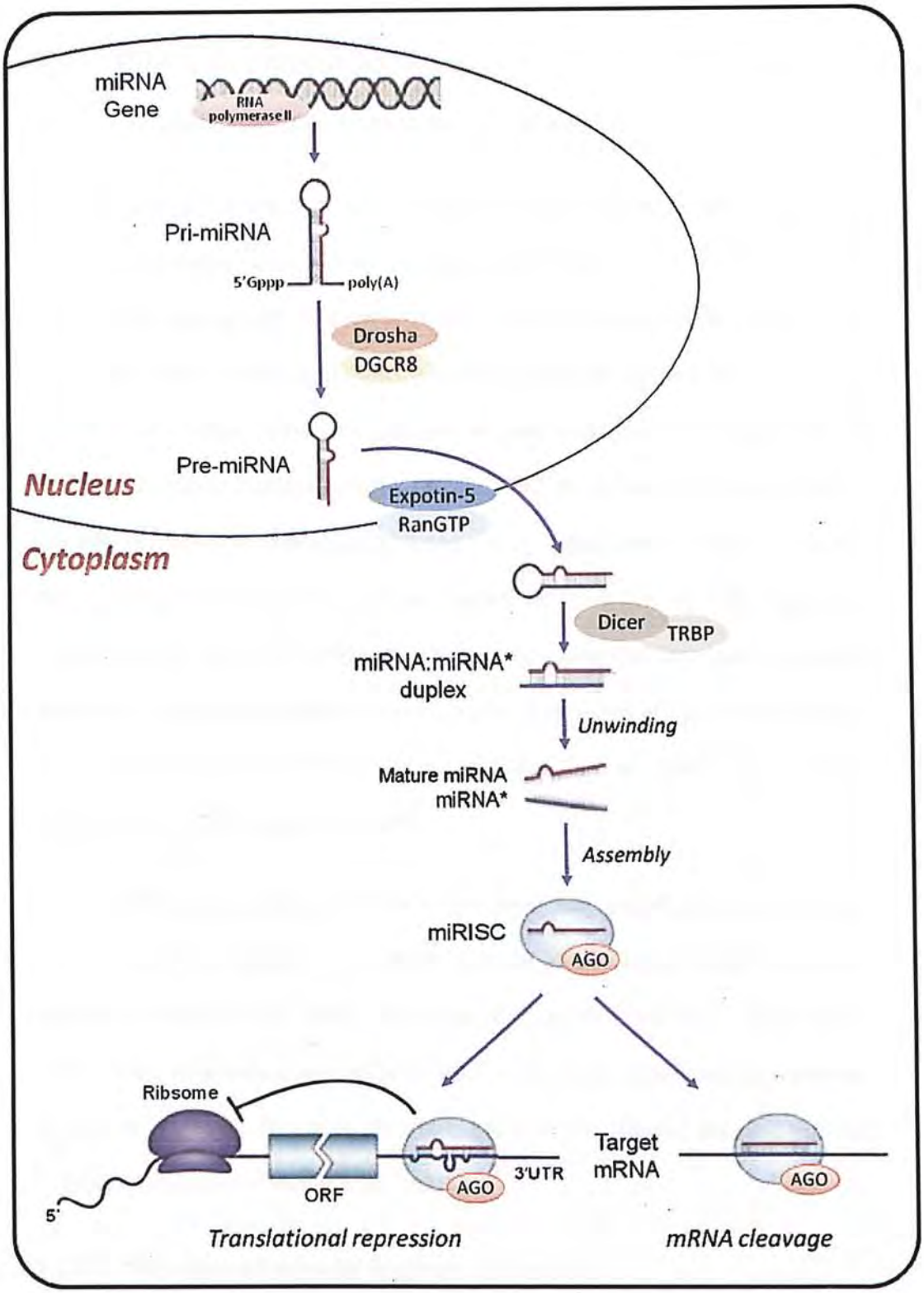

Figure 1.2 Overview of miRNA biogenesis.

1.2.2 MiRNA involvement in Cancer

1.2.2.1 Dysregulation of miRNAs in human malignancies

The linkage between miRNA and cancer has been established since the premier study demonstrating downregulated miR-15a and miR-16-1 expression levels in B-cell chronic lymphocytic leukaemia (CLL). Both of these miRNAs are clustered within the chromosome l3ql4 locus, which is commonly deleted in this disorder (Calin *et al.*, 2002). Advanced genomic analysis highlighted the importance of miRNAs in human tumorigenesis by revealing that about half of all miRNA genes are mapped to cancer-related genomic regions or fragile sites (Calin *et al.*, 2004). Subsequently, high-throughput profiling studies indicated that miRNA expressions were frequently altered in many different types of cancer and that specific miRNA expression signature is distinct among tumors of different origin. These findings suggest a pivotal role miRNAs play in oncogenesis (Liu *et al.*, 2004; Lu *et al.*, 2005; Volinia *et al.*, 2006; Visone *et al.*, 2009).

The aberrant expression of miRNAs in cancers may arise from several aspects, such as mutations (Calin *et al.*, 2005; Raveche *et al.*, 2007), single nucleotide polymorphisms (Hu *et al.*, 2008), chromosomal instability (Calin *et al.*, 2004; Zhang *et al.*, 2006), epigenetic modifications (Fabbri *et al.*, 2010), transcriptional regulation (Chang *et al.*, 2007; Woods *et al.*, 2007; Ma *et al.*, 2010) and deficient miRNA biogenesis machinery (Winter *et al.*, 2011).

1.2.2.2 Function and potential application of miRNAs

On the basis of miRNA expression profiles, it was wondered whether this widespread deregulation of miRNA has an important role in tumorigenesis.

Functional studies have demonstrated that many abnormally expressed miRNAs are involved in crucial cellular processes in cancer formation, such as cell proliferation, apoptosis, migration, invasion, differentiation, and angiogenesis. MiRNAs show oncogenic or tumor suppressive properties through negative regulation of tumor suppressor or oncogene targets, respectively. For examples, miR-15/16 cluster displays a tumor suppressive role through repressing the anti-apoptotic B-cell CLL/lymphoma 2 (BCL2) expressioin and thereafter activates the apoptotic signalling pathway in CLL (Cimmino *et al.*, 2005); whereas the oncogenic property of miR-155 is refleced by its direct targeting of TP53 inducible nuclear protein 1 (TP53INP1), an important mediator of TP53 pro-apoptotic activities in pancreatic ductal adenocarcinoma (Gironella *et al.*, 2007).

In summary, having shown a tumor-specific expression signature and diverse roles in cellular processes involved in tumorigenesis, miRNA has been implicated in cancer diagnosis, prognosis and therapeutic targets, which provide new insights into understanding and treatment of this malignancy (Tricoli *et al.*, 2007; Trang *et al.*, 2008).

1.2.3 Role of miRNAs in glioma

1.2.3.1 miRNAs in OTs

To date, the significance of miRNA in OTs remains poorly understood. A limited number of papers deciphering miRNA in OTs have been published (Nelson *et al.*, 2006; Silber *et al.*, 2008; Sasayama *et al.*, 2009)

In an attempt to identify deregulated miRNAs in OTs, Nelson *et al.* performed the miRNA microarray on formalin-fixed paraffin-embedded (FFPE) human brains and oligodendroglial tumors (Nelson *et al.*, 2006). Their results exhibited miR-9 upregulation and miR-124 downregulation in 20 human oligodendrogliomas compared to 6 adult cortex tissues confirmed by locked nucleic acid based *in situ* hybridization. No association between miR-9 expression and tumor grade or tumor cell proliferative activity was observed. Additionally, since three of the four *AGO* genes *(AGO1, AGO3*, and *AGO4*) map to chromosome 1p, the authors asked whether loss of 1p would affect the miRNA expression. The results showed that miRNA expression patterns between oligodendrogliomas with or without 1p allelic loss were similar, suggesting that allelic losses of three *AGO* genes did not substantially alter miRNAs in oligodendrogliomas (Nelson *et al.*, 2006).

In another study, miR-124 and miR-137 were among the miRNAs down-regulated in high-grade astrocytoma by expression analysis. Reduced expression of these 2 miRNAs in mouse oligodendroglioma stem cells relative to mouse neuronal stem cells (NSCs) were also demonstrated (Silber *et al.*, 2008), suggesting an aberrant expression in early stage of OT formation.

A recent study identified frequent miR-10b overexpression in a cohort of glioma,

including 6 oligodendrogliomas (Sasayama *et al.*, 2009). The miR-10b expression was correlated with that of RAS homolog gene family member C (RHOC), a well-characterized pro-metastatic gene in 43 gliomas studied. The association was probably mediated through the direct suppression of a RHOC upstream regulator, homeobox D10 (HOXD10) by miR-10b which was previously proved in breast cancer (Ma *et al.*, 2007). These results were in line with the finding of elevated RHOC expression observed in a profiling study of 17 oligodendrogliomas (Huang *et al.*, 2004).

1.2.3.2 miRNAs in GBM

There were multiple studies reporting global miRNA expression profiles in GBM (Ciafre *et al.*, 2005; Godlewski *et al.*, 2008; Silber *et al.*, 2008; Guan *et al.*, 2010; Malzkorn *et al.*, 2010; Rao *et al.*, 2010). These investigations have highlighted numerous critical miRNAs that might be involved in the development and progression of GBM (summarized in Table 1.2 and Table 1.3). The dysregulated miRNAs indicated by more than 2 studied include upregulated miR-9, miR-10b, miR-15a, miR-16, miR-19a, miR-21, miR-25, miR-130a, miR-130b, miR-210 and miR-221, and downregulated miR-124, miR-128, miR-132, miR-137, miR-138, miR-139, miR-184, miR-218, miR-323 and miR-328.

Given that up-regulated miRNA may function as oncogenes by targeting tumor-suppressor genes, whereas down-regulated miRNA may function as tumor suppressors by repressing oncogenes, some of the dysregulated miRNAs are focused and subjected to further functional characterization in recent years.

Table 1.2 Upregulated miRNAs identified in GBM.

Ciafre *et al.* 2005 (n=9)[1]	**Godlewski *et al.* 2008 (n=3)[1]**	**Silber *et al.* 2008 (n=4)[1]**	**Rao *et al.* 2010 (n=26)[1]**			**Malzkorn *et al.* 2010 (n=4)[2]**	**Guan *et al.* 2010 (n=74)[2]**
miR-9-2	**miR-10b**	**miR-10b**	**miR-9**	miR-96	miR-195	**miR-9**	miR-15b
miR-10b	**miR-21**	**miR-21**	miR-10a	miR-99a	miR-199a-3p	**miR-15a**	**miR-21**
miR-21	miR-26a	miR-155	**miR-10b**	miR-105	miR-199b-5p/3p	**miR-16**	miR-135b
miR-25	miR-383	**miR-210**	**miR-15a**	miR-106a	miR-215	miR-17	miR-196a
miR-123	miR-451		miR-15b	miR-106b*	miR-320a	**miR-19a**	miR-196b
miR-125b-1	miR-486		**miR-16**	miR-122	miR-362-3p	miR-20a	miR-363
miR-125b-2	miR-516-3p		miR-17*	**miR-130a**	miR-374a	**miR-21**	
miR-130a	miR-519d		**miR-19a**	**miR-130b**	miR-374b	**miR-25**	
miR-221			miR-19b	miR-135b	miR-424	miR-28	
			miR-20b*	miR-142-5p/3p	miR-450a	**miR-130b**	
			miR-21	miR-144	miR-497	miR-140	
			miR-23a	miR-146a	miR-505	**miR-210**	
			miR-25	miR-152	miR-532-5p		
			miR-32	miR-155	miR-542-5p		
			miR-92a	miR-181a-2*	miR-550		
			miR-92b	miR-182	miR-660		
			miR-93	miR-193a-3p	miRPlus-A1083		

[1]Relative to non-tumorous brain tissues.

[2]Relative to low-grade gliomas.

Bold indicates miRNA identified by 2 or more profiling studies.

Table 1.3 Downregulated miRNAs identified in GBM.

Ciafre *et al.* 2005 (n=9)[1]	**Godlewski *et al.* 2008 (n=3)[1]**	**Silber *et al.* 2008 (n=4)[1]**		**Rao *et al.* 2010 (n=26)[1]**		**Malzkorn *et al.* 2010 (n=4)[2]**	**Guan *et al.* 2010 (n=74)[2]**
miR-128-1	**miR-124**	miR-7	miR-149	**miR-124**	miR-338-5p	**miR-184**	miR-105
miR-181a	**miR-128-1**	miR-29b	miR-153	**miR-128**	miR-432	**miR-328**	miR-128b
miR-181b	miR-128-2	miR-31	miR-154	miR-129*	miR-483-5p		**miR-184**
miR-181c	**miR-137**	miR-101	miR-185	miR-129-3p	miR-485-3p		miR-302b
	miR-139	miR-107	miR-187	miR-129-5p	miR-498		miR-302d
	miR-190	**miR-124**	miR-203	**miR-132**	miR-584		miR-367
	miR-218	miR-124-2	**miR-218**	**miR-138**	miR-628-3p		miR-383
	miR-299	**miR-128-1**	**miR-323**	miR-187*	miR-637		miR-504
	miR-323	miR-129	**miR-328**	miR-1908	miR-638		miR-517c
	miR-483	**miR-132**	miR-330	miR-198	miR-665		miR-601
	miR-511-1	miR-133a		miR-219-2-3p	miR-765		
		miR-133b		miR-219-5p	miRPlus-A1027		
		miR-137		miR-323-3p	miRPlus-A1056		
		miR-138		miR-329	miRPlus-D1036		
		miR-139		miR-338-3p			

[1]Relative to non-tumorous brain tissues.

[2]Relative to low-grade gliomas.

Bold indicates miRNA identified by 2 or more profiling studies.

MiR-21 upregulation was consistently demonstrated in GBM by a number of studies (Chan *et al.,* 2005; Ciafre *et al.,* 2005; Gabriely *et al.,* 2008; Godlewski *et al.,* 2008; Silber *et al.,* 2008; Conti *et al.,* 2009). Functional study demonstrated that knockdown of miR-21 in glioblastoma cells resulted in suppressed cell growth, increased apoptotic activity, reduced cell invasion and more importantly, decreased tumorigenicity in mouse model (Chan *et al.,* 2005; Corsten *et al.,* 2007; Gabriely *et al.,* 2008; Li *et al.,* 2009; Shi *et al.,* 2010; Zhou *et al.,* 2010). Target identification has uncovered multiple molecular mechanisms underlying the oncogenic role of miR-21. These downregulated targets include key factors involving in the p53 pathway (TP63 and DAXX), the transforming growth factor-β pathway (TGFBR2 and PDCD4) and the mitochondrial apoptosis tumor-suppressive signaling pathway (APAF1). Alterations of these targets were in line with miR-21 regulation on cell cycle and apoptosis (Chen *et al.,* 2008; Papagiannakopoulos *et al.,* 2008). Additionally, miR-21 also targeted RECK and TIMP3 to promote glioblastoma cell migration and invasion by activating matrix metalloproteinases (MMPs) (Gabriely *et al.,* 2008). The GBM-related tumor suppressor gene PTEN is also verified as a target of miR-21. However, it was also shown that knockdown of miR-21 could lead to suppression of EGFR, AKT2 and signal transducer and activator of transcription 3 (STAT3) pathways independent of PTEN status (Zhou *et al.,* 2010). Interestingly, miR-21 regulation on leucine rich repeat interacting protein 1 (LRRFIP1) contributed to glioblastoma cell chemoresistance to VM-26 through NF-κB activation (Li *et al.,* 2009). In addition, TMZ-induced apoptosis can be rescued by miR-21 expression in glioblastoma cells (Shi *et al.,* 2010). Taken together, miR-21 promotes glioblastoma proliferation and invasion and inhibited apoptosis through negative control of multiple targets in the carcinogenic network actively.

The miR-221/222 cluster is overexpressed in GBM and cell lines (Ciafre *et al.*, 2005; Conti *et al.*, 2009; Lukiw *et al.*, 2009). The expression level of miR-221 is associated with glioma grade (Conti *et al.*, 2009; Lukiw *et al.*, 2009). Inhibition of miR-221/222 led to inhibited cell proliferation, induced G1 cell cycle arrest and suppressed tumorigenicity in glioblastoma cells. Consistent with such observation, the cyclin-dependent kinase inhibitors p27 and p57 were found to be under negative regulation by miR-221/222 (Gillies *et al.*, 2007; le Sage *et al.*, 2007; Zhang *et al.*, 2009). Moreover, it was shown that when quiescent glioblastoma cells were triggered to proliferate, miR-221 and miR-222 expressions were enhanced and such upregulation facilitated tumor cells to enter S phase (Medina *et al.*, 2008). Collectively, these findings strongly indicate that miR-221/222 plays an important role in cell cycle progression in GBM.

In GBM, numerous downregulated miRNAs have been characterized. Expression of miR-7 was decreased in GBM versus adjacent or non-neoplastic brain tissues (Kefas *et al.*, 2008; Silber *et al.*, 2008). Further elucidation revealed markedly lower level of pre-miR-7 but comparable abundance of pri-miR-7 in GBM, suggesting that miR-7 inactivation might result from impaired processing of pri-miR-7. It was also demonstrated that delivery of miR-7 in glioblastoma cells induced apoptosis, inhibited viability and suppressed invasiveness. Notably, dramatic suppression of EGFR, IRS1 and IRS2 proteins and activation of AKT and ERK1/2 were observed following transfection of miR-7 (Kefas *et al.*, 2008; Webster *et al.*, 2009). EGFR and IRS2 are further proven to be direct targets of miR-7 (Kefas *et al.*, 2008). It is well believed that the AKT pathway can be activated by its upstream regulators, IRS1 and IRS2, as well as EGFR, of which amplification is frequent in GBM. Hence, the effect of miR-7 is probably mediated by its negative regulation on

the EGFR/AKT pathway, which plays key role in glioblastoma formation (Wong *et al.,* 1987; Haas-Kogan *et al.,* 1998).

The brain-enriched miRNA, miR-128 has been observed downregulated in astrocytoma, including GBM and cell lines by several studies (Ciafre *et al.,* 2005; Godlewski *et al.,* 2008; Zhang *et al.,* 2009; Cui *et al.,* 2010). Its abundance was lower in malignant gliomas compared to low-grade gliomas (Cui *et al.,* 2010). The reduced expression may be not due to epigenetic alteration, since treatment with DNA demethylating agent, 5-aza-2'-deoxycytidine (5-aza-dC), and/or the histone deacetylase inhibitor, trichostatin A (TSA), did not affect miR-128 level in T98G glioblastoma cells (Zhang *et al.,* 2009). Functional analysis indicated that overexpression of miR-128 inhibited cell proliferation and suppressed xenograft growth in GBM (Godlewski *et al.,* 2008; Zhang *et al.,* 2009; Cui *et al.,* 2010). MiRNA-128 is a negative regulator of BMI1, a polycomb factor implicated as an oncogene. Ectopic expression of miR-128 led to a decrease in histone $H3K27me^3$ methylation and AKT phosphorylation as well as $p21^{CIP1}$ up-regulation, which was previously shown to be associated with BMI1 knockdown. Moreover, overexpression of miR-128 in glioblastoma-derived stem-like neurosphere cultures blocked glioma stem cell self-renewal, supporting the notion that BMI1 is a key modulator in stem cell self-renewal (Godlewski *et al.,* 2008). This finding provided for the first time a linkage between miRNA and neuronal stem cell property. Another direct target of miR-128, E2F transcription factor 3 (E2F3), is a transcription factor participating in control of entry into S phase during cell-cycle progression. E2F3 was established as a functional target of miR-128 in glioblastoma cells based on the findings that E2F3 knockdown caused similar phenotype as miR-128 overexpression, and E2F3 could partly rescue the proliferation inhibition resulted from miR-128

(Zhang *et al.,* 2009). Recently, a novel computational predicted target, angiopoietin-related protein 5 (ARP5), was found to be negatively regulated by miR-128. Similar to BMI1 and E2F3, ARP5 was overexpressed in low-grade gliomas and even at higher level in glioblastomas (Cui *et al.,* 2010). Whether there exists a direct interaction between miR-128 and ARP5 transcript requires further investigation.

Additional brain-specific miRNAs displaying decreased expression in glioblastoma are miR-124 and miR-137 (Silber *et al.,* 2008). Both of them inhibited proliferation and induced G0/G1 cell cycle arrest in glioblastoma cells by targeting cyclin-dependent kinase 6 (CDK6), a crucial regulator in G1-S transition that repressed pRB. Notably, miR-124 and miR-137 were also involved in differentiation of mouse NSCs. When mouse NSCs were induced for differentiation upon growth factor withdrawal, upregulation of miR-124 and miR-137 was detected. In line with such observation, ectopic expression of miR-124 and miR-137 induced neuronal-like differentiation of mouse NSCs and glioblastoma-derived stem cells (Silber *et al.,* 2008).

In addition, several lines of evidence suggest that miR-124 is involved in neurogenesis. First, miR-124 was induced during neuronal differentiation in mouse embryonic carcinoma cells and embryonic stem cells (ESCs) (Smirnova *et al.,* 2005; Krichevsky *et al.,* 2006). Second, miR-124 was preferentially expressed in neurons (Smirnova *et al.,* 2005). Third, miR-124 directly inhibited polypyrimidine tract binding protein 1 (PTBP1), a repressor of neuron-specific splicing, and thereby allowing a switch from non-neuronal to neuronal-specific alternative splicing pattern during induced neuronal differentiation of mouse neuroblastoma cells (Makeyev *et al.,* 2007). Fourth, miR-124 could suppress small C-terminal domain phosphatase 1

(SCP1), leading to resultant inhibition of the REST/SCP1 anti-neural pathway (Visvanathan *et al.,* 2007). Fifth, in the subventricular zone of the mouse cortex, miR-124 expression mediated neuron formation by inhibiting sex determining region Y-box 9 (SOX9), which drives stem cell self-renewal (Cheng *et al.,* 2009).

Thus downregulation of three brain-specific miRNAs, miR-124, miR-128 and miR-137, may contribute to tumorigenesis through maintaining proliferating and undifferentiated state of stem cells. The potential treatment of glioblastoma with these miRNAs targeting glioma stem cells may be a novel therapeutic approach and deserves further investigations.

Downregulation of miR-181 family, miR-181a/181b/181c has been reported in both primary glioblastoma and cell lines (Ciafre *et al.,* 2005; Shi *et al.,* 2008; Conti *et al.,* 2009). Among them, expression level of miR-181a appeared to be negatively correlated with tumor grade of grade II-IV gliomas, whereas miR-181b showed more pronounced deregulation in high-grade than in low-grade gliomas. Transfection of miR-181a or miR-181b in glioblastoma cell inhibited growth, triggered apoptosis, reduced anchorage-independent growth as well as suppressed invasive capacity (Shi *et al.,* 2008). Moreover, miR-181a expression was observed decreased in glioblastoma cells upon radiation treatment. Ectopic expressed miR-181a sensitized glioblastoma cells to radiation treatment with concurrent reduction of Bcl-2 protein level, indicating stimulated apoptosis (Chen *et al.,* 2010). In addition, miR-181b and miR-181c were significantly downregulated in glioblastoma in response to concomitant chemoradiotherapy with temozolomide (Slaby *et al.,* 2010). Low expression of mir-181b has been shown associated with poor survival in astrocytoma patients (Zhi *et al.,* 2010). Although direct targets have not yet been identified, miR-

181 family may represent candidate glioblastoma suppressors and predictor for glioblastoma diagnosis, prognosis and sensitivity to therapeutic treatment.

Another potential tumor suppressor regulating important cancer signaling pathways is miR-34a, whose expression is reduced in GBM compared with normal brain (Li *et al.,* 2009). Transcriptionally activated by p53, miR-34a level was markedly lower in p53-mutant GBM relative to p53-wild-type GBM. Ectopic expression of miR-34a resulted in significantly reduced glioblastoma cell proliferation, survival, invasion *in vitro* and glioblastoma xenograft growth *in vivo* (Li *et al.,* 2009; Luan *et al.,* 2010). In glioma stem cells, similar results were also observed with an additional finding of induced differentiation following miR-34a enhanced expression (Guessous *et al.,* 2010). The tumor suppressive role of miR-34a was addressed to its inhibitory effect on several oncogenic targets, such as MET, NOTCH1, NOTCH2 and SIRT1 (Li *et al.,* 2009; Luan *et al.,* 2010).

Collectively, miRNAs are demonstrated to play an important role in the development and progression of glioma through regulation of multiple cellular pathways. Table 1.4 summarizes the functions and targets of deregulated miRNAs identified in gliomas. These tiny RNA molecules are also promising therapeutic targets for treatment of glioma.

Table 1.4 miRNAs involved in glioblastoma pathogenesis

miRNA	Function				Targets	References
	proliferation	apoptosis	invasion	differentiation		
Upregulated						
miR-17-92	√	√			CTGF	Ernst *et al.*, 2010
miR-21	√	√	√		PTEN, RECK, TIMP3, DAXX, TP63, TGFBR2, PDCD4, LRRFIP1	Corsten *et al.*, 2007; Chan *et al.*, 2008; Chen *et al.*, 2008; Gabriely *et al.*, 2008; Papagiannakopoulos *et al.*, 2008; Conti *et al.*, 2009; Li *et al.*, 2009; Zhou *et al.*, 2010
miR-10b			√		-	Silber *et al.*, 2008; Sasayama *et al.*, 2009
miR-15b	√				Cyclin E1	Xia *et al.*, 2009
miR-26a	√				PTEN	Huse *et al.*, 2009
miR-125b	√	√			BMF	Ciafre *et al.*, 2005; Xia *et al.*, 2009
miR-221/222	√	√	√		CNDN1B/p27^{Kip1}, CNDN1C/p57^{Kip2}	Ciafre *et al.*, 2005; Gillies *et al.*, 2007; le Sage *et al.*, 2007; Medina *et al.*, 2008; Conti *et al.*, 2009; Lukiw *et al.*, 2009; Zhang *et al.*, 2009
miR-451	√	√	√	√	CAB39	Godlewski *et al.*, 2008; Gal *et al.*, 2008; Godlewski *et al.*, 2010; Nan *et al.*, 2010
Downregulated						
miR-7	√	√	√		EGFR and IRS2	Kefas *et al.*, 2008; Webster *et al.*, 2009
miR-34a	√	√	√	√	NOTCH1, NOTCH2, SIRT1, MET	Li *et al.*, 2009, Li *et al.*, 2010, Luan *et al.*, 2010
miR-124	√			√	CDK6, PTBP1, SCP1, SOX9	Makeyev *et al.*, 2007; Silber *et al.*, 2008
miR-128	√			√	BMI1, E2F3, ARP5	Ciafre *et al.*, 2005; Godlewski *et al.*, 2008; Zhang *et al.*, 2009; Cui *et al.*, 2010
miR-137	√			√	CDK6	Silber *et al.*, 2008
miR-146b	√		√		MMP16	Xia *et al.*, 2009
miR-153	√	√			BCL2 and MCL1	Xu *et al.*, 2010
miR-181a/181b	√	√	√		-	Ciafre *et al.*, 2005; Shi *et al.*, 2008

1.3 miR-137

Since allelic loss of 1p has been reported as a frequent event in OTs, it was proposed that this region may harbor miRNAs that may be involved in gliomagenesis. There are 38 miRNAs mapped to chromosome 1p (Table 1.5) according to miRBase (http://www.mirbase.org/; release 16.0, September 2010). One candidate mapped to 1p36.22 is miR-34a, which was shown to play an important role in the development of GBM (Li *et al.,* 2009). Another candidate is miR-137. Expression of miR-137 was demonstrated to be downregulated in GBM in two profiling studies (Godlewski *et al.,* 2008; Silber *et al.,* 2008). It is hypothesized that miR-137 may also be involved in development of other glioma subtypes. The following sections highlight the biology of miR-137.

1.3.1 Biology of miR-137

The miR-137 gene resides on chromosomal arm 1p21.3 (98511626-98511727, negative strand). Both the precursor and mature miR-137 sequences are highly conserved across a broad range of vertebrate species, indicating the significance miR-137 (Figure 1.3). miR-137 is recognized as a brain-enriched miRNA in both human and mouse (Lagos-Quintana *et al.,* 2002; Sempere *et al.,* 2004; Beuvink *et al.,* 2007; Landgraf *et al.,* 2007; Liang *et al.,* 2007; Chiang *et al.,* 2010). Human miR-137 expression in brain was at least 2-fold higher than in other organs (Sempere *et al.,* 2004). MiR-137 is also detectable in endocrine gland, placenta and peripheral blood mononuclear cells (Landgraf *et al.,* 2007; Liang *et al.,* 2007).

Table 1.5 A list of 38 miRNAs located on chromosome arm 1p according to miRBase

ID	Start	End	Strand
miR-1302-2	30366	30503	+
miR-200b	1102484	1102578	+
miR-200a	1103243	1103332	+
miR-429	1104385	1104467	+
miR-4251	3044539	3044599	+
miR-551a	3477259	3477354	-
miR-4252	6489894	6489956	-
miR-34a	9211727	9211836	-
miR-1273d	10287776	10287861	+
miR-3675	17185444	17185516	-
miR-1290	19223565	19223642	-
miR-1256	21314807	21314925	-
miR-4253	23189652	23189719	-
miR-3115	23370798	23370865	+
miR-3917	26232853	26232945	-
miR-1976	26881033	26881084	+
miR-4254	32224261	32224336	-
miR-3605	33797994	33798093	-
miR-552	35135200	35135295	-
miR-4255	37627164	37627235	+
miR-3659	38554903	38555001	+
miR-30e	41220027	41220118	+
miR-30c-1	41222956	41223044	+
miR-761	52302016	52302074	-
miR-3116-1	62544458	62544531	+
miR-3116-2	62544461	62544528	-
miR-3671	65523438	65523525	-
miR-101-1	65524117	65524191	-
miR-3117	67094123	67094200	+
miR-1262	68649201	68649293	-
miR-186	71533314	71533399	-
miR-760	94312388	94312467	+
miR-137	98511626	98511727	-
miR-553	100746797	100746864	+
miR-197	110141515	110141589	+
miR-4256	113004392	113004455	-
miR-320b-1	117214371	117214449	+
miR-942	117637265	117637350	+

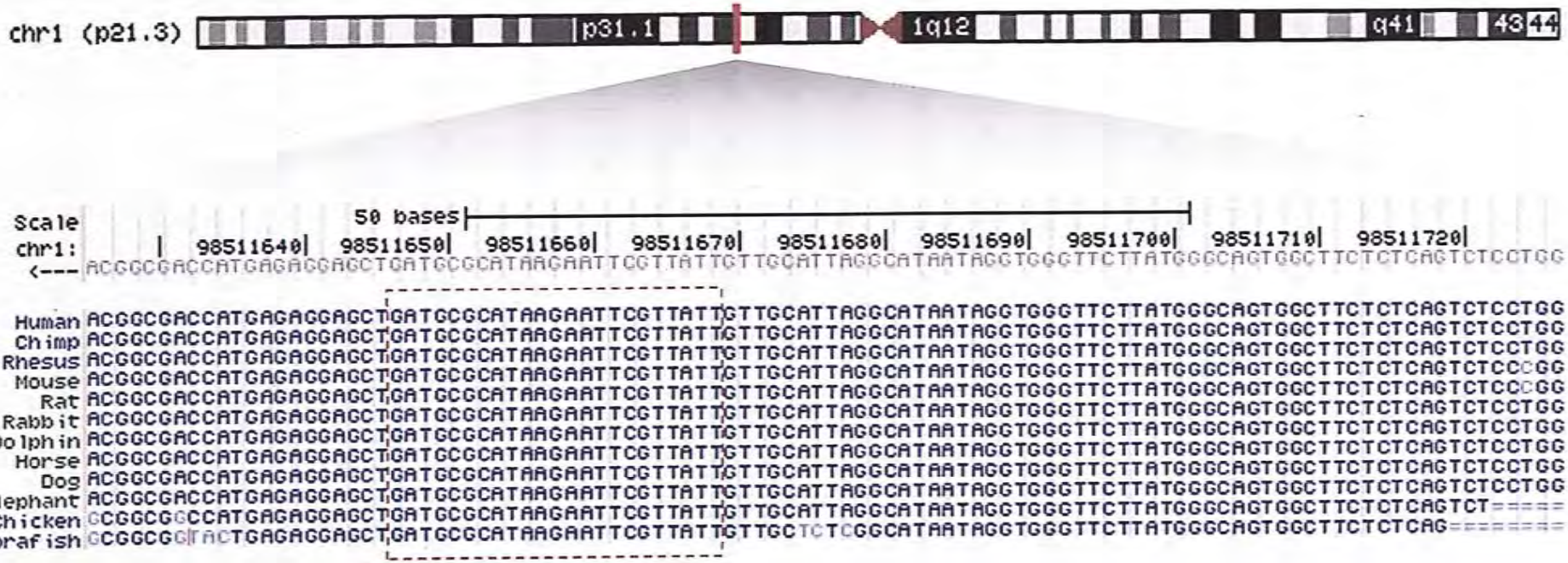

Figure 1.3 Evolutionary conservation of miR-137 precursor (whole sequence, 102-nt) and mature miR-137 region (dashed box, 23-nt) across 12 vertebrate species. Data was obtained from miRBase and UCSC Gemone bioinformatics database (http://genome.ucsc.edu/).

1.3.2 Role of miR-137 in carcinogenesis

1.3.2.1 Deregulation of miR-137 in cancer

The relevance of miR-137 in human tumors was first highlighted by quantitative expression analysis of its expression levels in tumors and cancer cell lines relative to those of normal tissues or cells. Abnormal miR-137 expression was detected in numerous cancer types, with majority of them showing miR-137 downregulation (Table 1.6). As mentioned in section 1.2.3.2, miR-137 displayed significantly low level in astrocytomas of all WHO grades (Silber *et al.*, 2008; Zhi *et al.*, 2010). Its downregulation was more pronounced in high-grade astrocytomas than in low-grade (Zhi *et al.*, 2010), indicating a significant association of miR-137 with clinical grade. Reduced miR-137 transcript level was also identified in central nervous system tumor (Gaur *et al.*, 2007), neuroblastoma (Chen *et al.*, 2007), colorectal tumor (Bandres *et al.*, 2006; Balaguer *et al.*, 2010), oral squamous cell carcinoma (Kozaki *et al.*, 2008), lung adenocarcinoma (Dacic *et al.*, 2010) and uveal melanoma (Chen *et al.*, 2010). However, miR-137 overexpression was reported in squamous cell carcinoma of the tongue (Wong *et al.*, 2008). Taken together, these findings have implicated a role of miR-137 in the development of multiple cancers.

1.3.2.2 Regulation of miR-137 expression in cancer

Since miR-137 was frequently suppressed in a number of cancers, the mechanism underlying such downregulation has also been investigated. Emerging studies showed that miR-137 inactivation was tightly linked to epigenetic regulation in several tumors including gliomas (Table 1.6).

Genomic analysis revealed a high CpG content in putative promoter region of

miR-137, suggesting that miR-137 may be epigenetically modulated. Examination of methylation status demonstrated high incidence of DNA hypermethylation on the promoter region in gastric cancer (Ando *et al.*, 2009), colorectal cancer (Bandres *et al.*, 2009; Balaguer *et al.*, 2010) and oral squamous cell carcinoma (Kozaki *et al.*, 2008; Langevin *et al.*, 2010), but absence of such alteration in normal tissue or cells. An inverse correlation between the expression and promoter methylation status of miR-137 was observed in colorectal cancer (Balaguer *et al.*, 2010) and squamous cell carcinoma of head and neck (Kozaki *et al.*, 2008; Langevin *et al.*, 2010). Moreover, miR-137 expression was restored in response to demethylation treatment in cell lines derived from glioblastoma (Silber *et al.*, 2008), colorectal cancer (Bandres *et al.*, 2009; Balaguer *et al.*, 2010) and uveal melanoma (Chen *et al.*, 2010). The promoter of miR-137 was demethylated following demethylation treatment in colorectal tumor cells (Bandres *et al.*, 2009; Balaguer *et al.*, 2010). These observations suggested that epigenetic modulation was a major mechanism responsible for miR-137 expression. More importantly, patients with squamous cell carcinoma of head and neck carrying methylated miR-137 showed poor prognosis compared with patients with tumors harboring unmethylated miR-137, providing prognostic potential for epigenetic status of miR-137 (Langevin *et al.*, 2010).

In particular, Bemis *et al.*, (2008) provided new insight into miR-137 regulation by indentifying a 15-bp variable nucleotide tandem repeat (VNTR), located 6-bp upstream of pre-miR-137 sequence, that was associated with miR-137 expression level in melanoma cell lines. Sequencing analysis detected the presence of 3 to 12 VNTRs in different melanoma cell lines. When constructs containing pri-miR-137 complementary DNA (cDNA) fragment with 3 or 12 VNTRs were transfected in melanoma cells, it was found that the construct containing 3 VNTRs expressed miR-

137 more efficiently, suggesting that miR-137 expression may also be modulated by copy number of the 15-bp VNTR.

Table 1.6 Expression and epigenetics of miR-137 in cancers

Cancer type	miR-137 down-regulation	Promoter hypermethylation	Correlation between expression and methylation status	After demethylating treatment		Reference
				promoter demethylation	miR-137 restoration	
Central nervous system tumor	√					Gaur *et al.*,2007
Neuroblastoma	√					Chen *et al.*, 2007
Glioblastoma	√				√	Silber *et al.*, 2008
Astrocytoma	√					Zhi *et al.*, 2010
Colorectal tumor	√	√		√	√	Bandres *et al.*, 2006, 2009
	√	√	√	√	√	Balaguer *et al.*, 2010
Gastric tumor		√				Ando *et al.*, 2009
Lung adenocarcinoma	√					Dacic *et al.*, 2010
Oral squamous cell carcinoma	√	√	√			Kozaki *et al.*, 2008
		√				Langevin *et al.*, 2010
Squamous cell carcinoma of the head and neck		√	√			Langevin *et al.*, 2010
Uveal melanoma	√				√	Chen *et al.*, 2010

1.3.2.3 Biological functions of miR-137 in cancer

Since miR-137 expression level is downregulated in many types of human cancer, it is believed that miR-137 plays a key role in tumor formation. Recently, several functional studies have demonstrated the biological effects of miR-137 in tumor cells identified its targets (Table 1.7).

In human glioblastoma (Silber *et al.*, 2008) and oral squamous cell carcinoma cells (Kozaki *et al.*, 2008), forced miR-137 expression suppressed tumor cell proliferation and induced G0/G1 cell cycle arrest. CDK6 was the first direct miR-137 target identified through multiple experimental approaches in both tumor types. The protein level of CDK6 decreased following forced miR-137 expression, and the direct interaction was validated by luciferase reporter assay. As a cell cycle regulator, CDK6 promotes G1-S transition and contributes to cell proliferation. Involvement of CDK6 in differentiation and transformation of human cancers has been reported as well (Meyerson *et al.*, 1994; Grossel *et al.*, 2006). Moreover, elevated CDK6 expression has been demonstrated in these tumors (Lam *et al.*, 2000; Poomsawat *et al.*, 2010), suggesting that CDK6 may play an oncogenic role.

Another study on melanoma indicated that miR-137 regulates microphthalmia-associated transcription factor (MITF) (Bemis *et al.*, 2008). MITF has been characterized as a master regulator of melanocyte growth, maturation, apoptosis, as well as melanoma progression and prognosis (Garraway *et al.*, 2005; Levy *et al.*, 2006). The regulation of miR-137 on CDK6 and MITF was also observed in uveal melanoma (Chen *et al.*, 2010). In addition, both ectopic miR-137 expression and RNA interference (RNAi)-mediated MITF knockdown showed inhibitory effects on

uveal melanoma cell growth and cell cycle progression. These results strongly suggested miR-137 may act as a tumor suppressor miRNA via negative regulation of CDK6 and MITF in melanoma.

The role of miR-137 in carcinogenesis is also investigated in colorectal cancer. In addition to inhibition on cell proliferation, miR-137 also affected invasive ability of colorectal tumor cells. The potential tumor-suppressive function of miR-137 was addressed to its direct inhibition of cell division cycle 42 (CDC42). CDC42 is a member of the Rho GTPase family, its elevated expression has been documented in several types of human tumors including colorectal cancer (Gomez Del Pulgar *et al.*, 2008). CDC42 has been implicated in diverse cellular processes, such as cell proliferation, migration and apoptosis, which resulted in its tight linkage to cancer initiation and progression. Indeed, CDC42 knockdown in colorectal tumor cells led to inhibition of cell cycle progression and invasion, these biological effects were similar to those observed after miR-137 overexpression *in vitro* (Liu *et al.*, 2010). Hence, miR-137 contributes, in part through negative regulation of CDC42, to the development of colorectal tumors.

In addition, Balaguer *et al.*, 2010 have identified another miR-137 target, lysine (K)-specific demethylase 1A (LSD1, also known as KDM1A), in colon cancer. Elevated LSD1 expression has been illustrated in prostate cancer (Metzger *et al.*, 2005) and neuroblastoma (Schulte *et al.*, 2009), where LSD1 is related to maintaining the undifferentiated phenotype and tumor cell proliferation. On the other hand, the demethylating activity of LSD1 can stabilize DNA (cytosine-5-)-methyltransferase 1 (DNMT1) in addition to demethylating histone H3 on lysine 4 (H3K4) and lysine 9 (H3K9) (Wang *et al.*, 2009). DNMT1 is known to be crucial in

maintaining global DNA methylation and has been shown overexpression in many human cancers (Ting *et al.,* 2004). Although the expression and biological role of LSD1 in colon cancer remain largely elusive, the evidence gives rise to a potential miR-137-*LSD1-DNMT1* axis in epigenetic machinery, which may play a role in carcinogenesis.

Overall, these studies suggest that miR-137 may play suppressive roles in tumor cell proliferation and invasion through negative regulation of multiple targets (CDK6, MITF, LSD1 and CDC42) involved in diverse cellular processes.

1.3.3 Role of miR-137 in differentiation and neurogenesis

As miR-137 is a brain-enriched miRNA in human and rodent, several studies have provided evidence supporting a linkage between miR-137 and mouse neuronal differentiation by assessing its expression during stem cell differentiation process and its effects on stem cell self-renewal and differentiation.

Silber *et al.,* 2008 investigated miRNA expression alterations during *in vitro* differentiation of mouse NSCs isolated from the subventricular zone by withdrawal of growth factor in culture. Their results showed that miR-137 expression was elevated 20-fold in a 5-day interval, accompanied with enhanced expression of neuronal marker, β-tubulin III (Tuj1). In line with this observation was induced miR-137 upregulation in glioblastoma spheroid upon all-trans retinoic acid-induced differentiation (Ernst *et al.,* 2010). Moreover, ectopic expression of miR-137 increased percentage of Tuj1 positive (+) cell with a rounded or trapezoidal cellular morphologic characteristic in differentiating mouse NSCs. Meanwhile, the cell fraction that showed glial fibrillary acidic protein (GFAP, an astrocytic marker) was

not affected. Again, in mouse oligodendroglioma-derived and human glioblastoma-derived tumor stem cells, ectopic expression of miR-137 also resulted in neuronal-like differentiation without neuronal morphologic change. These studies implicate a role of miR-137 in neuronal differentiation.

However, opposite effects of miR-137 were observed in proliferating mouse NSCs (Szulwach *et al.,* 2010). Ectopic expression of miR-137 promoted DNA synthesis in actively proliferating NSCs both *in vitro* and *in vivo*. Meanwhile, the Tuj1 and GFAP expression were suppressed, suggesting miR-137 enhanced NSCs proliferation at the expense of differentiation when differentiation is not triggered by other stimulus. Another functional target of miR-137, enhancer of zeste homolog 2 (*Ezh2*), was identified, which showed declined expression during NSC differentiation (Sher *et al.,* 2008) and has been functionally associated with NSCs fate decision. (Pereira *et al.,* 2010).

In addition, miR-137 also participates in maturation of young neurons by negatively regulating neuronal dendritic morphogenesis, phenotypic maturation, and spine development both *in vitro* and *in vivo* (Smrt *et al.,* 2010). MiR-137-mediatd direct suppression of mindbomb homolog 1 (Mib1), a ubiquitin ligase modulating neurodevelopment (Ossipova *et al.,* 2009), was shown. In the study, Mib1 was demonstrated as a miR-137 target that was responsible for the inhibitory effect of miR-137 on dendritic complexity, the final step in neurogenesis. The above observations illustrated that miR-137 plays multiple roles in different stages of adult neurogenesis.

The role of miR-137 in neurogenesis was further supported by investigation on mouse embryonic stem cells (ESCs) (Tarantino *et al.,* 2010). Undetectable in

undifferentiated ESCs, miR-137 expression was induced upon differentiation. Furthermore, miR-137 cooperated with miR-34a and miR-100 to enhance expression of early neuronal differentiation maker in differentiating ESCs. Inhibition of this miRNA mix led to elevated stemness markers expression in ESCs undergoing differentiation induction. In this study, the authors identified lysine (K)-specific demethylase 5B (Jarid1b, also known as Kdm5b) as a target of miR-137. Jarid1b is a histone H3K4 demethylase, whose constitutive expression in ESCs prevents cell differentiation and sustains the expression of stemness markers (Dey *et al.*, 2008). The role of Jarid1b in cell differentiation may responsible for function of miR-137 observed.

Table 1.7 Functions and targets for miR-137

Cell type	Function				Target	Reference
	proliferation	invasion	differentiation	neurogenesis		
Tumor cells						
Mouse OT stem cells			√		-	Silber *et al.*, 2008
GBM and cancer stem cells	√		√		CDK6	Silber *et al.*, 2008
Oral squamous cell carcinoma	√				CDK6	Kozaki *et al.*, 2008
Melanoma					MITF	Bemis *et al.*, 2008
Uveal melanoma	√				CDK6, MITF	Chen *et al.*, 2010
Colorectal tumor	√	√			LSD1, CDC42	Balaguer *et al.*, 2010; Liu *et al.*, 2010
Normal cells						
Mouse neural stem cells	√		√		Ezh2	Szulwach *et al.*, 2010
Mouse embryonic stem cells			√		Jarid1b	Tarantino *et al.*, 2010
Mouse primary neurons				√	Mib1	Smrt *et al.*, 2010

CHAPTER 2 AIMS OF STUDY

As previously reviewed, loss of chromosome 1p is the most frequent genetic abnormality in OTs, suggesting the presence of candidate tumor suppressor gene (TSG) (Bello *et al.,* 1994; Reifenberger *et al.,* 1994; Bigner *et al.,* 1999; Husemann *et al.,* 1999; Smith *et al.,* 1999). Although numerous candidate TSGs located on 1p had been found downregulated in OTs, none of them showed a key functional role in OTs. (Husemann *et al.,* 1999; Dong *et al.,* 2002; Barbashina *et al.,* 2005; McDonald *et al.,* 2005; McDonald *et al.,* 2006; Ngo *et al.,* 2007; Tews *et al.,* 2007; Riemenschneider *et al.,* 2008; Benetkiewicz *et al.,* 2009; Pang *et al.,* 2010) Recently investigations discovered that miRNAs represent a new class of molecular complexity in various cancer types including glioma. Therefore, it is speculated that chromosome 1p may carry glioma-related miRNAs. Identification and functional characterization of such miRNAs will improve our understanding on molecular mechanism of glioma and may stem new potential avenues for treatment of this malignancy.

Among the 38 miRNAs mapped to chromosome 1p, miR-34a has been reported to function as a tumor suppressor in GBM (Li *et al.,* 2009; Luan *et al.,* 2010). However, the role of other miRNAs in glioma formation remains elusive. Three independent profiling studies have reported reduced expression of miR-137, a brain-

enriched miRNA, in astrocytomas compared to normal or non-neoplastic brain tissues (Godlewski *et al.,* 2008; Silber *et al.,* 2008; Zhi *et al.,* 2010). The functional significance of miR-137 was demonstrated by the finding of its growth inhibitory effects on GBM, as well as melanoma and colorectal tumor (Kozaki *et al.,* 2008; Silber *et al.,* 2008; Balaguer *et al.,* 2010; Chen *et al.,* 2010; Liu *et al.,* 2010). These findings strongly suggested that miR-137 might be involved in the development of glioma. Hence, this study aimed to investigate the potential involvement of miR-137 in OTs and its biological functions in gliomagenesis. The specific aims were:

i. To quantify miR-137 expression in primary OTs and glioma cell lines and evaluate the clinical significance of miR-137 in OT patients by correlating the miR-137 expression level with clinicopathological parameters,

ii. To investigate the mechanisms responsible for miR-137 differential expression in OTs by examining the 1p status and epigenetic involvement,

iii. To characterize the functional roles of ectopic miR-137 expression in glioma cell proliferation, apoptosis, invasiveness and differentiation,

iv. To elucidate miR-137 by identification of its downstream target(s) in glioma cells by combined computational and experimental approaches,

v. To examine the transcript and protein expression levels of verified miR-137 target in the same panel of OT specimens and explore the functional effects of miR-137 target in glioma cell proliferation, apoptosis and invasiveness following small interfering RNA (siRNA) mediated target gene knockdown.

CHAPTER 3 MATERIALS AND METHODS

3.1 Tumor samples

A panel of 36 OTs was collected from Huashan Hospital, Fudan University, Shanghai, P. R. China. Histological classification of all tumors was performed according to WHO Classification of Tumors of the Central Nervous System (2007). Tumor tissues resected from surgery were immediately immersed in RNALater® solution (Ambion, Austin, U.S.A.) and stored at80°C until use to preserve RNA integrity. The series consisted of 13 oligodendrogliomas, 7 anaplastic oligodendrogliomas, 13 oligoastrocytomas, and 3 anaplastic oligoastrocytomas. In adult patients, the male/female ratio was 1.25:1 and the median age was 42 years, ranging from 28 to 77 years. There was 1 pediatric case (Table 3.1).

Table 3.1 Clinicopathological and follow-up information of 36 OTs studied.

Case number	Diagnosis[1]	Sex	Age (years)	Survival time (months)[3]		
				Overall	Progression-free	status
HS390	OD	M	10	72	72	alive
HS460	OD	M	29	50	50	alive
HS380	OD	M	35	80	62	alive
HS469	OD	F	36	49	49	alive
HS378	OD	F	38	80	80	alive
HS466	OD	F	40	49	49	alive
HS324	OD	M	42	93	93	alive
HS331	OD	F	46	78	78	alive
HS400	OD	F	49	48	48	dead
HS329	OD	F	69	78	78	dead
HS303	OD	M	48	-	-	-
HS332	OD	M	53	-	-	-
HS467	OD	F	56	-	-	-
HS382	OA	F	37	79	79	alive
HS458	OA	M	37	52	41	alive
HS393	OA	F	49	71	70	alive
HS314	OA	F	38	81	57	dead
HS375	OA	M	28	-	-	-
HS381	OA	F	28	-	-	-
HS384	OA	M	30	-	-	-
HS394	OA	F	31	-	-	-
HS399	OA	M	34	-	-	-
HS462	OA	M	39	-	-	-
HS362[2]	OA	M	41	-	-	-
HS301	OA	M	43	-	-	-
HS368	OA	F	61	-	-	-
HS333	AOD	F	43	12	12	dead
HS358	AOD	F	50	42	8	dead
HS360	AOD	M	51	2	2	dead
HS461	AOD	M	53	14	14	dead
HS377	AOD	M	77	48	42	dead
HS302	AOD	M	35	-	-	-
HS312	AOD	M	53	-	-	-
HS366	AOA	M	35	-	-	-
HS364	AOA	F	48	-	-	-
HS457	AOA	M	52	-	-	-

[1] OD, oligodendroglioma; OA, oligoastrocytoma; AOD, anaplastic oligodendroglioma; AOA, anaplastic oligoastrocytoma.

[2] Due to lack of corresponding FFPE section, this case was not included in the immunohistochemical analysis.

[3] Survival time was measured from the date of surgery to January 2010 or to the time of death. -, data not available.

3.2 Cell lines and culture conditions

Three human OT cell lines (GOS-3, HOG and TC620) and seven human glioblastoma cell lines (A172, LNZ308, T98G, U118MG, U138MG, U373MG and U87MG) were used in this study. GOS-3 cell was obtained from German Collection of Microorganisms and Cell Cultures (Braunschweig, Germany), HOG and TC620 cells were kindly provided as gifts from Dr. Glyn Dawson, University of Chicago, U.S.A. and Dr. Rainer Probstmeier, University of Bonn, Germany, respectively. The A172, U118MG, U138MG, U373MG and U87MG cells were purchased from American Type Culture Collection (Manassas, U.S.A.).

A172, GOS-3, HOG, LNZ308, TC620, U118MG and U373MG cells were cultured in Dulbecco's modified Eagle medium (DMEM; Invitrogen, Carlsbad, U.S.A.), U138MG and U87MG were grown in alpha-minimal essential medium (Invitrogen). All growth media were supplemented with 10% (v/v) fetal bovine serum (Invitrogen). The cell lines were maintained at 37°C in a humidified atmosphere supplied with 5% carbon dioxide. The morphology of cells was continuously monitored under an inverted microscope during culture. Cells of ~70% confluency were trypsinized and sub-cultivated at a ratio of 1:5. To prevent clonal selection during culture, fresh cells rejuvenated from cryopreservation every 3 months were used. Mycoplasma test was also performed to guarantee the absence of contamination.

3.3 Fluorescence in situ hybridization (FISH)

To determine the allelic status of chromosomes 1p and 19q, dual-color interphase FISH analysis was performed on FFPE tissue sections as reported (Dong *et al.,* 2004). Sections of 5-μm thickness were deparaffinized, rehydrated, treated with 1 M sodium thiocyanate at 80°C for 10 minutes, digested in pepsin solution (5 mg/ml in 0.2 N HCl; Sigma-Aldrich, St. Louis, U.S.A.) for 30 minutes, rinsed in phosphate buffered saline (PBS) and dehydrated. The sections were treated with microwave (600 W) for 10 minutes, baked at 80°C for 30 minutes and then subjected to hybridization.

Four bacterial artificial chromosome (BAC) clones used to prepare locus-specific FISH probes were RP11-62M23 on 1p36.3 (target), RP11-162L13 on 1q25.3-q31.1 (reference), CTD-2571L23 on 19q13.3 (target) and RP11-420K14 on 19p12 (reference). The genomic clones were purchased from Invitrogen Corporation. Five μg of BAC DNA was labeled using nick-translation in a 50-μl reaction containing 100 mM Tris-HCl (pH 7.5), 10 mM magnesium chloride ($MgCl_2$), 0.01% bovine serum albumin (BSA), 0.1 mM deoxyadenosine triphosphate (dATP), 0.1 mM deoxycytidine triphosphate (dCTP), 0.1 mM deoxyguanosine triphosphate (dGTP), 0.1 nM deoxythimidine triphosphate (dTTP), 0.1 nM β-mercaptoethanol, 0.03 U of DNase I (Roche Diagnostics Ltd., Hong Kong), 20 U of *E. coli* DNA polymerase I (Roche), and 1.9 nmol of SpectrumOrange™-deoxyuridine triphosphate (dUTP)

(Enzo Life Sciences Inc., Farmingdale, U.S.A.) for target probe or 0.85 nmol of digoxigenin-11-dUTP (Roche) for reference probe at 15°C for 1 hour. The reaction was stopped by adding 1 μl of 0.5 M ethylenediaminetetraacetic acid (EDTA) and 0.5 μl of 10% sodium dodecyl sulfate (SDS) followed by incubation at 65°C for 10 minutes.

Labeled probes were mixed with salmon sperm DNA (Invitrogen) and human Cot-1 DNA (Invitrogen) in Hybrisol VI solution (Appligene Oncor, Illkirch Graffenstaden, France) to suppress cross-hybridization to human repetitive DNA and to reduce the background. The probe mix was denatured and applied onto sections. Hybridization was carried out at 37°C overnight. Sections were washed with 1.5 M urea / 1× saline sodium citrate (SSC) at 45°C for 30 minutes, 2× SSC at 45°C for 15 minutes, treated with anti-digoxigenin-fluorescein antibody (Roche) at 37°C for 1.5 hours. The sections were then washed in phosphate-buffered detergent (Appligene Oncor, Ullkirch Graffenstaden, France) and counterstained with Vectashield mounting medium with anti-fade solution of 4,6-diamidino-2-phenylindole (DAPI; Vector Laboratories, Inc., Burlingame, U.S.A.).

Sections were viewed under an Axioplan 2 fluorescence microscope (Carl Zeiss MicroImaging Co., Ltd., Oberkochen, Germany). Images were independently captured through three separate band pass filters for rhodamine, fluorescein isothiocyanate (FITC) and DAPI by a cooled charge-coupled device. At least 100

non-overlapping tumor nuclei were counted on each section. A sample with more than 60% of counted nuclei exhibited one target signal (red) and two reference signals (green) was considered having deletion of 1p or 19q locus.

3.4 Cell transfection

3.4.1 Transfection of oligonucleotides

3.4.1.1 Oligonucleotide preparation

In the study of miR-137 overexpression in glioma cells, miRIDIAN hsa-miR-137 mimic (5'-UUAUUGCUUAAGAAUACGCGUAG-3') and the negative control #1 was used (Dharmacon, Inc., Lafayette, U.S.A.). For knockdown of CSE1L expression, 2 short interfering RNA (siRNA) oligonucleotides specifically targeting exon 18 and exon 15 of human CSE1L transcripts (NCBI reference sequence: NM_001316.2) were obtained from Applied Biosystems (Foster City, U.S.A.) (siCSE1L-1, s3588: 5'-GCAAUAUGUUUAUCCAUAAtt-3', and siCSE1L-2, s3589: 5'-GAACAUCUUUUAGUCUCGAtt-3'). The siRNA negative control #1 oligonucleotide (Applied Biosystems) was used as control.

The miRIDIAN miRNA mimics and siRNA oligonucleotides were dissolved in DEPC-treated H_2O to 20 μM and 5 μM respectively as stock and stored at -20°C in aliquots until use.

3.4.1.2 Optimization of transfection condition

Cells were seeded on 24-well plate one day before to yield a confluency of 20%-30% at the time of transfection. Lipofectamine™ 2000 (Invitrogen) was used to

introduce oligonucleotides into glioma cells according to the manufacturer's recommendation. In order to achieve optimized transfection efficiencies, different amounts of both Lipofectamine™ 2000 reagent and miRNA mimic or siRNA were tested for each cell line.

For miRNA mimic, the transfection efficiency was monitored using siGLO green transfection indicator from Dharmacon. Transfected cells were viewed under a fluorescent microscope and optimized condition was determined when greater than 80% cell showed green fluorescent signals. For siRNA, the transfection condition was optimized using a siGAPDH concentration that suppressed at least 70% of GAPDH protein level detected by western blotting.

3.4.2 Cotransfection of plasmids and miRNA mimic

3.4.2.1 Optimization of transfection condition

When glioma cells were subjected to plasmid and miRNA mimic cotransfection, cells of approximately 90% confluency were transfected using Lipofectamine™ 2000 reagent. In optimization study, the firefly luciferase reporter plasmid pMIR-REPORT™ miRNA Expression Reporter Vector (Ambion) and reference *renilla* luciferase expressed plasmid pRL-TK Vector (Promega, Madison, U.S.A.) were involved. The transfection efficiency of both plasmids was evaluated by the luciferase activity of transfected cells using Dual-Luciferase® Reporter Assay System

(Promega). The percentage of miRNA mimic-transfected cell was monitored by siGLO green transfection indicator as mentioned in section 3.4.1.2.

3.4.2.2 Procedure of transfection

Cells grown at log phase were trysinized, plated onto a 24-well plate the day before transfection and maintained in growth medium. Lipofectamine™ 2000 of 1-1.5 μl was diluted in 50 μl Opti-MEM® I reduced serum media (Invitrogen) and then incubated at room temperature for 5 minutes. Plasmid DNA (0.2-1 μg) and 10-20 pmol of miRNA mimic were diluted in 50 μl of Opti-MEM® I reduced serum media. The DNA mixture and diluted Lipofectamine™ 2000 were mixed gently and incubated for 20 minutes at room temperature. The DNA (μg): Lipofectamine (μl) ratio ranged from 1:1 to 1:5. The transfection mixture was added into relevant well and mixed by rocking the plate back and forth. Medium was removed after 24 hours and replaced by fresh growth medium.

3.5 Quantitative reverse transcription-polymerase chain reaction (qRT-PCR)

3.5.1 RNA extraction from frozen tissues and cell lines

Total RNA of frozen tumor tissues and cell lines was extracted using the TRIZOL® reagent (Invitrogen) according to the manufacturer's protocol. For frozen tissue, 1 ml of TRIZOL® per 50-100 mg tissue was added and the tissue was immediately homogenized using a Tissue-Tearor (BioSpec Products, Inc., Bartlesville, U.S.A.). For culture cells grown in monolayer, cells were washed twice with chilled PBS, added with TRIZOL® (1 ml per 10 cm^2 culture dish surface area), and lysed by repetitive pipetting with a small bore tip to ensure complete cell breakage and to shear genomic DNA. After incubation for 5 minutes at room temperature, 0.2 ml of chloroform per 1 ml of TRIZOL® was added. The contents were mixed by vigorous shaking for 15 seconds and allowed to stand at room temperature for 2 minutes. Following centrifugation at 12,000 × *g*, 4°C for 15 minutes, total RNA in the upper aqueous phase was carefully collected. RNA was precipitated by mixing with 0.5 ml of isopropanol per 1 ml of TRIZOL® and incubated for 10 minutes at room temperature. The RNA pellet was collected by centrifugation at 12000 × *g* for 10 minutes at 4°C, washed with 70% (v/v) ethanol in DEPC-treated water, air-dried completely and then dissolved in DEPC-treated water. All RNA samples were stored in aliquots at -80°C.

RNA concentration was determined by measurement of optical density (OD) at wavelength of 260 nm, using NanoDrop ND-1000 Spectrometer (NanoDrop products, Wilmington, U.S.A.). RNA concentration was calculated using a conversion factor of 1 unit of OD at 260 nm equivalent to 40 μg/ml RNA. An RNA sample with an OD_{260nm}/OD_{280nm} ratio of 1.8 to 2 and an OD_{260nm}/OD_{230nm} ratio of 1.8 or greater was considered of good quality.

3.5.2 qRT-PCR for miR-137

The expression level of mature miR-137 in normal brains and OTs was determined using TaqMan miRNA assay (Applied Biosystems). Briefly, reverse transcription (RT) was performed in a 15-μl reaction containing 20 ng of total RNA, 50 nM of miR-137-specific stem-loop RT primer, 1× RT buffer, 1 mM deoxyribonucleoside triphosphates (dNTPs), 50 U of MultiScribe™ reverse transcriptase and 3.8 U of RNase inhibitor. The reactions were incubated for 30 minutes at 16°C to allow primer binding to miR-137, 30 minutes at 42°C for RT, and 5 minutes at 85°C to inactivate reverse transcriptase.

PCR was performed in a 10-μl volume containing 0.67 μl (1 ng) of reversed transcribed product, 1× TaqMan Universal PCR master mix, and 1× TaqMan miRNA assay reagent. The reaction was performed in triplicates and carried out in 384-well optical tray on the ABI7900HT real-time PCR system (Applied Biosystems). The thermal cycling conditions were as follows: 95°C for 10 minutes to activate

polymerase, followed by 40 cycles of 95°C for 15 seconds to denature and 60°C for 1 minute to anneal and extend. Threshold cycle (C_T) was analyzed using the SDS software version 2.3 (Applied Biosystems). To adjust for variations in starting input, miR-137 expression was normalized with miR-16 as an internal reference. Total RNA of normal brains was obtained from BD Biosciences Clontech (Palo Alto, U.S.A.), BioChain (Hayward, U.S.A.) and Ambion.

The expression fold change of miR-137 in tumors and cell lines relative to normal brains were assessed using the comparative C_T ($\Delta\Delta C_T$) method. The ΔC_T value is determined by subtracting the average C_T value of the target from that of internal reference. The $\Delta\Delta C_T$ is obtained by subtracting the ΔC_T value of tumors from that of normal brains. The calculated $2^{-\Delta\Delta CT}$ represents the relative target expression fold in tumor samples normalized to internal control as compared to normal tissues. (Livak *et al.* 2001)

3.5.3 qRT-PCR for CSE1L and ERBB4 transcripts

To prevent amplification from genomic DNA, total RNA from each sample was subjected to DNase treatment. One μg of RNA was incubated, in a total volume of 10 μl containing l U of RQ1 RNase-free DNase and l× DNase reaction buffer (Promega), at 37°C for 30 minutes. One μl of stop solution [20 mM ethylene glycol tetraacetic acid (EGTA), pH 8.0] was added followed by incubation at 65°C for 10 minutes to inactive the DNase. PCR containing DNase-treated RNA without reverse

transcription was performed to ensure thorough elimination of genomic DNA.

Complementary DNA (cDNA) was synthesized from total RNA using MultiScribe™ reverse transcriptase and random hexamers (Applied Biosystems) according to manufacturer's protocol. Briefly, one μg of DNase-treated total RNA was used as template in a reaction mix of 20 μl containing 1× RT buffer, 5.5 mM $MgCl_2$, 500 μM dNTP mix, 2.5 μM random hexamers, 8 U of RNase inhibitor and 25 U of MultiScribe™ reverse transcriptase. The reaction was incubated at 25°C for 10 minutes to maximize primer–RNA template binding, followed by 48°C for 30 minutes to synthesize cDNA and 95°C for 5 minutes to inactivate reverse transcriptase.

SYBR® Green-based PCR analysis was performed to quantify gene expression. This method is based on the binding of Sybr Green I dye to the minor-groove of double-stranded DNA and the amount of bound dye is a measure of DNA quantity.

PCR reaction was performed in a 10-μl reaction mix containing 0.6 μl of RT product, 1× FastStart Universal SYBR® Green master mix (Roche) and 0.4 μM of forward and reverse primer. Amplification was carried out under the conditions of 95°C for 10 minutes, followed by 40 cycles of 95°C for 15 seconds, and 60°C for 1 minute. The product was subjected to melt curve analysis, in which a signal peak in dissociation curve indicates a single product and absence of nonspecific amplification including primer-dimers. Agarose gel electrophoresis was also

performed to ensure product was of correct size.

Relative standard curves were generated with a serial dilution of RT product to confirm the same amplification efficiency of CSE1L, ERBB4, and GAPDH. The expression levels of CSE1L and ERBB4 were normalized to the endogenous reference gene GAPDH. Expressions of CSE1L and ERBB4 in tumors are compared with the mean expression level of 3 normal brain samples. The $\Delta\Delta C_T$ method was used to determine change in CSE1L and ERBB4 expression. All quantitative PCR was carried out in triplicates, and the experiment was performed three times. Primers used in qRT-PCR are listed in Table 3.2.

Table 3.2 Primers used in this study.

Gene	GeneBank Accession no.	Forward primer sequence (5' to 3')[1]	Reverse primer sequence (5' to 3')[1]	Annealing temperature (°C)	Product size (bp)
qRT-PCR					
CSE1L	NM_001316	GCTCTCACACTTCCTGGCTC	GGGATGTAGGGGATTATGGC	62	98
ERBB4	NM_001042599	CATGGCCTTCCAACTTGACT	GGCAATGATTTTCTGTGGGT	60	108
GAPDH	NM_002046	AGCCGAGCCACATCGCTCA	TGGCAACAATATCCACTTTACCAGAGTT	60	122
3'UTR cloning					
AKT2-site1	NM_001626	ATGGTAACTAGTGTGTCGTGCTGGTGTCTG	AACGTTAAGCTTATCCATAGGGTGAGGACAGT	54	361
AKT2-site2	NM_001626	ACCGTTACTAGTTCCCTATCCCATCTCCTGTA	ACCGTTAAGCTTTAGCCTAAGCAGCACTGAG	54	488
CDC42-1	NM_001039802	TCTTGGGGGTTTGAATGTTT	GAAAAGAGGAGGGGCAAGAT	58	904
CDC42-2	NM_001039802	ACCGTTGAGCTCATCTCTCCAGAGCCCTTTC	ACCGTTAAGCTTATGTCCCAGATTACTCTCCAG	52	420
CSE1L	NM_001316	AGAGTTACTAGTTAACCTGAACCTTGAGCAAA	AGAGTAAAGCTTAACCTGCCCTTAAGATGTTC	58	414
ERBB4	NM_001042599	ATGGTTACTAGTTGTGGTTCAGGAAAACTACTG	ATGACTAAGCTTATCCACTCGCATTCCTTC	56	424
NRP1	NM_003873	AGAGAAACTAGTAACTGAGCGAAATCCAAGAT	AGAGTAAAGCTTCCAAGGATTTGTGTTTTTGT	56	412
Sequencing					
pCR2.1-TOPO		CAGGAAACAGCTATGAC	TAATACGACTCACTATAGGG	60	178
pMIR-REPORT		GGCCTCTTCGCTATTACGC	TGTTGTGGACGAAGTACCG	60	365

[1]Underlined nucleotides indicate restriction enzyme recognition sites. (SpeI: ACTAGT, HindIII: AAGCTT, SacI: GAGCTC)

3.6 5-aza-2'-deoxycytidine (5-aza-dC) and Trichostatin A (TSA) treatment

DNA demethylating agent 5-aza-dC (Sigma-Aldrich) and histone deacetylase inhibitor TSA (Sigma-Aldrich) were dissolved in dimethyl sulfoxide (DMSO) to 10 mM and 1 mM, respectively, and stored at -80°C in aliquots.

Human glioma cell lines A172, U373MG and TC620 were incubated with medium containing 2, 5 or 10 μM of 5-aza-dC for a period equivalent to 2 cell doublings (3 days for A172, U373MG and 4 days for TC620). Growth medium containing fresh 5-aza-dC was replaced every day. For TSA treatment, cells were incubated with 0.33 or 1 μM TSA for 24 hours. Combinational effect of 5-aza-dC and TSA was tested by treating cells with 5-aza-dC for 3 days followed by TSA for 24 hours. Cells treated with same volume of DMSO were used as control.

3.7 Western blotting

3.7.1 Preparation of cell lysate

Cells were collected by trypsinization and washed twice with chilled PBS. Cell pellet was resuspended in radio-immunoprecipitation assay (RIPA) lysis buffer [50 mM Tris-HCl (pH 7.4), 150 mM NaCl, 1% (v/v) NP-40, 0.1% (w/v) SDS, and 0.25% (w/v) sodium deoxycholate] freshly supplemented with protease inhibitors [1× cOmplete, Mini protease inhibitor cocktail (Roche) and 1 mM phenylmethylsulfonyl fluoride (PMSF; Sigma-Aldrich)] and phosphatase inhibitors [5 mM sodium orthovanadate (Na_2VO_4) and 10 mM sodium fluoride (NaF) (Sigma-Aldrich)]. The content was incubated on ice for 15 minutes followed by centrifugation at 14,000 rpm for 15 minutes. The supernatant containing soluble protein was collected and stored at -80°C until use.

3.7.2 Measurement of protein concentration

Protein concentration was measured by Bio-Rad Protein Assay (Bio-Rad, Hercules, U.S.A.) in a 96-well plate. Dye reagent was prepared by diluting 1 volume of Dye Reagent concentrate with 4 volume of MilliQ water and then filtered through 3MM chromatography paper (Whatman Inc., Florham Park, U.S.A.) to remove particulates. A series of concentrations (0, 0.0625, 0.125, 0.25, 0.375 and 0.5 μg/μl) of BSA was used to generate a standard curve. Ten μl of protein standard or diluted

sample plated on a 96-well plate were added with 200 µl of diluted dye reagent. After incubation at room temperature for 10 minutes, OD at 595 nm for each sample was measured using VICTOR^3 Multilabel Readers (PerkinElmer, Waltham, Massachusetts, U.S.A.). The standard curve was generated by plotting BSA concentration against corresponding average value of OD_{595nm} from triplicates. A linear equation obtained was used to calculate protein concentration of each sample.

3.7.3 Sodium dodecyl sulfate-polyacrylamide gel electrophoresis (SDS-PAGE)

SDS-PAGE is used to separate proteins based on size. The SDS-coated, negatively charged protein molecules migrates in the gel and are resolved according to their molecular weights. The Mini-PROTEAN Tetra Cell electrophoresis system (Bio-Rad) was used for polyacrylamide gel casting and SDS-PAGE.

Polyacrylamide gels of 0.75 mm thickness were cast using the Mini-PROTEAN gel cassette assembly and casting stand according to the manufacturer's protocol (Bio-Rad). The stacking gel (4%) and resolving gel (7.5%, 10%, or 12.5%) solution were prepared by mixing a stock solution of 40% (w/v) acrylamide/N,N'-methylene-bis-acrylamide (29:1) in 1× gel buffer [4× stacking gel buffer (0.4% SDS, 0.5 M Tris-HCl, pH 6.8) or 8× resolving gel buffer (0.8% SDS, 3 M Tris-HCl, pH 8.8)]. Resolving gels of different percentages were used to separate proteins of different

sizes. The components for preparing stacking and resolving gels are listed in Table 3.3. Polymerization catalysts 10% (w/v) ammonium persulfate (APS) (USB, Cleveland, U.S.A.) and N,N,N',N'-tetramethylethylenediamine (TEMED) (Bio-Rad) were added freshly to gel mix to start polymerization.

After resolving gel solution was introduced into the gel cassette sandwiches and overlaid with isopropanol to prevent oxygen from inhibiting polymerization, the acrylamide/bis was allowed to polymerize for 1 hour at room temperature. Overlaying isopropanol was then removed and the resolving gel surface was rinsed with distilled water. After absorbing the residual water trapped between plates by filter paper, stacking gel solution was poured on top of resolving gel until top of the short plate is reached. A comb was inserted immediately into each gel sandwich. The stacking gel was allowed to be polymerized for 30 minutes and the comb was removed just before use. After wells were rinsed with running buffer (25 mM Tris, 192 mM glycine, 0.1% SDS, pH 8.3), gels were pre-run 70 V for 10 minutes before samples were loaded.

Samples were prepared by mixing cell lysates with 6× SDS loading buffer (375 mM Tris, 12% SDS, 60% glycerol, 0.012% bromophenol blue, 30% β-mercaptoethanol, pH 6.8) in a ratio of 5:1 (v/v), denatured at 95°C for 5 minutes, and cooled down on ice. In this step, proteins were denatured, linearized and coated with negatively charged SDS molecules, and β-mercaptoethanol assisted protein

denaturation by reducing all disulfide bonds. Samples containing equal amounts of protein were loaded to the wells of acrylamide gels, as well as the molecular weight marker Spectra™ Multicolor broad range protein ladder (Fermentas Inc., Glen Burnie, U.S.A.) to monitor protein migration during SDS-PAGE and to estimate protein band size after blotting. Electrophoresis was performed at 120 V for 2 hours or until the dye front reached the bottom of the gels.

3.7.4 Electroblotting of proteins

After electrophoresis, resolved proteins were transferred from gel to Hybond-P polyvinylidene fluoride (PVDF) Membrane (GE Healthcare, Buckinghamshire, UK) using the Mini Trans-Blot® Electrophoretic Transfer Cell (Bio-Rad). PVDF membrane was cut into same size as gels and pre-wetted in methanol for 5 minutes for activation and then equilibrated in pre-chilled transfer buffer (25 mM Tris, 192 mM glycine, 20% methanol, pH 8.3) for 10 minutes. Gels removed from the gel sandwiches, together with fiber pads and filter paper of suitable size, were soaked in transfer buffer before blotting. The fiber pad-filter paper-gel-membrane-filter paper-fiber pad transfer cassette sandwich was then assembled. To remove air bubbles that may block protein transfer, a 15-ml tube was rolled horizontally over the sandwich. A magnetic stir bar and a cooling unit were placed in the buffer tank to maintain even ion distribution and buffer temperature throughout the transfer. Electroblotting was carried out at 100 V for 1 hour or 30 V overnight depending on size of protein.

3.7.5 Immunoblotting

After blotting, non-specific proteins on the membrane were blocked by incubation in 5% (w/v) non-fat milk powder in Tris-buffered saline with Tween 20 (TBST) buffer [20 mM Tris-HCl (pH 7.6), 0.1% (v/v) Tween 20, and 137 mM NaCl] for 1 hour with gentle shaking at room temperature. The blot was incubated with

Table 3.3 Components of polyacylamide gels for SDS-PAGE

Reagent	Stacking gel	Resolving gel		
	4%	7.5%	10%	12%
40% acrylamide/bis-acrylamide (29:1)	0.4 ml	1.88 ml	2.5 ml	3 ml
4× stacking buffer	1.0 ml	-	-	-
8× resolving buffer	-	1.25 ml	1.25 ml	1.25 ml
10% (w/v) APS	40 µl	100 µl	100 µl	100 µl
100% TEMED	8 µl	20 µl	20 µl	20 µl
MilliQ water	2.6 ml	6.75 ml	6.13 ml	5.63 ml
Total volume	4.0 ml	10.0 ml	10.0 ml	10.0 ml

diluted primary antibody (Table 3.4) in 5% (w/v) non-fat milk powder in TBST with shaking. After that, the blot was washed with TBST three times for 10 minutes each at room temperature with shaking. According to the source of primary antibody, horseradish peroxidase-conjugated sheep anti-mouse antibody (NA931V, GE Healthcare) or donkey anti-rabbit antibody (NA934V, GE Healthcare) were used as secondary antibodies and incubated with the blot in 1:5000 dilution in TBST with 5% milk for 1 hour with shaking at room temperature. The blot was then washed and subjected to chemiluminescence detection.

Chemiluminescent signals were detected and visualized by using SuperSignal West Pico Chemiluminescent Substrate (Thermo Scientific, Rockford, U.S.A.) according to the manufacturer's instructions. Briefly, substrate was applied onto membrane and the light emitted in the reaction was captured by Fuji Super RX Blue Medical X-Ray Films (Fujifilm, Tokyo, Japan). The intensity of bands on the film was quantified using ImageJ software (National Institutes of Health, Bethesda, U.S.A.). Fold difference of target proteins were normalized to GAPDH or β-actin as loading control.

Table 3.4 Experimental conditions used in Western blotting

	Protein size (kDa)	% of resolving gel used	Amount of cell lysate loaded (μg)	Transfer condition	Antibody dilution	Incubation	Antibody species	Source and catalog number
CSE1L	110	7.5%	30	30V, overnight	1:200	4°C, overnight	Mouse	Abnova, Taiwan, H00001434-M08
cleaved PARP	89	10%	30	100V, 1 hour	1:1000	4°C, overnight	Rabbit	Cell Signaling Technology, Denvers, U.S.A., #9541
β-tubulin III	50	12%	30	100V, 1 hour	1:500	4°C, overnight	Mouse	R&D Systems, Minneapolis, U.S.A., MAB1195
GFAP	50	12%	30	100V, 1 hour	1:100	4°C, overnight	Mouse	DakoCytomation, Glostrup, Denmark, M0761
GAPDH	37	12%	5	100V, 1 hour	1:10000	4°C, overnight	Mouse	Abnova, Taiwan, H00002597-M01
β-actin	42	12%	5	100V, 1 hour	1:10000	4°C, overnight	Mouse	Abcam, Cambridge, U.S.A., ab8224

3.8 Dual-luciferase reporter assay

Dual-luciferase reporter assay (Promega, Madison, U.S.A.) was used to investigate whether miR-137 could interact with the predicted MRE in 3'UTR of target genes. Briefly, predicted miR-137 MRE was cloned downstream of the firefly luciferase gene in the pMIR-reporter vector. The recombinant plasmid would then be co-transfected with miR-137 into glioma cells and then assayed for luciferase activity. Reduced luciferase activity indicated an interaction between miR-137 and the MRE.

3.8.1 Construction of reporter plasmids

3.8.1.1 Experimental outline

To generate the reporter plasmid, a DNA fragment containing the predicted miR-137 MRE of candidate gene was amplified from genomic DNA using primers linked with restriction enzyme sites. The fragment was first cloned into pCR®2.1-TOPO® by TA cloning, sequenced and subcloned downstream of the luciferase gene at specific restriction sites in the pMIR-reporter vector. Additionally, plasmid DNA containing mutated miR-137 MRE was also created using *in vitro* site-directed mutagenesis to serve as negative control in the luciferase assay.

3.8.1.2 PCR Amplification of MREs

The 3'UTR fragment containing the predicted MRE was amplified from human

genomic DNA by PCR. Each 20-μl PCR mix contained 40 ng of genomic DNA, 1× GeneAmp PCR buffer II, 2.5 mM $MgCl_2$, 0.2 mM dNTP mix, 0.4 μM of primer pair, and 1 U of AmpliTaq Gold® DNA polymerase (Applied Biosystems). PCR was carried out at 95°C for 10 minutes, followed by 40 cycles of denaturation at 95°C for 30 seconds, annealing at 52-58°C for 30 seconds, extension at 72°C for 1 minute, and a final extension at 72°C for 10 minutes. All primers were designed using Primer3 (http://frodo.wi.mit.edu/primer3/) and synthesized by Invitrogen (Table 3.2) The PCR products were resolved by electrophoresis in 1.5% agarose gel containing 1 μl/ml RedSafe™ nucleic acid staining solution (iNtRON Biotechnology, Seoul, Korea) and visualized under ultraviolet light.

For CDC42, since there are pseudogenes in the human genome, a nested PCR approach was employed to isolate the CDC42-specific 3'UTR fragment. First round PCR amplified a 904-bp fragment spanning intron 7 and exon 8 using CDC42-specific primer pair CDC42-1 (Table 3.2). This fragment was gel purified using the MEGA-spin agarose gel DNA extraction kit (iNtRON Biotechnology), and then subjected to second round PCR using primer pair CDC42-2 to produce a 420-bp fragment containing the miR-137 MRE.

3.8.1.3 TA cloning

PCR products were cloned using the TOPO TA cloning® technology, which is

based on the efficient ligating activity of topisomerase I for single nucleotide overhang (Invitrogen). A 5-µl TA cloning mix contained 2 µl of PCR product, 0.5 µl pCR®2.1-TOPO® vector (linearized with topiosomerase I covalently bound to each 3' phosphate), 0.5 µl salt solution and 2 µl H_2O. The mix was incubated for 30 minutes at room temperature, and then placed on ice until transformation.

3.8.1.4 Transformation

Ligation mix was added to 100 µl of E. coli TOP10 competent cells (Invitrogen), mixed gently and incubated on ice for 30 min. The cells were heat shocked at 42°C for 45 seconds and immediately cooled on ice for at least 2 minutes. Two hundred µl of Luria Bertani (LB) broth (USB) supplemented with 2 mM glucose was added to the cells and the mixture was incubated in a 37°C shaker with 250 rpm horizontal shaking for 1 hour. After incubation, 100 µl of cells was spread onto a LB agar plate supplemented with 100 µg/ml ampicillin that had been pre-spread with 40 µl of 40 mg/ml X-gal (dissolved in dimethylformamide). The plates were incubated inverted at 37°C overnight.

3.8.1.5 Blue/white screening and validation of recombinants

The blue-white selection is an effective method for selecting recombinant clones containing insets (white colonies) versus those without inserts (blue colonies). From each LB plate spread with ligation mix, at least 5 white colonies and 1 blue colony

(as negative control) were picked individually into 20 µl of LB broth. After thorough mixing, 1 µl of cell suspension was transferred to 20 µl of PCR mix with composition identical to that described in section 3.8.1.2, except for the primers used (Table 3.2). PCR was carried out as stated in section 3.8.1.2 and products were resolved by 1.5% agarose gel electrophoresis. Clones that showed products of expected size were inoculated into 2 ml of LB broth supplemented with 100 µg/ml ampicillin and allowed to grow overnight at 37°C with shaking at 250 rpm. A mini preparation of plasmid DNA from the culture was performed using DNA-spin™ plasmid DNA extraction kit (iNtRON). Quantity and quality of DNA were determined by spectrometry at 260 nm and 280 nm. Concentration of DNA (in µg/µl) was calculated using the formula OD_{260nm} × 50 ng /µl × dilution factor. A ratio of OD_{260nm}/OD_{280nm} in the range of 1.8-2.0 indicates a DNA prep of high quality. Positive recombinant clones were confirmed by restriction enzymes digestion and sequencing (Tech Dragon Limited, Hong Kong). For long-term storage, a 10% glycerol stock of cell culture was prepared and stored at -80 °C.

3.8.1.6 Subcloning of 3'UTR fragments into pMIR-reproter vector

Validated recombinant clones containing 3'UTR fragments of AKT2, CSE1L, ERBB4 and NRP1 were digested with restriction endonucleases SpeI and HindIII (New England Biolabs, Ipwich, U.S.A.) to release the inserts. The digestion mixture of 20-µl volume containing 10 µg of DNA, 20 U of SpeI, 20 U of HindIII and 0.1

μg/μl BSA in 1× NEBuffer 2 was incubated at 37°C for 90 minutes, followed by 65°C for 20 minutes to inactivate the enzyme activity. To release the CDC42 3'UTR fragment, recombinant clones were treated with SacI and HindIII. The pMIR-reporter vector was prepared for ligation by digesting with HindIII and SpeI or SacI. Restricted DNA was resolved by agarose gel electrophoresis and purified by MEGA-spin Agarose Gel DNA Extraction Kit (iNtRON). To ligate the released 3'UTR fragment to pMIR-reporter, a 20-μl reaction containing ~300 ng of vector DNA, ~60 ng of each insert (molar ratio 1:3), 1 U of T4 DNA ligase (Invitrogen), and 1× T4 DNA ligase buffer was prepared and incubated overnight at 16°C.

Bacterial transformation was conducted as described in section 3.8.1.4. Because blue-white selection was not feasible with the pMIR-reporter vector, a quick screen for recombinant clones by PCR was conducted using primer pairs as listed in Table 3.2. Positive recombinant clones were validated by restriction mapping (HindIII + BamHI, HindIII + XbaI, HindIII + XhoI) and sequencing. A large preparation of each validated recombinant plasmid DNA was prepared using PureLink™ HiPure plasmid DNA purification kit according to manufacturer's recommendation (Invitrogen). Purified DNA was stored in aliquots at -20 °C. These clones were termed pMIR-GENE, where GENE was the name of target gene.

3.8.2 Site-directed mutagenesis

To generate mutated miR-137 MRE that could serve as negative control in reporter assay, specific bases in MRE of pMIR-GENE were mutated using in vitro site-directed mutagenesis. The method involves 2 steps: the synthesis of mutant strands of plasmid DNA using two synthetic oligonucleotides containing desired mutations and a proofreading DNA polymerase, followed by digestion of methylated non-mutated parental template with methylation-sensitive restriction endonuclease DpnI.

The site-directed mutagenesis steps were conducted according to Strategene's Quickchange multi-site mutagenesis kit with modifications. The mutagenic oligonucleotide primers were designed in such a way that substituted nucleotides were introduced at sites in the UTRs (482^{nd}-488^{th} bases of CSE1L and 1139^{th}-1146^{th} of ERBB4) that are thought to interact with the seed region of miR-137 (Table 3.5). To maintain GC content in the primers the nucleotides targeted for mutations were converted to complementary bases. The primers were allowed to hybridize to pMIR-GENE and mutant strands were synthesized using *pfx* DNA polymerase with 3' to 5' proofreading exonuclease activity. A 50-µl reaction consisted of 1× *Pfx* amplification buffer, 0.3 mM dNTP mix, 1 mM $MgSO_4$, 0.3 µM of each mutagenic primer, 100 ng of template plasmid (pMIR-GENE) and 2.5 U of *Pfx* DNA polymerase. The reaction was incubated at 94°C for 2 min followed by 18 thermal cycles of 95°C for 1 min, 68°C for 10 min and a final extension at 68°C for 10 min. After chilling the reaction

on ice, 1 µl of DpnI (New England Biolabs) was added and the mixture was incubated at 37°C for 1 hour to allow digestion of parental methylated DNA. The DpnI-treated DNA was then subjected to bacterial transformation as described in section 3.8.1.4. Colonies selected were grown in culture and subjected to direct DNA sequencing to confirm mutations.

3.8.3 Plasmid and miRNA mimic cotransfection

Human glioblastoma LNZ308 cells were seeded at a density of 1.2×10^5 cells/well on a 24-well plate. After incubation for 24 hours when the cell confluency reached ~90%, cells were transfected with a DNA mixture containing 500 ng of pMIR-GENE or pMIR-reporter, 100 ng of pRL-TK *renilla* luciferase expression plasmid (as an internal control), 10 pmol of either miRIDIAN miR-137 mimic or miRNA negative control #1, 1 µl of Lipofectamine 2000 reagent in 100 µl of Opti-MEM® I and incubated at 37°C overnight.

3.8.4 Determination of luciferase activity

Dual-luciferase reporter assay (Promega) was performed 24 hours post transfection. After removal of media, cells were washed twice with PBS and lysed in 100 µl 1× Passive Lysis Buffer. The plates were placed on an orbital shaker with gentle shaking at room temperature for 15 min to ensure complete and even coverage of the cell monolayer. Sequential measurements of firefly and *renilla* luciferase

activities in cell lysates were then performed. The firefly luciferase substrate Luciferase Assay Reagent II was prepared by resuspending 1 vial of lyophilized Luciferase Assay Substrate in 10 ml of the supplied Luciferase Assay Buffer II. The *renilla* luciferase substrate 1× Stop & Glo® reagent, which quenched the firefly luciferase luminescence, was prepared by diluting 1 volume of 50× Stop & Glo® substrate in 50 volumes of Stop & Glo® buffer. For each measurement, 10 µl of cell lysate was transferred into a 96-well black plate followed by mixing with 50 µl Luciferase Assay Reagent II. The firefly luciferase activity was measured in the IVIS 100 imaging system (Xenogen Corporation, Hopkinto, MA). Fifty µl of the Stop & Glo® reagent was added to the reaction mixture and the *renilla* luciferase activity was measured immediately. A lysate of nontransfected control cells was included to determine the background contribution. All experiments were performed in triplicate and repeated 3 times. The firefly luminescence was normalized to the *renilla* luciferase activity in the same sample. Results were expressed as relative firefly luminescence in cells transfected with pMIR-GENE and miR-137 mimic compared to control cells transfected with pMIR-reporter with miR-137.

Table 3.5 Oligonucleotides for site-directed mutagenesis.

Primer	Sequence (5' to 3')[1]	Annealing temperature (°C)	Length (bp)
CSE1L-mut-sense	GCAGTGCACATTTCATAGTTTCAAATCTGTAATCTCGTTATAAAATCCTAAAATATGTACCTAAGAACATCTTAAGG	77	77
CSE1L-mut-antisense	CCTTAAGATGTTCTTAGGTACATATTTTAGGATTTTATAACGAGATTACAGATTTGAAACTATGAAATGTGCACTGC		77
ERBB4-mut-sense	GTTCTTTTTCTGAACTCCATTTTGGATTTTGAATCTTCGTTATTGGAAGCAACCAGCAAATTAACTAATTTAAGTAC	75	77
ERBB4-mut-antisense	GTACTTAAATTAGTTAATTTGCTGGTTGCTTCCAATAACGAAGATTCAAAATCCAAAATGGAGTTCAGAAAAAGAAC		77

[1]Underlined nucleotides indicate mutated sites.

3.9 Functional assays

3.9.1 Cell growth and proliferation assay

Cell growth was evaluated by measuring cellular metabolic activity, whereas cell proliferation was assessed by cell counting and BrdU incorporation during DNA synthesis.

3.9.1.1 3-(4,5-Dimethyl thiazol-2-yl)-2,5-diphenyl tetrazolium bromide (MTT) assay

The colorimetric MTT assay was used to monitor cell growth. This method is based on the principle that metabolically active cells can convert yellow tetrazolium salt MTT to a water-insoluble violet formazan by succinate dehydrogenase in the mitochrondria. The amount of formazan crystals formed, after dissolution, can be quantified by spectrophotometry at 500-600 nm. Since succinate dehydrogenase is active in living cells, its activity level is a measure of cell growth.

A total of 1500 cells were seeded in each well of a 96-well plate and allowed to grow for 24 hours in 100 µl of culture medium. Cells were transfected with miR-137 mimic, CSE1L-targeting siRNA or corresponding negative control RNA with Lipofectamine 2000 at optimized concentrations (see section 3.4.1). At 24, 48, 72 and 96 hours after transfection, MTT assay was performed. Fifteen µl of MTT

reagent (5 mg/ml stock solution in PBS stored at 4°C and protected from light) was added to each well. After incubation at 37°C in a humidified atmosphere for 4 hours, culture medium was removed and the purple formazan crystals were dissolved in 100 µl of DMSO with shaking on a horizontal shaker for 15 min at room temperature. The optical density at 570 nm and 690 nm in each well was measured sequentially using Victor^3 Multilabel Plate Reader. Wells with medium only served as background control. Each test was measured in triplicate and the experiment was repeated 3 times.

3.9.1.2 Cell counting

Viable cells with intact cell membrane were distinguished from dead cells by exclusion of trypan blue, which stained dead cells only. Eight thousand cells were plated in each well of a 24-well plate. After incubation for 24 hr, transfection with miR-137 mimic or siRNAs was performed as described in the MTT assay. Each day for 4 consecutive days cells were harvested by trypsinization and resuspended in 1 ml medium. Equal volumes of cell suspension and 0.4% trypan blue solution (Sigma-Aldrich) were mixed and 10 µl of stained cells were transferred to a hemocytometer. The number of unstained living cells was then counted. The total number of viable cells was calculated as the number of unstained cells counted $\times$ 2 $\times 10^4$. Experiments were carried out in triplicates and repeated 3 times independently.

3.9.1.3 5-Bromo-2'-deoxyuridine (BrdU) incorporation assay

DNA synthesis is a useful indicator of cell proliferation. As an analogue of thymidine, BrdU is incorporated into DNA of replicating cells during the S phase of cell cycle. The amount of BrdU in the newly synthesized DNA can be detected with BrdU-specific antibody followed by an ELISA-based colorimetric assay. In this study, the Cell Proliferation ELISA, BrdU assay (Roche Diagnostics) was used to quantify cell proliferation.

Cells were plated and transfected as described in section 3.9.1.1. At 24, 48, 72 and 96 hours post-transfection, 10 µl of 1× BrdU labeling reagent (100 µM BrdU in culture medium) was added to each well of a 96-well plate to a final BrdU concentration of 9.1 µM. After incubation for 4 hours, the culture medium was removed. Cells were fixed and the DNA was denatured to expose the incorporated BrdU by adding 200 µl/well of FixDenat reagent, and the mixture was let stand for 30 min at room temperature. The FixDenat solution was then removed thoroughly by flicking off and tapping. One hundred µl of mouse monoclonal anti-BrdU antibody conjugated with peroxidase (anti-BrdU-POD) (100-fold dilution from stock solution with antibody dilution solution provided in the kit) was added to each well and allowed to incubate for 90 min at room temperature. Cells were washed three times with PBS to remove unbound antibody. The immune complexes were detected by adding 100 µl of substrate (tetramethyl-benzidine) solution and mixture was incubated for 30 min at room temperature. The reaction product was quantified by

measuring the optical density at 370 nm (peak absorbance wavelength) and 490 nm (reference wavelength) using a multiwell spectrophotometer. Relative proliferating cell numbers were calculated as a ratio of optical density measured from cells transfected with miR-137 or siCSE1L to cells transfected with negative control miRNA or siRNA. The data were obtained from triplicates in three independent experiments.

3.9.2 Apoptosis assay

During apoptosis, the 116-kDa nuclear poly (ADP-ribose) polymerase (PARP) is cleaved to amino-terminal DNA binding domain (24 kDa) and carboxy-terminal catalytic domain (89 kDa) fragments by activated caspases. The detection of the 89-kDa PARP catalytic fragment is a marker of apoptosis.

Cells of 20-30% confluency in 60-mm culture dishes were transfected with miR-137, CSE1L siRNA or negative control RNA as mentioned in section 3.8.1.1. At 48 and 96 hours post-transfection, cell lysates was prepared and subjected to Western blotting as described in section 3.7. The 89-kDa PARP fragment was detected using an antibody specific to cleaved PARP (Cell Signaling; Table 3.4)

3.9.3 Anchorage-independent growth assay

The ability of cells to grow in an anchorage-independent manner was examined

using the soft agar assay. Agar solutions of 0.6% and 1% agar were prepared in distilled water and autoclaved. To prepare the base layer, 1% agar solution was melted in a microwave oven and cooled to 55°C in a water bath, mixed with equal volume of 2× culture medium warmed to 37°C to give a final concentration of 0.5, poured into each well (2 ml/well) in 6-well plates, and allowed to solidified at room temperature. Transfected cells were trysinized and resuspended in 37°C 2× culture medium. Cell suspension ($2\text{-}4\times10^5$) was mixed with equal volume of 0.6% agar (warmed to 42°C) and 1 ml of this mixture was layered on top of the base layer. After agar solidification, the plates were incubated at 37°C. Several drops of culture medium were added to the plate every 3 days to feed the cells.

After three weeks of incubation, cell clusters of greater than 100 μm diameter were considered as colonies. The number of colonies was scored in 10 fields of view (200×) under a microscope. All experiments were performed in triplicates for 3 times.

3.9.4 Wound healing assay

The wound healing assay was performed to assess glioma cell motility *in vitro*. A172 cells (3×10^5) were seeded on a 6-well plate and allowed to grow overnight. Cells of 70% confluency were transfected with 40 nM miR-137, 6 nM CSE1L siRNA, or negative RNA controls. After 16 hours, artificial wounds were made by streaking a line in 100%-confluent cell monolayer using sterile 200-μl pipette tips.

Cell debris was removed by rinsing the plate with medium. Cells were then incubated as usual. Closure of the open gaps was monitored for 40 hours until wounds were completely closed. Photos were captured using a phase-contrast microscope under 40× magnification. Widths of the wounds were measured using Image-Pro Plus software version 5.1 (Media Cybernetics, Silver Spring, U.S.A.).

3.9.5 Matrigel invasion assay

The invasive ability of glioma cells was evaluated using BD BioCoat™ Matrigel™ Invasion Chamber (BD Bioscience, Bedford, U.S.A.) system. The chamber contains an 8-micron pore polyethylene terephthalate membrane covered with a thin layer of Matrigel basement membrane matrix. Cells that could pass the Matrigel and migrate through the pores to the underside of chamber were considered invasive.

Briefly, the chamber was removed from -20°C storage, equilibrated to room temperature for 1 hour, and rehydrated with 500 µl of warm serum-free culture medium for 2 hours at 37°C. After rehydration, medium was removed carefully. transfected cells were prepared in serum-free medium. Culture medium (750 µl) supplemented with 10% FBS was used as a chemoattractant and added to each well of a tissue culture plate (BD Falcon, Franklin Lakes, U.S.A.). Chambers were transferred to wells containing chemoattractant followed by addition of 500 µl of cell

suspension containing different numbers of cells (2×10^5 for TC620, 1×10^5 for A172, U87MG and U373MG cells) into each chamber. After incubation for 16 hours, the non-invading cells on the upper surface of the membrane were removed by scrubbing using cotton tipped swab. Invaded cells on the lower surface of the membrane were fixed with 500 µl of methanol for 2 minutes and then stained with 500 µl of 1% Toluidine blue (in 1% borax; Sigma-Aldrich) for another 2 minutes. Cells were photographed using a phase-contrast microscope under 40× magnification. Cell numbers in 3 randomly selected fields of each insert were counted. Experiments were performed in duplicates for 3 times.

3.9.6 Cell differentiation assay

In glioma cells transfected with miRNA for 48 hours, expressions of β-tubulin III and GFAP were detected as neuronal and astrocytic markers, respectively, by Western blotting as described in section 3.7.

3.10 Immunohistochemical analysis

Expressions of CSE1L and Ki-67 were examined by immunohistochemistry in 35 OTs. For controls, FFPE blocks of 5 autopsy samples and 8 non-neoplastic brain tissues with medial temporal sclerosis or brain chronic inflammation were retrieved from Department of Anatomical and Cellular Pathology, Prince of Wales Hospital, Hong Kong. FFPE tissues were cut into 5-μm thick sections and subjected to hematoxylin and eosin (H&E) staining and immunohistochemistry (IHC).

3.10.1 H&E staining

After heated on a 40°C hot plate, FFPE sections were deparaffinized with xylene three times for 5 minutes, rehydrated through a series of graded alcohol (100% ×2, 95% and 70%) and then washed briefly in distilled water.

Sections were stained in Mayer's haematoxylin for 10 minutes and washed in running tap water for 5 minutes. Cytoplasmic component was decolorized with acid alcohol (1% HCl in 70% ethanol) for 2 seconds. After thorough rinsing in tap water, slides were treated in Scott's tap water substitute for 2 minutes to blue up and washed in running tap water again. The sections were thereafter stained with 1% eosin for 2 minutes, followed by a running tap water wash. Stained sections were dehydrated in graded alcohol series (70%, 95% and 100% ×2, 5 minutes each), cleared in 2 changes of xylene for 5 minutes each, and finally mounted with xylene based mounting

medium. The H&E stained slides were subjected to histological review for diagnosis and localization of representative tumor area.

3.10.2 Detection of Ki-67 expression

Sections were deparaffinized and rehydrated as described in section 3.10.1. Antigen retrieval was carried out by boiling the sections in EDTA buffer (1 mM EDTA, pH 8.0) in a microwave oven. After antigen exposure, immunohistochemical staining was preceded with the program 32 min-i in Ventana NexES IHC automated slide stainers system using iVIEW DAB Detection Kit (Ventana Medical Systems Inc., Tucson, USA). Tissue sections were incubated with primary monoclonal antibody against Ki-67 antigen (clone MIB-1, 1:100 dilution, Dako, Carpinteria, USA) at 37°C for 32 minutes. Negative control sections were incubated in parallel without primary antibodies. A section of multi-tissue spring-roll block (including tonsil, thyroid, lung and colonic tissues, etc.) was mounted on slide as positive control to ensure that the immunostaining was working correctly.

3.10.3 Detection of CSE1L expression

Deparaffinized and rehydrated sections were subjected to antigen retrieval in boiled citrate buffer (10 mM citric acid, pH 6.0) in a microwave oven. Endogenous horseradish peroxidase (HRP) activity was blocked 3% hydrogen peroxide (H_2O_2) for 5 minutes. After blocking in 2% normal swine serum (Dako, Carpinteria, USA)

for 5 minutes at room temperature, the CSE1L antibody (clone 3D8; 1:50 dilution; Abnova, Taiwan) were applied onto the specimens and incubated overnight at 4°C. Sections were then washed three times with TBST followed by incubation with Dako EnVision+ HRP labeled anti-mouse at room temperature for 50 minutes. Sections were then washed three times in TBST before the addition of 3,3'-diaminobenzidine (DAB) chromogen substrate in DakoCytomation EnVision+ System-HRP (DAB), allowed to react for 3 minutes and washed well in running tap water. The DAB chromogen resulted in a brown precipitate where antigen was located can be visualized under a light microscopy. Finally, sections were counterstained with Mayer's hematoxylin to stain the nucleus blue. A non-neoplastic specimen and a section of colorectal cancer tissue array showing positive CSE1L staining were employed as positive staining control.

3.10.4 Scoring methods

For each case, a total of 1,000 cells in 5 high-power fields (400×) with the maximal nuclear staining areas were counted. The Ki-67 labeling index was determined as the percentage of the number of stained nuclei over the total number of nuclei counted.

The nuclear expression of CSE1L was evaluated by using an immunoreactive score (IRS) system, in which IRS = SI (staining intensity) × PP (percentage of positive cells). The staining intensity score was assigned for the intensity of positive

cells (0, negative; 1, weak; 2, moderate; 3, strong). The PP score was determined according to percentage of cells with positive nuclear staining (0, 0%; 1, 0-10%; 2, 10–50%; 3, 50-80%; 4, >80% positive cells). The resultant IRS scores ranged from 0 to 12. The expression of CSE1L was categorized as negative (IRS=0, 1), low (IRS=2, 3), medium (IRS=4, 6) or high (IRS=8, 9, 12).

3.11 Bioinformatic analysis

To identify putative downstream targets of hsa-miR-137, a total of 4 computational programs based on different criteria were employed. These are microCosm (Griffiths-Jones *et al.,* 2006), miRanda (Enright *et al.,* 2003; John *et al.,* 2004), PicTar (Grun *et al.,* 2005; Krek *et al.,* 2005) and TargetScan (Lewis *et al.,* 2003; Lewis *et al.,* 2005). Multiple features are taken into consideration by these algorithms to filter out false positive hits, including 1) base pairing pattern between miRNAs (especially the seed region) and target transcript, 2) thermodynamic stability of the miRNA-mRNA duplex, 3) evolutionary conservation in vertebrate of the target sites, and 4) relative position of binding sites in 3'UTR (Table 3.6). Four criteria were used for selection of candidate miR-137 targets. These included 1) genes predicted by at least 2 of the prediction algorithms, 2) conserved miR-137 MRE across vertebrates, 3) overexpression in human cancer, and 4) implicated oncogenic function.

Table 3.6 Computational algorithms for predicting miR-137 targets

Algorithm	Prediction criteria				URL
	Complementarity	Thermodynamics	Conservation	Site location	
microCosm	√	√	√		http://www.ebi.ac.uk/enright-srv/microcosm/htdocs/targets/v5/
miRanda	√	√	√		http://www.microrna.org/
PicTar	√	√	√		http://pictar.mdc-berlin.de/
TargetScan	√		√	√	http://www.targetscan.org/

3.12 Statistical analysis

Expressions of miR-137 in tumors, cell lines and normal brains were compared by Mann-Whitney U-test. Association of miR-137 expression levels with Ki-67 labeling index was examined by the Spearman's correlation analysis. Dual-luciferase reporter analysis and functional effects of miR-137 or CSE1L knockdown were assessed by the Student's *t*-test.

Patient follow-up was conducted by telephone contact. Survival time was measured from the date of surgery to Janurary 2010 or to the time of death. Survival analysis between study groups was performed using the Kaplan-Meier survival curve with the log-rank test. A *p*-value of less than 0.05 (2-sided) was considered statistically significant. All statistical analyses were performed using SPSS software version 16.0 (SPSS, Inc., Chicago, U.S.A.).

CHAPTER 4 RESULTS

4.1 Expression of miR-137 in glioma cells and clinical significance

4.1.1 Description of 36 OT samples

We have recruited a total of 13 oligodendrogliomas, 7 anaplastic oligodendrogliomas, 13 oligoastrocytomas and 3 anaplastic oligoastrocytomas according to WHO classification for our study (Representative H&E photos in Figure 4.1). The male/female ratio was 1.25:1 and the median age was 41.5 years, ranging from 10 to 77 years. There was 1 pediatric case among all 36 patients.

As OT was characterized by chromosome 1p and 19q co-deletion, we also detected the status of 1p and 19q in these samples using dual-color FISH. Copy number of 1p36.3 and 19q13.3 in each case are listed in Table 4.1.

There were 50.0% (18/36, including 10 of 20 ODs and 8 of 16 OAs) and 47.2% (17/36, including 10 of 20 ODs and 7 of 16 OAs) of OTs showing allelic loss of 1p36 and 19q13, respectively. Among the 18 samples with loss of either region, co-deletion was observed in 17 (94%) cases, except for only 1 OA case (HS375). Chi-square or Fisher's exact test was employed to assess whether 1p36 or 19q13 status was associated with clinical data. As shown in Table 4.2, no significant correlation was detected between allelic status of 1p36 or 19q13 and any clinical

parameter, such as histological subtype, tumor grade, patient sex and age.

To evaluate the proliferative activity in these OTs, Ki-67 expression was examined by IHC analysis. Ki-67 immunoreactivity was observed in the nuclei of tumor cells and was quantified by nuclear labeling index (LI), which represents the percentage of positive staining nucleus. Ki-67 LI in OTs investigated showed great variation. The index ranged from 0.0% to 37.2% in 35 OTs with a median value of 3.7% and a mean value of 6.5%. For the non-neoplastic brain tissues, the index was 0% to 0.1%. Significant higher Ki-67 LI was found in 20 ODs (p=0.007) and 15 OAs (p=0.045) when compared to non-tumorous tissues (Figure 4.2). Between 20 ODs and 15 OAs, there was no significant difference in Ki-67 LI (p=0.386).

When tumors of WHO grade II or III were compared, the Ki-67 LI in grade III tumors were significant higher than that in grade II tumors (p=0.014, Figure 4.3), indicating that high grade tumor cells showed higher proliferative activity. Furthermore, statistical analysis revealed a correlation between Ki-67 LI and patient age (p=0.005), suggesting older patients having higher Ki-67 index. No significant relationship was found between Ki-67 LI and patient sex or 1p/19q allelic status (Table 4.3).

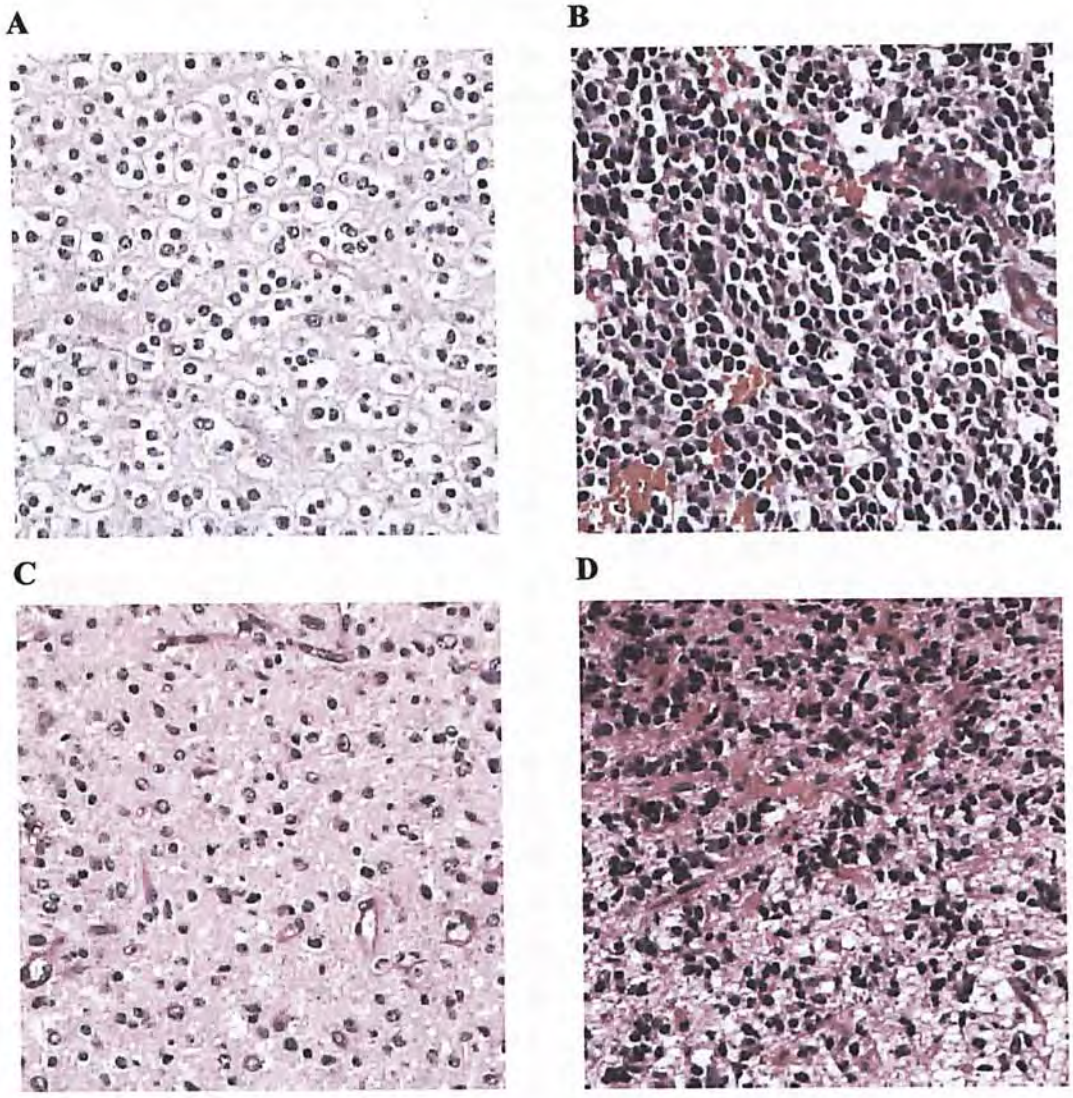

Figure 4.1 Histological appearance of OTs. (A) oligodendroglioms, HS303, (B) anaplastic oligodendroglioma, HS302, (C) oligoastrocytoma, HS381, and (D) anaplastic oligoastrocytoma, HS364, under microscope (400×magnification).

Table 4.1 Summary of clinical parameters, 1p/19q status, Ki-67 labeling index and miR-137 expression level in 36 OTs examined.

Case number	Diagnosis[1]	Sex	Age (years)	1p status[2]	19q status[2]	Ki-67 LI (%)[3]	miR-137 expression (fold change)[4]
HS467	OD	F	56	R	R	7.9	1.2
HS331	OD	F	46	L	L	1.2	-1.6
HS469	OD	F	36	L	L	1.6	-2.0
HS390	OD	M	10	R	R	0.7	-2.3
HS378	OD	F	38	R	R	3.7	-2.5
HS329	OD	F	69	L	L	1.0	-2.8
HS303	OD	M	48	L	L	7.8	-3.0
HS400	OD	F	49	L	L	1.2	-3.5
HS466	OD	F	40	L	L	0.9	-3.7
HS324	OD	M	42	R	R	0.5	-4.0
HS332	OD	M	53	L	L	2.1	-8.6
HS460	OD	M	29	R	R	0.2	-59.7
HS380	OD	M	35	L	L	6.0	-119.4
HS381	OA	F	28	L	L	0.0	-2.0
HS301	OA	M	43	L	L	1.5	-2.7
HS375	OA	M	28	L	R	0.0	-2.7
HS393	OA	F	49	R	R	0.3	-5.4
HS382	OA	F	37	L	L	2.0	-7.0
HS368	OA	F	61	R	R	16.1	-7.4
HS384	OA	M	30	R	R	2.1	-9.9
HS394	OA	F	31	L	L	8.9	-11.0
HS462	OA	M	39	L	L	5.5	-27.9
HS362	OA	M	41	R	R	N/A[5]	-77.2
HS399	OA	M	34	R	R	12.1	-320.9
HS314	OA	F	38	R	R	4.2	-401.8
HS458	OA	M	37	L	L	6.9	-955.4
HS377	AOD	M	77	L	L	12.0	5.3
HS302	AOD	M	35	R	R	23.7	-10.6
HS312	AOD	M	53	R	R	37.2	-16.0
HS360	AOD	M	51	R	R	17.5	-90.5
HS333	AOD	F	43	R	R	8.5	-207.9
HS461	AOD	M	53	L/R[6]	L/R[6]	20.7	-337.8
HS358	AOD	F	50	R	R	4.9	-477.7
HS366	AOA	M	35	R	R	1.7	-22.8
HS457	AOA	M	52	L	L	5.7	-45.3
HS364	AOA	F	48	R	R	0.0	-56.6

[1] OD, oligodendroglioma; AOD, anaplastic oligodendroglioma; OA, oligoastrocytoma; AOA, anaplastic oligoastrocytoma.

[2] L or R stands for allelic loss or retention determined by FISH.

[3] Ki-67 labeling index indicated percentage of positive staining nucleus examined by IHC.

[4] miR-137 expression fold change relative to 3 normal brain RNA samples was determined by qRT-PCR, + or – represents upregulation or downregulation.

[5] Ki-67 labeling index is not available due to lack of FFPE section.

[6] Different chromosomes 1p and 19q status were shown in heterogeneous tumor cells in this case.

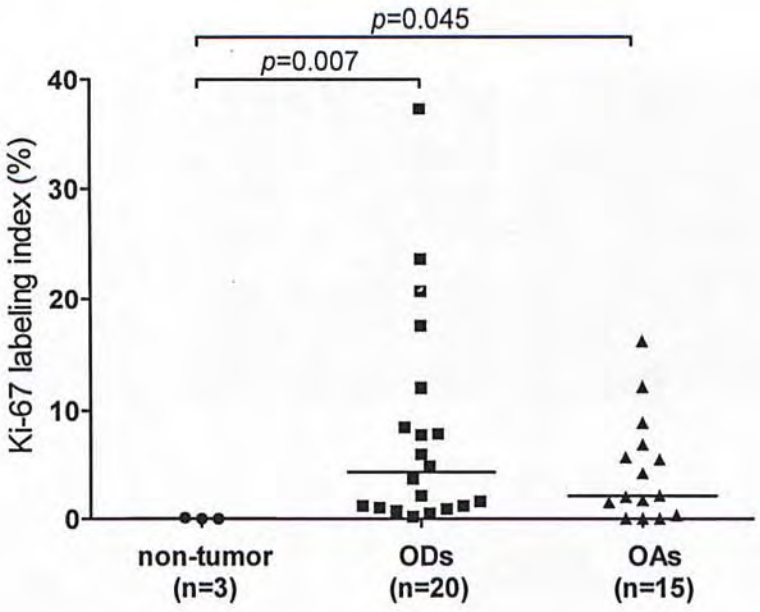

Figure 4.2 Ki-67 labeling index in OTs compared to non-tumorous brain samples by IHC. Both 20 oligodendrogliomas (ODs) and 15 oligoastrocytoma (OAs) showed significant higher Ki-67 expression than 3 non-neoplastic brain tissues.

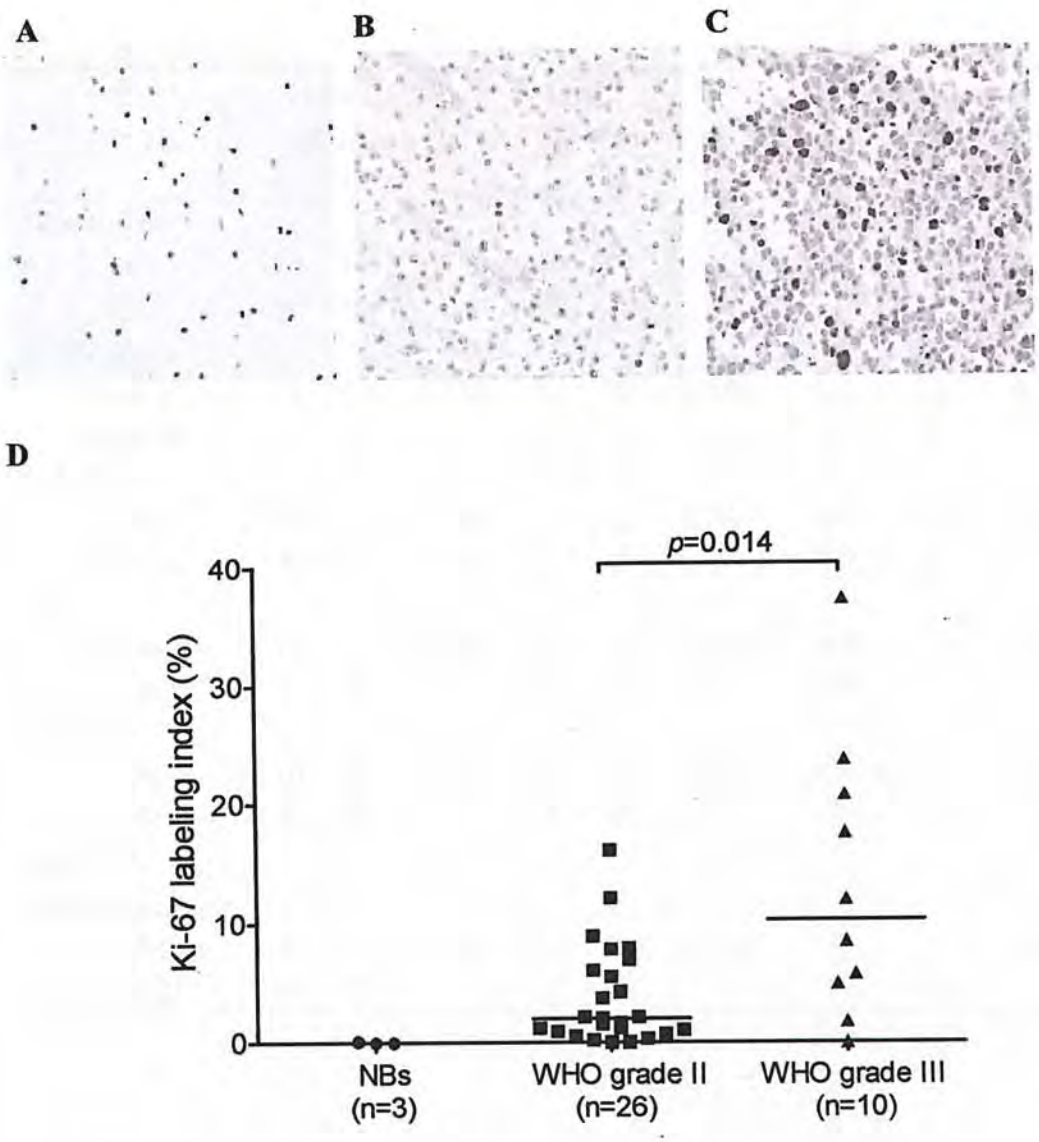

Figure 4.3 Expression of Ki-67 in WHO grade II and III OTs and non-tumorous brain tissue. Representative IHC staining photos in a non-neoplastic brain sample (A), an oligodendroglioma, grade II, HS303 (B) and an anaplastic oligodendroglioma, grade III, HS302 (C) are shown here. D. Labeling index in ODs and OAs are significantly higher than that in non-tumorous brain tissues. Furthermore, grade III tumors displayed higher Ki-67 expression than grade II tumors.

Table 4.2 Association analysis of 1p36/19q13 status with clinicopathological parameters in 36 OTs.

	1p36 status		p-value	19q13 status		p-value	1p36/19q13 co-deletion		p-value
	L	R		L	R		Yes	No	
Tumor type									
OD	10	10	1.000	10	10	0.709	10	10	0.709
OA	8	8		7	9		7	9	
WHO grade									
grade II	15	11	0.137	14	12	0.199	14	12	0.199
grade III	3	7		3	7		3	7	
Gender									
male	10	10	1.000	9	11	0.765	9	11	0.765
female	8	8		8	8		8	8	
Age									
<50 years	13	13	1.000	12	14	0.836	12	14	0.836
>=50 years	5	5		5	5		5	5	
Ki-67 LI									
<3%	10	7	0.365	9	8	0.615	9	8	0.615
>3%	8	10		8	10		8	10	
miR-137 down-regulation									
<2-fold	2	1	1.000	2	1	0.593	2	1	0.593
>2-fold	16	17		15	18		15	18	

Table 4.3 Association analysis of Ki-67 labeling index with clinicopathological parameters in 35 OTs.

	N	Ki-67 labeling index (%)			p-value
		Range	Median	Mean	
Tumor type					
OD	20	0.2~37.2	4.3	8.0	0.385
OA	15	0~16.1	3.2	4.5	
WHO grade					
grade II	25	0~16.1	2.0	3.8	0.014
grade III	10	0~37.2	10.3	12	
Gender					
male	19	0~37.2	5.7	8.6	0.148
female	16	0~16.1	1.8	3.9	
Age					
<50 years	25	0~23.7	1.7	4.0	0.005
>=50 years	10	1.0~37.2	12.0	12.5	
1p status					
loss	18	0~20.7	2.1	4.7	0.507
intact	17	0~37.2	4.2	8.3	
19q status					
loss	17	0~20.7	2.1	5.0	0.884
intact	18	0~37.2	4.0	7.9	
1p/19q co-deletion					
yes	17	0~20.7	2.1	5.0	0.884
no	18	0~37.2	4.0	7.9	
miR-137 down-regulation					
<2-fold	3	1.2~7.9	1.6	3.7	0.528
>2-fold	32	0~37.2	4.0	6.7	

4.1.2 miR-137 level in oligodendroglial tumors and glioma cells

Previous studies screening for miRNA expressions showed that miR-137 was significantly down-regulated in astrocytomas of different grades (Silber *et al.*, 2008; Zhi *et al.*, 2010) relative to non-tumorous brain tissues. In order to investigate whether miR-137 was involved in tumorigenesis of OT, qRT-PCR analysis was performed to evaluate the expression levels of miR-137 in 36 frozen OT specimens (composed of 20 oligodendrogliomas and 16 oligoastrocytomas), 10 glioma cell lines and 3 commercial normal brain RNA samples. Detection of miR-16, whose expression was more robust than small RNA U6B, was selected as an endogenous control for normalization. A significant downregulation of miR-137 level was observed in oligodendrogliomas ($p=0.016$), oligoastrocytomas ($p=0.009$) and glioma cell lines ($p=0.007$) when compared with that in normal brain samples (Figure 4.4). Downregulation of miR-137 (>2-fold decrease) was found in 17 out of 20 (85.0%) OD and all 16 (100%) OA cases, up to 478- and 955-fold, respectively. All 10 glioma cell lines showed reduced miR-137 expression by 8.5- to 2190-fold. Among 36 OTs, there was no significant difference of miR-137 levels between 20 ODs and 16 OAs ($p=0.220$, Figure 4.4). These data indicated that reduction of miR-137 was a frequent event in human OT.

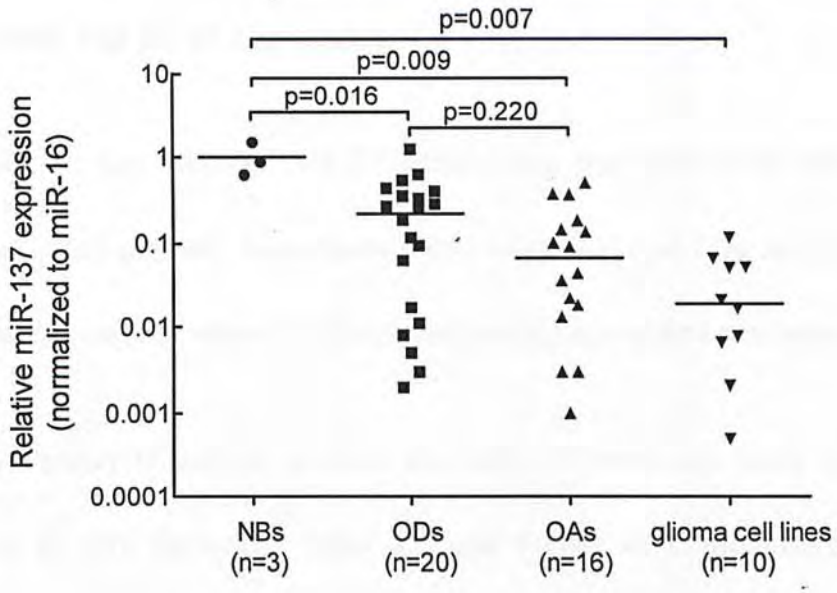

Figure 4.4 Expression levels of miR-137 in 20 ODs, 16 OAs and 10 glioma cell lines compared to that in 3 normal brain (NB) samples by qRT-PCR. Both primary OTs and glioma cell lines showed significant reduced miR-137 expression.

4.1.3 Association of miR-137 expression with clinicopathological features, 1p/19q status and Ki-67 expression

In order to test whether miR-137 expression was associated with clinical parameters of OT patients, the relative levels of miR-137 of OTs to normal brain samples were compared when 36 OTs are categorized into different groups.

Mann-Whitney U analysis revealed that miR-137 levels was lower in grade III than grade II OTs ($p=0.010$, Table 4.4 and Figure 4.5). Moreover, miR-137 expression was inversely correlated with Ki-67 LI in 35 OTs examined ($p=0.009$, $r=-0.436$, Figure 4.7). It was further confirmed by a significantly lower miR-137 level in Ki-67 high expression (>3%) group ($p=0.002$, Figure 4.7). These suggested that miR-137 may play a role in regulating OT cell proliferation.

Although located in chromosome 1p, miR-137 expression levels showed no significant difference between 1p intact or loss OT groups ($p=0.115$, Figure 4.6). In addition, no significant difference was found in miR-137 level when patients were grouped by tumor type ($p=0.219$), sex ($p=0.092$), age (50 years as a cut-off, $p=0.533$), or 19q status ($p=0.215$) (Table 4.4).

Survival analysis was also performed to study the clinical significance of above parameters in 19 OTs with available survival data (Figure 4.8). It was showed that there was significant association between tumor grade and overall or

progression-free survival ($p<0.001$). We also found elder patients with a worse prognosis than younger patients ($p<0.001$). No significant difference was observed between male and female patients.

All the 19 cases showed concurrent statús of chromosome 1p and 19q by FISH analysis. However, 1p/19q status did not significantly correlate with patients' survival. Furthermore, patients with lower Ki-67 LI showed a better clinical outcome for both overall and progression-free survival ($p=0.049$ and $p=0.017$, respectively). Patients with higher miR-137 expression had more favorable prognosis, but it was not statistically significant in our study ($p=0.215$ and $p=0.103$, respectively).

Table 4.4 Association analysis of miR-137 levels with clinicopathological parameters in 36 OTs.

	N	miR-137 expression (fold change)			p-value
		Range	Median	Mean	
Tumor type					
OD	20	1.2 ~ -477.7	-4.6	-3.8	0.219
OA	16	-2.0 ~ -955.4	-14.9	-7.9	
WHO grade					
grade II	26	1.2 ~ -955.4	-4.7	-3.8	0.010
grade III	10	-5.3 ~ -477.7	-50.9	-22.2	
Gender					
male	20	-2.3 ~ -955.4	-18.8	-8.1	0.092
female	16	1.2 ~ -477.7	-4.4	-3.3	
Age					
<50 years	26	-1.6 ~ -955.4	-8.2	-5.1	0.533
>=50 years	10	1.2 ~ -477.7	-11.2	-4.7	
1p status					
loss	18	-1.6 ~ -955.4	-4.4	-4.2	0.115
intact	18	1.2 ~ -477.7	-18.8	-6.0	
19q status					
loss	17	-1.6 ~ -955.4	-5.3	-4.4	0.215
intact	19	1.2 ~ -477.7	-16.0	-5.6	
1p/19q co-deletion					
yes	17	-1.6 ~ -955.4	-5.3	-4.4	0.215
no	19	1.2 ~ -477.7	-16.0	-5.6	
Ki-67 LI					
<3%	17	-1.6 ~ -59.7	-3.7	-3.7	0.002
>3%	18	1.2 ~ -955.4	-34.5	-6.8	

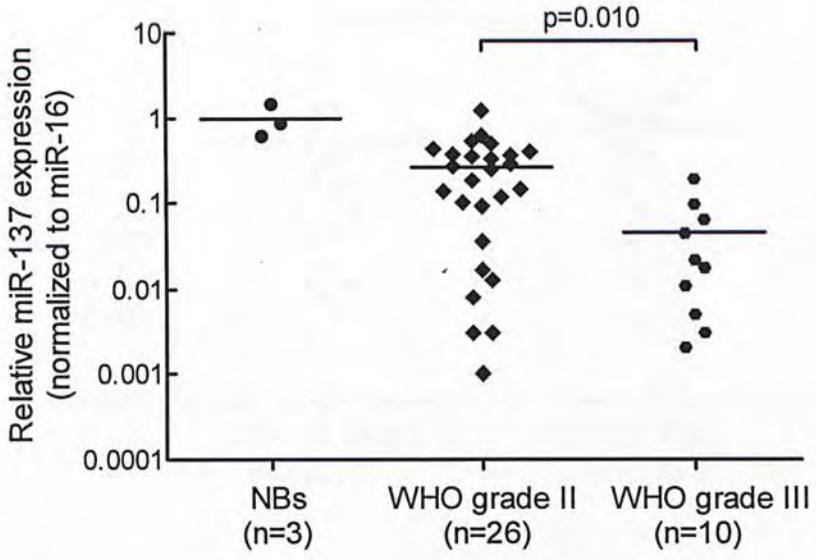

Figure 4.5 miR-137 levels in WHO grade II and III OTs and normal brain samples. Significant lower miR-137 expression was detected in grade III than grade II tumors.

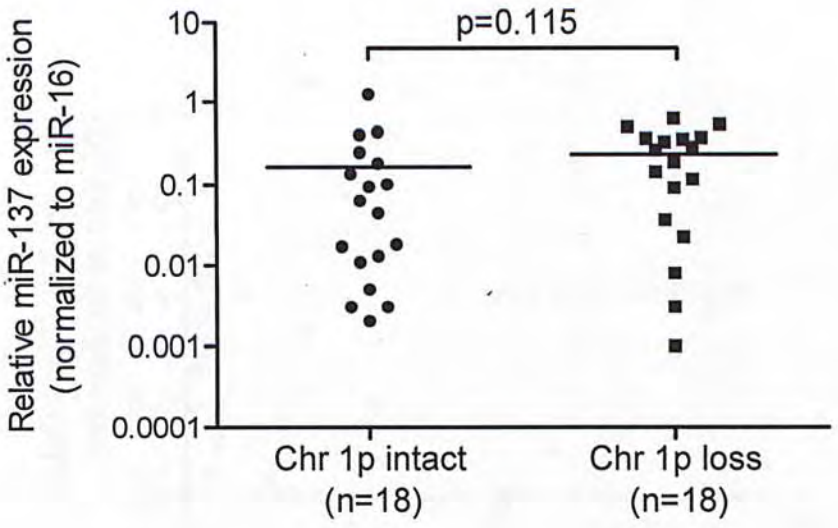

Figure 4.6 Relationship of miR-137 and chromosome 1p status in OTs. No significant difference of miR-137 levels was observed between 1p intact and loss tumors by Mann-Whitney U analysis (p=0.115).

A

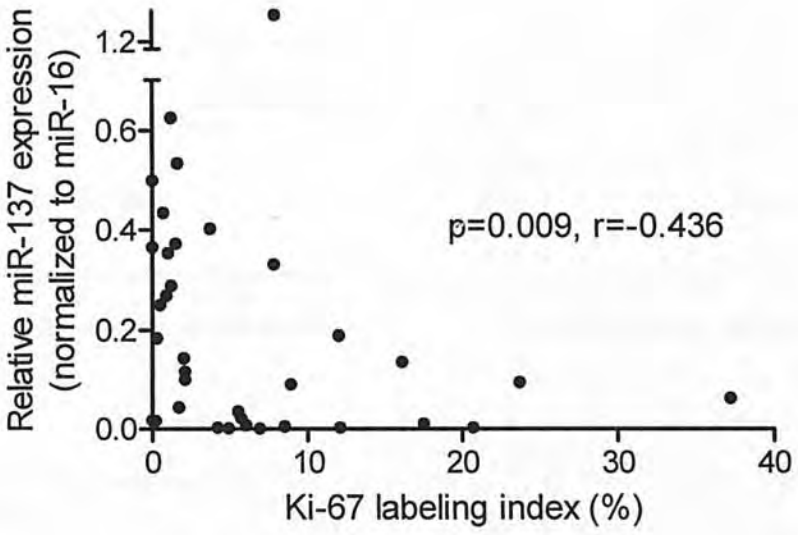

B

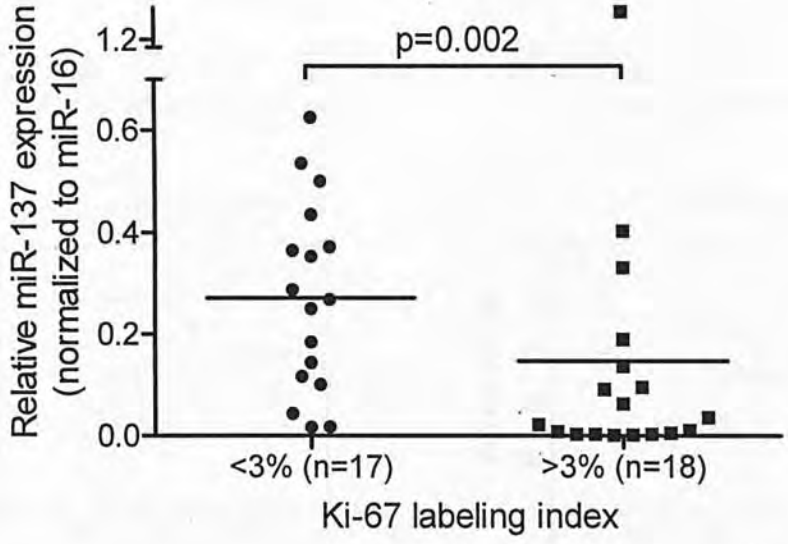

Figure 4.7 Relationship of miR-137 and Ki-67 expression in OTs. A. Significant inverse correlation observed using spearman's correlation analysis (p=0.009, r=-0.436). B. Significant lower miR-137 levels in Ki-67 high expression group by Mann-Whitney U analysis (p=0.002).

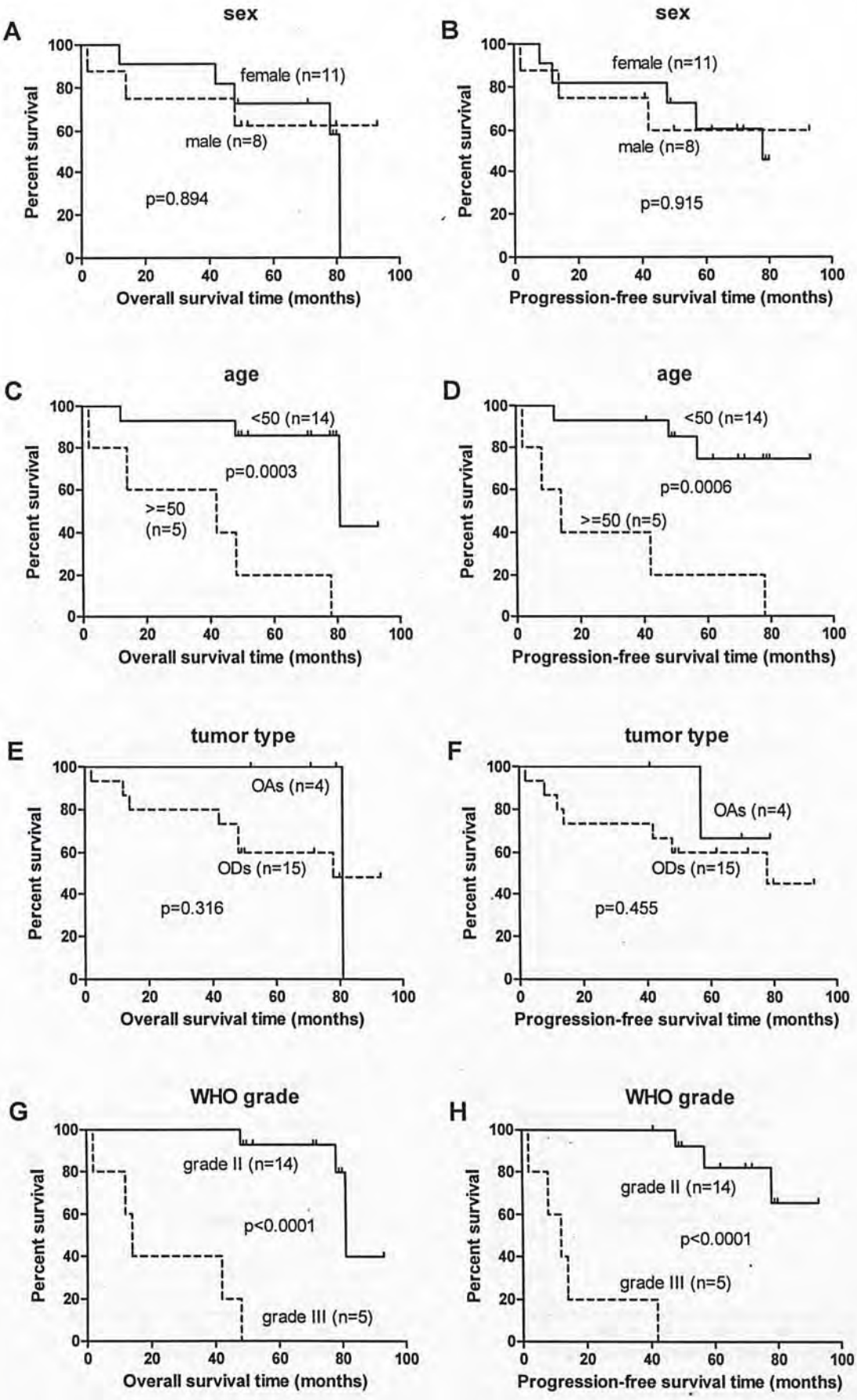
A
sex
Percent survival
female (n=11)
male (n=8)
p=0.894
Overall survival time (months)
B
sex
Percent survival
female (n=11)
male (n=8)
p=0.915
Progression-free survival time (months)
C
age
Percent survival
<50 (n=14)
p=0.0003
>=50
(n=5)
Overall survival time (months)
D
age
Percent survival
<50 (n=14)
p=0.0006
>=50 (n=5)
Progression-free survival time (months)
E
tumor type
Percent survival
OAs (n=4)
ODs (n=15)
p=0.316
Overall survival time (months)
F
tumor type
Percent survival
OAs (n=4)
ODs (n=15)
p=0.455
Progression-free survival time (months)
G
WHO grade
Percent survival
grade II (n=14)
p<0.0001
grade III (n=5)
Overall survival time (months)
H
WHO grade
Percent survival
grade II (n=14)
p<0.0001
grade III (n=5)
Progression-free survival time (months)

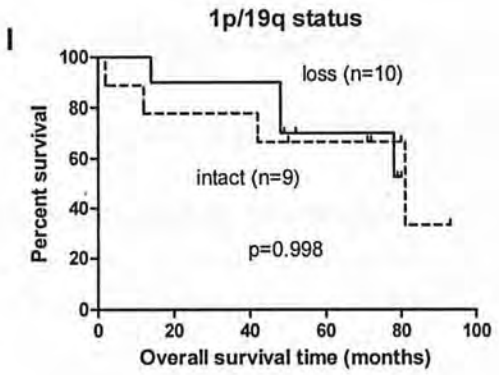
I
1p/19q status
loss (n=10)
intact (n=9)
p=0.998
Percent survival
Overall survival time (months)

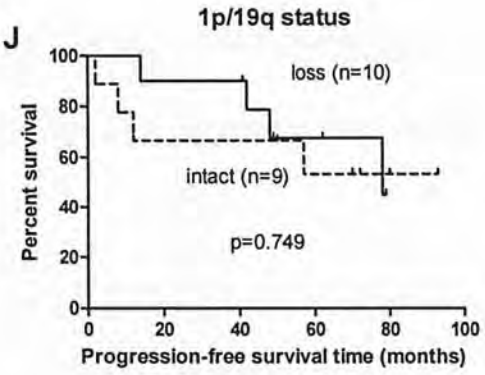
J
1p/19q status
loss (n=10)
intact (n=9)
p=0.749
Percent survival
Progression-free survival time (months)

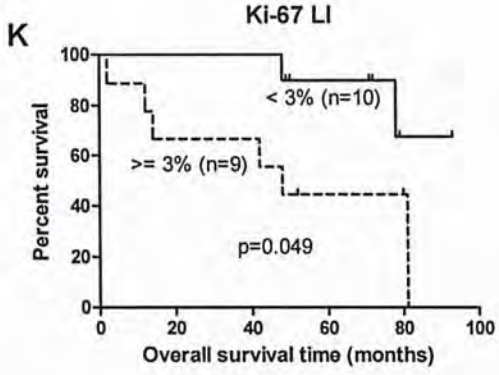
K
Ki-67 LI
< 3% (n=10)
>= 3% (n=9)
p=0.049
Percent survival
Overall survival time (months)

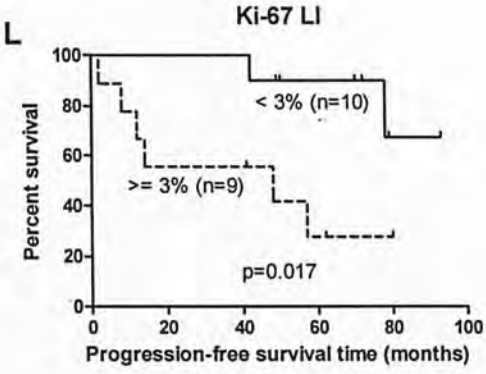
L
Ki-67 LI
< 3% (n=10)
>= 3% (n=9)
p=0.017
Percent survival
Progression-free survival time (months)

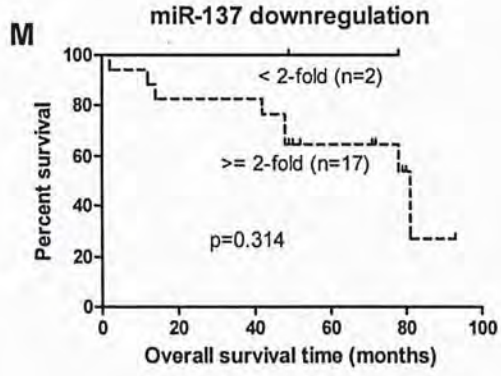
M
miR-137 downregulation
< 2-fold (n=2)
>= 2-fold (n=17)
p=0.314
Percent survival
Overall survival time (months)

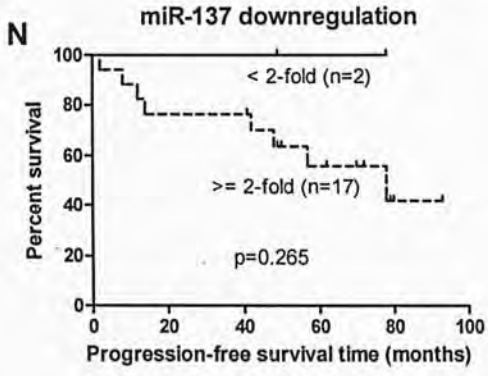
N
miR-137 downregulation
< 2-fold (n=2)
>= 2-fold (n=17)
p=0.265
Percent survival
Progression-free survival time (months)

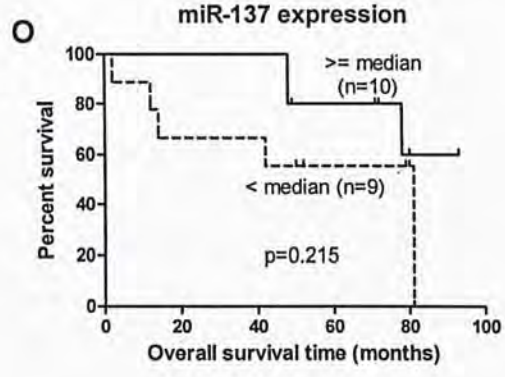
O
miR-137 expression
>= median (n=10)
< median (n=9)
p=0.215
Percent survival
Overall survival time (months)

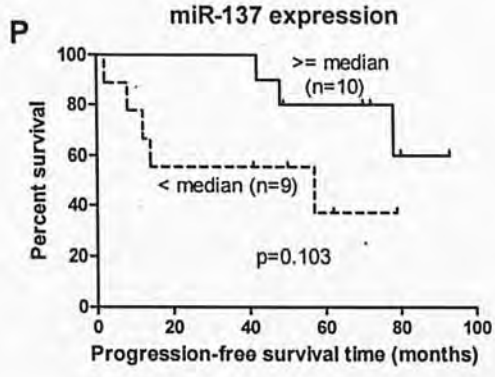
P
miR-137 expression
>= median (n=10)
< median (n=9)
p=0.103
Percent survival
Progression-free survival time (months)

Figure 4.8 Kaplan–Meier overall survival curves (left panel) and progression-free survival curves (right panel) with log-rank test for 19 OT patients with various clinicopathological parameters.

4.2 miR-137 levels in glioma cells after demethylation treatment

Accumulating studies revealed that the promoter CpG islands region of miR-137 was more frequently methylated in oral squamous cell carcinoma (Kozaki *et al.*, 2008; Langevin *et al.*, 2010), gastric cancer cell lines (Ando *et al.*, 2009) and colorectal cancer (Bandres *et al.*, 2009; Balaguer *et al.*, 2010) compared to corresponding normal controls. Moreover, the methylation status of miR-137 promoter was found correlated with its low expression in oral squamous cell carcinoma cells (Kozaki *et al.*, 2008), suggesting promoter methylation may contribute to miR-137 downregulation in cancers. This was supported by several evidence that miR-137 expression was restored after 5-aza-dC or TSA treatment in different cancers (Silber *et al.*, 2008; Bandres *et al.*, 2009; Balaguer *et al.*, 2010), accompanied with the promoter region demethylation (Bandres *et al.*, 2009; Balaguer *et al.*, 2010).

To investigate whether miR-137 was epigenetically regulated in glioma, miR-137 expression in TC620, A172 and U373MG glioma cells was measured followed by 5-aza-dC and/or TSA treatment. It has been determined that miR-137 expression in the 3 cell lines was 478, 15 and 60-fold lower than that in normal brain samples, respectively in section 4.1.1. Quantitative analysis of miR-137 expression revealed a significant increase by 5.0~9.6-fold after TC620 oligodendroglioma cells were incubated with 2, 5 or 10 μm of 5-aza-dC for a period of 2 doubling time

compared to untreated cell ($p<0.001$). When cells were subjected to a subsequent treatment of TSA, the miR-137 expression was further enhanced to 11.2~17.4-fold significantly ($p<0.001$). A dose-dependent effect was observed in mean value of miR-137 expression, but the differences among 2, 5 and 10 μm of 5-aza-dC or 0.33 and 1 μm of TSA was not statistically significant. No significant increase of miR-137 expression was detected in TC620 cells treated only by TSA relative to untreated cells. (Table 4.5, Figure 4.9A)

However, there was no significant change in miR-137 levels in A172 and U373MG cells treated after either drug treatment (Table 4.5, Figure 4.9B-C).

These data suggested that miR-137 expression was reduced by DNA methylation and histone deacetylation in TC620 oligodendroglioma cells. miR-137 expression in A172 and U373MG glioblastoma cells may not be regulated by this mechanism.

Table 4.5 miR-137 expression fold change after 5-aza-dC and/or TSA treatment in 3 glioma cell lines by qRT-PCR relative to untreated cells. Data shown are mean value from 3 independent experiments performed in triplicate.

	Relative miR-137 expression		5-aza-dC (μM)			
			0	2	5	10
TC620	TSA (μM)	0	1.00	5.03	6.44	9.59
		0.33	1.53	11.57	12.02	17.05
		1	1.74	11.18	14.57	17.37
	Relative miR-137 expression		5-aza-dC (μM)			
			0	2	5	10
A172	TSA (μM)	0	1.00	0.94	1.19	1.14
		0.33	1.08	1.06	1.05	0.98
		1	0.89	0.99	1.00	0.83
	Relative miR-137 expression		5-aza-dC (μM)			
			0	2	5	10
U373MG	TSA (μM)	0	1.00	1.09	1.07	0.95
		0.33	1.14	0.95	0.87	1.22
		1	1.12	1.08	1.01	1.02

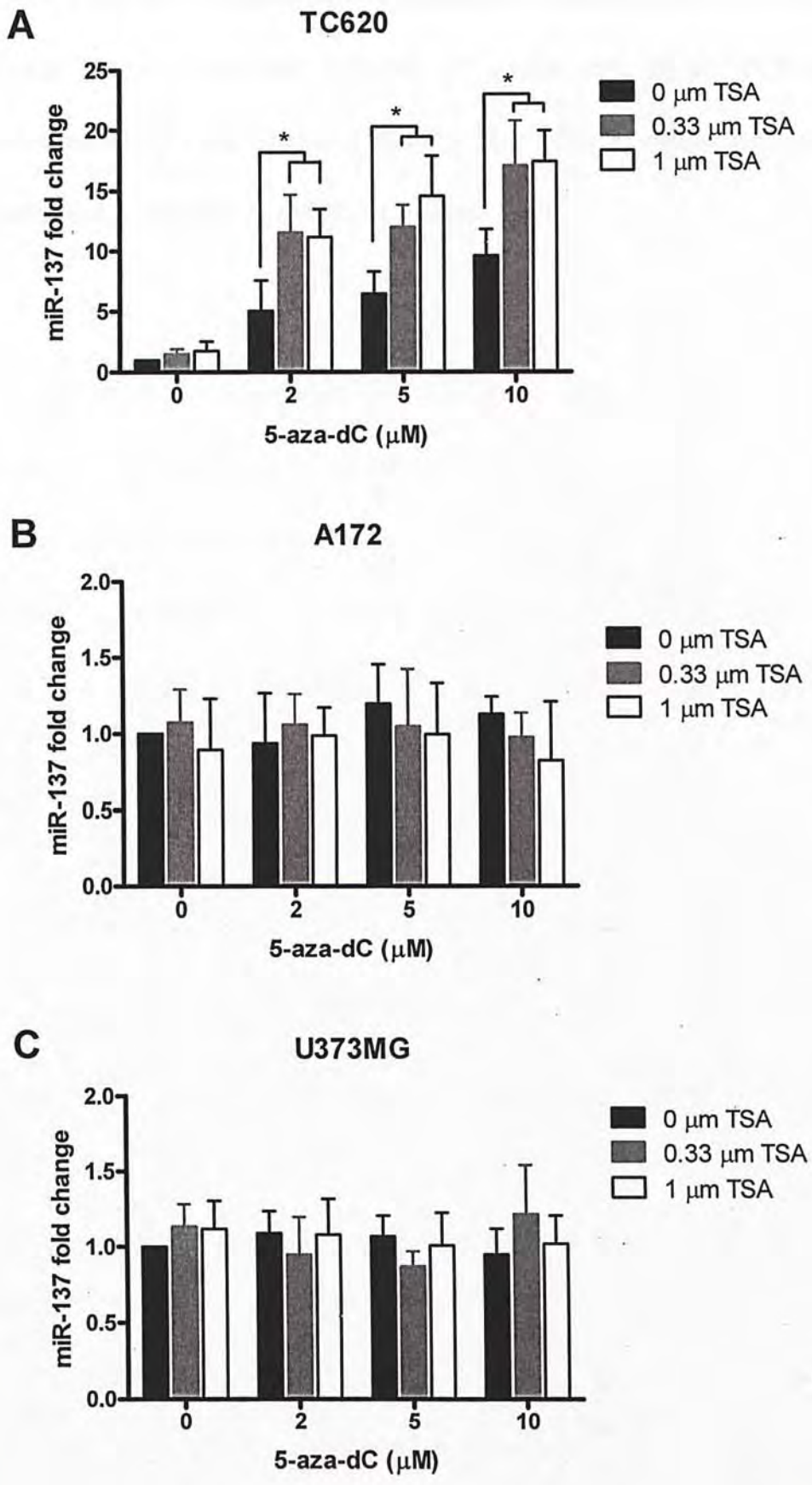
A
TC620
miR-137 fold change
25
20
15
10
5
0
*
*
*
0
2
5
10
5-aza-dC (μM)
0 μm TSA
0.33 μm TSA
1 μm TSA
B
A172
miR-137 fold change
2.0
1.5
1.0
0.5
0.0
0
2
5
10
5-aza-dC (μM)
0 μm TSA
0.33 μm TSA
1 μm TSA
C
U373MG
miR-137 fold change
2.0
1.5
1.0
0.5
0.0
0
2
5
10
5-aza-dC (μM)
0 μm TSA
0.33 μm TSA
1 μm TSA

Figure 4.9 miR-137 expression fold change after 5-aza-dC and/or TSA treatment in TC620 (A), A172 (B) and U373MG (C) glioma cells by qRT-PCR relative to untreated cells. Data represent mean ± SD from 3 independent experiments performed in triplicate. *, $p<0.05$ by student's t test.

4.3 Biological effects of miR-137 overexpression in glioma cells

It has been reported that miR-137 inhibited cell proliferation in glioblastoma (Silber *et al.,* 2008), oral squamous cell carcinoma (Kozaki *et al.,* 2008) and colorectal cancer cells (Liu *et al.,* 2010) and suppressed invasive ability of colon cancer cells (Liu *et al.,* 2010), indicating a role of miR-137 in tumorigenesis. To characterize the biological function of miR-137 in glioma, the effects of miR-137 on glioma cell malignancy variables including cell viability, cell cycle, anchorage-independent growth, cell apoptosis, invasion and differentiation were assessed following ectopic transient expression of miR-137 mimic or negative control miRNA.

4.3.1 Cell growth

4.3.1.1 Cell viability

Our data in section 4.1 revealed the expression of miR-137 was inversely related to Ki-67 level in OTs *in vivo.* Therefore, we firstly tested whether miR-137 affected glioma cell growth. Effect of miR-137 expression on cell viability was assessed by MTT assay in 8 glioma cell lines, including TC620, HOG and GOS-3 OT cells and A172, U87MG, U373MG, LNZ308 and T98G GBM cells. The changes of relative cell viability in subsequent 24, 48, 72 and 96 hours after cells were transfected with miRNA mimic or lipofectamine control were shown in Figure 4.10.

The effect of miR-137 was measured as percentage of cell metabolic activity in cells treated with miR-137 compared to that transfected with negative control miRNA. As shown in Table 4.6 and Figure 4.10, miR-137 induced significant decrease on cell viability at 48~72 hours post-transfection ($p<0.05$). Forced expression of miR-137 mimic resulted in a concordant suppression on cell viability in all 8 cell lines examined. The inhibition ranged from 30% to 74% at 96 hours in these cells.

These data demonstrated that transfection of miR-137 significantly reduced cell growth in all cell lines tested, suggesting that miR-137 has a growth suppressor function in glioma cells.

Table 4.6 Effect of miR-137 on cell viability in 8 glioma cell lines relative to negative control miRNA.

Cell line	Time after transfection (hours)	Cell viability		Cell line	Time after transfection (hours)	Cell viability	
		% of negative control	p value			% of negative control	p value
TC620	24	90.0%	0.107	A172	24	92.3%	0.074
	48	84.5%	0.098		48	89.5%	<0.001
	72	79.7%	0.021		72	85.3%	0.006
	96	52.8%	0.035		96	49.2%	0.001
U87MG	24	85.2%	0.087	U373MG	24	93.7%	0.404
	48	78.9%	<0.001		48	69.2%	<0.001
	72	46.4%	<0.001		72	40.8%	<0.001
	96	32.8%	<0.001		96	26.1%	<0.001
GOS-3	24	91.7%	0.202	HOG	24	101.9%	0.886
	48	77.2%	0.014		48	91.4%	0.017
	72	75.4%	<0.001		72	87.9%	0.008
	96	61.9%	<0.001		96	79.6%	0.003
LNZ308	24	87.0%	0.323	T98G	24	94.4%	0.611
	48	78.2%	<0.001		48	80.3%	0.658
	72	67.9%	<0.001		72	68.6%	<0.001
	96	75.0%	<0.001		96	58.7%	<0.001

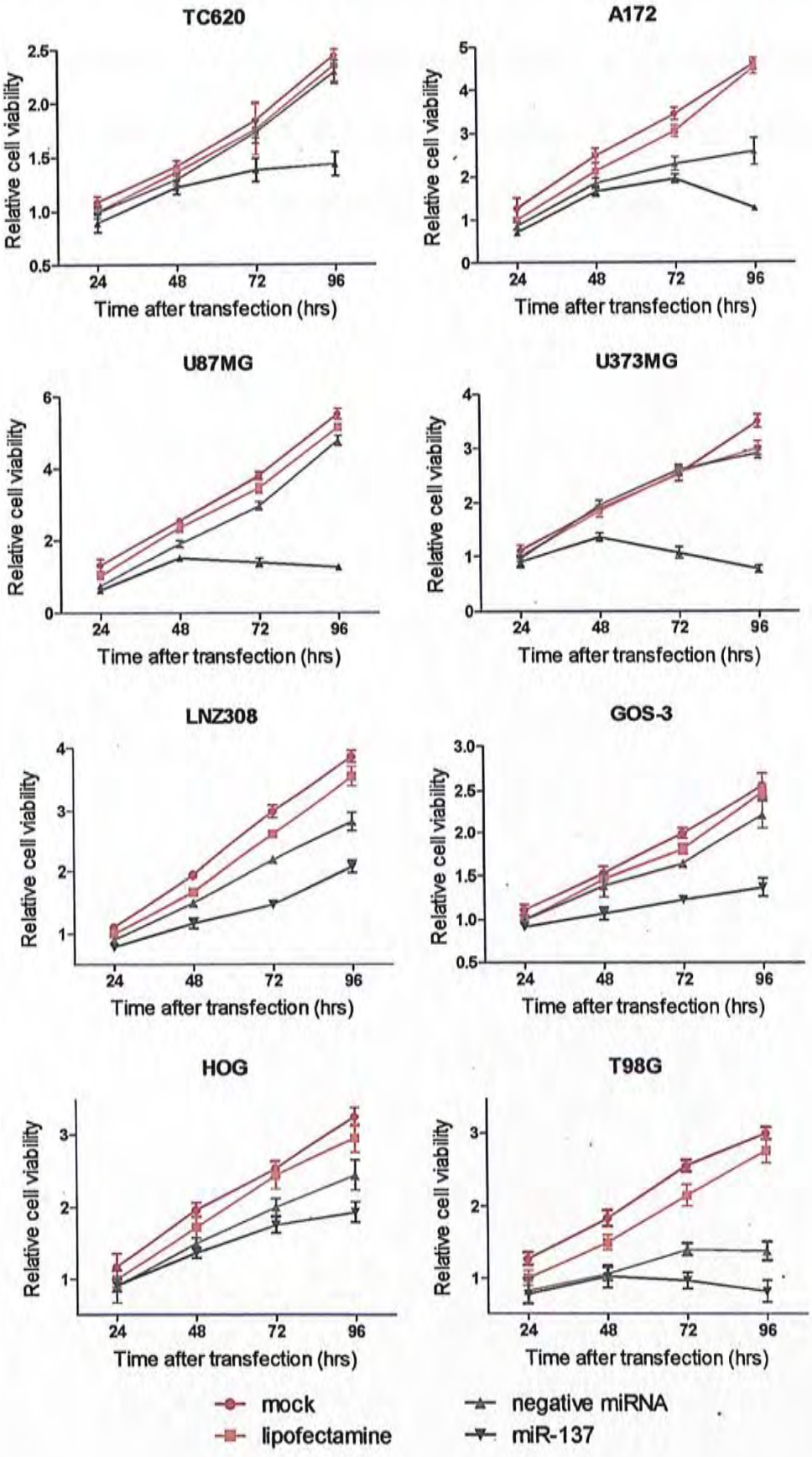
TC620
A172
U87MG
U373MG
LNZ308
GOS-3
HOG
T98G
Relative cell viability
Time after transfection (hrs)
24
48
72
96
mock
lipofectamine
negative miRNA
miR-137

Figure 4.10 Effect of ectopic miR-137 expression on glioma cell viability. Cell metabolic activity of 8 glioma cell lines are measured by MTT assay 24~96 hours after transfected with miR-137, negative control miRNA or lipofectamine treatment. The points showed means ± SD from 3 independent experiments performed in triplicate. Cell viability was significantly reduced in all cell lines.

4.3.1.2 Cell number

The effect of miR-137 on cell growth was further validated by cell count in these glioma cells. Transfection and time of cell number measurement are performed same as above in MTT assay.

As shown in Table 4.7 and Figure 4.11, the cell number of all cell lines tranfected with miR-137 were significantly dropped when compared to cells tranfected with negative control miRNA viability since 48~72 hours post-transfection ($p<0.05$). The inhibitory effect ranged from 40% to 64% at 96 hours in these cells. Consistent with data from MTT assay in section 4.3.1.1, this further confirming that ectopic expression of miR-137 suppressed proliferation of glioma cells.

Table 4.7 Effect of miR-137 on cell number in 8 glioma cell lines relative to negative control miRNA.

Cell line	Time after transfection (hours)	Cell number		Cell line	Time after transfection (hours)	Cell number	
		% of negative control	p value			% of negative control	p value
TC620	24	82.4%	0.064	A172	24	102.2%	0.776
	48	75.8%	<0.001		48	69.4%	0.010
	72	55.2%	<0.001		72	71.0%	0.008
	96	45.0%	<0.001		96	39.9%	<0.001
U87MG	24	80.5%	0.072	U373MG	24	91.2%	0.396
	48	69.5%	<0.001		48	81.0%	0.023
	72	55.2%	<0.001		72	46.6%	<0.001
	96	40.3%	<0.001		96	36.0%	<0.001
GOS-3	24	94.7%	0.583	HOG	24	95.7%	0.694
	48	75.4%	0.003		48	89.1%	0.259
	72	62.7%	<0.001		72	76.9%	0.012
	96	60.1%	0.015		96	62.0%	<0.001
LNZ308	24	96.6%	0.762	T98G	24	93.6%	0.604
	48	91.8%	0.344		48	88.1%	0.021
	72	79.7%	0.005		72	79.4%	0.004
	96	67.7%	<0.001		96	68.3%	0.015

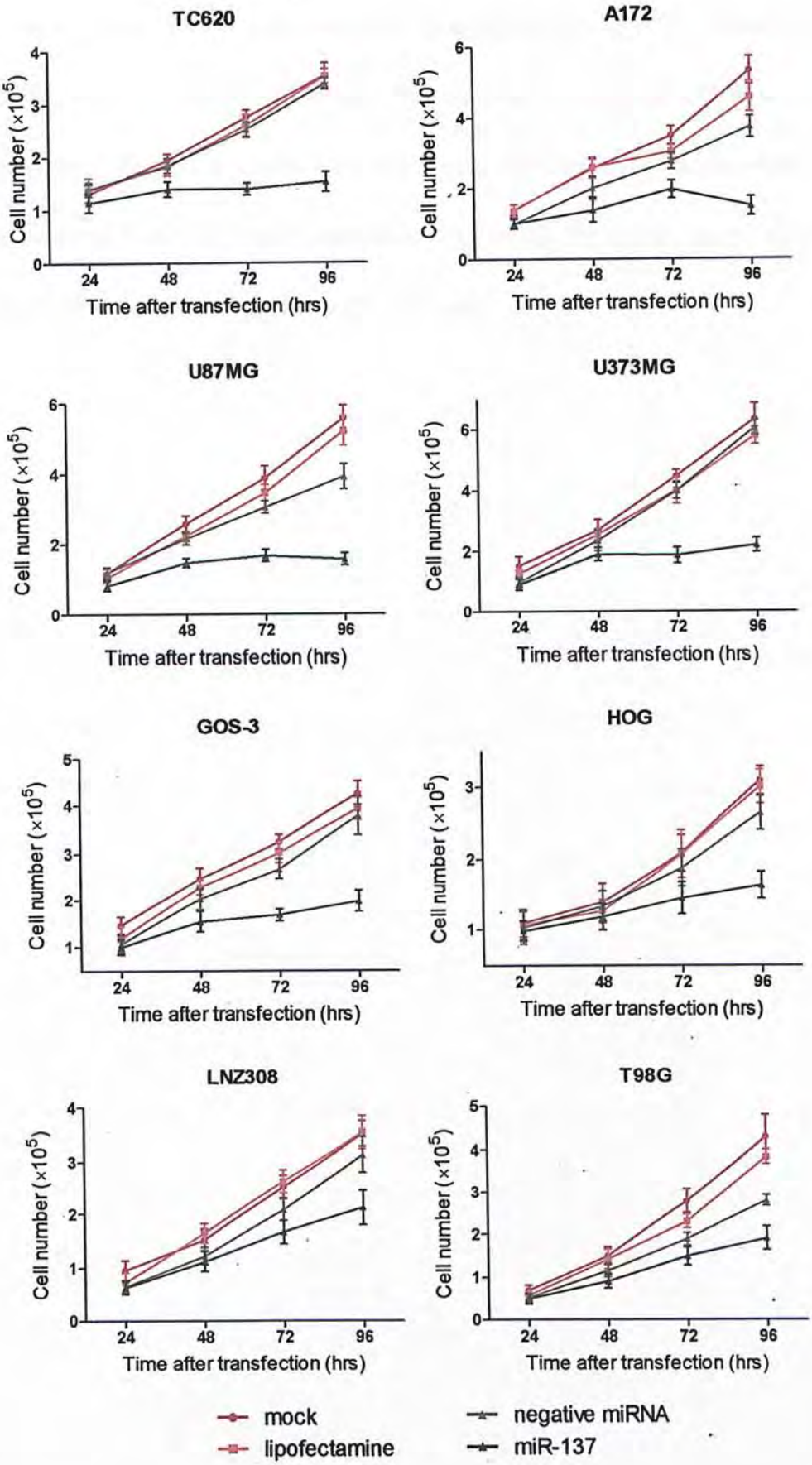
TC620
A172
U87MG
U373MG
GOS-3
HOG
LNZ308
T98G
Cell number (×10^5)
Time after transfection (hrs)
24
48
72
96
mock
lipofectamine
negative miRNA
miR-137

Figure 4.11 Effect of ectopic miR-137 expression on glioma cell growths. Growth curves represent glioma cells and cells transfected with miR-137 mimic, miRNA negative control or lipofectamine only. The numbers of viable cells at 24 to 96 hours after transfection were assessed by cell count. All lines show suppression of cell growth upon miR-137 forced expression. The points showed means ± SD from 3 independent experiments performed in triplicate.

4.3.1.3 Cell cycle analysis

Given that miR-137 inhibited glioma cell growth obviously *in vitro*, we tried to determine the potential mechanism by cell cycle and apoptosis analyses. Four glioma cells (TC620, A172, U87MG and U373MG), which showed more reduction of cell growth following miR-137 transfection, were transfected with miR-137 mimic, negative control. BrdU incorporation at following 24~96 hours was determined by a colorimetric immunoassay to quantify DNA synthesis during cell proliferation.

As shown in Table 4.8 and Figure 4.12, the cell proliferative activity dropped continuously in miR-137 transfected TC620 and U87MG cells compared with negative control since 24 hours post-transfection ($p<0.05$). Similar effect was observed in A172 and U373MG cells, whereas the significant difference started from 48 hours ($p<0.05$). DNA synthesis was decreased by 24.7% to 86.2% in TC620, 8% to 56.9% in A172, 47.6% to 86.2% in U87MG, and 1.5% to 84.0% in U373MG during 1~4 days afterwards.

Moreover, a flow cytometry analysis showed that G0/G1 cell cycle arrest was induced in miR-137 transfected TC620 cells at 48 hours post-transfection. Above data indicated that miR-137 suppressed cell proliferation by blocking DNA replication in cell cycle progression.

Table 4.8 Effect of miR-137 on DNA synthesis in 4 glioma cell lines relative to negative control miRNA by BrdU incorporation assay.

Cell line	Time after transfection (hours)	BrdU incorporation	
		Average % of negative control	p value
TC620	24	75.3%	0.009
	48	44.0%	<0.001
	72	22.0%	<0.001
	96	13.8%	<0.001
A172	24	92.0%	0.181
	48	55.8%	0.004
	72	50.2%	<0.001
	96	43.1%	0.010
U87MG	24	52.4%	<0.001
	48	40.0%	0.003
	72	19.2%	<0.001
	96	13.8%	<0.001
U373MG	24	98.5%	0.854
	48	41.6%	<0.001
	72	24.0%	<0.001
	96	16.0%	<0.001

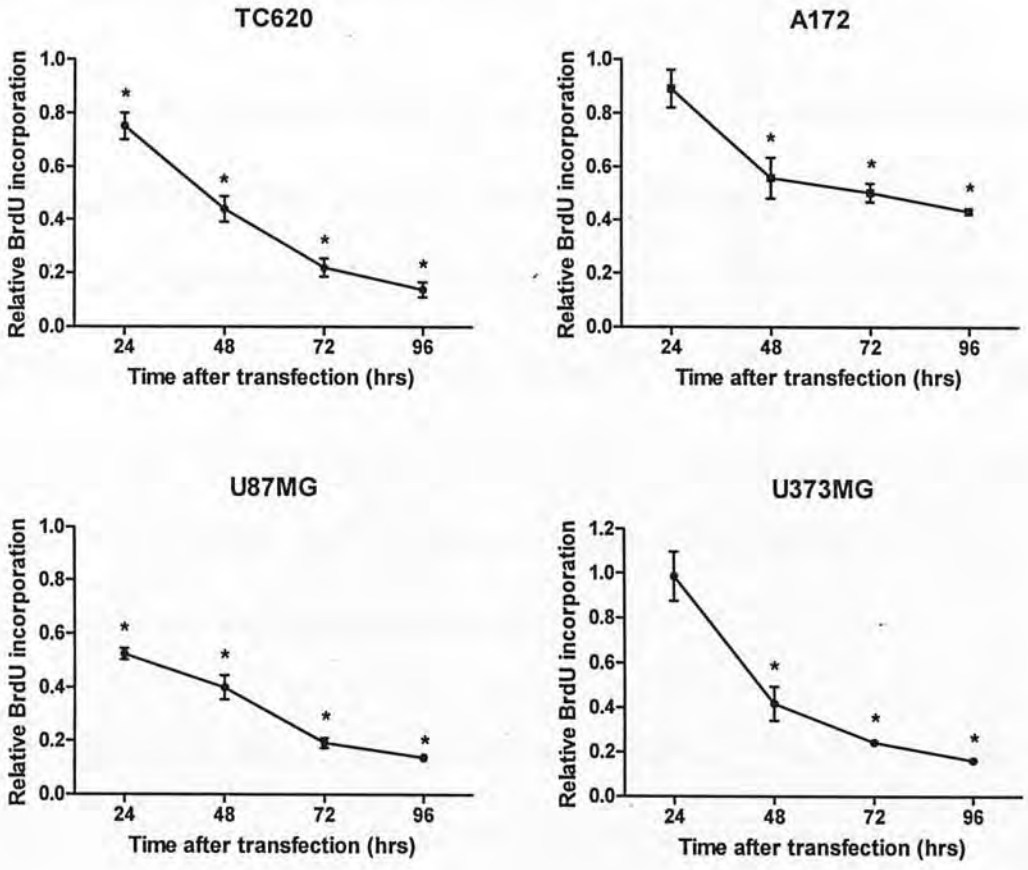

Figure 4.12 Effect of ectopic miR-137 expression on glioma cell DNA synthesis. By BrdU incorporation assay, the relative proliferating cells at 24 to 96 hours after transfection were assessed. All lines show suppression of cell proliferation following miR-137 forced expression. The points showed means ± SD from 3 independent experiments performed in triplicate. *, $p<0.05$ between miR-137 and negative control miRNA transfected group by student's t test.

4.3.2 Anchorage-independent cell growth

To determine whether the miR-137 would aggravate the transforming potential of glioma cells, anchorage-independent soft agar growth assay was performed on TC620, A172, U87MG and U373MG glioma cells. In our preliminary test for colony forming ability of these cells in soft agar, cell colonies were observed in all cell lines except for U373 MG cells in soft agar after a incubation time of 14 days (Representative images of colony showed in Figure 4.13). Therefore, TC620, A172 and U87MG cells were included in this assay.

miR-137 or negative control miRNA was transfected into the 3 cell lines and the numbers of colonies formed with diameter larger than 100 μm were counted. It was found that miR-137 was able to reduce the colony forming ability of TC620, A172 and U87MG cells by 80.5%, 71.3% and 75.3% compared with the negative control, respectively ($p<0.001$, Figure 4.14). This result suggested that miR-137 could inhibit the anchorage-independent cell growth in glioma cells.

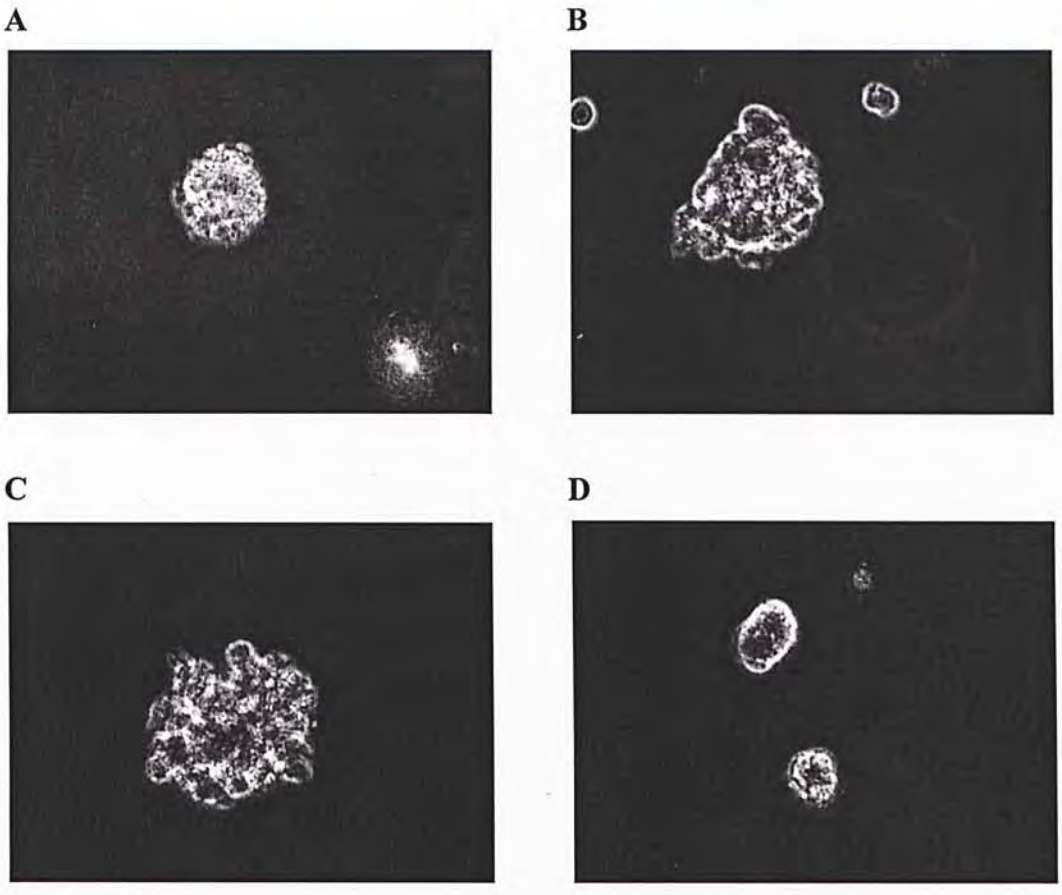

Figure 4.13 Microscopic views of glioma cell colonies in soft agar. Colonies were observed in TC620 (A), A172 (B), U87MG (C), but not U373MG (D) cells under microscope at 200× magnification.

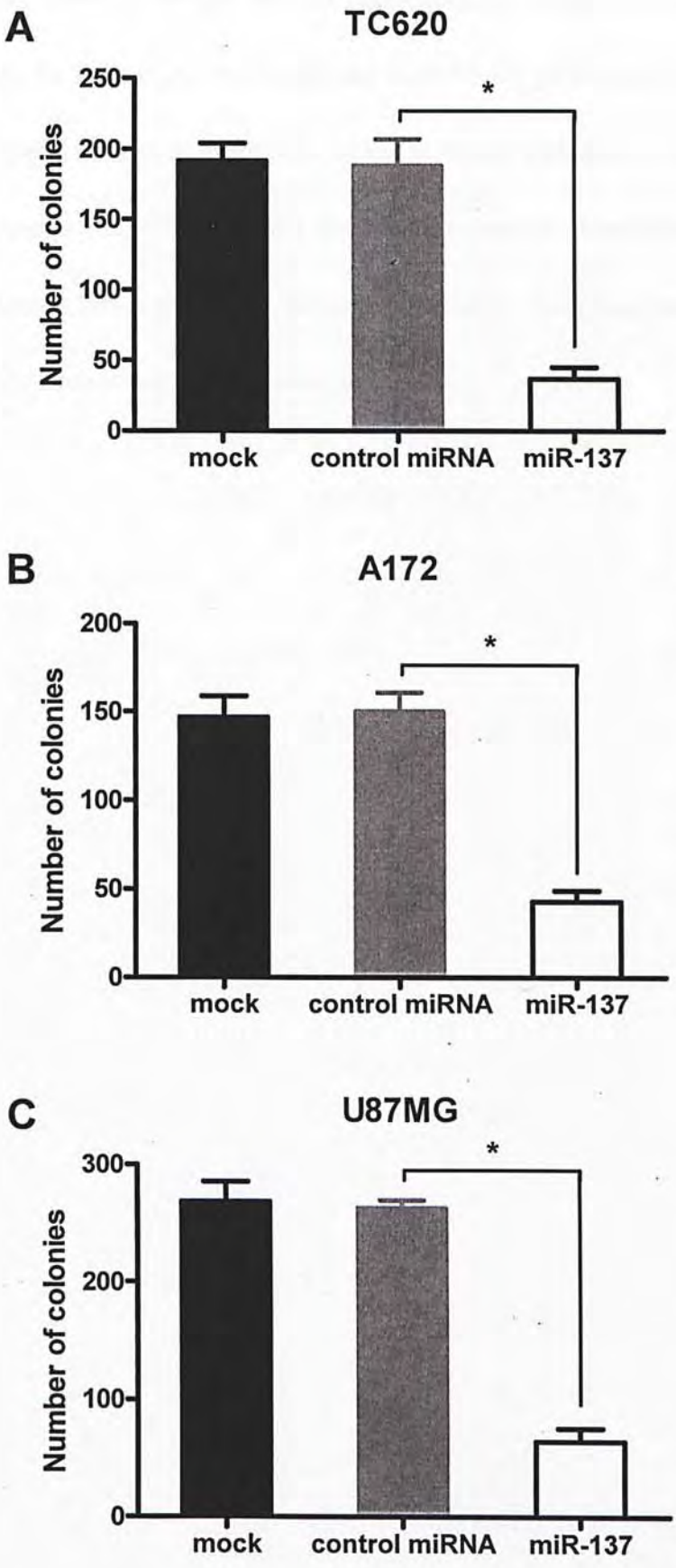
A
TC620
Number of colonies
250
200
150
100
50
0
*
mock
control miRNA
miR-137
B
A172
Number of colonies
200
150
100
50
0
*
mock
control miRNA
miR-137
C
U87MG
Number of colonies
300
200
100
0
*
mock
control miRNA
miR-137

Figure 4.14 Effect of ectopic miR-137 expression on number of colonies formed in glioma cells. In TC620 (A), A172 (B) and U87MG (C) glioma cells transfected with miR-137, negative control miRNA or mock. Colonies with sizes of greater than 100 μm were counted. miR-137 led to a significant reduction in numbers of colonies in all 3 cell lines when compared to the negative control. Results represent the average of three independent experiments done in triplicate. *, $p<0.001$.

4.3.3 Cell apoptosis

Besides induction of cell cycle arrest, we also sought to identify whether miR-137 was involved in glioma cell apoptosis, which may also contribute to cell growth suppression. An apoptotic marker, cleaved PARP, was examined by western blot in glioma cells following transfected with miR-137 compared to negative control. The protein level of cleaved PARP elevated gradually in TC620 and A172 cells in subsequent 4 days following miR-137 transfection. A dramatic enhancement of cleaved PARP was observed at 48 hours in U87MG and U373MG cells, whereas no further induction at 96 hours (Figure 4.15). The data indicated that miR-137 forced expression resulted in cellular apoptosis in glioma cells.

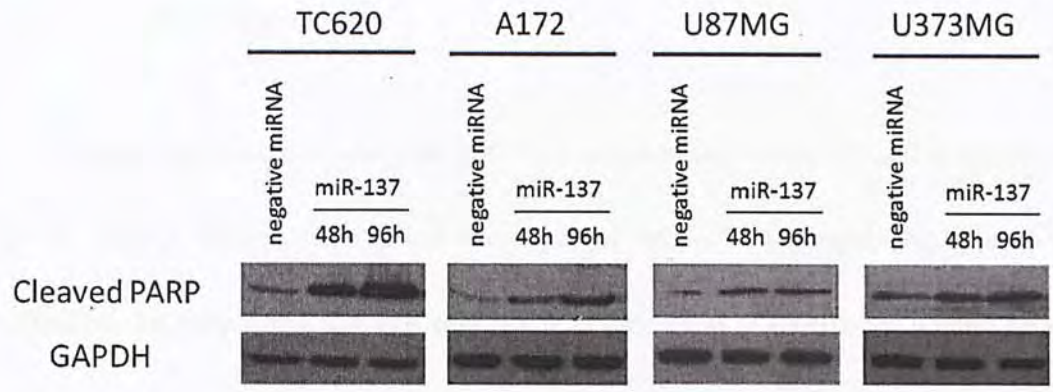

Figure 4.15 Effect of ectopic miR-137 expression on cleaved PARP expression in glioma cells. Protein levels of cleaved PARP were remarkably up-regulated following miR-137 ectopic expression compared to negative control miRNA in 4 glioma cells. GAPDH was included as loading control.

4.3.4 Cell motility

It has been demonstrated that miR-137 could block colorectal cell invasion (Liu *et al.,* 2010). Hence, to explore the roles of miR-137 in regulating glioma cell motility, we examined the cell migration ability of A172 cells by wound healing assay. As shown in Figure 4.16, the rate of wound closure was significantly slower in miR-137 transfected cells than negative miRNA transfectants at 16 hours ($p=0.040$). Note that negative miRNA tranfected cells closed the wound at 32 hours, miR-137 transfected cells closed 67% of the wound. This indicates that forced miR-137 expression led to suppression of glioblastoma cell migration.

To further study the effect of miR-137 on glioma cell invasive capacity, matrigel invasion assay was also performed. Number of invaded cell in response to FBS enriched medium was significantly reduced by 38.9%~52.6% in all glioma cell lines tested upon ectopic miR-137 expression (Table 4.9 and Figure 4.17). It indicated that glioma cell invasion into extracellular matrix was affected by miR-137. Together, these results supported that miR-137 overexpressed glioma cells have lower ability of both migration and invasion.

A

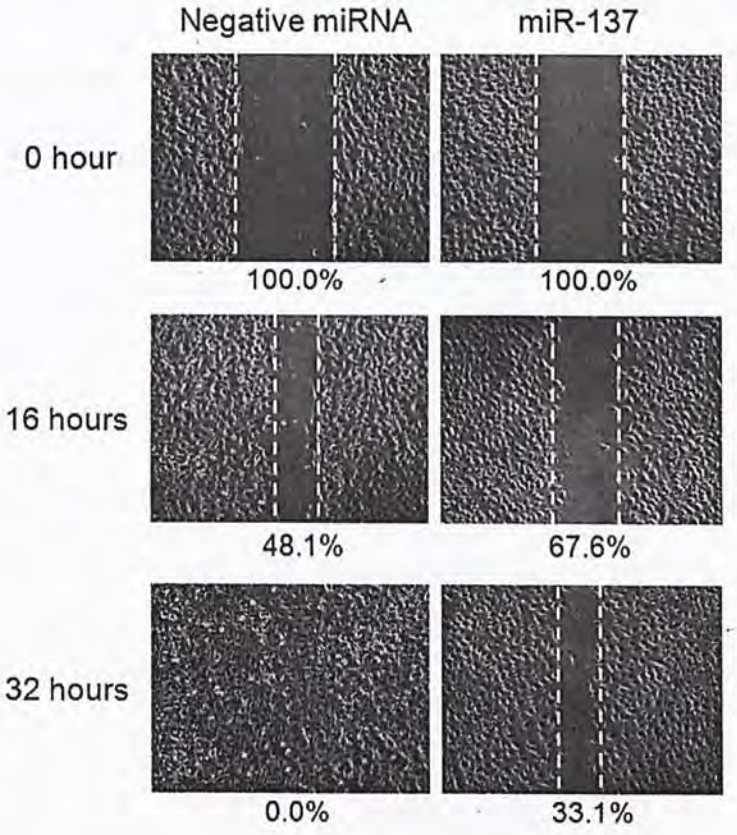

B

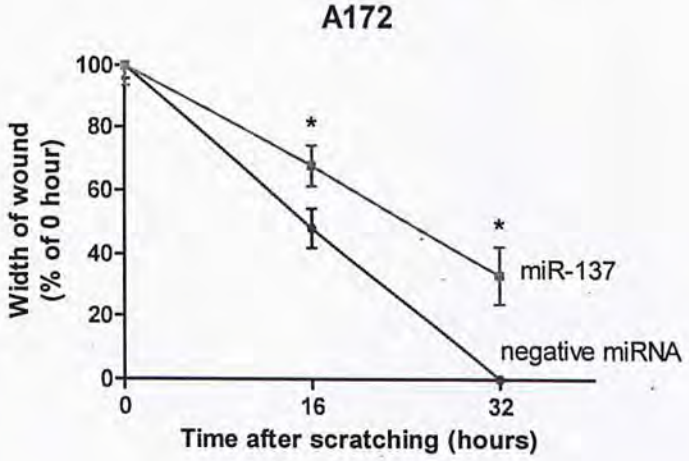

Figure 4.16 Effect of miR-137 on A172 GBM cell migration. In wound healing assay, wound was induced using a yellow pipette tip on the full confluent monolayer A172 cells transfected with miR-137 or negative control miRNA. A. The rate of wound closure was monitored at different time points afterwards. Representative

photos were taken under 40× magnifications. Lines indicated the differential migration rate of cells. B. The migration rate was significant slower in miR-137 transfected cells. *, $p<0.05$.

Table 4.9 Effect of miR-137 overexpresssion on cell invasion of 4 glioma cell lines by matrigel invasion assay.

Cell line	Mean number of invaded cells			% of negative control	p value
	mock	negative miRNA	miR-137		
TC620	238.3	251.2	153.4	61.1%	<0.001
A172	128.0	117.3	60.8	51.8%	<0.001
U87MG	329.0	321.1	167.4	52.1%	<0.001
U373MG	226.3	223.6	105.9	47.4%	<0.001

A

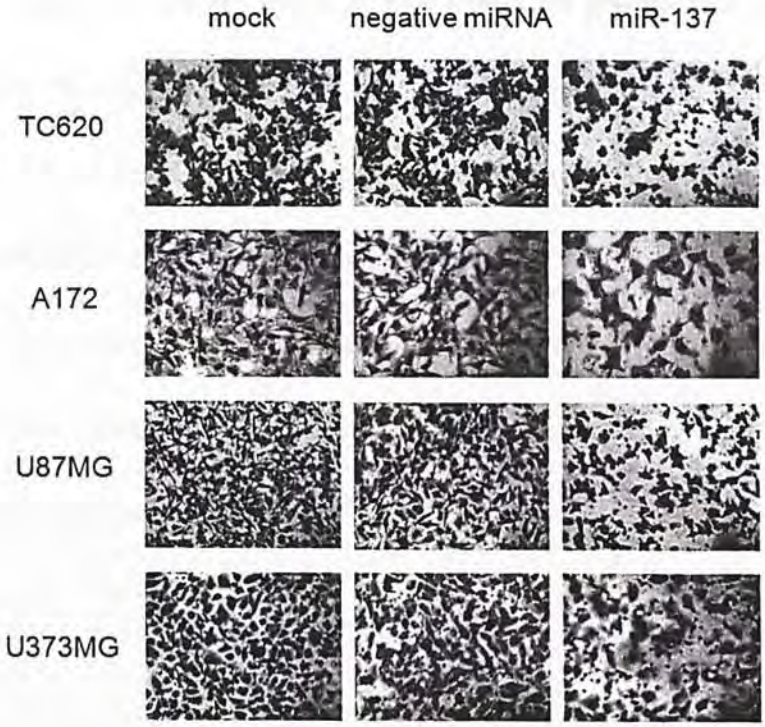
mock
negative miRNA
miR-137
TC620
A172
U87MG
U373MG

B

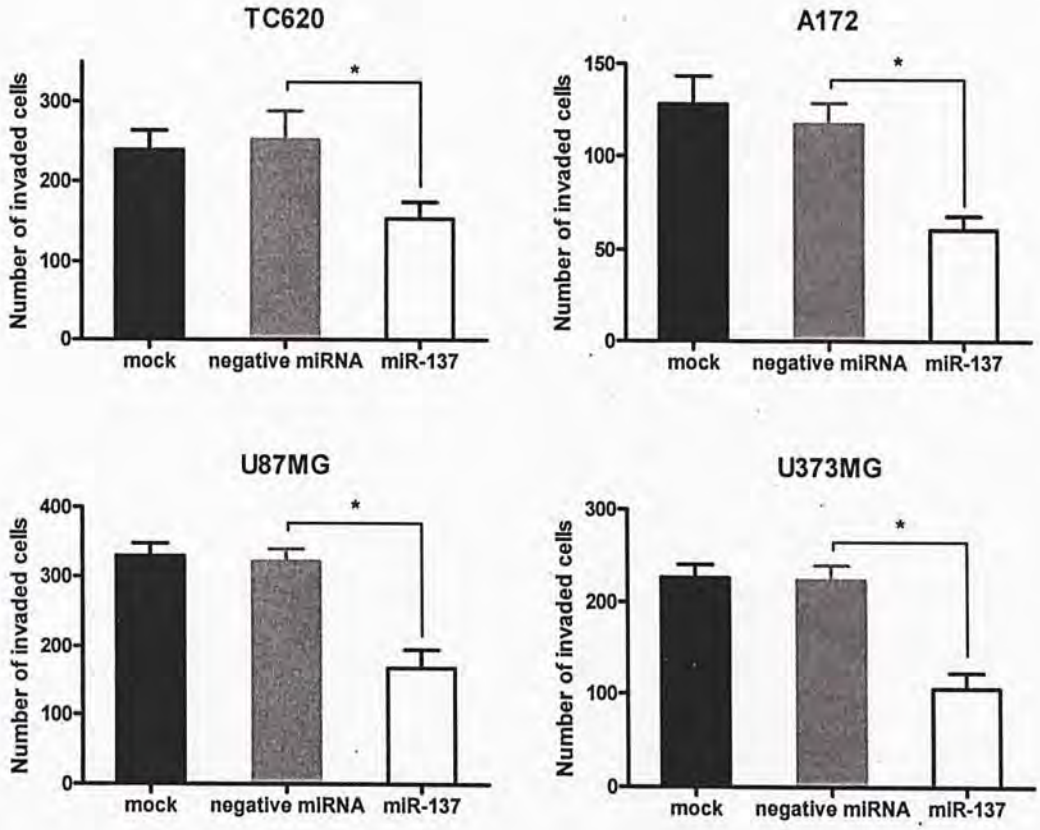
TC620
A172
U87MG
U373MG
Number of invaded cells
mock
negative miRNA
miR-137
*

Figure 4.17 Effect of ectopic miR-137 expression on glioma cell invasion. The invasive ability of 4 glioma cell lines after transfected with miR-137 or negative control miRNA were assessed by matrigel invasion assay. Cells invaded to the lower surface of matrigel-coated chambers were quantified 16 hours after plating. A. Invaded cells were stained and observed under microscopy at 40× magnification. B. Significant fewer cells were able to invade after transfected with miR-137 than negative control miRNA transfectants. *, $p<0.001$.

4.3.5 Cell differentiation

To investigate the role of miR-137 in cell differentiation, neuronal and astrocyte marker were determined by western blot. β-tubulin III protein level was enhanced after miR-137 restoration in U87MG and U373MG cells compared to cells transfected with negative control miRNA. No change in GFAP expression was observed in any of these cells. Meanwhile, morphology of cells was also monitored. U87MG cells rounded up after miR-137 transfection compared to cells transfected with negative control miRNA. The well-defined boundary of TC620 cells was disrupted and cellular protrusion was observed. No prominent morphological change was observed in A172 and U373MG cells (Figure 4.18). This suggested that miR-137 may play a role in neuronal differentiation in glioblastoma cells.

A

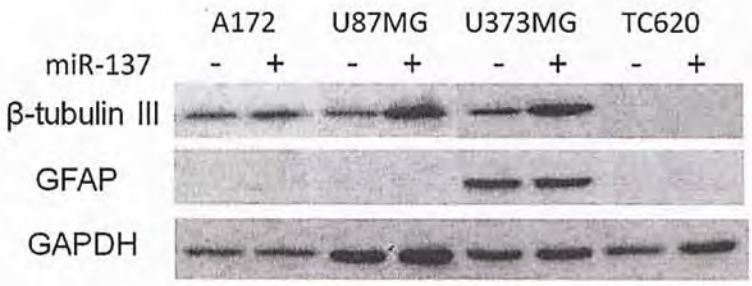

B

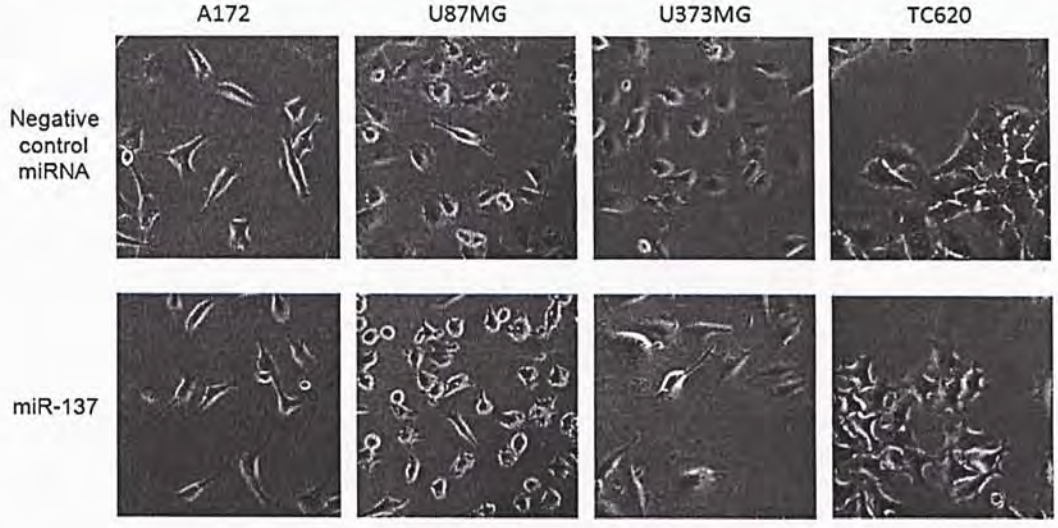

Figure 4.18 Effect of ectopic miR-137 expression on neuronal and astrocytic marker expression in glioma cell. A. Protein levels of neuron-specific β-tubulin III and astrocyte marker, GFAP by western blot 48 hours after transfection with miR-137 or negative control miRNA. B. Microscopic views of cell morphology at 48 hours. MiR-137 enhanced expression of β-tubulin III in U87MG and U373MG glioblastoma cells, without obvious neuronal-like morphological alteration.

4.4 Identification of miR-137 targets

Above studies revealed multiple roles of miR-137 in glioma cells. To further elucidate the mechanism underlying observed miR-137 function, we attempted to identify downstream targets of miR-137 in gliomas by a series of computational and experimental approaches. Briefly, potential targets were obtained from *in silico* prediction algorithms followed by experimental validation, such as dual-luciferase assay, qRT-PCR and western blot to determine whether miR-137 bind to the predicted targets and induce a negative regulation.

4.4.1 *In silico* prediction of potential miR-137 targets

Bioinformatic analysis of potential miR-137 target sites was performed by 4 commonly used computational prediction algorithms, microCosm, miRanda, PicTar and TargetScan

To reduce false positive results, we retrieved putative target genes with high level complementarity between the seed region of miR-137 and miRNA recognition elements (MREs) in 3'UTR, which were predicted by at least 2 of the programs. The predicted targets whose MRE was conserved across species (human, mouse, rat, dog and chicken) are also preferred. In addition, in order to address our observation of miR-137 function in glioma cell, we search for candidates which were previously observed overexpressed in glioma or implicated in oncogenic behaviors, such as cell

proliferation, apoptosis, or migration.

Based on these criteria, 6 potential miR-137 recognition sites located in 3'UTR of 5 gene transcripts were selected for further validation (Table 4.10). Chosen miR-137 target candidates were CSE1 chromosome segregation 1-like (yeast) (*CSE1L*), v-erb-a erythroblastic leukemia viral oncogene homolog 4 (avian) (*ERBB4*), neuropilin 1 (*NRP1*), cell division cycle 42 (*CDC42*) and v-akt murine thymoma viral oncogene homolog 2 (*AKT2*). In the following sections, different experiments were performed to validate interaction and functional inhibition of miR-137 on potential targets.

Table 4.10 5 miR-137 target candidates by bioinformatic analysis.

Predicted target	Predicted pairing of target region (top) in 3'UTR and miR-137 (bottom)	Conservation of MREs among species	Number of predicted programs	Related function
CSE1L	5' ...UUCAAAUCUGUAAUC---AGCAAUAA... 3' GAUGCGCAUAAGAAUUCGUUAU	human, mouse, rat, dog	4	proliferation, apoptosis, invasion
ERBB4	5' ...UUUGGAUUUUGAAUCAAGCAAUA... 3' GAUGCGCAUAAGAA--UUCGUUAU	human, mouse, rat, dog, chicken	2	proliferation
NRP1	5' ...UCAGCUCUGUUUACG-AAGCAAUA... 3' GAUGCGCAUAAGAAUUCGUUAU	human, mouse, rat, dog, chicken	2	proliferation, angiogenesis
CDC42	5' ...UCGGCAUCAUACUAAAAGCAAUG... 3' GAUGCGCAUAAGAA-UUCGUUAU	human, mouse, rat, dog, chicken	2	cell cycle, apoptosis, migration
AKT2	5' ...CUAUGGGGGCAGAAAAGCAAUAA... 3' GAUGCGCAUAAGAAUUCGUUAUU	human, mouse, rat, dog	3	proliferation, apoptosis, metastasis
	5' ...UAUUUGUACGGUACAAGCAAUAA... 3' GAUGCGCAUAAGAAUUCGUUAUU	human, mouse, rat, dog	3	

4.4.2 Experimental validation of miR-137 targets by dual-luciferase reporter assay

Having identified 5 potential miR-137 targets using multiple computational algorithms, we would like to screen and validate the target candidates by several experimental approaches in subsequent sections. First of all, luciferase reporter assay was employed to test whether miR-137 bind to predicted 3'UTR region of target candidates directly.

In this assay, each predicted miR-137 MRE region located in 3'UTR of potential target genes was cloned downstream of the firefly luciferase gene in pMIR-REPORTER vector, respectively. Therefore, the luciferase activity indicated the gene expression, which may be regulated by the interaction of the miR-137 with the potential binding sites after miR-137 and the construct were both introduced into glioma cells. Decreased firefly luciferase activity when miR-137 was transfected demonstrated a direct inhibitory effect of miR-137 to the expression of corresponding target gene.

According to our previously observation, LNZ308 cells showed the lowest endogenous miR-137 expression among the set of glioma cell lines studied. Ectopic miR-137 expression may probably result in a noticeable effect in this cell line, so that it was chosen as the cell line model to perform this assay.

LNZ308 cells was co-transfected with miR-137 mimic or negative control miRNA, firefly luciferase reporter construct containing predicted miR-137 binding site, along with a *renilla* luciferase vector, which serve as a control for normalization of transfection efficiency. The measurement of luciferase activity demonstrated that forced miR-137 expression exerted a significantly reduced normalized firefly luciferase activity by 44% and 40% on the constructs harboring CSE1L and ERBB4 3'UTR region relative to negative control miRNA, respectively ($p<0.001$). Meanwhile, no significant suppression of luciferase signal was observed on original vector and constructs containing 3'UTR of other genes upon miR-137 ectopic expression (Figure 4.19). This suggested that only potential miR-137 binding sites in 3'UTR of CSE1L and ERBB4 were probably targeted by miR-137 among the 6 potential target sites evaluated,

To further validate the direct interaction, we introduced a 7-nucleotide and a 8- nucleotide mutation on miR-137 binding sites of CSE1L and ERBB4 corresponding to seed region of miR-137, which may be crucial in miRNA target recognition (Figure 4.20A). The wild-type or mutant vector was cotransfected into LNZ308 cells with miR-137 or negative control miRNA, as well as *renilla* luciferase reporter vector. As shown in Figure 4.20B, miR-137 significantly decreased the relative luciferase activity of wild-type CSE1L and ERBB4 3'UTR, whereas the inhibitory effect was abolished when the 3'UTR are mutated. Taken together, these findings suggested that CSE1L and ERBB4 are direct

downstream targets of miR-137 in glioma cells. Moreover, the pairing between miR-137 seed region and 3'UTR is important to this regulation.

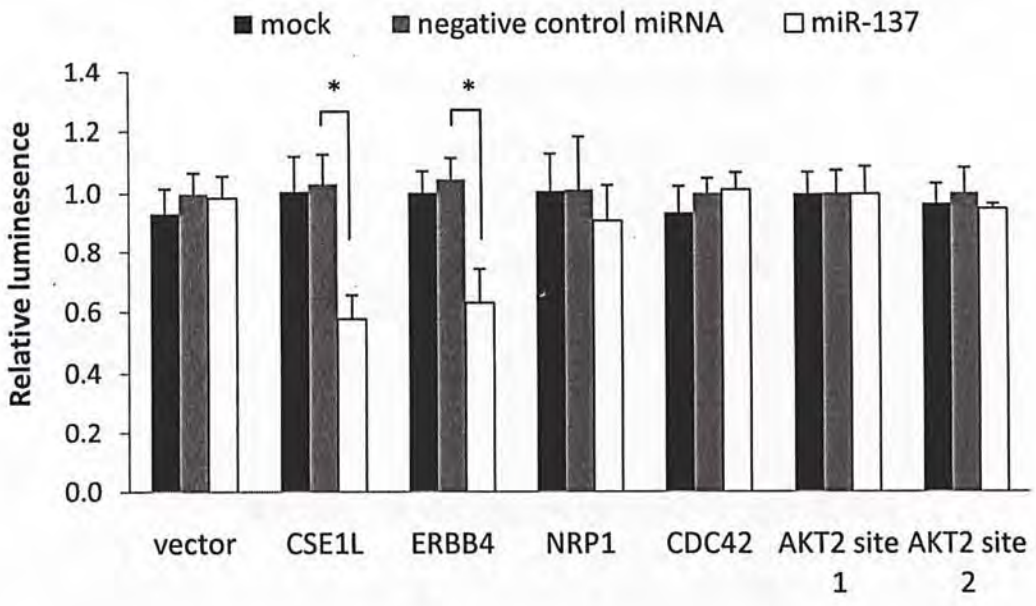

Figure 4.19 Dual-luciferase reporter assay for 5 miR-137 target candidates. LNZ308 cells were cotransfected with luciferase reporter constructs containing predicted miR-137 MRE, miR-137 mimic or negative control miRNA, as well as *renilla* luciferase vector. Firefly luciferase activity was determined and normalized with *renilla* luciferase activity. A significant decrease of luciferase activity was detected in LNZ308 cells cotransfected with miR-137 and construct harboring predicted miR-137 MRE in CSE1L and ERBB4. For original vector and constructs containing 3'UTR of other genes, miR-137 showed no significant effect on luciferase activity. *, $p<0.05$.

A

CSE1L	5'	...UUCAAAUCUGUAAUCAGCAAUAA...	3'
		||||||||	
hsa-miR-137	3'	GAUGCGCAUAAGAAUUCGUUAUU	5'
CSE1L-MUT	5'	...UUCAAAUCUGUAAUCUCGUUAUA...	3'
ERBB4	5'	... UUGGAUUUUGAAUCAAGCAAUAU...	3'
		||||||||	
hsa-miR-137	3'	GAUGCGCAUAAGAAUUCGUUAUU	5'
ERBB4-MUT	5'	... UUGGAUUUUGAAUCUUCGUUAUU...	3'

B

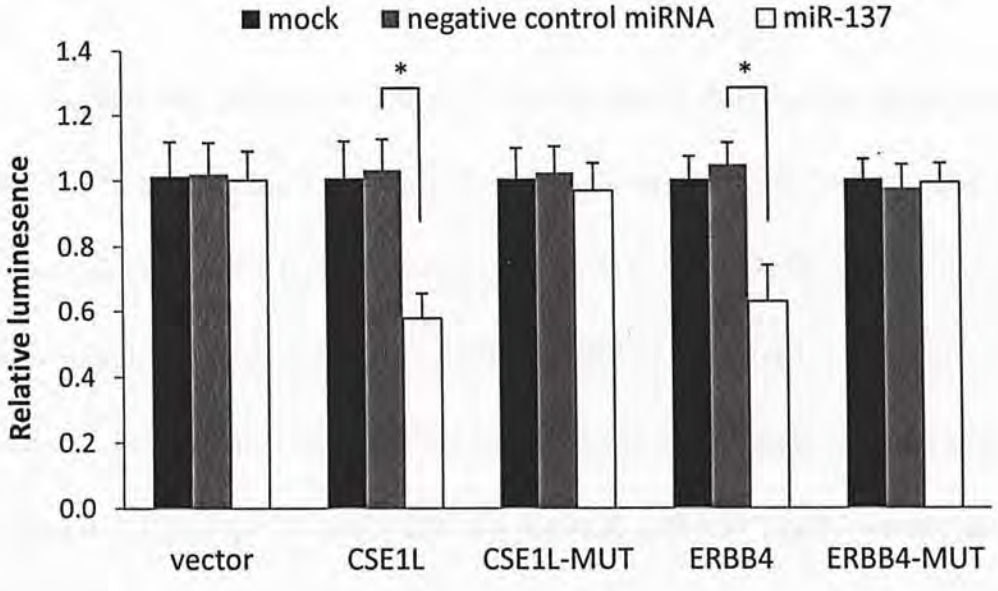

Figure 4.20 Validation of interaction between miR-137 and predicted binding sites in 3'UTR of CSE1L and ERBB4 by dual-luciferase reporter assay. A. miR-137 and predicted binding sequences in CSE1L and ERBB4 3'UTR. Mutated binding sites (underlined) were designed corresponding to the miR-137 seed region by site-directed mutagenesis. Vertical lines indicate Watson-Crick base pairing. B. Relative luminescence of LNZ308 cells following co-transfected with miR-137 or negative control miRNA along with wild type or mutated CSE1L or ERBB4 reporter constructs. *, $p<0.001$.

4.4.3 Expression of miR-137 candidate targets, CSE1L and ERBB4 in glioma cells

Having demonstrated that miR-137 interacted with the potential binding sites of CSE1L and ERBB4, we tried to investigate the involvement of CSE1L and ERBB4 by detecting their mRNA expression levels in 10 glioma cell lines firstly by qRT-PCR analysis.

Our previous data in section 4.1.1 has revealed a common deregulation of miR-137 in all 10 glioma cell lines. In the same series of cell lines, 8 out of 10 showed elevated CSE1L mRNA expression by 2- to 5.4-fold compared to normal brain samples (Figure 4.21A). In contrast, ERBB4 displayed a markedly low transcript level by 6.5- to 2521-fold in all 10 cell lines below normal samples (Figure 4.21B). Hence, it seems that as a potential miR-137 target, overexpressed CSE1L was observed when miR-137 was found down-regulated. In addition, we note that according to TargetScan and PicTar, which allow prediction of miRNAs that may target given gene, miR-137 is the only miRNA that may regulate CSE1L. Taken together, miR-137 was probably an important regulator of CSE1L in glioma. Therefore, we focused on validation of CSE1L as a miR-137 target, as well as its biological function in gliomas in our following study.

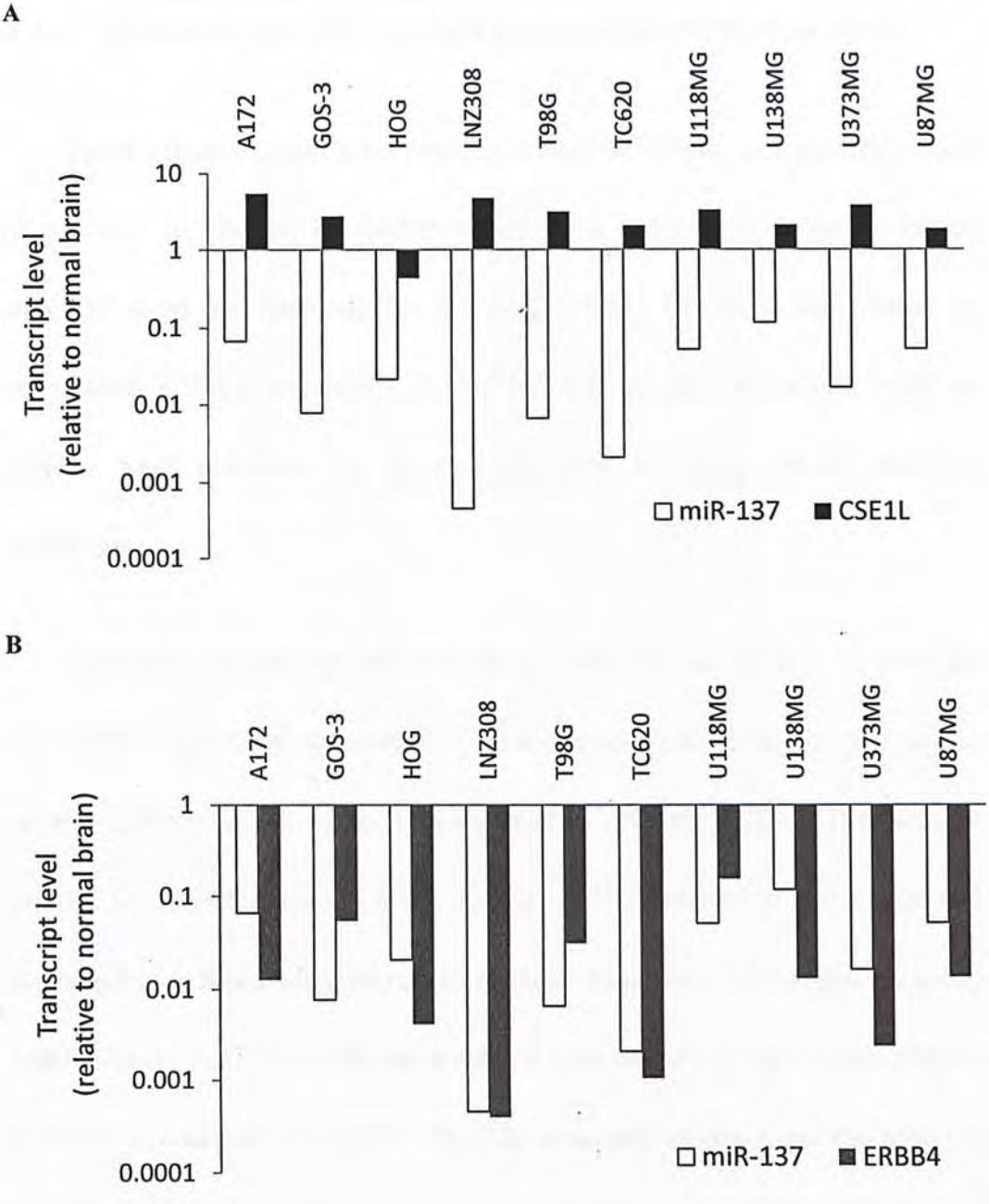

Figure 4.21 Comparison of relative expression of miR-137 with CSE1L (A) and ERBB4 (B) in glioma cell lines.

4.4.4 Effects of miR-137 on CSE1L transcript and protein levels

Above results in section 4.4 strongly suggested CSE1L as a potential target of miR-137 in glioma. To further validate this and also investigate whether miR-137 exert its functions by inducing CSE1L transcript degradation or suppressing CSE1L translation, the mRNA and protein expression levels of CSE1L were measured in glioma cell lines following forced miR-137 expression.

Trasfection of miR-137 into LNZ308 glioblastoma and GOS-3 OT cells did not result in significant alteration of CSE1L transcript levels relative to negative control miRNA at 48 hours post-transfection (Figure 4.22A). However, at protein level, endogenous CSE1L in miR-137 transfected glioma cells was dramatically reduced when compared to those transfected with negative control miRNA in all 3 OT and 4 glioblastoma cell lines tested by western blot analysis at the same time point (Figure 4.22B). The observations suggested that miR-137 inhibited CSE1L expression at translational, but not transcriptional level.

Taken the luciferase reporter assay results into account, the evidence supported that miR-137 directly interacted with 3'UTR of CSE1L, leading to the suppression of CSE1L protein expression in glioma cells.

A

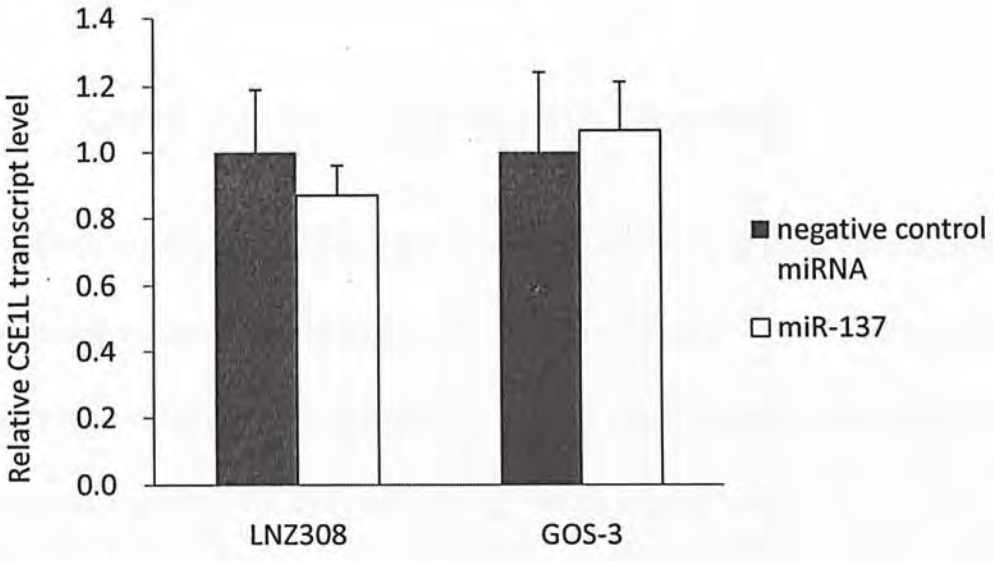

B

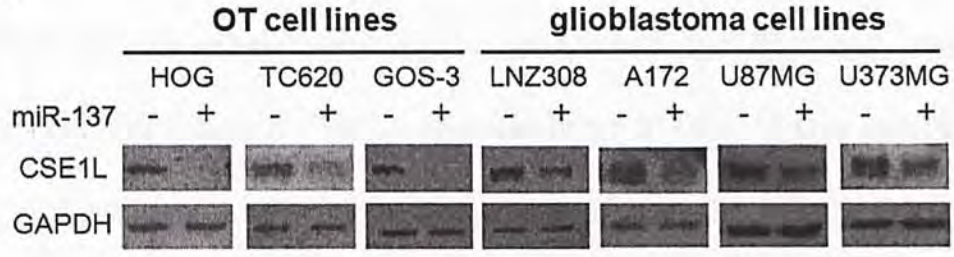

Figure 4.22 Alteration of CSE1L mRNA and protein expression in glioma cells following enhanced miR-137 transfection. A, CSE1L mRNA was quantified by qRT-PCR normalized to GAPDH. Transfection of miR-137 did not affect CSE1L mRNA transcript levels at 48 hours relative to cells transfected with negative control miRNA. B, CSE1L protein expression was markedly reduced as determined by western blot in response to miR-137 transfection.

4.5 Expression of CSE1L in OTs

4.5.1 CSE1L expression in OTs by qRT-PCR and IHC

Since CSE1L showed significant overexpression in glioma cell lines, this suggested an involvement of CSE1L in gliomagenesis. To determine CSE1L expression in OTs *in vivo*, the mRNA and protein levels in our cohort of 36 OTs were examined by qRT-PCR and IHC approaches, respectively.

At mRNA level, CSE1L expression in 36 OT patient tissues and 3 normal brain samples was normalized by the expression of GAPDH in each sample. The overall distribution of CSE1L expression in the 20 ODs, 16 OAs and 10 glioma cell lines relative to 3 normal brain samples were shown in Figure 4.23 and Table 4.11. CSE1L was overexpressed more than 2-fold in 6 out of 20 (30%) OD and 12 of 16 (75%) OA cases, up to 3.3- and 12.7-fold, respectively. In glioma cell lines, 8 of 10 cell lines showed CSE1L overexpression by 2- to 5.4-fold. Statistical analysis showed that the CSE1L mRNA expressions was significantly higher in both ODs and OAs ($p=0.039$ and $p=0.006$, respectively), as well as in glioma cell lines ($p=0.014$).

On the other hand, CSE1L protein expression levels in 35 OTs and 13 non-tumorous brain tissues were assessed by IHC. Nucleus staining of CSE1L was observed in both tumor and non-neoplastic tissues. In non-tumorous tissues,

positive staining of CSE1L of neurons and glial cells was observed in both cortex and white matter areas. Neurons displayed a strong staining intensity, whereas surrounding glial cells showed negative or weak IHC activity (Figure 4.24). The differential staining intensity was described as negative, weak, moderate or strong in scoring (Figure 4.25).

Representative CSE1L staining pictures in non-tumorous brain tissue and OTs are showed in Figure 4.26. Take both percentage of positive staining cells and the intensity of staining into accounts, CSE1L expression was scored as negative, low, medium or high expression. Table 4.12 summerized the comparison of CSE1L expression distribution between non-tumorous brain tissues and subtypes of OT. Among the 13 non-neoplastic tissues, 11 (84.6%) showed negative~low CSE1L expression and only 2 (15.4%) cases showed medium expression. No case was defined as high expression. For the 35 tumor tissues, 6 of them (17.1%) displayed low CSE1L expression, 13 (37.1%) and 16 cases (45.7%) showed medium and high expression of CSE1L, respectively. Chi-square analysis revealed a significant higher expression of CSE1L in OTs relative to non-tumorous tissues ($p<0.001$). This was also found in each histological subtype. These results suggest overexpression of CSE1L in OTs at both mRNA and protein levels, implicating its involvement in human gliomagenesis.

Table 4.11 Summary of CSE1L mRNA and protein expression in 36 OTs.

Case number	Diagnosis[1]	Sex	Age (years)	CSE1L mRNA expression (fold change)[2]	CSE1L protein expression[3]
HS380	OD	M	35	0.85	high
HS467	OD	F	56	1.16	high
HS466	OD	F	40	1.18	high
HS460	OD	M	29	1.32	high
HS324	OD	M	42	1.52	low
HS378	OD	F	38	1.63	low
HS390	OD	M	10	1.75	medium
HS400	OD	F	49	1.98	medium
HS329	OD	F	69	2.30	high
HS332	OD	M	53	2.47	medium
HS469	OD	F	36	2.65	high
HS331	OD	F	46	2.92	high
HS303	OD	M	48	3.26	low
HS314	OA	F	38	1.37	medium
HS394	OA	F	31	1.89	low
HS462	OA	M	39	2.66	medium
HS381	OA	F	28	3.19	high
HS301	OA	M	43	3.74	medium
HS382	OA	F	37	4.18	low
HS362	OA	M	41	4.36	N/A[4]
HS375	OA	M	28	4.92	high
HS399	OA	M	34	5.72	high
HS384	OA	M	30	6.45	high
HS458	OA	M	37	6.80	medium
HS393	OA	F	49	8.39	medium
HS368	OA	F	61	12.70	medium
HS333	AOD	F	43	0.31	low
HS461	AOD	M	53	1.15	medium
HS360	AOD	M	51	1.30	medium
HS377	AOD	M	77	1.42	medium
HS312	AOD	M	53	1.52	high
HS302	AOD	M	35	1.87	high
HS358	AOD	F	50	2.54	medium
HS457	AOA	M	52	1.35	high
HS366	AOA	M	35	1.72	high
HS364	AOA	F	48	2.19	high

[1] OD, oligodendroglioma; OA, oligoastrocytoma; AOD, anaplastic

oligodendroglioma; AOA, anaplastic oligoastrocytoma.

[2] CSE1L expression fold change relative to 3 normal brain RNA samples was determined by qRT-PCR.

[3] CSE1L protein expression based on IRS by IHC.

[4] CSE1L protein expression is not available due to lack of FFPE section.

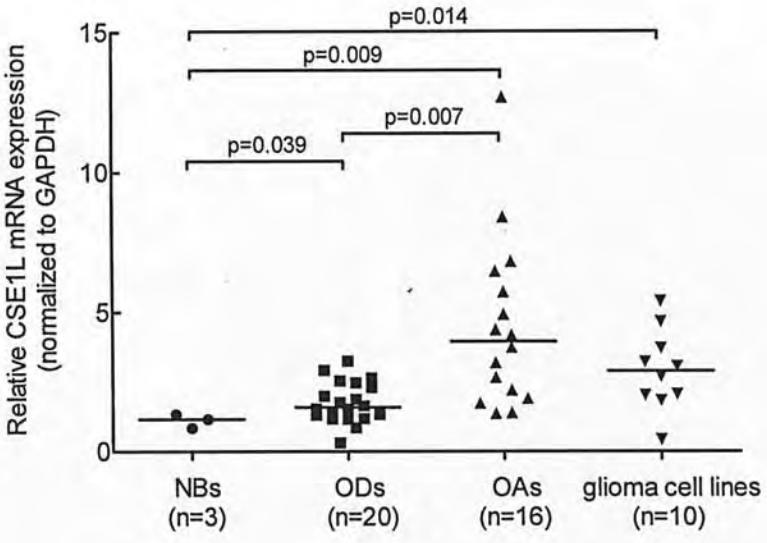

Figure 4.23 mRNA expression levels of CSE1L in OTs and glioma cell lines. Both primary OTs [20 oligodendrogliomas (ODs) and 16 oligoastrocytomas (OAs)] and 10 glioma cell lines showed significant CSE1L overexpression than 3 normal brain samples by qRT-PCR. CSE1L mRNA levels were significantly higher in OAs than in OTs.

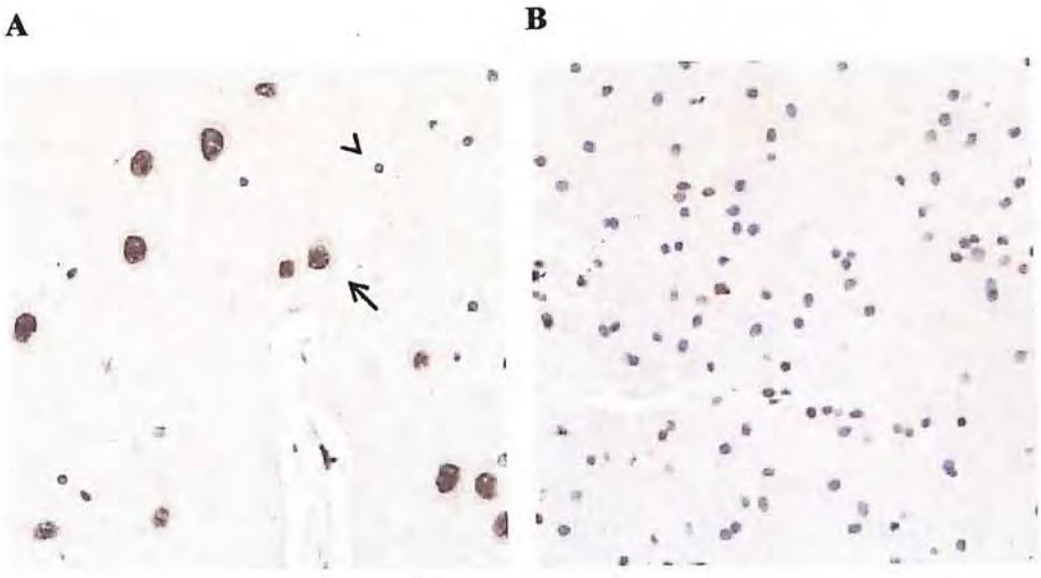

Figure 4.24 Representative CSE1L staining in non-neoplastic brain tissue by IHC. Positive staining was observed in both cortex (A) and white matter (B) areas. Neuron (arrow) and glial cell (arrowhead) showed nuclear CSE1L expression. Photos were taken under microscopic view of 400× magnification.

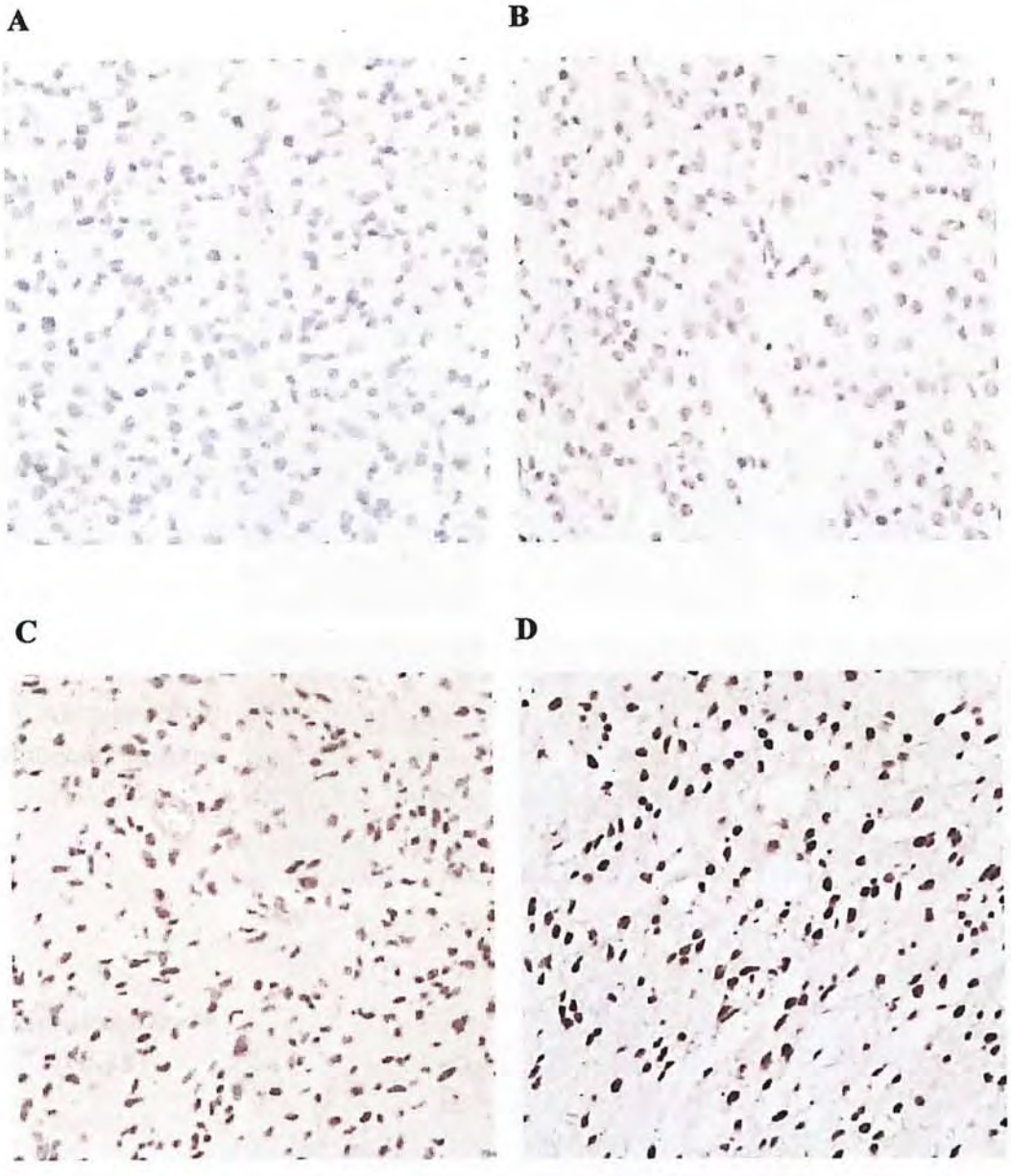

Figure 4.25 CSE1L staining in OT tissues by IHC. Differential CSE1L staining intensity was described as negative (A, HS378), weak (B, HS458), moderate (C, HS384) or strong (D, HS460). Photos were taken under microscopic view of 400× magnification.

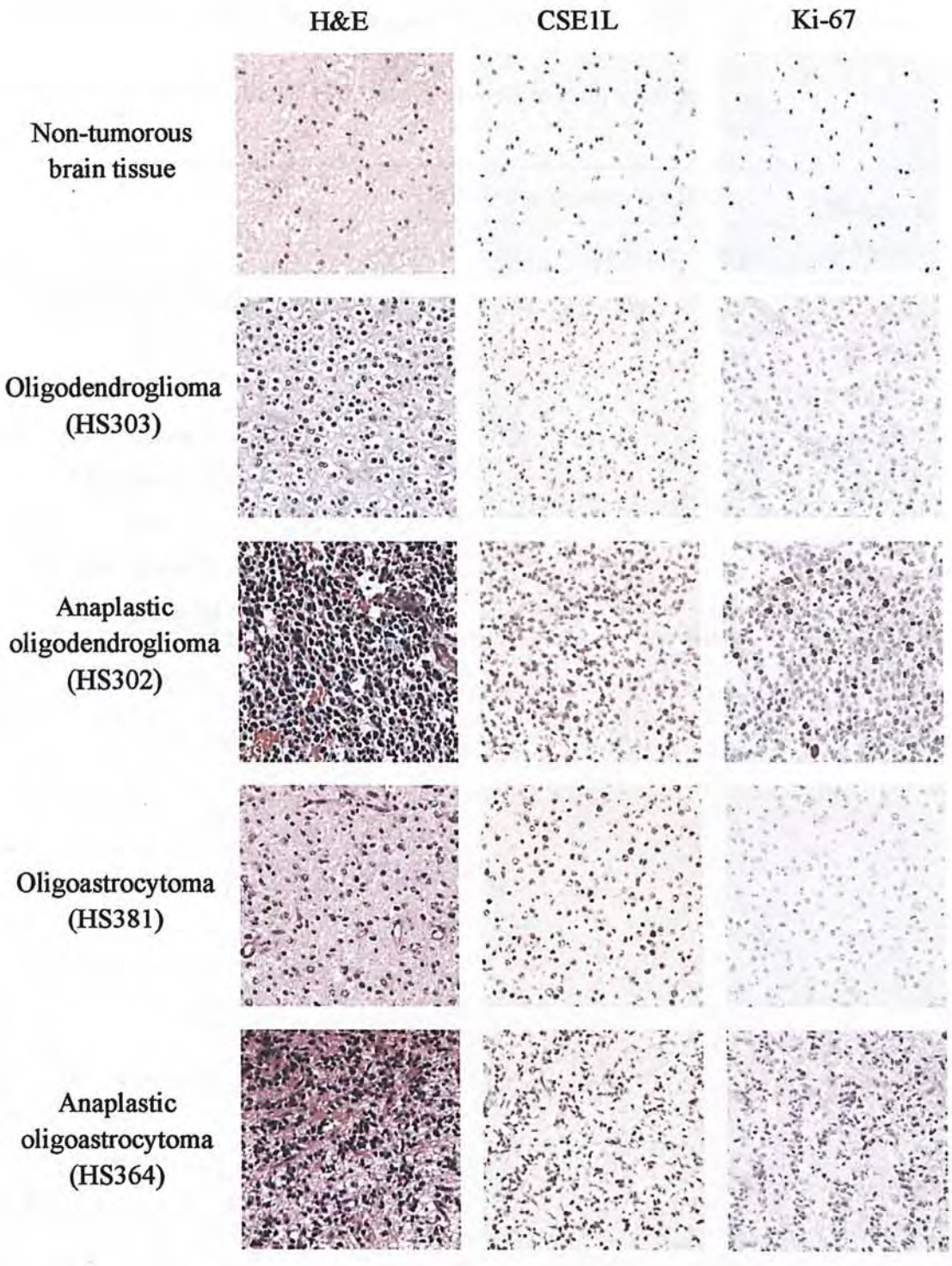

Figure 4.26 Comparison of CSE1L and Ki-67 expression in OTs and non-tumorous tissue by IHC.

Table 4.12 CSE1L protein expression in 20 ODs and 15 OAs compared to that in 13 non-tumorous brain samples by IHC. Both ODs and OAs showed significant higher CSE1L expression, as well as each subtype.

	N	CSE1L expression by IHC				Chi-square p-value
		negative	low	medium	high	
Non-tumorous tissue	13	7	4	2	0	
OT	35	0	6	13	16	<0.001
OD	20	0	4	7	9	<0.001
OD, grade II	13	0	3	3	7	<0.001
OD, grade III	7	0	1	4	2	<0.001
OA	15	0	2	6	7	<0.001
OA, grade II	12	0	2	6	4	<0.001
OA, grade III	3	0	0	0	3	<0.001

4.5.2 Correlation of CSE1L expression with clinicopathological features

To identify the clinical significance of CSE1L, the relationships between CSE1L expression level and clinicopathological characteristics of the 36 OT patients were investigated. As summarized in Table 4.13, CSE1L mRNA levels in 16 OAs were significant higher than those in 20 ODs (p=0.007, Figure 4.23). However, protein expression was not significantly different between these 2 histological subtypes (p=0.867). As summarized in Table 4.13, there is no significant correlation between CSE1L overexpression and tumor grade, patient sex, 1p/19q status, miR-137 down-regulation or Ki-67 expression (p>0.05). Although CSE1L acted as a miR-137 target in glioma, the abundance of CSE1L mRNA or protein showed no significant correlation was miR-137 level in OTs (p=0.326 and p=0.300, respectively).

To study the association of CSE1L expression and prognosis, survival analysis was performed. There was no significant relationship between CSE1L mRNA expression and patient overall survival (p=0.516) or progression-free survival (p=0.355). When patients were grouped by CSE1L protein expression of negative~low or medium~high, no significant difference in overall survival (p=0.346) or progression-free survival (p=0.310) was found (Figure 4.27).

Table 4.13 Association analysis of CSE1L expression with clinicopathological parameters, 1p/19q status, miR-137 down-regulation and Ki-67 expression in 36 OTs.

	CSE1L expression							
	mRNA upregulation		**p value**	**protein expression**				**p value**
	<2-fold	>2-fold		negative	low	medium	high	
Tumor type								
OD	14	6	0.006	0	4	7	9	0.867
OA	4	12		0	2	6	7	
WHO grade								
grade II	10	16	0.060	0	5	9	11	0.777
grade III	8	2		0	1	4	5	
Gender								
male	11	9	0.502	0	2	8	9	0.506
female	7	9		0	4	5	7	
Age								
<50	12	14	0.457	0	6	7	12	0.107
>=50	6	4		0	0	6	4	
1p status								
loss	7	11	0.182	0	3	7	8	0.976
intact	11	7		0	3	6	8	
19q status								
loss	7	10	0.317	0	3	7	7	0.861
intact	11	8		0	3	6	9	
1p/19q co-deletion								
yes	7	10	0.317	0	3	7	7	0.861
no	11	8		0	3	6	9	
miR-137 down-regulation								
<2-fold	1	2	1.000	0	0	0	3	0.143
>2-fold	17	16		0	6	13	13	
Ki-67 LI								
<3%	6	11	0.063	0	2	5	10	0.312
>3%	12	6		0	4	8	6	

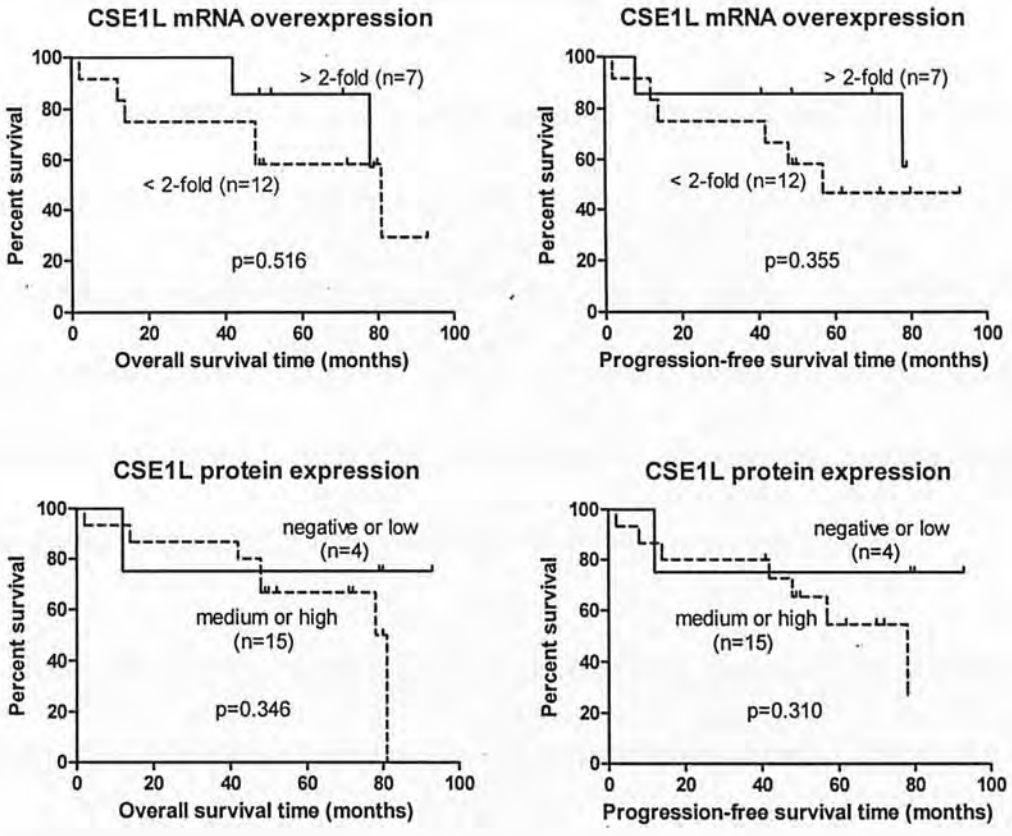

Figure 4.27 Kaplan–Meier overall (left panel) and progression-free (right panel) survival curves with log-rank test for 19 OT patients with low and high CSE1L mRNA (upper) or protein (bottom) expression.

4.6 Effects of CSE1L knockdown in glioma cells

Given that CSE1L showed overexpression in glioma cells and was a direct target of miR-137, the function of CSE1L in development of gliomas was examined. To further determine the functional role of CSE1L in gliomagenesis and whether CSE1L contribute to our previously demonstrated effects of miR-137, the effect of CSE1L knockdown on glioma cell proliferation, anchorage-independent growth, apoptosis and motility were evaluated.

Here, two specific siRNAs against CSE1L mRNA were used. As shown in Figure 4.28, both siRNAs dramatically reduced the protein level of CSE1L at 24 and 48 hours post-transfection.

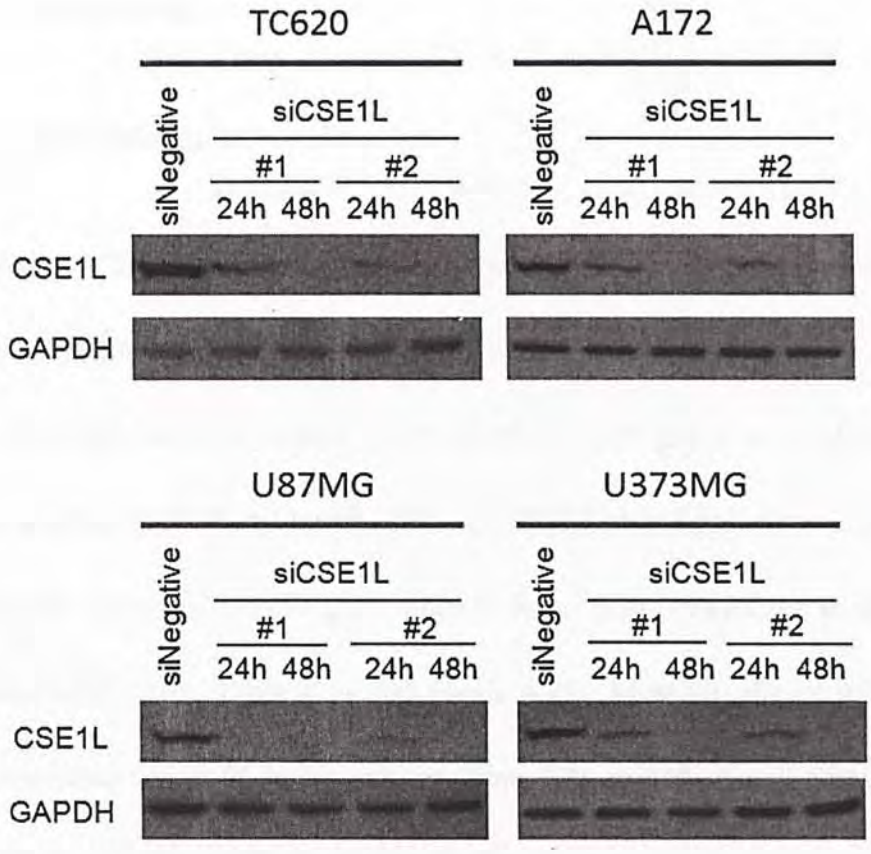

Figure 4.28 siRNA-mediated knockdown effect of CSE1L. Efficient knockdown of CSE1L was observed at 24 and 48 hours after glioma cells transfected with either siCSE1L as compared to negative control siRNA.

4.6.1 Cell growth

4.6.1.1 Cell viability

Effect of CSE1L knockdown on cell viability in 1 oligodendroglioma cell and 3 glioblastoma cell lines was assessed by MTT assay at 24, 48, 72 and 96 hours after cells were transfected with siCSE1L, siNegative or lipofectamine control. Results showed that knockdown of CSE1L led to significant decrease of cell viability compared to siNegative since 72 hours post-transfection in all 4 cell lines studied ($p<0.05$, Table 4.14 and Figure 4.29). Most significant inhibitory effect was observed at 96 hours, ranging from 32% to 44% for siCSE1L-1 and from 19% to 34% for siCSE1L-2, respectively.

Table 4.14 Effect of CSE1L knockdown on cell viability in 4 glioma cell lines relative to negative control siRNA.

Cell line	Time after transfection (hours)	Cell viability			
		siCSE1L-1		siCSE1L-2	
		% of negative control	p value	% of negative control	p value
TC620	24	95.6%	0.217	94.1%	0.147
	48	94.8%	0.356	93.4%	0.242
	72	80.1%	0.010	82.8%	0.013
	96	63.2%	<0.001	80.9%	0.001
A172	24	99.8%	0.793	101.7%	0.873
	48	91.2%	0.349	96.6%	0.754
	72	80.0%	<0.001	83.8%	0.028
	96	56.2%	0.001	66.1%	0.002
U87MG	24	94.1%	0.153	100.2%	0.963
	48	87.6%	0.561	91.6%	0.277
	72	74.9%	0.002	74.8%	0.032
	96	66.9%	<0.001	69.2%	0.001
U373MG	24	96.4%	0.276	101.1%	0.723
	48	93.2%	0.105	90.3%	0.136
	72	79.4%	<0.001	85.6%	0.018
	96	67.6%	<0.001	68.9%	<0.001

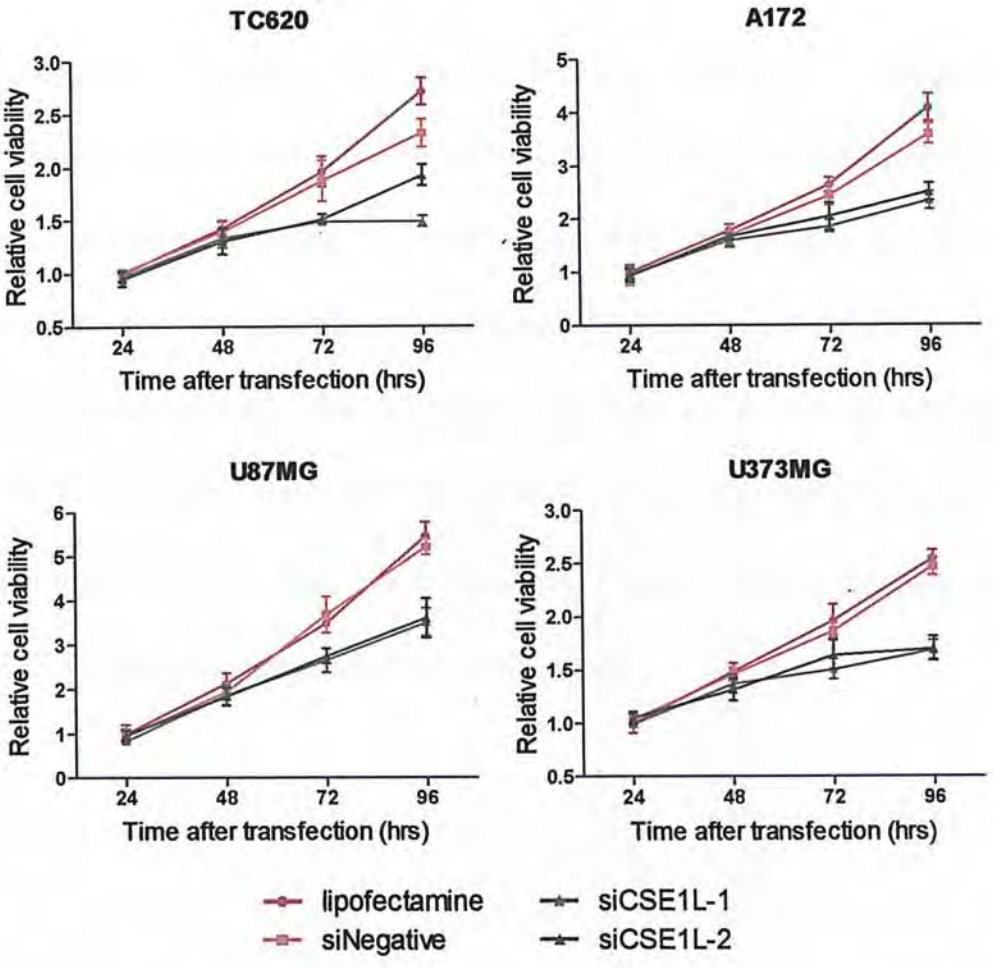

Figure 4.29 Effect of CSE1L knockdown on cell viability in 4 glioma cell lines. Metabolic activity of 4 glioma cell lines were measured by MTT assay 24~96 hours after transfected with siCSE1L-1 or -2, negative control siRNA or lipofectamine treatment. The points showed means±SD from 3 independent experiments performed in triplicate. Cell viability was significantly reduced upon knockdown of CSE1L in all cell lines at 72 and 96 hours.

4.6.1.2 Cell number

Alteration of glioma cell growth following siCSE1L or siNegative transfection was also evaluated by cell counting at same time points as MTT assay. As shown in Table 4.15 and Figure 4.30, cell number in CSE1L knockdown cells was significant less than cells transfected with siNegative at 72 and 96 hours ($p<0.05$). The suppression increased up to 27% to 49% for siCSE1L-1 and from 26% to 43% for siCSE1L-2 when compared to siNegative, respectively. This is in line with data from MTT assay, further confirming that CSE1L knockdown suppressed glioma cells growth.

Table 4.15 Effect of CSE1L knockdown on cell number in 4 glioma cell lines relative to negative control siRNA.

Cell line	Time after transfection (hrs)	Cell number			
		siCSE1L-1		siCSE1L-2	
		% of negative control	p value	% of negative control	p value
TC620	24	98.9%	0.416	99.6%	0.564
	48	87.0%	0.149	93.3%	0.312
	72	75.3%	0.001	83.2%	0.033
	96	51.4%	<0.001	61.3%	<0.001
A172	24	98.2%	0.864	105.8%	0.180
	48	83.5%	0.063	89.1%	0.091
	72	80.9%	0.004	84.9%	0.012
	96	59.0%	<0.001	65.4%	<0.001
U87MG	24	90.2%	0.205	90.0%	0.404
	48	76.8%	0.068	83.7%	0.081
	72	74.2%	<0.001	76.2%	<0.001
	96	73.0%	<0.001	74.2%	<0.001
U373MG	24	97.9%	0.145	98.7%	0.901
	48	93.5%	0.211	94.8%	0.524
	72	87.0%	0.041	87.0%	0.046
	96	60.9%	<0.001	57.5%	<0.001

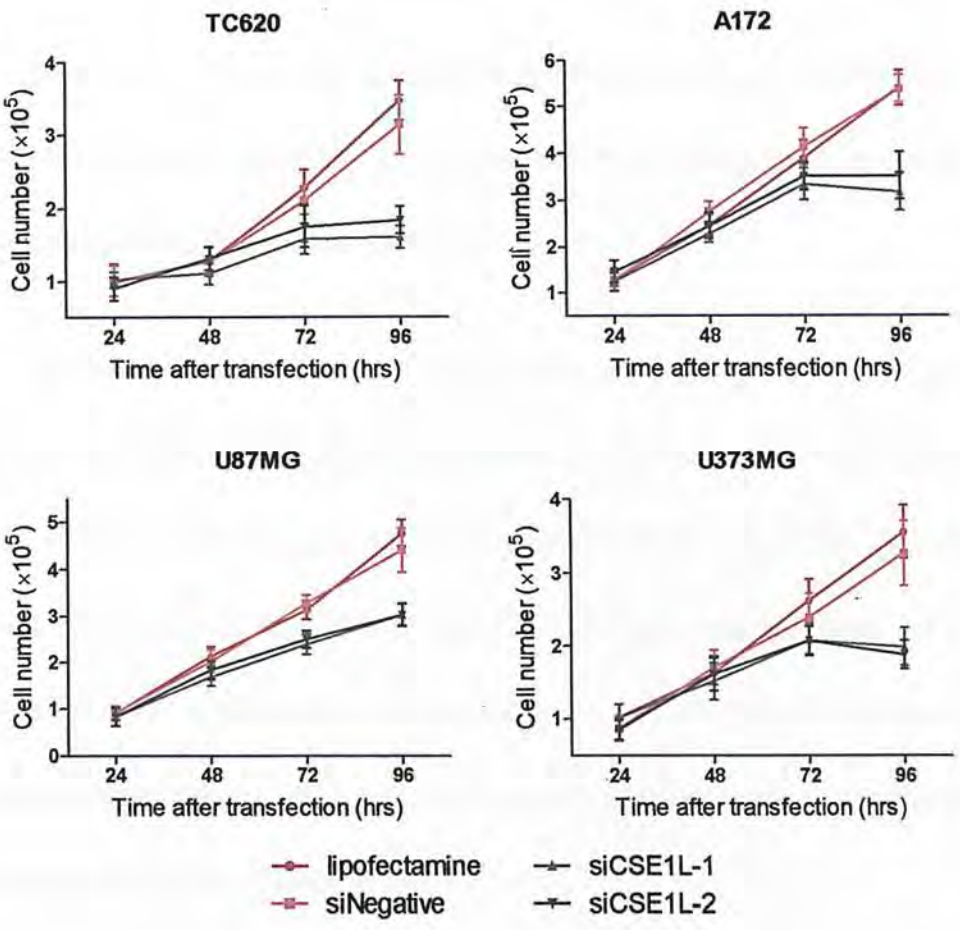

Figure 4.30 Effect of CSE1L knockdown on cell growth in 4 glioma cell lines. By cell count, growth curves indicated viable glioma cells transfected with siCSE1L, siRNA negative control or lipofectamine only at 24 to 96 hours. All lines showed suppression of cell growth upon miR-137 forced expression. The points showed means ± SD from 3 independent experiments performed in triplicate.

4.6.1.3 Cell cycle analysis

To further elucidate the mechanism underlying cell growth inhibition by CSE1L knockdown, change of DNA synthesis during cell cycle progression was assessed by BrdU incorporation activity.

As shown in Table 4.16 and Figure 4.31, the BrdU incorporation activity significantly reduced in CSE1L knockdown TC620 and A172 cells compared with negative control since 48 hours post-transfection ($p<0.05$). Significant effect was observed in U87MG and U373MG cells started from 72 hours ($p<0.05$). DNA synthesis was decreased up to 45%~63% at 96 hours. These results indicated that CSE1L knockdown could inhibit glioma cell proliferation through suppression of DNA synthesis.

Table 4.16 Effect of CSE1L knockdown on DNA synthesis in 4 glioma cell lines relative to negative control siRNA by BrdU incorporation assay.

Cell line	Time after transfection (hours)	siCSE1L	
		% of negative control	p value
TC620	24	102.4%	0.626
	48	74.4%	0.020
	72	57.8%	<0.001
	96	49.5%	<0.001
A172	24	82.9%	0.083
	48	80.5%	0.008
	72	64.2%	0.006
	96	37.5%	<0.001
U87MG	24	92.7%	0.088
	48	88.9%	0.176
	72	84.6%	0.029
	96	55.5%	<0.001
U373MG	24	104.0%	0.768
	48	104.5%	0.166
	72	88.3%	0.024
	96	49.2%	0.001

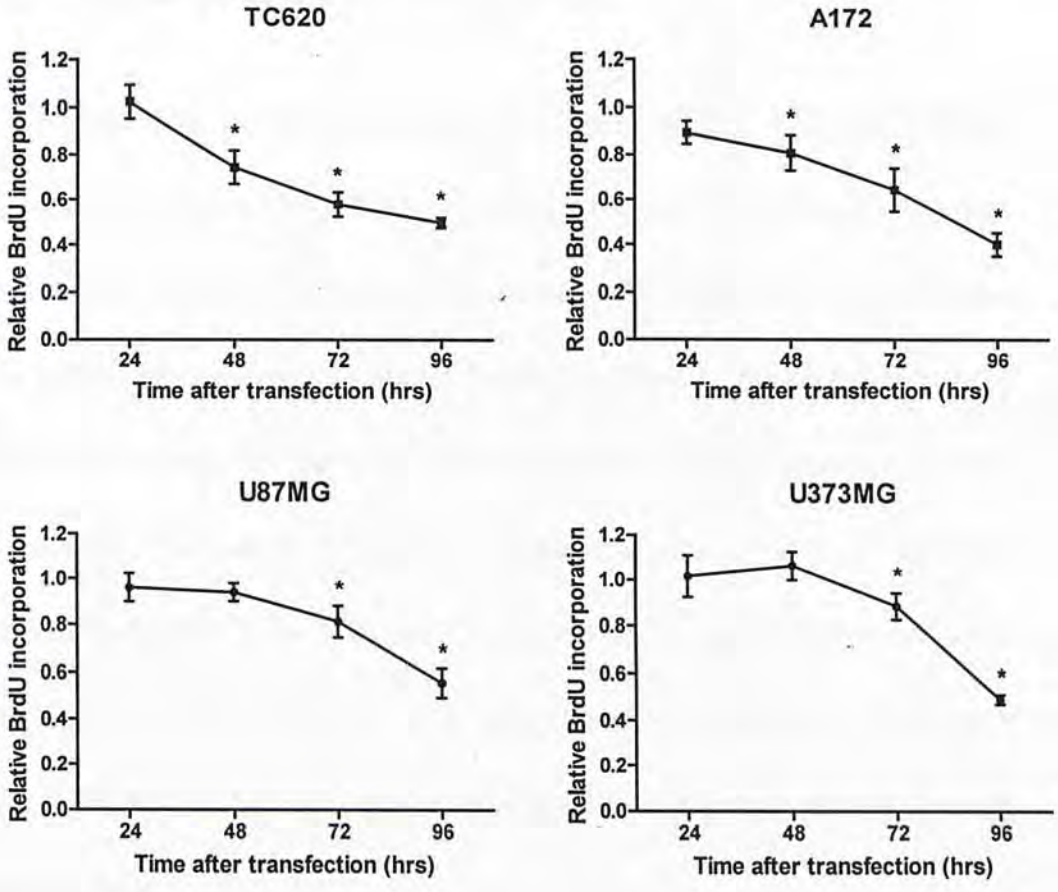

Figure 4.31 Effect of CSE1L knockdown on DNA synthesis in 4 glioma cell lines, By BrdU incorporation assay, the relative BrdU incorporation at 24 to 96 hours after transfection were assessed. All cell lines show suppression of cell proliferation following siCSE1L transfection compared to siNegative. The points showed means ± SD from 3 independent experiments performed in triplicate. *, $p<0.05$ between siCSE1L and siNegative transfected group by student's t test.

4.6.2 Anchorage-independent cell growth

To study whether the transforming potential of TC620, A172 and U87MG cells could be affected by CSE1L, anchorage-independent soft agar assay was performed in siCSE1L or siNegative transfected cells. After growing in soft agar for 3 weeks, the numbers of colonies formed in siCSE1L transfected cells were significantly lower than those of cells transfected with siNegative ($p<0.001$, Figure 4.32). The number of colonies decreased to 31.7% and 31.1% inTC620 cell, 42.0% and 39.3% in A172 cell, 34.3% and 39.7% in U87MG cell of those in siNegative transfected cells for siCSE1L-1 and -2, respectively. This result suggested that CSE1L knockdown reduce the anchorage-independent cell growth in glioma cells.

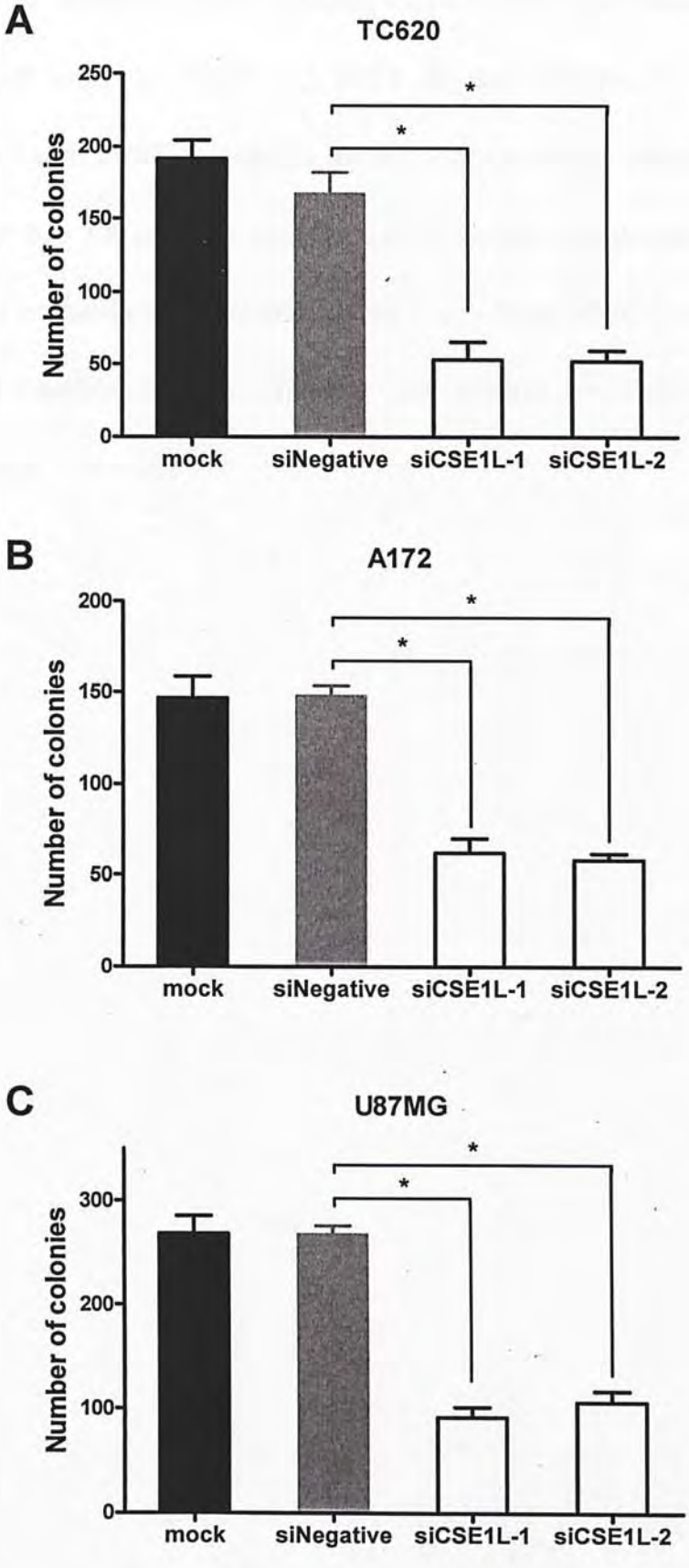
A
TC620
Number of colonies
250
200
150
100
50
0
*
*
mock
siNegative
siCSE1L-1
siCSE1L-2
B
A172
Number of colonies
200
150
100
50
0
*
*
mock
siNegative
siCSE1L-1
siCSE1L-2
C
U87MG
Number of colonies
300
200
100
0
*
*
mock
siNegative
siCSE1L-1
siCSE1L-2

Figure 4.32 Effect of CSE1L knockdown on number of colonies formed in 3 glioma cell lines. In TC620 (A), A172 (B) and U87MG (C) glioma cells transfected with siCSE1L, negative control siRNA or mock. Colonies with sizes of greater than 100 μm were counted. CSE1L knockdown showed a significant reduction in numbers of colonies in all 3 cell lines when compared to the negative controls. Results represent the average of three independent experiments. *, $p<0.001$.

4.6.3 Cell apoptosis

To identify whether CSE1L was involved in glioma cell apoptosis, cleaved PARP, was examined by western blot in glioma cells following transfected with siCSE1L compared to negative control siRNA. The protein level of cleaved PARP elevated in all 4 cells at both 48 and 96 hours following CSE1L knockdown. The enhancement of cleaved PARP was similar between 48 and 96 hours. However, a further induction was observed for siCSE1L-2 treatment in TC620 cells at 96 hours (Figure 4.33). The results indicated that CSE1L knockdown led to cellular apoptosis in glioma cells, which also contributed to suppression of cell growth.

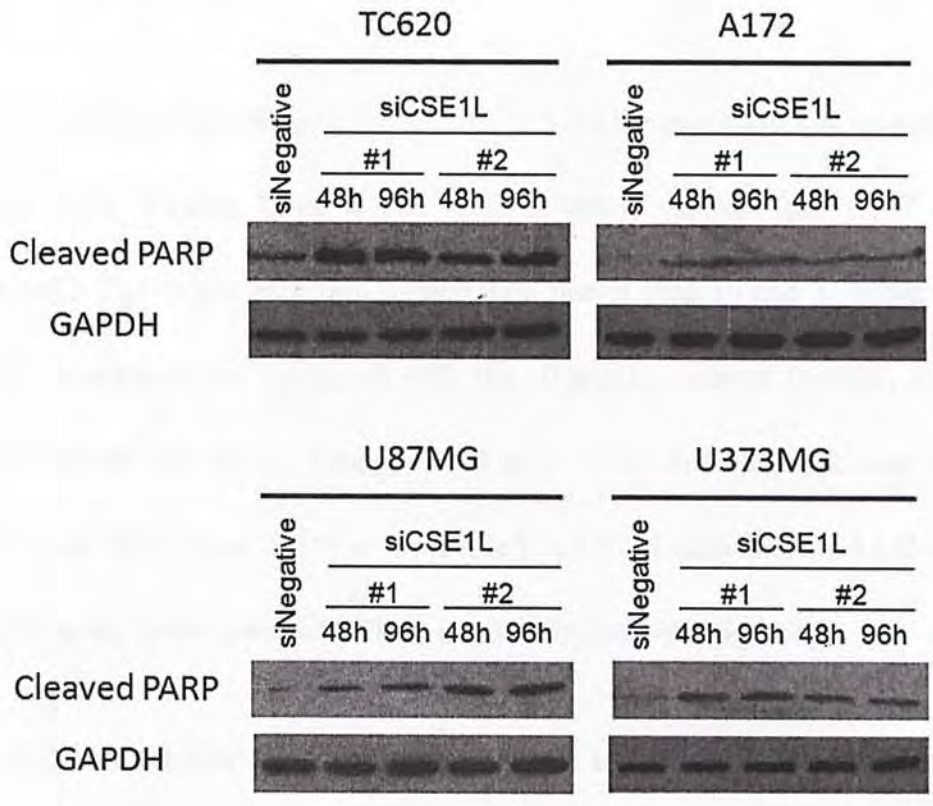

Figure 4.33 Effect of CSE1L knockdown on cleaved PARP expression in 4 glioma cell lines. Protein levels of cleaved PARP were remarkably up-regulated following CSE1L knockdown compared to negative control siRNA in 4 glioma cells. GAPDH was included as loading control.

4.6.4 Cell motility

We next investigated the effect of siCSE1L on the migration and invasion of glioma cells. Results from wound healing assay showed that A172 cells exhibited a significant reduction in migration rate at both 16 and 32 hours after CSE1L knockdown as compared with the siNegative control ($p<0.05$, Figure 4.34). Notably, the wound almost closed at 32 hours in siNegative transfected A172 cells. There was 29.1% of wound left in CSE1L knockdown A172 cells, suggesting an involvement of CSE1L in glioblastoma cell migration.

Moreover, cell invasive ability in response to FBS enriched medium was quantified by matrigel invasion assay. Results demonstrated that number of invaded glioma cell was significantly decreased by 15%~40% and 20%~69% in all glioma cell lines examined following CSE1L silencing by 2 siCSE1L transfection, respectively (Table 4.17 and Figure 4.35). This indicated that glioma cell invasion through extracellular matrix was impaired by CSE1L knockdown. Together, these results supported that CSE1L inactivated glioma cells have reduced ability of both migration and invasion.

A

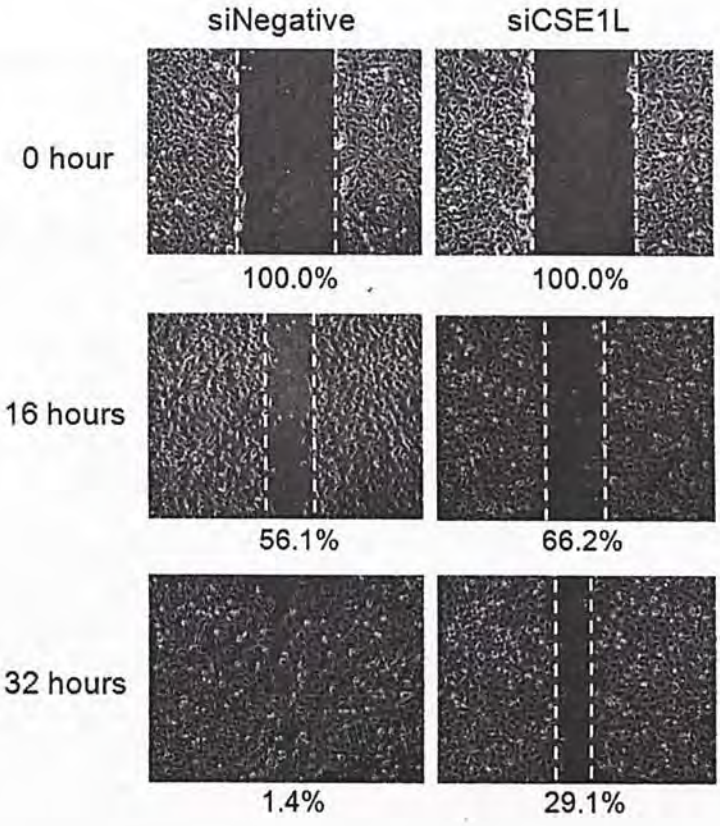

B

Figure 4.34 Effect of CSE1L knockdown on A172 GBM cell migration. In wound healing assay, wound was induced using a yellow pipette tip on the full confluent monolayer A172 cells transfected with CSE1L siRNA or negative

control siRNA. A. The rate of wound closure was monitored at different time points afterwards. Representative photos were taken under 40× magnifications. Lines indicated the differential migration rate of cells. B. The migration rate was significant slower in siCSE1L transfected cells. *, $p<0.05$.

Table 4.17 Effect of CSE1L knockdown on cell invasion of 4 glioma cell lines by matrigel invasion assay.

Cell line	Mean number of invaded cells				% of negative control		*p* value	
	mock	siNegative	siCSE1L-1	siCSE1L-2	siCSE1L-1	siCSE1L-2	siCSE1L-1	siCSE1L-2
TC620	238.3	246.6	210.4	196.2	85.4%	79.6%	0.019	0.002
A172	128.0	116.6	77.9	80.0	66.8%	68.6%	0.001	<0.001
U87MG	329.0	300.8	179.7	92.3	59.7%	30.7%	<0.001	<0.001
U373MG	226.3	214.3	144.7	129.2	67.5%	60.3%	<0.001	<0.001

A

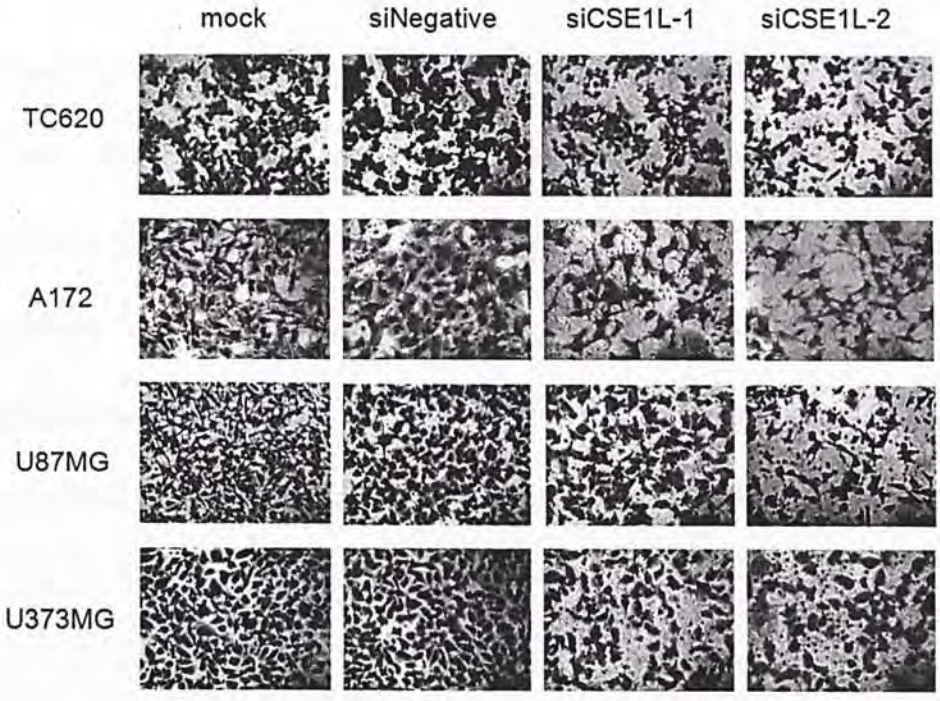
mock
siNegative
siCSE1L-1
siCSE1L-2
TC620
A172
U87MG
U373MG

B

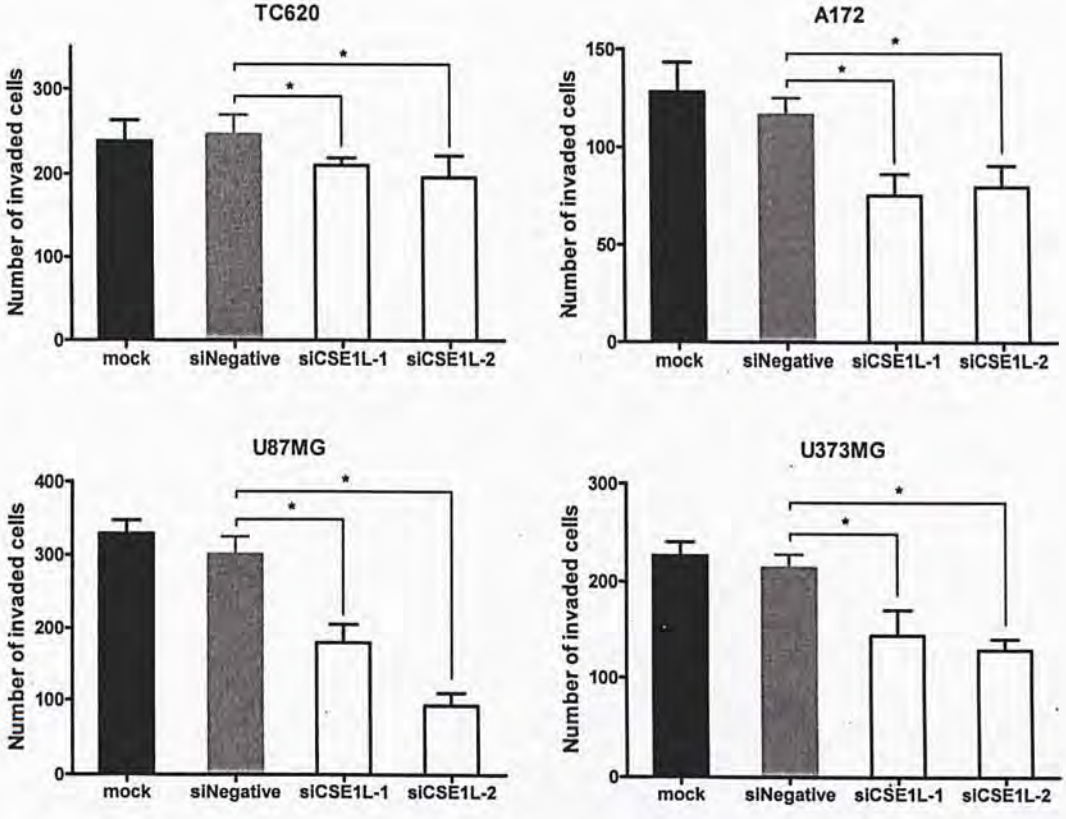
TC620
A172
U87MG
U373MG
Number of invaded cells
mock
siNegative
siCSE1L-1
siCSE1L-2
*

Figure 4.35 Effect of CSE1L knockdown on cell invasion in 4 glioma cell lines. The invasive ability of 4 glioma cell lines after transfection with siCSE1L or negative control siRNA were assessed by matrigel invasion assay. Cells invaded to the lower surface of matrigel-coated wells were counted 16 hours after plating. A. Invaded cells were stained and observed under microscope at 40× magnification. B. Significant fewer cells were able to invade after transfected with siCSE1L than negative control siRNA transfectants. *, $p<0.05$.

CHAPTER 5 DISCUSSION

5.1 Expression of miR-137 transcript level in OTs and glioma cell lines

Allelic loss of chromosome 1p is characterized as a major hallmark of OTs, suggesting the existence of tumor suppressive gene(s) or miRNA(s) involved in development of OT. Among all 38 miRNAs residing on chromosome 1p, miR-137 was found downregulated in WHO grade I-IV astrocytomas (Godlewski *et al.,* 2008; Silber *et al.,* 2008; Zhi *et al.,* 2010). Functionally, expression of miR-137 inhibited proliferation of GBM cells and induced neuronal-like differentiation in mouse neural stem cells and tumor stem cells derived from mouse OT and human GBM (Silber *et al.,* 2008). Therefore, we focused on this miRNA to investigate its role in pathogenesis of OT and GBM.

In the current study, it was demonstrated for the first time a significantly reduced miR-137 transcript level in 34 out of 36 (94%) OTs examined with a median of 9.3-fold reduction compared with normal brain samples. Similarly, in cultured OT and GBM cells, notable decrease in miR-137 expression was observed in all 10 cell lines studied. In line with my findings, remarkable downregulation of miR-137 has been earlier uncovered in astrocytoma of all WHO grades as compared to normal or non-tumor brain tissues (Godlewski *et al.,* 2008; Silber *et al.,* 2008; Zhi *et al.,* 2010). Therefore, miR-137 downregulation is common in both astrocytic and oligodendroglial tumors. Moreover, the preferential expression of miR-137 in brain (Sempere *et al.,* 2004; Beuvink *et al.,* 2007; Landgraf *et al.,* 2007; Liang *et al.,* 2007) also emphasizes the importance of miR-137 in glioma pathogenesis.

Downregulation of miR-137 is not limited to glioma. It has also been involved in other cancer types, such as neuroblastoma (Chen *et al.,* 2007), colorectal cancer (Bandres *et al.,* 2006; Balaguer *et al.,* 2010), oral squamous cell carcinoma (Kozaki *et al.,* 2008), lung adenocarcinoma (Dacic *et al.,* 2010) and uveal melanoma (Chen *et al.,* 2010). In combination with these findings, it is reinforced that miR-137 may be involved in cancer development including glioma.

5.2 Association of miR-137 expression with OT clinical and molecular parameters

To evaluate the clinical significance of miR-137 in OTs, association analysis was performed to correlate miR-137 expression level to clinicopathological information, including sex, age, tumor subtype, tumor grade as well as 1p status and Ki-67 LI.

Here, the abundance of miR-137 transcript was found dramatically lower in 10 WHO grade III OTs than those of 26 OTs diagnosed as WHO grade II ($p=0.010$), suggesting that inactivation of miR-137 may contribute to progression of OT. This association was concordant with study showing more pronounced miR-137 repression in 76 high-grade astrocytomas than those of 48 low-grade astrocytomas (Zhi *et al.*, 2010). Thus, reduction of miR-137 may play a role in both development and progression of gliomas.

On the other hand, high-grade OTs displayed a higher Ki-67 labeling index than those of low-grade in our study ($p=0.014$). Ki-67 is a nuclear antigen expressed in all phases during the cell cycle except the G_0 phase and widely used as a proliferative marker in FFPE samples using IHC (Gerdes *et al.*, 1983; Gerdes *et al.*, 1984). High mitotic activity is one of the features of anaplastic OT (Reifenberger *et al.*, 2007). The survival analysis demonstrated a prognostic role of Ki-67 in OTs, which is in parallel with previous reports (Heegaard *et al.*, 1995; Kayaselcuk *et al.*, 2002; Kuo *et al.*, 2009).

It is notable that association analysis uncovered a novel relationship that miR-137 expression level was inversely correlated with Ki-67 immunoreactivity ($p=0.009$)

in the 35 OT cases. It was further illustrated by the significantly different miR-137 expression of two groups based on Ki-67 LI of less or greater than 3% (p=0.002). This is the first study showing an inverse correlation between miR-137 levels to proliferative activity in primary tumor, providing a high possibility that miR-137 involvement in OT cell proliferation.

In the current study, the chromosomes 1p and 19q statuses in OTs were determined by FISH analysis. The probe specifically bind to 1p36.3 and 19q13 region respectively, which represent the minimally deleted region (Husemann *et al.*, 1999; Smith *et al.*, 1999; Smith *et al.*, 2000; Dong *et al.*, 2004). Furthermore, the allelic loss mostly affect the entire 1p/19q arm (Felsberg *et al.*, 2004; Barbashina *et al.*, 2005), probably due to the unbalanced translocation involving chromosomes 1 and 19 (Griffin *et al.*, 2006; Jenkins *et al.*, 2006). Hence, it is believed that examinination of one loci in each chromosome arm region in FFPE section by FISH is a reliable method to investigate the status of 1p and 19q arm in glioma. According to our comparison of miR-137 levels in OTs with or without LOH 1p, despite located on chromosome 1p, reduction of miR-137 did not show a correlation with 1p loss in OTs. For other clinical characteristics, sex, age or tumor subtype seems do not associate with miR-137 expression. These data suggest that deregulation of miR-137 may be a frequent event in OTs of all sex, age and histological groups.

5.3 Prognostic significance of clinical features and miR-137 expression in OTs

By Kaplan-Miere survival analysis, favorable prognosis of the 19 OT patients in our study is statistically associated with younger patient age and low tumor grade at the time of diagnosis. In line with the results, such correlation has been reported in earlier population-based investigations (Okamoto *et al.*, 2004; Ohgaki *et al.*, 2005; Reifenberger *et al.*, 2007).

Investigations have indicated that 1p/19q codeletion is a prognostic marker for OT patients including clinical trials involving hundreds of cases (Cairncross *et al.*, 1998; Bauman *et al.*, 2000; Ino *et al.*, 2001; Cairncross *et al.*, 2006; Jenkins *et al.*, 2006; Kanner *et al.*, 2006; van den Bent *et al.*, 2006; van den Bent *et al.*, 2007). However, in our panel of 19 OT patients (14 WHO grade II and 5 WHO grade III) whose follow-up data were available, the overall or progression-free survival time was not statistically different between 1p/19q loss and intact groups. I did not look into survival data in only grade II or grade III OTs, due to the small sample size (Capelle *et al.*, 2009; Kuo *et al.*, 2009).

In this study, a Ki-67 LI of more than 3% was associated with shorter overall (p=0.049) and progression-free survival (p=0.017), which is consistent with previous studies (Heegaard *et al.*, 1995; Kros *et al.*, 1996; Coons *et al.*, 1997; Dehghani *et al.*, 1998; Kuo *et al.*, 2009).

For clinical relevance of miR-137, a trend was observed between longer overall and progression-free survival in miR-137 high-expressed OT patients (p=0.215 and p=0.103, respectively). The result is in accordance with the observation that miR-

137 correlated with tumor grade and Ki-67 immunoactivity in OTs. Whether miR-137 is a prognostic marker for OTs, requires more clinical cases with survival record.

5.4 Inactivation mechanisms of miR-137 in glioma

As miR-137 resides within a highly unstable chromosome arm in glioma (Bello *et al.*, 1995; Bigner *et al.*, 1999; Husemann *et al.*, 1999; Smith *et al.*, 1999; Ohgaki *et al.*, 2009) and promoter hypermethylation results in silencing of miR-137 in various cancers (Kozaki *et al.*, 2008; Silber *et al.*, 2008; Ando *et al.*, 2009; Bandres *et al.*, 2009; Balaguer *et al.*, 2010; Chen *et al.*, 2010; Langevin *et al.*, 2010), I sought whether chromosome 1p deletion or epigenetic regulation was responsible for miR-137 down-regulation in OTs and GBM cells.

In comparison with normal brain samples, the resulted showed miR-137 was downregulated in OT patients with intact chromosome 1p as well as 1p loss, indicating there are other mechanisms repressing miR-137 expression in OTs.

To investigate whether epigenetics played a role in modulating miR-137 expression, miR-137 level in OT and GBM cells was quantified following treatment of demethylating agent, 5-aza-dC and/or histone deacetylase inhibitor, TSA. A restoration of miR-137 level was observed in a dose-dependent manner in cultured TC620 oligodendroglioma cells when treated with 5-aza-dC of different concentrations. The elevation reached approximately 10-fold. Subsequent histone deacetylase inhibitor TSA treatment induced a further enhancement of miR-137 up to nearly 20-fold as compared to parental untreated cells. These indicated the control of miR-137 by synergetic DNA hypermethylation and histone deacetylation.

From the above 2 aspects, miR-137 downregulation in OTs with LOH 1p may result from both lp loss and epigenetic modulation including DNA hypermethylation and histone deacetylation. For OTs with intact 1p, miR-137 might be inactivated by

epigenetic aberration.

Promoter hypermethylation controlled miR-137 expression was uncovered in other tumors, such as gastric (Ando *et al.,* 2009), colorectal (Bandres *et al.,* 2009; Balaguer *et al.,* 2010) and oral squamous cell carcinoma (Kozaki *et al.,* 2008; Langevin *et al.,* 2010). Nonetheless, whether the mechanisms in glioma directly involve miR-137 promoter region or through indirect regulation requires further investigation.

In the 2 GBM cell lines examined, miR-137 expression was 15-fold and 60-fold below normal level in A172 and U373MG cells, respectively. Neither 5-aza-dC (or TSA) nor combined treatment altered miR-137 expression in both cell lines. Earlier investigation revealed 3~12-fold increased miR-137 expression in U87 and U251 GBM cells following similar treatment (Silber *et al.,* 2008). Therefore, epigenetic repression of miR-137 may occur in some of GBMs, and the underlying molecular mechanism remains unclear.

5.5 Biological effects of miR-137 overexpression in glioma cells

Having demonstrated that miR-137 deregulation was frequent and associated with tumor progression and proliferative activity in OTs, it was subsequently questioned whether miR-137 played a role in gliomagenesis.

In the present study, delivery of miR-137 into miR-137–deficient OT and GBM cells inhibited cell growth as evaluated by cell number and metabolic activity. The results of the 2 assays were in well agreement. The suppressive effect is also significant when cells grew in soft agar. Hence, we have proved that miR-137 inhibited glioma cell growth under both anchorage-dependent and -independent conditions.

Three possible cellular processes responsible for the growth inhibition affected by miR-137 were thereafter investigated. First, miR-137 suppressed DNA synthesis and induced G0/G1 cell cycle arrest in OT and GBM cells. In agreement with this, inhibited cell proliferation by miR-137 has been observed in several tumors, such as GBM (Silber *et al.*, 2008), colorectal cancer (Balaguer *et al.*, 2010; Liu *et al.*, 2010), oral squamous cell carcinoma (Kozaki *et al.*, 2008) and uveal melanoma (Chen *et al.*, 2010). Second, miR-137 induced programmed cell death as indicated by markedly elevated cleaved PARP levels in all glioma cell lines examined, which was a novel effect for miR-137 in human tumors. Above elucidation suggested that miR-137 exerted the cell growth suppressive effect in OT cell via cell cycle arrest and apoptosis.

The infiltrating property is a hallmark of diffuse gliomas, which make wholly surgical resection difficult and lead to high recurrence of this malignancy. In our

functional study, miR-137 affected migrating and invasive ability of glioma cells by monolayer cell wound healing assay and matrigel chamber invasion assay, which was demonstrated in colorectal cancer cells as well (Liu *et al.,* 2010).

Moreover, miR-137 may induce neuronal-like differentiation as indicated by notably increased expression of neuronal marker Tuj1 in U87MG and U373MG GBM cells, although no neuronal morphological alteration observed meanwhile. The expression of astrocytic marker, GFAP was not induced in both GFAP+ (U373MG) and GFAP- (A172, U87MG and TC620) cell lines. This result was supported by previous reports revealing neuronal differentiation promoting effect of miR-137 in glioma TSCs, NSCs (Silber *et al.,* 2008) as well as ESCs (Tarantino *et al.,* 2010).

Taken together, our data indicated that high tumor grade and proliferative activity in primary OT were associated with deregulation of miR-137 and miR-137 inhibited malignant behaviors in glioma.

5.6 CSE1L is a novel miR-137 target in glioma

MiRNAs execute diverse functional roles via post-transcriptional silencing of gene targets by interacting with 3'UTR of target transcript. Thus it is crucial to identify miRNA downstream targets for our understanding miRNA-mediated regulation. With respect to miR-137 targets, several targets has been reported in various normal and malignant cell types (Bemis *et al.,* 2008; Kozaki *et al.,* 2008; Silber *et al.,* 2008; Chen *et al.,* 2010; Liu *et al.,* 2010; Smrt *et al.,* 2010; Szulwach *et al.,* 2010; Tarantino *et al.,* 2010). Given that mammalian miRNA can have multiple targets (Lewis *et al.,* 2005; Lim *et al.,* 2005), I subsequently sought to identify novel miR-137 target gene(s) which is implicated in pathogenesis of glioma. In this study, *CSE1L* is established as a novel miR-137 target in glioma by integrated strategies constituting bioinformatic prediction and experimental validation.

Since mammalian miRNA exerts gene silencing via partial complementary with 3'UTR region of target mRNAs, the basic step in our screening is *in silico* prediction by 4 bioinformatic algorithms, miRanda (Enright *et al.*, 2003; John *et al.*, 2004), PicTar (Grun *et al.*, 2005; Krek *et al.*, 2005) and TargetScan (Lewis *et al.*, 2003; Lewis *et al.*, 2005) and microCosm (Griffiths-Jones *et al.*, 2006). As different criteria are covered in each of these programmes (Table 3.6), potential targets predicted by more algorithms may have higher chance to be true targets.

Here, *CSE1L* is predicted by all 4 programmes utilized. The putative miR-137 binding sites perfectly match the first 8 nucleotides at the 5'end of miR-137, covering the seed region (the 2^{nd}-8^{th} nuleotides) which is essential for miRNA target recognition (Bartel 2004; Lewis *et al.*, 2005; Bartel 2009). The thermodynamic

stability of the miRNA:mRNA hybrid is demonstrated by the free energy of −14.8 kcal/mol. In addition, the MRE region in the 3'UTR of *CSE1L* is conserved across different species including human, chimp, mouse, rat and dogs. These results suggest that CSE1L is a candidate target of miR-137 in glioma.

Moreover, despite there are dozens of human miRNAs predicted to potentially target CSE1L by all 4 bioinformatic algorithms, miR-137 is the only one hit with a broadly conserved MRE among vertebrates according to PicTar and TargetScan. MiR-137 also ranks the 1st among the 19 miRNAs which may regulating CSE1L as assessed by miRanda score, suggesting miR-137 might be a regulator for CSE1L.

Subsequent experimental validation, including dual-luciferase reporter assay, qRT-PCR and western blotting, have verified the suppression of CSE1L by miR-137 through direct interaction between miR-137 and predicted MRE in CSE1L 3'UTR. We observed a significantly reduced abundance of CSE1L protein in all 3 OT and 4 GBM cell lines after transfection with miR-137 mimic by western blot. Meanwhile, the CSE1L transcript level was not affected as determined by qRT-PCR analysis. Hence, CSE1L was negatively regulated by miR-137 via translational inhibition rather than mRNA degradation in glioma cells. Moreover, dual-luciferase reporter assay have confirmed this repression was mediated by the binding of miR-137 to the putative MRE in 3'UTR of CSE1L mRNA, where the base pairing at the seed region is essential for the interaction. Therefore, miR-137 directly suppressed *CSE1L* at translational level in glioma.

A previous study by Balaguer *et al.* attempted to identify miR-137 targets in colorectal cancer and took CSE1L as a candidate as well. In contrast to our result,

CSE1L protein expression was not altered following ectopic miR-137 expression in colorectal cancer cells (Balaguer *et al.,* 2010). This is probably due to human CSE1L transcript isoforms express in a tissue-specific manner (Brinkmann *et al.,* 1999). The MRE of miR-137 lies only in CSE1L mRNA variants those harboring an extended 3'UTR region. This isoform was found uniquely expressed in brain, spinal cord, peripheral nerves as well as fetal liver, but not in colon (Brinkmann *et al.,* 1999). The tissue-specific expression pattern of CSE1L may give rise to the tissue-dependent regulation of *CSE1L* by miR-137 and make the modulation more important.

5.7 Expression of *CSE1L* in glioma

Having demonstrated the tumor suppressive role of miR-137 and its negatively control of CSE1L in glioma, we subsequently wondered whether CSE1L displayed a enhanced expression in our panel of OTs and furthermore whether there was an inverse correlation between miR-137 and CSE1L expression level.

CSE1L transcript expression was enhanced in 50% (18/36) of OTs up to 12.7-fold elevation as compared to normal brain by qRT-PCR analysis. More than 2-fold overexpression of CSE1L mRNA was observed in 2 of 3 OT cells and 6 of 7 GBM cells. At protein level, IHC indicated a significant upregulation of CSE1L in the series of 36 OTs in comparison of 13 non-neoplastic brain tissues. Thus, CSE1L is overexpressed in OTs at both mRNA and protein levels.

CSE1L is the human homologue of the yeast gene chromosome segregation 1 (*CSE1*), which plays an essential role in the mitotic spindle checkpoint and therefore ensuring genomic stability during yeast cell division (Xiao *et al.,* 1993; Brinkmann *et al.,* 1995). Among normal human tissues, CSE1L preferentially expresses in testis and fetal liver, which contain lots of actively proliferating cells (Brinkmann *et al.,* 1995). Human *CSE1L* gene maps to chromosome 20q13.13, a locus with frequent gains in gliomas, especially in astrocytomas of all grades (Weber *et al.,* 1996; Nishizaki *et al.,* 1998; Paunu *et al.,* 2000; Weber *et al.,* 2001; Koschny *et al.,* 2002; Yakut *et al.,* 2007). Of particular interest, high resolution-CGH studies have unveiled an increased *CSE1L* copy number in 57% (8/14) of GBM and cell lines (Hui *et al.,* 2001), as well as during the progression of low-grade OTs (50%, 4/8) and astrocytomas (33%, 2/6) (Idbaih *et al.,* 2008). Such chromosomal gain of *CSE1L* is

observed in a spectrum of other tumor types, such as medulloblastoma (Tong *et al.*, 2004), nasopharyngeal carcinoma (Hui *et al.*, 2002), prostate cancer (Bar-Shira *et al.*, 2002), cervical cancer (Narayan *et al.*, 2010), primary cutaneous B-cell lymphoma (Mao *et al.*, 2002), gastro-esophageal cancer (Rosenberg *et al.*, 2002), leukemia, colorectal and breast cancers (Brinkmann *et al.*, 1996).

Apart from gene copy number gain, upregulation of CSE1L mRNA and protein products was documented in cancers of various origins, including hepatocellular carcinoma (Wellmann *et al.*, 2001; Shiraki *et al.*, 2006), colon cancer (Brinkmann *et al.*, 1995; Seiden-Long *et al.*, 2006), lung cancer (Brinkmann *et al.*, 1995), lymphoma (Brinkmann *et al.*, 1995; Wellmann *et al.*, 1997), melanoma (Boni *et al.*, 1999) and endometrial carcinoma (Peiro *et al.*, 2001). In combination of our findings, it is suggested that *CSE1L* may play a role in carcinogenesis.

The overexpression of CSE1L in glioma may attribute to several possible factors. In this study, CSE1L is identified negatively controlled by miR-137 in glioma. The results also demonstrated that among 33 OTs with a reduced miR-137 level and available CSE1L protein expression, 87% (29/33) of cases displayed an elevated CSE1L protein level. This suggested that miR-137 was a key regulator of CSE1L in OT.

In addition, although the genomic status of *CSE1L* has not been described to date, one potential explanation is copy number gain, which has been extensively demonstrated in various tumors as mentioned above in this section. More significantly, Peiro *et al.* has uncovered a correlation between CSE1L upregulation and chromosome 20q13 amplification in ovarian cancer (Peiro *et al.*, 2002). In GBM,

gain of *CSE1L* gene is observed in 57% of GBMs (Hui *et al.,* 2001), whereas we have shown an overexpression of CSE1L in 8 of 10 GBM cell lines. It is therefore suggested that copy number gain may result in the elevation of CSE1L transcript and protein in gliomas.

Another plausible molecular mechanism is elevation of CSE1L transcript and protein by hepatocyte growth factor (HGF) and its receptor MET signaling activation in colon cancer cells (Seiden-Long *et al.,* 2006). The CSE1L transcript expression showed strong correlation with MET in 30 normal and 93 colorectal tumors, suggesting the transcriptional regulation of CSE1L by MET. Moreover, the protein abundance of CSE1L is also KRAS-dependent, which may explain the differential expression pattern of CSE1L mRNA and protein observed *in vitro* as well as *in vivo* (Seiden-Long *et al.,* 2006). In concordance with our observation of CSE1L upregulation, HGF and proto-oncogene MET are highly expressed in glioma (Abounader *et al.,* 2005), supporting the potential enhance of CSE1L by activated HGF/MET signaling in glioma.

In addition, CSE1L may be regulated by other miRNAs besides miR-137, as the CSE1L 3'UTR region carries potential MREs for miR-19a, -19b, -23a, -23b, -128, -182, -194, -203, -377 and -384 according to miRanda and microCosm. Whether these miRNAs contribute to modulation of CSE1L in glioma remains to be explored.

5.8 Intracellular distribution of CSE1L in OTs

The IHC results clearly showed a nucleus staining of CSE1L in cells of OTs and non-neoplastic brain tissues. It differed from localization of CSE1L in cells of other tumors indicated by IHC. Cytoplasmic distribution of CSE1L is reported in hepatocellular carcinoma (Shiraki *et al.,* 2006), lymphoma (Wellmann *et al.,* 1997), melanoma (Boni *et al.,* 1999) and endometrial carcinoma cells (Peiro *et al.,* 2001). Two independent investigations revealed CSE1L IHC activity at nucleus and cytoplasm of ovarian cancer cells, respectively (Peiro *et al.,* 2002; Brustmann 2004). In colon cancer, several studies indicated cytoplasmic CSE1L IHC staining (Tsao *et al.,* 2009; Tung *et al.,* 2009; Tsai *et al.,* 2010), while both nucleus and cytoplasmic CSE1L expression was described by another research group (Seiden-Long *et al.,* 2006). Particularly, Behrens *et al.* discovered invasive breast cancers display a nuclear CSE1L expression pattern. In the contrary, benign lesions along with *in situ* carcinomas exhibited a predominately cytoplasmic CSE1L staining (Behrens *et al.,* 2001). More detailed characterization of the variable distribution of CSE1L came from Scherf *et al.* describing that CSE1L might be associated with microtubules in interphase cells while colocalized with the chromosome segregation spindle apparatus in mitotic cells by immunofluorescent staining in breast cancer cells (Scherf *et al.,* 1996).

The molecular basis of the diversity in CSE1L intracellular expression pattern may attribute to a role of CSE1L as a nuclear transport factor, which is necessary for recycling importin-α from the nucleus to the cytoplasm (Kutay *et al.,* 1997). Another study further elucidated that CSE1L intracellular distribution is determined by its phosphorylation via MAPK/ERK kinase 1 (MEK-1). Phosphorylated or

dephosphorylated CSE1L accumulates predominantly in the cytoplasm or in the nucleus, respectively (Scherf *et al.,* 1998). It was speculated that the cytoplasmic microtubule-associated CSE1L may act as a reservoir of CSE1L protein, the nuclear CSE1L however is related to the mitotic spindle during cell division.

Overall, the divergent localization of CSE1L in tumors of various origins, or even in differential degree of malignancy of same tumor suggested the distribution of CSE1L in cells may lead to alternative CSE1L functional role in cell proliferation and thereby affect the development of human tumors.

5.9 Correlation of CSE1L expression with clinicopathological and molecular features in OTs

Apart from the consistent upregulation of CSE1L in various tumors including glioma, CSE1L transcript level has been shown to positively correlated with higher metastatic and tumorigenic ability of nasopharyngeal carcinoma cells (Fang *et al.*, 2005) and metastatic property of colorectal tumors (Seiden-Long *et al.*, 2006). IHC analysis revealed correlation of CSE1L expression with i) tumor grade of hepatocellular carcinoma (Wellmann *et al.*, 2001), endometrial carcinoma (Peiro *et al.*, 2001) and ovarian cancer (Peiro *et al.*, 2002; Brustmann 2004); ii) tumor stage of melanoma (Boni *et al.*, 1999) and ovarian cancer (Peiro *et al.*, 2002); and iii) invasive capability of breast cancers (Behrens *et al.*, 2001).

More importantly, CSE1L showed strong correlation with Ki-67 staining in lymphoma (Wellmann *et al.*, 1997), proliferating cell nuclear antigen (PCNA) staining in hepatocellular carcinoma (Shiraki *et al.*, 2006) as well as cyclin D1 and mitotic activity in ovarian cancer (Peiro *et al.*, 2002; Brustmann 2004). Above reports implied a role of CSE1L in tumor progression as well as cell proliferation.

Unlike these findings, no significant correlation was observed between CSE1L expression and tumor grade or Ki-67 labeling index in OTs, suggesting the link may be tumor-specific. Meanwhile, to achieve a more accurate conclusion, more samples is required.

The survival analysis demonstrated CSE1L expression at mRNA or protein level was not associated with outcome of OT patients. It was previous illustrated that high expression of CSE1L has been linked with a shorter survival in endometrial

carcinoma (Peiro *et al.,* 2001) and ovarian cancer (Peiro *et al.,* 2002), but not in nasopharyngeal carcinoma (Kim *et al.,* 2010). The results suggested a variable prognostic significance of CSE1L in different tumor types. Larger sample size may lead to a more promising result.

5.10 CSE1L mediates effects of miR-137 in glioma cells

The next question to be resolved is to determine whether inhibition of CSE1L mediates the tumor suppressive role of miR-137 observed in glioma cells.

Here, CSE1L-specific siRNAs successfully knocked down CSE1L expression in CSE1L-abundant OT and GBM cells. Our results demonstrated that attenuation of CSE1L led to reduced proliferation, induced apoptosis and suppressed invasiveness in both OT and GBM cells. It was notable that these effects were similar to those observed after miR-137 overexpression, but to a less extent, suggesting that miR-137 may mediate its effect partly through CSE1L repression.

It is also implicated the existence of other target genes of miR-137, which may contribute to biological roles of miR-137 in glioma. CDK6 and MITF belong to such candidates. Earlier investigations have shown that CDK6 is inhibited by ectopic expression of miR-137 in U251 GBM cells (Silber *et al.,* 2008), oral squamous cell carcinoma (Kozaki *et al.,* 2008) and uveal melanoma cells (Chen *et al.,* 2010), where miR-137 resulting in cell cycle arrest. CDK6 is a well-known cell cycle regulator, which promotes G1-S transition and is important in cell proliferation (Meyerson *et al.,* 1994; Grossel *et al.,* 2006). Consistently, elevated CDK6 expression has been detected in 85.6% (12/14) of GBMs (Lam *et al.,* 2000). Therefore, it was highly possible that CSEIL and CDK6 act together to mediate the inhibitory effect of miR-137 on glioma cell proliferation.

In addition, miR-137 exerts its effect of reducing cell proliferation via suppressing MITF expression in uveal melanoma cells (Chen *et al.,* 2010). The expression of MITF is present in GBM according to TCGA microarray data.

Whether these miR-137 targets validated in other cell types are still repressed by miR-137 in glioma and are responsible for miR-137 effects require further investigations.

5.11 Biological roles of *CSE1L* in glioma cells

In my study, knockdown of CSE1L in glioma cells inhibited cell proliferation, induced cellular apoptosis and suppressed cell motility and invasiveness, suggesting multiple functions of *CSE1L*. These observations were in line with involvement of *CSE1L* with cancer cell proliferation, apoptosis as well as invasion in previous reports (Brinkmann 1998; Behrens et al., 2003; Tai et al., 2010).

5.11.1 *CSE1L* in glioma cell proliferation

CSE1L is the human homologue of the yeast gene *CSE1* with a protein product sequence showing 59% overall homology to the yeast CSE1 protein (Brinkmann *et al.*, 1995). Mutation of *CSE1* induced G2 phase or mitotic arrest and deficient cyclin B proteolysis (Xiao *et al.*, 1993; Irniger *et al.*, 1995). Later study showed depletion of *CSE1* resulted in disrupted DNA replication (Yu *et al.*, 2006). *CSE1* is therefore considered as an essential gene for yeast replication, giving rise to the postulation that *CSE1L* might be involved in mammalian cell proliferation.

In mouse model, Cse1l expression increased during mouse embryo development with high levels in adult proliferating tissues (Bera *et al.*, 2001). In regard to human *CSE1L*, Brinkmann *et al.* observed an abundant CSE1L expression in human leukemia, lymphoma, colon and lung cancer cells as well as some of human normal tissues containing many proliferating cells by northern blot analysis, such as testis, fetal liver and lymphoid, but only low levels in tissues those do not actively proliferate. *In vitro*, CSE1L expression levels changed in accompany with the proliferation status of WI-38 human fibroblasts (Brinkmann *et al.*, 1995). In concordance to the observation in the yeast, another study demonstrated that ectopic

expression CSE1L antisense cDNA led to arrest in G2 phase or mitosis along with cyclin B accumulation in HeLa human cervical cancer cells (Ogryzko *et al.,* 1997). Thus, CSE1L might be necessary in human cell cycle progression. Consequently, mounting evidence have indicated highly CSE1L expression in various cancers, with positive correlation with tumor grade or cell proliferation index in some of them as summarized in section 5.7 and 5.9. CSE1L was thus thought as a proliferation-associated protein, probably participating in tumor cell proliferation during cancer formation and progression.

In concordance with these findings, our results showed interruption of CSE1L in glioma cells induces a suppressed cell proliferation as evaluated by cell number, metabolic activity and DNA synthesis. This was in contrast to enhanced CSE1L expression in HT-29 colon cancer and MCF-7 breast cancer cells were not able to increase cell proliferation (Jiang *et al.,* 2004; Liao *et al.,* 2008). I therefore speculated that CSE1L might be necessary in cell cycle progression, but not sufficient alone to stimulate cancer cell proliferation. It is also plausible that the role of CSE1L in cell proliferation is cancer-specific. A better understanding of the underlying mechanisms for the differential phenotype deserves further investigation.

5.11.2 CSE1L in glioma cell apoptosis

Our study has revealed CSE1L inactivation in glioma cells resulted in elevated cellular apoptosis, which was in line with several previous finding. Bera *et al.* generated homozygous and heterozygous Cse1l knockout mice and observed that the Cse1l heterozygous mice were still phenotypically normal and fertile, homozygous Cse1l depleted mutant is however embryonically lethal. The *in vivo* experiments

emphasized the essential role of Cse1l for mouse embryonic growth and development (Bera *et al.,* 2001). In addition, CSE1L protein expression inversely correlated with apoptotic activity in human hepatocellular carcinoma by IHC analysis (Shiraki *et al.,* 2006). These suggested that CSE1L might be cell survival-related and protected cells from programmed cell death.

CSE1L has been widely implicated in chemotherapeutic drug-induced apoptosis. In MCF-7 breast cancer cells, however, CSE1L reduction conferred cell resistance to the ADP-ribosylating toxins *pseudomonas* exotoxin, diphtheria toxin and tumor necrosis factors, but showed no effect on the cell death induced by etoposide, staurosporine or cycloheximid (Brinkmann *et al.,* 1996). Interferon- γ treatment induced CSE1L expression in HT-29 colon cancer cells, where CSE1L overexpression enhanced interferon-γ-induced apoptosis (Jiang *et al.,* 2001). CSE1L knockdown also attenuated MCF-7 and HT-29 cell apoptosis induced by UV light as well as a series of chemotherapeutic drugs, including oxorubicin, 5-fluorouracil, cisplatin, and tamoxifen, with a concurrent p53 protein accumulation (Tanaka *et al.,* 2007; Liao *et al.,* 2008). The positive effects of CSE1L in drug-induced apoptosis may be mediated by its association with promoter of some p53 targets (Tanaka *et al.,* 2007) and/or enhancement in apoptosome formation (Kim *et al.,* 2008).

In contrast, CSE1L inhibited paclitaxel-induced apoptosis, G2/M phase cell cycle arrest and aster formation of cancer cells (Liao *et al.,* 2008). Paclitaxel serves as a chemotherapy drug by targeting the microtubule assembly and activating pro-apoptotic signaling pathways (Yvon *et al.,* 1999; Zhou *et al.,* 2005). It was in well agreement with the earlier observed *CSE1L* association with microtubule (Scherf *et al.,* 1996), which appears in turn to protect microtubule from paclitaxel binding and

thereby escape from apoptosis.

5.11.3 CSE1L in glioma cell invasion

In my study, CSE1L knockdown reduced glioma cell mobility, which was in line with CSE1L function in other tumors. Expression of CSE1L correlated with metastatic ability in nasopharyngeal carcinoma cells (Fang *et al.,* 2005) and colon cancer (Seiden-Long *et al.,* 2006). It was also shown that sera CSE1L was most prevalent in a collection of metastatic cancers, followed by invasive and primary cancers of various origins (Tung *et al.,* 2009; Tsai *et al.,* 2010).

Functional assays gave evidence that CSE1L overexpression enhanced cell migration, invasion and matrix metalloproteinase 2 (MMP2) secretion in MCF-7 breast cancer cells, where CSE1L and MMP2 colocalized (Liao *et al.,* 2008; Tai *et al.,* 2010). CSE1L reduction inhibited the metastasis of B16-F10 melanoma cells in mice, validating the effect *in vivo* (Liao *et al.,* 2008; Tsai *et al.,* 2010).

MMP2 is a member of MMP family, which possess proteolytic activity against extracellular matrix (ECM) components and herein plays critical role in glioma cell invasion. Elevated MMP2 expression was found in gliomas, whereas inhibition of MMP2 led to reduced glioma cell invasion. (Fillmore *et al.,* 2001; Rao 2003) Together with our results in glioma, it is speculated that CSE1L is important in modulation of glioma cell invasion, potentially through regulating MMP2.

CHAPTER 6 CONCLUSIONS

The main aim of my study was to elucidate the role of miR-137, a chromosome 1p encoded miRNA in gliomas with a focus on OTs.

The expression level of miR-137 was demonstrated to be frequently down-regulated in 94% (34/36) of OTs as compared to those of normal brains. A statistically significant difference was observed in miR-137 expression between normal brain samples and 20 oligodendrogliomas (p=0.016) or 16 oligoastrocytomas (p=0.009). All 3 OT and 7 GBM cultured cells displayed decreased miR-137 expression (p=0.007). The miR-137 level was significantly lower in WHO grade III OTs than those of WHO grade II (p=0.010). The expression of miR-137 was inversely correlated with Ki-67 labeling index in OTs (p=0.009). These results strongly suggest reduced miR-137 level may play a role in OT development and progression.

The mechanisms responsible for reduced miR-137 expression were investigated. In OT cells, DNA demethylation and histion deacetylating inhibition treatment induced a synergetic miR-137 restoration (p<0.001). Expression of miR-137 showed no correlation with loss of chromosome 1p (p=0.115), where miR-137 is mapped. Therefore, miR-137 inactivation in OTs may result from aberrant epigenetic modification rather than 1p allelic loss.

Ectopic expression of miR-137 significantly inhibited both anchorage-dependent and –independent cell growth, through suppressing cell proliferation and inducing apoptosis in one OT and three glioblastoma cells (p<0.015). Cell invasiveness was repressed by enhanced miR-137 expression in these cells as well (p<0.001). In

addition, neuronal-like differentiation was induced by miR-137 ectopic expression in two GBM cells. These observations strongly suggested that miR-137 is a potential tumor suppressive miRNA in OT and GBM.

CSE1L, *ERBB4*, *NRP1*, *CDC42* and *AKT2* were predicted as miR-137 target candidates by bioinformatic analysis. Among the 5 genes, miR-137 specifically interacted with 3'UTR of CSE1L and ERBB4 transcripts in glioma cells. CSE1L protein, but not mRNA, levels were reduced after miR-137 transfection in glioma cells. The results indicated that miR-137 binds to 3'UTR of CSE1L mRNA and negatively regulated CSE1L through translational inhibition in glioma.

Examinations of *CSE1L* encoded product expression were subsequently performed. Elevated CSE1L transcript level was detected in 30% (6/20) of oligodendrogliomas and 75% (12/16) of oligoastrocytomas cases, up to 3.3- and 12.7-fold, when compared to normal brains, respectively (p=0.022). CSE1L mRNA was overexpressed in 2 of 3 OT cells and 6 of 7 GBM cells (p=0.014). At protein level, a significant upregulation of CSE1L in the cohort of 36 OTs in comparison of 13 non-neoplastic brain tissues was observed (p<0.001). However, the abundance of CSE1L mRNA or protein showed no significant correlation with miR-137 level in OTs (p=0.326 and p=0.300, respectively). These data have revealed overexpression of CSE1L in OTs at both mRNA and protein levels, suggesting CSE1L is potentially implicated in gliomagenesis.

Investigations on functional role of CSE1L in OT and GBM cells were carried out using CSE1L loss-of-function approach. CSE1L knockdown led to significant reduced proliferation, induced apoptosis and suppressed invasiveness in glioma cells

(p<0.001). These effects were similar to those observed after miR-137 overexpression, but to a less extent, suggesting that miR-137 may mediate its effect partially through CSE1L.

In summary, we present the first study on miR-137 in human OTs, suggesting that miR-137 plays an important role in the development of OT and GBM. Our results increased the understanding of pathogenesis of gliomas, and the miR-137-*CSE1L* pathway may serve as a potential therapeutic target in treatment of gliomas.

CHAPTER 7 FUTURE STUDIES

7.1 Molecular mechanisms for miR-137 inactivation in glioma

Our results in this study along with previous findings have uncovered a reduced miR-137 expression in oligodendroglial and astrocytic gliomas (Silber et al., 2008; Zhi et al., 2010). The mechanisms underlie miR-137 silencing are poorly understood. Our data raise aberrant epigenetic modification as a plausible reason rather than chromosome 1p loss in OTs. However, whether miR-137 promoter hypermethylation or an indirect regulation is responsible remains elusive. Therefore, analysis of miR-137 promoter methylation in OTs is required. Bisulfate sequencing and methylation-specific PCR on the CpG islands located within putative miR-137 promoter region can be utilized to determine the miR-137 promoter methylation status, and to test whether miR-137 downregulation shows a correlation with promoter hypermethylation. Alteration of miR-137 promoter methylation status after DNA demethylating treatment can also provide hints to understand this regulation in OT cells.

In addition, other potential mechanisms, such as VNTR variation upstream pre-miR-137, defects in miR-137 biogenesis machinery and mutation at coding sequence, deserve further investigation to explain silencing of miR-137 in glioma.

7.2 Identification of more miR-137 targets in glioma

Given that CSE1L partially mediated miR-137 effects in glioma, it is worthwhile to study other target genes of miR-137 to explore the miR-137 regulated pathways. In other tumor types or stem cells, several miR-137 target genes have been

documented, including MITF, LSD1 and Ezh2 (Bemis *et al.*, 2008; Balaguer *et al.*, 2010; Szulwach *et al.*, 2010). Whether these genes are controlled by miR-137 and moreover, account for miR-137 effects in glioma needs to be verified.

On the other hand, high-throughput array analysis can provide potential targets with decreased expression following miR-137 ectopic expression in glioma cells. By coupling such gene expression profiling results with bioinformatic predictions, more promising targets can be discovered. Those validated targets may probably establish a miR-137 regulatory network, which will largely enhance our knowledge on role of miR-137 in gliomagenesis.

7.3 Role of miR-137 and CSE1L in drug-induced apoptosis in glioma

As chromosome 1p deletion is predictive of chemosensitivity in OT patients and CSE1L has been implicated in drug-induced cellular apoptosis, whether miR-137 and CSE1L render glioma cells sensitive to chemotherapeutic drugs becomes an important but unsolved question. To test this issue, miR-137 or siCSE1L transfected glioma cells can be exposed to several chemotherapeutic drugs, such as procarbazine, lomustine, vincristine, TMZ, paclitaxel and cisplatin. The cell survival after drug treatment can reflect the chemotherapeutic drug sensitivity as evaluated by MTT assay. If the potential significance of miR-137 and CSE1L here is proved, it may help to improve outcome following chemotherapy.

7.4 Deciphering dysregulated and clinical relevant miRNAs in glioma

Up to data, the pool of miRNA database is continuously increasing since

discovery of this class of tiny molecules nearly 2 decades ago. Although some earlier miRNA profiling studies have uncovered a series of miRNAs with abnormal expression levels in glioma compared to normal brains or lower-grade gliomas, suggesting an important role these miRNAs play in glioma development and progression, our understanding of aberrant expressed miRNA in gliomagenesis is still inadequate. Further miRNA expression profiling containing probes specific to newly discovered miRNAs is necessary to characterize the roles of these short mRNAs in pathogenesis of glioma.

On the other hand, by correlate miRNA expression with patient survival time, some miRNAs with prognostic significance may be identified. This would provide novel clues for clinical relevance of miRNA in glioma.

7.5 Effects of miR-137 in vivo and the therapeutic potential in glioma treatment

Our study has shown a potential tumor suppressive role of miR-137 in vitro, but the in vivo biological effects has not been defined. By using an induced intracranial glioma model in mouse, we can test whether miR-137 restored expression can be employed as a potential therapeutic strategy for glioma treatment in the future.

Nowadays, miRNA or siRNA as a feasible therapeutic approach for glioma is challenged by numerous issues, including selection of suitable miRNA or gene targets, development of efficient and specific delivery systems, determination of optimized treatment dose and administration schedule as well as measurement system of a validated clinical response (Guo *et al.*, 2010). Future testing and clinical trials are required to resolve these existing problems with a hope.

REFERENCES

Abounader R and Laterra J. Scatter factor/hepatocyte growth factor in brain tumor growth and angiogenesis. ***Neuro Oncol*** 2005;7:436-451.

Ando T, Yoshida T, Enomoto S, Asada K, Tatematsu M, Ichinose M, Sugiyama T and Ushijima T. DNA methylation of microRNA genes in gastric mucosae of gastric cancer patients: its possible involvement in the formation of epigenetic field defect. ***Int J Cancer*** 2009;124:2367-2374.

Aylon Y and Oren M. Living with p53, dying of p53. ***Cell*** 2007;130:597-600.

Balaguer F, Link A, Lozano JJ, Cuatrecasas M, Nagasaka T, Boland CR and Goel A. Epigenetic silencing of miR-137 is an early event in colorectal carcinogenesis. ***Cancer Res*** 2010;70:6609-6618.

Balss J, Meyer J, Mueller W, Korshunov A, Hartmann C and von Deimling A. Analysis of the IDH1 codon 132 mutation in brain tumors. ***Acta Neuropathol*** 2008;116:597-602.

Bandres E, Agirre X, Bitarte N, Ramirez N, Zarate R, Roman-Gomez J, Prosper F and Garcia-Foncillas J. Epigenetic regulation of microRNA expression in colorectal cancer. ***Int J Cancer*** 2009;125:2737-2743.

Bandres E, Cubedo E, Agirre X, Malumbres R, Zarate R, Ramirez N, Abajo A, Navarro A, Moreno I, Monzo M and Garcia-Foncillas J. Identification by Real-time PCR of 13 mature microRNAs differentially expressed in colorectal cancer and non-tumoral tissues. ***Mol Cancer*** 2006;5:29.

Bar-Shira A, Pinthus JH, Rozovsky U, Goldstein M, Sellers WR, Yaron Y, Eshhar Z and Orr-Urtreger A. Multiple genes in human 20q13 chromosomal region are involved in an advanced prostate cancer xenograft. ***Cancer Res*** 2002;62:6803-6807.

Barbashina V, Salazar P, Holland EC, Rosenblum MK and Ladanyi M. Allelic losses at 1p36 and 19q13 in gliomas: correlation with histologic classification, definition of a 150-kb minimal deleted region on 1p36, and evaluation of CAMTA1 as a candidate tumor suppressor gene. ***Clin Cancer Res*** 2005;11:1119-1128.

Bartel DP. MicroRNAs: genomics, biogenesis, mechanism, and function. ***Cell*** 2004;116:281-297.

Bartel DP. MicroRNAs: target recognition and regulatory functions. ***Cell*** 2009;136:215-233.

Bauman GS, Ino Y, Ueki K, Zlatescu MC, Fisher BJ, Macdonald DR, Stitt L, Louis DN and Cairncross JG. Allelic loss of chromosome 1p and radiotherapy plus chemotherapy in patients with oligodendrogliomas. ***Int J Radiat Oncol Biol Phys*** 2000;48:825-830.

Behrens P, Brinkmann U, Fogt F, Wernert N and Wellmann A. Implication of the proliferation and apoptosis associated CSE1L/CAS gene for breast cancer development. ***Anticancer Res*** 2001;21:2413-2417.

Bello MJ, Leone PE, Vaquero J, de Campos JM, Kusak ME, Sarasa JL, Pestana A and Rey

JA. Allelic loss at 1p and 19q frequently occurs in association and may represent early oncogenic events in oligodendroglial tumors. ***Int J Cancer*** 1995;64:207-210.

Bello MJ, Vaquero J, de Campos JM, Kusak ME, Sarasa JL, Saez-Castresana J, Pestana A and Rey JA. Molecular analysis of chromosome 1 abnormalities in human gliomas reveals frequent loss of 1p in oligodendroglial tumors. ***Int J Cancer*** 1994;57:172-175.

Bemis LT, Chen R, Amato CM, Classen EH, Robinson SE, Coffey DG, Erickson PF, Shellman YG and Robinson WA. MicroRNA-137 targets microphthalmia-associated transcription factor in melanoma cell lines. ***Cancer Res*** 2008;68:1362-1368.

Benetkiewicz M, Idbaih A, Cousin PY, Boisselier B, Marie Y, Criniere E, Hoang-Xuan K, Delattre JY, Sanson M and Delattre O. NOTCH2 is neither rearranged nor mutated in t(1;19) positive oligodendrogliomas. ***PLoS One*** 2009;4:e4107.

Bera TK, Bera J, Brinkmann U, Tessarollo L and Pastan I. Csell is essential for early embryonic growth and development. ***Mol Cell Biol*** 2001;21:7020-7024.

Beuvink I, Kolb FA, Budach W, Garnier A, Lange J, Natt F, Dengler U, Hall J, Filipowicz W and Weiler J. A novel microarray approach reveals new tissue-specific signatures of known and predicted mammalian microRNAs. ***Nucleic Acids Res*** 2007;35:e52.

Bigner SH, Matthews MR, Rasheed BK, Wiltshire RN, Friedman HS, Friedman AH, Stenzel TT, Dawes DM, McLendon RE and Bigner DD. Molecular genetic aspects of oligodendrogliomas including analysis by comparative genomic hybridization. ***Am J Pathol*** 1999;155:375-386.

Boni R, Wellmann A, Man YG, Hofbauer G and Brinkmann U. Expression of the proliferation and apoptosis-associated CAS protein in benign and malignant cutaneous melanocytic lesions. ***Am J Dermatopathol*** 1999;21:125-128.

Boulay JL, Miserez AR, Zweifel C, Sivasankaran B, Kana V, Ghaffari A, Luyken C, Sabel M, Zerrouqi A, Wasner M, Van Meir E, Tolnay M, Reifenberger G and Merlo A. Loss of NOTCH2 positively predicts survival in subgroups of human glial brain tumors. ***PLoS One*** 2007;2:e576.

Bourne TD and Schiff D. Update on molecular findings, management and outcome in low-grade gliomas. ***Nat Rev Neurol*** 2010;6:695-701.

Brandes AA, Tosoni A, Cavallo G, Reni M, Franceschi E, Bonaldi L, Bertorelle R, Gardiman M, Ghimenton C, Iuzzolino P, Pession A, Blatt V and Ermani M. Correlations between O6-methylguanine DNA methyltransferase promoter methylation status, 1p and 19q deletions, and response to temozolomide in anaplastic and recurrent oligodendroglioma: a prospective GICNO study. ***J Clin Oncol*** 2006;24:4746-4753.

Brinkmann U, Brinkmann E, Bera TK, Wellmann A and Pastan I. Tissue-specific alternative splicing of the CSE1L/CAS (cellular apoptosis susceptibility) gene. ***Genomics*** 1999;58:41-49.

Brinkmann U, Brinkmann E, Gallo M and Pastan I. Cloning and characterization of a cellular apoptosis susceptibility gene, the human homologue to the yeast

chromosome segregation gene CSE1. ***Proc Natl Acad Sci U S A*** 1995;92:10427-10431.

Brinkmann U, Brinkmann E, Gallo M, Scherf U and Pastan I. Role of CAS, a human homologue to the yeast chromosome segregation gene CSE1, in toxin and tumor necrosis factor mediated apoptosis. ***Biochemistry*** 1996;35:6891-6899.

Brinkmann U, Gallo M, Polymeropoulos MH and Pastan I. The human CAS (cellular apoptosis susceptibility) gene mapping on chromosome 20q13 is amplified in BT474 breast cancer cells and part of aberrant chromosomes in breast and colon cancer cell lines. ***Genome Res*** 1996;6:187-194.

Bromberg JE and van den Bent MJ. Oligodendrogliomas: molecular biology and treatment. ***Oncologist*** 2009;14:155-163.

Brustmann H. Expression of cellular apoptosis susceptibility protein in serous ovarian carcinoma: a clinicopathologic and immunohistochemical study. ***Gynecol Oncol*** 2004;92:268-276.

Cairncross G, Berkey B, Shaw E, Jenkins R, Scheithauer B, Brachman D, Buckner J, Fink K, Souhami L, Laperierre N, Mehta M and Curran W. Phase III trial of chemotherapy plus radiotherapy compared with radiotherapy alone for pure and mixed anaplastic oligodendroglioma: Intergroup Radiation Therapy Oncology Group Trial 9402. ***J Clin Oncol*** 2006;24:2707-2714.

Cairncross JG, Ueki K, Zlatescu MC, Lisle DK, Finkelstein DM, Hammond RR, Silver JS, Stark PC, Macdonald DR, Ino Y, Ramsay DA and Louis DN. Specific genetic predictors of chemotherapeutic response and survival in patients with anaplastic oligodendrogliomas. ***J Natl Cancer Inst*** 1998;90:1473-1479.

Calin GA, Dumitru CD, Shimizu M, Bichi R, Zupo S, Noch E, Aldler H, Rattan S, Keating M, Rai K, Rassenti L, Kipps T, Negrini M, Bullrich F and Croce CM. Frequent deletions and down-regulation of micro- RNA genes miR15 and miR16 at 13q14 in chronic lymphocytic leukemia. ***Proc Natl Acad Sci U S A*** 2002;99:15524-15529.

Calin GA, Ferracin M, Cimmino A, Di Leva G, Shimizu M, Wojcik SE, Iorio MV, Visone R, Sever NI, Fabbri M, Iuliano R, Palumbo T, Pichiorri F, Roldo C, Garzon R, Sevignani C, Rassenti L, Alder H, Volinia S, Liu CG, Kipps TJ, Negrini M and Croce CM. A MicroRNA signature associated with prognosis and progression in chronic lymphocytic leukemia. ***N Engl J Med*** 2005;353:1793-1801.

Calin GA, Sevignani C, Dumitru CD, Hyslop T, Noch E, Yendamuri S, Shimizu M, Rattan S, Bullrich F, Negrini M and Croce CM. Human microRNA genes are frequently located at fragile sites and genomic regions involved in cancers. ***Proc Natl Acad Sci U S A*** 2004;101:2999-3004.

Capelle L, Oei P, Teoh H, Hamilton D, Palmer D, Low I and Campbell G. Retrospective review of prognostic factors, including 1p19q deletion, in low-grade oligodendrogliomas and a review of recent published works. ***J Med Imaging Radiat Oncol*** 2009;53:305-309.

Chan JA, Krichevsky AM and Kosik KS. MicroRNA-21 is an antiapoptotic factor in human glioblastoma cells. ***Cancer Res*** 2005;65:6029-6033.

Chang TC, Wentzel EA, Kent OA, Ramachandran K, Mullendore M, Lee KH, Feldmann G, Yamakuchi M, Ferlito M, Lowenstein CJ, Arking DE, Beer MA, Maitra A and Mendell JT. Transactivation of miR-34a by p53 broadly influences gene expression and promotes apoptosis. ***Mol Cell*** 2007;26:745-752.

Chen G, Zhu W, Shi D, Lv L, Zhang C, Liu P and Hu W. MicroRNA-181a sensitizes human malignant glioma U87MG cells to radiation by targeting Bcl-2. ***Oncol Rep*** 2010;23:997-1003.

Chen X, Wang J, Shen H, Lu J, Li C, Hu D, Dong XE, Yan D and Tu L. Epigenetics, MicroRNAs, and Carcinogenesis: Functional Role of MicroRNA-137 in Uveal Melanoma. ***Invest Ophthalmol Vis Sci*** 2010.

Chen Y, Liu W, Chao T, Zhang Y, Yan X, Gong Y, Qiang B, Yuan J, Sun M and Peng X. MicroRNA-21 down-regulates the expression of tumor suppressor PDCD4 in human glioblastoma cell T98G. ***Cancer Lett*** 2008;272:197-205.

Chen Y and Stallings RL. Differential patterns of microRNA expression in neuroblastoma are correlated with prognosis, differentiation, and apoptosis. ***Cancer Res*** 2007;67:976-983.

Cheng LC, Pastrana E, Tavazoie M and Doetsch F. miR-124 regulates adult neurogenesis in the subventricular zone stem cell niche. ***Nat Neurosci*** 2009;12:399-408.

Chiang HR, Schoenfeld LW, Ruby JG, Auyeung VC, Spies N, Baek D, Johnston WK, Russ C, Luo S, Babiarz JE, Blelloch R, Schroth GP, Nusbaum C and Bartel DP. Mammalian microRNAs: experimental evaluation of novel and previously annotated genes. ***Genes Dev*** 2010;24:992-1009.

Ciafre SA, Galardi S, Mangiola A, Ferracin M, Liu CG, Sabatino G, Negrini M, Maira G, Croce CM and Farace MG. Extensive modulation of a set of microRNAs in primary glioblastoma. ***Biochem Biophys Res Commun*** 2005;334:1351-1358.

Cimmino A, Calin GA, Fabbri M, Iorio MV, Ferracin M, Shimizu M, Wojcik SE, Aqeilan RI, Zupo S, Dono M, Rassenti L, Alder H, Volinia S, Liu CG, Kipps TJ, Negrini M and Croce CM. miR-15 and miR-16 induce apoptosis by targeting BCL2. ***Proc Natl Acad Sci U S A*** 2005;102:13944-13949.

Conti A, Aguennouz M, La Torre D, Tomasello C, Cardali S, Angileri FF, Maio F, Cama A, Germano A, Vita G and Tomasello F. miR-21 and 221 upregulation and miR-181b downregulation in human grade II-IV astrocytic tumors. ***J Neurooncol*** 2009;93:325-332.

Coons SW, Johnson PC and Pearl DK. The prognostic significance of Ki-67 labeling indices for oligodendrogliomas. ***Neurosurgery*** 1997;41:878-884; discussion 884-875.

Cooper LA, Gutman DA, Long Q, Johnson BA, Cholleti SR, Kurc T, Saltz JH, Brat DJ and Moreno CS. The proneural molecular signature is enriched in oligodendrogliomas and predicts improved survival among diffuse gliomas. ***PLoS One*** 2010;5:e12548.

Corsten MF, Miranda R, Kasmieh R, Krichevsky AM, Weissleder R and Shah K. MicroRNA-21 knockdown disrupts glioma growth in vivo and displays synergistic cytotoxicity with neural precursor cell delivered S-TRAIL in human gliomas. ***Cancer Res*** 2007;67:8994-9000.

Criniere E, Kaloshi G, Laigle-Donadey F, Lejeune J, Auger N, Benouaich-Amiel A, Everhard S, Mokhtari K, Polivka M, Delattre JY, Hoang-Xuan K, Thillet J and Sanson M. MGMT prognostic impact on glioblastoma is dependent on therapeutic modalities. ***J Neurooncol*** 2007;83:173-179.

Cui JG, Zhao Y, Sethi P, Li YY, Mahta A, Culicchia F and Lukiw WJ. Micro-RNA-128 (miRNA-128) down-regulation in glioblastoma targets ARP5 (ANGPTL6), Bmi-1 and E2F-3a, key regulators of brain cell proliferation. ***J Neurooncol*** 2010;98:297-304.

Dacic S, Kelly L, Shuai Y and Nikiforova MN. miRNA expression profiling of lung adenocarcinomas: correlation with mutational status. ***Mod Pathol*** 2010;23:1577-1582.

Dalmay T. Identification of genes targeted by microRNAs. ***Biochem Soc Trans*** 2008;36:1194-1196.

Dehghani F, Schachenmayr W, Laun A and Korf HW. Prognostic implication of histopathological, immunohistochemical and clinical features of oligodendrogliomas: a study of 89 cases. ***Acta Neuropathol*** 1998;95:493-504.

Dey BK, Stalker L, Schnerch A, Bhatia M, Taylor-Papidimitriou J and Wynder C. The histone demethylase KDM5b/JARID1b plays a role in cell fate decisions by blocking terminal differentiation. ***Mol Cell Biol*** 2008;28:5312-5327.

Dong S, Pang JC, Hu J, Zhou LF and Ng HK. Transcriptional inactivation of TP73 expression in oligodendroglial tumors. ***Int J Cancer*** 2002;98:370-375.

Dong Z, Pang JS, Ng MH, Poon WS, Zhou L and Ng HK. Identification of two contiguous minimally deleted regions on chromosome 1p36.31-p36.32 in oligodendroglial tumours. ***Br J Cancer*** 2004;91:1105-1111.

Ducray F, Idbaih A, de Reynies A, Bieche I, Thillet J, Mokhtari K, Lair S, Marie Y, Paris S, Vidaud M, Hoang-Xuan K, Delattre O, Delattre JY and Sanson M. Anaplastic oligodendrogliomas with 1p19q codeletion have a proneural gene expression profile. ***Mol Cancer*** 2008;7:41.

Ekstrand AJ, Sugawa N, James CD and Collins VP. Amplified and rearranged epidermal growth factor receptor genes in human glioblastomas reveal deletions of sequences encoding portions of the N- and/or C-terminal tails. ***Proc Natl Acad Sci U S A*** 1992;89:4309-4313.

Enright AJ, John B, Gaul U, Tuschl T, Sander C and Marks DS. MicroRNA targets in Drosophila. ***Genome Biol*** 2003;5:R1.

Ernst A, Campos B, Meier J, Devens F, Liesenberg F, Wolter M, Reifenberger G, Herold-Mende C, Lichter P and Radlwimmer B. De-repression of CTGF via the miR-17-92 cluster upon differentiation of human glioblastoma spheroid cultures. ***Oncogene*** 2010;29:3411-3422.

Esteller M, Garcia-Foncillas J, Andion E, Goodman SN, Hidalgo OF, Vanaclocha V, Baylin SB and Herman JG. Inactivation of the DNA-repair gene MGMT and the clinical response of gliomas to alkylating agents. ***N Engl J Med*** 2000;343:1350-1354.

Fabbri M and Calin GA. Epigenetics and miRNAs in human cancer. ***Adv Genet*** 2010;70:87-99.

Fang WY, Liu TF, Xie WB, Yang XY, Wang S, Ren CP, Deng X, Liu QZ, Huang ZX, Li X, Ding YQ and Yao KT. Reexploring the possible roles of some genes associated with nasopharyngeal carcinoma using microarray-based detection. ***Acta Biochim Biophys Sin (Shanghai)*** 2005;37:541-546.

Felsberg J, Erkwoh A, Sabel MC, Kirsch L, Fimmers R, Blaschke B, Schlegel U, Schramm J, Wiestler OD and Reifenberger G. Oligodendroglial tumors: refinement of candidate regions on chromosome arm 1p and correlation of 1p/19q status with survival. ***Brain Pathol*** 2004;14:121-130.

Felsberg J, Rapp M, Loeser S, Fimmers R, Stummer W, Goeppert M, Steiger HJ, Friedensdorf B, Reifenberger G and Sabel MC. Prognostic significance of molecular markers and extent of resection in primary glioblastoma patients. ***Clin Cancer Res*** 2009;15:6683-6693.

Ferrer-Luna R, Mata M, Nunez L, Calvar J, Dasi F, Arias E, Piquer J, Cerda-Nicolas M, Taratuto AL, Sevlever G, Celda B and Martinetto H. Loss of heterozygosity at 1p-19q induces a global change in oligodendroglial tumor gene expression. ***J Neurooncol*** 2009;95:343-354.

Filipowicz W, Bhattacharyya SN and Sonenberg N. Mechanisms of post-transcriptional regulation by microRNAs: are the answers in sight? ***Nat Rev Genet*** 2008;9:102-114.

Fillmore HL, VanMeter TE and Broaddus WC. Membrane-type matrix metalloproteinases (MT-MMPs): expression and function during glioma invasion. ***J Neurooncol*** 2001;53:187-202.

Gabriely G, Wurdinger T, Kesari S, Esau CC, Burchard J, Linsley PS and Krichevsky AM. MicroRNA 21 promotes glioma invasion by targeting matrix metalloproteinase regulators. ***Mol Cell Biol*** 2008;28:5369-5380.

Gal H, Pandi G, Kanner AA, Ram Z, Lithwick-Yanai G, Amariglio N, Rechavi G and Givol D. MIR-451 and Imatinib mesylate inhibit tumor growth of Glioblastoma stem cells. ***Biochem Biophys Res Commun*** 2008;376:86-90.

Garraway LA, Widlund HR, Rubin MA, Getz G, Berger AJ, Ramaswamy S, Beroukhim R, Milner DA, Granter SR, Du J, Lee C, Wagner SN, Li C, Golub TR, Rimm DL, Meyerson ML, Fisher DE and Sellers WR. Integrative genomic analyses identify MITF as a lineage survival oncogene amplified in malignant melanoma. ***Nature*** 2005;436:117-122.

Gaur A, Jewell DA, Liang Y, Ridzon D, Moore JH, Chen C, Ambros VR and Israel MA. Characterization of microRNA expression levels and their biological correlates in human cancer cell lines. ***Cancer Res*** 2007;67:2456-2468.

Gerdes J, Lemke H, Baisch H, Wacker HH, Schwab U and Stein H. Cell cycle analysis of a cell proliferation-associated human nuclear antigen defined by the monoclonal antibody Ki-67. ***J Immunol*** 1984;133:1710-1715.

Gerdes J, Schwab U, Lemke H and Stein H. Production of a mouse monoclonal antibody reactive with a human nuclear antigen associated with cell proliferation. ***Int J***

Cancer 1983;31:13-20.

Gillies JK and Lorimer IA. Regulation of p27Kip1 by miRNA 221/222 in glioblastoma. ***Cell Cycle*** 2007;6:2005-2009.

Gironella M, Seux M, Xie MJ, Cano C, Tomasini R, Gommeaux J, Garcia S, Nowak J, Yeung ML, Jeang KT, Chaix A, Fazli L, Motoo Y, Wang Q, Rocchi P, Russo A, Gleave M, Dagorn JC, Iovanna JL, Carrier A, Pebusque MJ and Dusetti NJ. Tumor protein 53-induced nuclear protein 1 expression is repressed by miR-155, and its restoration inhibits pancreatic tumor development. ***Proc Natl Acad Sci U S A*** 2007;104:16170-16175.

Godlewski J, Nowicki MO, Bronisz A, Nuovo G, Palatini J, De Lay M, Van Brocklyn J, Ostrowski MC, Chiocca EA and Lawler SE. MicroRNA-451 regulates LKB1/AMPK signaling and allows adaptation to metabolic stress in glioma cells. ***Mol Cell*** 2010;37:620-632.

Godlewski J, Nowicki MO, Bronisz A, Williams S, Otsuki A, Nuovo G, Raychaudhury A, Newton HB, Chiocca EA and Lawler S. Targeting of the Bmi-1 oncogene/stem cell renewal factor by microRNA-128 inhibits glioma proliferation and self-renewal. ***Cancer Res*** 2008;68:9125-9130.

Gomez Del Pulgar T, Valdes-Mora F, Bandres E, Perez-Palacios R, Espina C, Cejas P, Garcia-Cabezas MA, Nistal M, Casado E, Gonzalez-Baron M, Garcia-Foncillas J and Lacal JC. Cdc42 is highly expressed in colorectal adenocarcinoma and downregulates ID4 through an epigenetic mechanism. ***Int J Oncol*** 2008;33:185-193.

Griffin CA, Burger P, Morsberger L, Yonescu R, Swierczynski S, Weingart JD and Murphy KM. Identification of der(1;19)(q10;p10) in five oligodendrogliomas suggests mechanism of concurrent 1p and 19q loss. ***J Neuropathol Exp Neurol*** 2006;65:988-994.

Griffiths-Jones S. miRBase: microRNA sequences and annotation. ***Curr Protoc Bioinformatics*** 2010;Chapter 12:Unit 12 19 11-10.

Griffiths-Jones S, Grocock RJ, van Dongen S, Bateman A and Enright AJ. miRBase: microRNA sequences, targets and gene nomenclature. ***Nucleic Acids Res*** 2006;34:D140-144.

Grossel MJ and Hinds PW. From cell cycle to differentiation: an expanding role for cdk6. ***Cell Cycle*** 2006;5:266-270.

Grun D, Wang YL, Langenberger D, Gunsalus KC and Rajewsky N. microRNA target predictions across seven Drosophila species and comparison to mammalian targets. ***PLoS Comput Biol*** 2005;1:e13.

Guan Y, Mizoguchi M, Yoshimoto K, Hata N, Shono T, Suzuki SO, Araki Y, Kuga D, Nakamizo A, Amano T, Ma X, Hayashi K and Sasaki T. MiRNA-196 is upregulated in glioblastoma but not in anaplastic astrocytoma and has prognostic significance. ***Clin Cancer Res*** 2010;16:4289-4297.

Guessous F, Zhang Y, Kofman A, Catania A, Li Y, Schiff D, Purow B and Abounader R. microRNA-34a is tumor suppressive in brain tumors and glioma stem cells. ***Cell Cycle*** 2010;9.

Guo D, Wang B, Han F and Lei T. RNA interference therapy for glioblastoma. ***Expert Opin Biol Ther*** 2010;10:927-936.

Haas-Kogan D, Shalev N, Wong M, Mills G, Yount G and Stokoe D. Protein kinase B (PKB/Akt) activity is elevated in glioblastoma cells due to mutation of the tumor suppressor PTEN/MMAC. ***Curr Biol*** 1998;8:1195-1198.

He L, Thomson JM, Hemann MT, Hernando-Monge E, Mu D, Goodson S, Powers S, Cordon-Cardo C, Lowe SW, Hannon GJ and Hammond SM. A microRNA polycistron as a potential human oncogene. ***Nature*** 2005;435:828-833.

Heegaard S, Sommer HM, Broholm H and Broendstrup O. Proliferating cell nuclear antigen and Ki-67 immunohistochemistry of oligodendrogliomas with special reference to prognosis. ***Cancer*** 1995;76:1809-1813.

Hegi ME, Diserens AC, Gorlia T, Hamou MF, de Tribolet N, Weller M, Kros JM, Hainfellner JA, Mason W, Mariani L, Bromberg JE, Hau P, Mirimanoff RO, Cairncross JG, Janzer RC and Stupp R. MGMT gene silencing and benefit from temozolomide in glioblastoma. ***N Engl J Med*** 2005;352:997-1003.

Hoang-Xuan K, Capelle L, Kujas M, Taillibert S, Duffau H, Lejeune J, Polivka M, Criniere E, Marie Y, Mokhtari K, Carpentier AF, Laigle F, Simon JM, Cornu P, Broet P, Sanson M and Delattre JY. Temozolomide as initial treatment for adults with low-grade oligodendrogliomas or oligoastrocytomas and correlation with chromosome 1p deletions. ***J Clin Oncol*** 2004;22:3133-3138.

Homma T, Fukushima T, Vaccarella S, Yonekawa Y, Di Patre PL, Franceschi S and Ohgaki H. Correlation among pathology, genotype, and patient outcomes in glioblastoma. ***J Neuropathol Exp Neurol*** 2006;65:846-854.

Houillier C, Lejeune J, Benouaich-Amiel A, Laigle-Donadey F, Criniere E, Mokhtari K, Thillet J, Delattre JY, Hoang-Xuan K and Sanson M. Prognostic impact of molecular markers in a series of 220 primary glioblastomas. ***Cancer*** 2006;106:2218-2223.

Hu QD, Ang BT, Karsak M, Hu WP, Cui XY, Duka T, Takeda Y, Chia W, Sankar N, Ng YK, Ling EA, Maciag T, Small D, Trifonova R, Kopan R, Okano H, Nakafuku M, Chiba S, Hirai H, Aster JC, Schachner M, Pallen CJ, Watanabe K and Xiao ZC. F3/contactin acts as a functional ligand for Notch during oligodendrocyte maturation. ***Cell*** 2003;115:163-175.

Hu Z, Chen J, Tian T, Zhou X, Gu H, Xu L, Zeng Y, Miao R, Jin G, Ma H, Chen Y and Shen H. Genetic variants of miRNA sequences and non-small cell lung cancer survival. ***J Clin Invest*** 2008;118:2600-2608.

Huang H, Okamoto Y, Yokoo H, Heppner FL, Vital A, Fevre-Montange M, Jouvet A, Yonekawa Y, Lazaridis EN, Kleihues P and Ohgaki H. Gene expression profiling and subgroup identification of oligodendrogliomas. ***Oncogene*** 2004;23:6012-6022.

Hui AB, Lo KW, Teo PM, To KF and Huang DP. Genome wide detection of oncogene amplifications in nasopharyngeal carcinoma by array based comparative genomic hybridization. ***Int J Oncol*** 2002;20:467-473.

Hui AB, Lo KW, Yin XL, Poon WS and Ng HK. Detection of multiple gene amplifications

in glioblastoma multiforme using array-based comparative genomic hybridization. ***Lab Invest*** 2001;81:717-723.

Huse JT, Brennan C, Hambardzumyan D, Wee B, Pena J, Rouhanifard SH, Sohn-Lee C, le Sage C, Agami R, Tuschl T and Holland EC. The PTEN-regulating microRNA miR-26a is amplified in high-grade glioma and facilitates gliomagenesis in vivo. ***Genes Dev*** 2009;23:1327-1337.

Husemann K, Wolter M, Buschges R, Bostrom J, Sabel M and Reifenberger G. Identification of two distinct deleted regions on the short arm of chromosome 1 and rare mutation of the CDKN2C gene from 1p32 in oligodendroglial tumors. ***J Neuropathol Exp Neurol*** 1999;58:1041-1050.

Ichimura K, Pearson DM, Kocialkowski S, Backlund LM, Chan R, Jones DT and Collins VP. IDH1 mutations are present in the majority of common adult gliomas but rare in primary glioblastomas. ***Neuro Oncol*** 2009;11:341-347.

Idbaih A, Carvalho Silva R, Criniere E, Marie Y, Carpentier C, Boisselier B, Taillibert S, Rousseau A, Mokhtari K, Ducray F, Thillet J, Sanson M, Hoang-Xuan K and Delattre JY. Genomic changes in progression of low-grade gliomas. ***J Neurooncol*** 2008;90:133-140.

Ino Y, Betensky RA, Zlatescu MC, Sasaki H, Macdonald DR, Stemmer-Rachamimov AO, Ramsay DA, Cairncross JG and Louis DN. Molecular subtypes of anaplastic oligodendroglioma: implications for patient management at diagnosis. ***Clin Cancer Res*** 2001;7:839-845.

Irniger S, Piatti S, Michaelis C and Nasmyth K. Genes involved in sister chromatid separation are needed for B-type cyclin proteolysis in budding yeast. ***Cell*** 1995;81:269-278.

Jenkins RB, Blair H, Ballman KV, Giannini C, Arusell RM, Law M, Flynn H, Passe S, Felten S, Brown PD, Shaw EG and Buckner JC. A t(1;19)(q10;p10) mediates the combined deletions of 1p and 19q and predicts a better prognosis of patients with oligodendroglioma. ***Cancer Res*** 2006;66:9852-9861.

Jeuken JW, von Deimling A and Wesseling P. Molecular pathogenesis of oligodendroglial tumors. ***J Neurooncol*** 2004;70:161-181.

Jiang MC and Liao CF. CSE1/CAS overexpression inhibits the tumorigenicity of HT-29 colon cancer cells. ***J Exp Clin Cancer Res*** 2004;23:325-332.

Jiang MC, Lin TL, Lee TL, Huang HT, Lin CL and Liao CF. IRF-1-mediated CAS expression enhances interferon-gamma-induced apoptosis of HT-29 colon adenocarcinoma cells. ***Mol Cell Biol Res Commun*** 2001;4:353-358.

John B, Enright AJ, Aravin A, Tuschl T, Sander C and Marks DS. Human MicroRNA targets. ***PLoS Biol*** 2004;2:e363.

Kanner AA, Staugaitis SM, Castilla EA, Chernova O, Prayson RA, Vogelbaum MA, Stevens G, Peereboom D, Suh J, Lee SY, Tubbs RR and Barnett GH. The impact of genotype on outcome in oligodendroglioma: validation of the loss of chromosome arm 1p as an important factor in clinical decision making. ***J Neurosurg*** 2006;104:542-550.

Kanu OO, Hughes B, Di C, Lin N, Fu J, Bigner DD, Yan H and Adamson C. Glioblastoma Multiforme Oncogenomics and Signaling Pathways. ***Clin Med Oncol*** 2009;3:39-52.

Kayaselcuk F, Zorludemir S, Gumurduhu D, Zeren H and Erman T. PCNA and Ki-67 in central nervous system tumors: correlation with the histological type and grade. ***J Neurooncol*** 2002;57:115-121.

Kefas B, Godlewski J, Comeau L, Li Y, Abounader R, Hawkinson M, Lee J, Fine H, Chiocca EA, Lawler S and Purow B. microRNA-7 inhibits the epidermal growth factor receptor and the Akt pathway and is down-regulated in glioblastoma. ***Cancer Res*** 2008;68:3566-3572.

Kim DH, Mohapatra G, Bollen A, Waldman FM and Feuerstein BG. Chromosomal abnormalities in glioblastoma multiforme tumors and glioma cell lines detected by comparative genomic hybridization. ***Int J Cancer*** 1995;60:812-819.

Kim HE, Jiang X, Du F and Wang X. PHAPI, CAS, and Hsp70 promote apoptosome formation by preventing Apaf-1 aggregation and enhancing nucleotide exchange on Apaf-1. ***Mol Cell*** 2008;30:239-247.

Kim VN. MicroRNA biogenesis: coordinated cropping and dicing. ***Nat Rev Mol Cell Biol*** 2005;6:376-385.

Kim YH, Nobusawa S, Mittelbronn M, Paulus W, Brokinkel B, Keyvani K, Sure U, Wrede K, Nakazato Y, Tanaka Y, Vital A, Mariani L, Stawski R, Watanabe T, De Girolami U, Kleihues P and Ohgaki H. Molecular classification of low-grade diffuse gliomas. ***Am J Pathol*** 2010;177:2708-2714.

Kim YJ, Go H, Wu HG, Jeon YK, Park SW and Lee SH. Immunohistochemical study identifying prognostic biomolecular markers in nasopharyngeal carcinoma treated by radiotherapy. ***Head Neck*** 2010.

Kitange G, Misra A, Law M, Passe S, Kollmeyer TM, Maurer M, Ballman K, Feuerstein BG and Jenkins RB. Chromosomal imbalances detected by array comparative genomic hybridization in human oligodendrogliomas and mixed oligoastrocytomas. ***Genes Chromosomes Cancer*** 2005;42:68-77.

Kleihues P, Burger PC, Aldape KD, Brat DJ, Biernat W, Bigner DD, Nakazato Y, H. PK, Giangaspero F, von Deimling A, Ohgaki H and Cavenee WK. Glioblastoma. In: ***WHO classification of tumours of the central nervous system.***Louis DN, Ohgaki H, Wiestler OD and Cavenee WK, eds. 2007. International Agency for Research on Cancer, Lyon. pp. 33-49.

Koschny R, Koschny T, Froster UG, Krupp W and Zuber MA. Comparative genomic hybridization in glioma: a meta-analysis of 509 cases. ***Cancer Genet Cytogenet*** 2002;135:147-159.

Kouwenhoven MC, Kros JM, French PJ, Biemond-ter Stege EM, Graveland WJ, Taphoorn MJ, Brandes AA and van den Bent MJ. 1p/19q loss within oligodendroglioma is predictive for response to first line temozolomide but not to salvage treatment. ***Eur J Cancer*** 2006;42:2499-2503.

Kozaki K, Imoto I, Mogi S, Omura K and Inazawa J. Exploration of tumor-suppressive microRNAs silenced by DNA hypermethylation in oral cancer. ***Cancer Res***

2008;68:2094-2105.

Krek A, Grun D, Poy MN, Wolf R, Rosenberg L, Epstein EJ, MacMenamin P, da Piedade I, Gunsalus KC, Stoffel M and Rajewsky N. Combinatorial microRNA target predictions. ***Nat Genet*** 2005;37:495-500.

Krichevsky AM, Sonntag KC, Isacson O and Kosik KS. Specific microRNAs modulate embryonic stem cell-derived neurogenesis. ***Stem Cells*** 2006;24:857-864.

Krol J, Loedige I and Filipowicz W. The widespread regulation of microRNA biogenesis, function and decay. ***Nat Rev Genet*** 2010;11:597-610.

Kros JM, Hop WC, Godschalk JJ and Krishnadath KK. Prognostic value of the proliferation-related antigen Ki-67 in oligodendrogliomas. ***Cancer*** 1996;78:1107-1113.

Kuo LT, Kuo KT, Lee MJ, Wei CC, Scaravilli F, Tsai JC, Tseng HM, Kuo MF and Tu YK. Correlation among pathology, genetic and epigenetic profiles, and clinical outcome in oligodendroglial tumors. ***Int J Cancer*** 2009;124:2872-2879.

Kutay U, Bischoff FR, Kostka S, Kraft R and Gorlich D. Export of importin alpha from the nucleus is mediated by a specific nuclear transport factor. ***Cell*** 1997;90:1061-1071.

Lagos-Quintana M, Rauhut R, Yalcin A, Meyer J, Lendeckel W and Tuschl T. Identification of tissue-specific microRNAs from mouse. ***Curr Biol*** 2002;12:735-739.

Lam PY, Di Tomaso E, Ng HK, Pang JC, Roussel MF and Hjelm NM. Expression of p19INK4d, CDK4, CDK6 in glioblastoma multiforme. ***Br J Neurosurg*** 2000;14:28-32.

Landgraf P, Rusu M, Sheridan R, Sewer A, Iovino N, Aravin A, Pfeffer S, Rice A, Kamphorst AO, Landthaler M, Lin C, Socci ND, Hermida L, Fulci V, Chiaretti S, Foa R, Schliwka J, Fuchs U, Novosel A, Muller RU, Schermer B, Bissels U, Inman J, Phan Q, Chien M, Weir DB, Choksi R, De Vita G, Frezzetti D, Trompeter HI, Hornung V, Teng G, Hartmann G, Palkovits M, Di Lauro R, Wernet P, Macino G, Rogler CE, Nagle JW, Ju J, Papavasiliou FN, Benzing T, Lichter P, Tam W, Brownstein MJ, Bosio A, Borkhardt A, Russo JJ, Sander C, Zavolan M and Tuschl T. A mammalian microRNA expression atlas based on small RNA library sequencing. ***Cell*** 2007;129:1401-1414.

Lang FF, Miller DC, Koslow M and Newcomb EW. Pathways leading to glioblastoma multiforme: a molecular analysis of genetic alterations in 65 astrocytic tumors. ***J Neurosurg*** 1994;81:427-436.

Langevin SM, Stone RA, Bunker CH, Grandis JR, Sobol RW and Taioli E. MicroRNA-137 promoter methylation in oral rinses from patients with squamous cell carcinoma of the head and neck is associated with gender and body mass index. ***Carcinogenesis*** 2010;31:864-870.

Langevin SM, Stone RA, Bunker CH, Lyons-Weiler MA, Laframboise WA, Kelly L, Seethala RR, Grandis JR, Sobol RW and Taioli E. MicroRNA-137 promoter methylation is associated with poorer overall survival in patients with squamous cell carcinoma of the head and neck. ***Cancer*** 2010.

le Sage C, Nagel R, Egan DA, Schrier M, Mesman E, Mangiola A, Anile C, Maira G,

Mercatelli N, Ciafre SA, Farace MG and Agami R. Regulation of the p27(Kip1) tumor suppressor by miR-221 and miR-222 promotes cancer cell proliferation. ***EMBO J*** 2007;26:3699-3708.

Lee RC, Feinbaum RL and Ambros V. The C. elegans heterochronic gene lin-4 encodes small RNAs with antisense complementarity to lin-14. ***Cell*** 1993;75:843-854.

Lee Y, Jeon K, Lee JT, Kim S and Kim VN. MicroRNA maturation: stepwise processing and subcellular localization. ***EMBO J*** 2002;21:4663-4670.

Levy C, Khaled M and Fisher DE. MITF: master regulator of melanocyte development and melanoma oncogene. ***Trends Mol Med*** 2006;12:406-414.

Lewis BP, Burge CB and Bartel DP. Conserved seed pairing, often flanked by adenosines, indicates that thousands of human genes are microRNA targets. ***Cell*** 2005;120:15-20.

Lewis BP, Shih IH, Jones-Rhoades MW, Bartel DP and Burge CB. Prediction of mammalian microRNA targets. ***Cell*** 2003;115:787-798.

Li Y, Guessous F, Zhang Y, Dipierro C, Kefas B, Johnson E, Marcinkiewicz L, Jiang J, Yang Y, Schmittgen TD, Lopes B, Schiff D, Purow B and Abounader R. MicroRNA-34a inhibits glioblastoma growth by targeting multiple oncogenes. ***Cancer Res*** 2009;69:7569-7576.

Li Y, Li W, Yang Y, Lu Y, He C, Hu G, Liu H, Chen J, He J and Yu H. MicroRNA-21 targets LRRFIP1 and contributes to VM-26 resistance in glioblastoma multiforme. ***Brain Res*** 2009;1286:13-18.

Liang Y, Ridzon D, Wong L and Chen C. Characterization of microRNA expression profiles in normal human tissues. ***BMC Genomics*** 2007;8:166.

Liao CF, Luo SF, Li LT, Lin CY, Chen YC and Jiang MC. CSE1L/CAS, the cellular apoptosis susceptibility protein, enhances invasion and metastasis but not proliferation of cancer cells. ***J Exp Clin Cancer Res*** 2008;27:15.

Liao CF, Luo SF, Shen TY, Lin CH, Chien JT, Du SY and Jiang MC. CSE1L/CAS, a microtubule-associated protein, inhibits taxol (paclitaxel)-induced apoptosis but enhances cancer cell apoptosis induced by various chemotherapeutic drugs. ***BMB Rep*** 2008;41:210-216.

Lim LP, Lau NC, Garrett-Engele P, Grimson A, Schelter JM, Castle J, Bartel DP, Linsley PS and Johnson JM. Microarray analysis shows that some microRNAs downregulate large numbers of target mRNAs. ***Nature*** 2005;433:769-773.

Liu CG, Calin GA, Meloon B, Gamliel N, Sevignani C, Ferracin M, Dumitru CD, Shimizu M, Zupo S, Dono M, Alder H, Bullrich F, Negrini M and Croce CM. An oligonucleotide microchip for genome-wide microRNA profiling in human and mouse tissues. ***Proc Natl Acad Sci U S A*** 2004;101:9740-9744.

Liu M, Lang N, Qiu M, Xu F, Li Q, Tang Q, Chen J, Chen X, Zhang S, Liu Z, Zhou J, Zhu Y, Deng Y, Zheng Y and Bi F. miR-137 targets Cdc42 expression, induces cell cycle G1 arrest, and inhibits invasion in colorectal cancer cells. ***Int J Cancer*** 2010.

Liu X, Fortin K and Mourelatos Z. MicroRNAs: biogenesis and molecular functions. ***Brain Pathol*** 2008;18:113-121.

Livak KJ and Schmittgen TD. Analysis of relative gene expression data using real-time quantitative PCR and the 2(-Delta Delta C(T)) Method. ***Methods*** 2001;25:402-408.

Louis DN, Ohgaki H, Weistler OD and Cavenee WK, eds. ***WHO classification of tumours of the central nervous system.*** World Health Organization classification of tumours. 2007. International Agency for Research on Cancer, Lyon.

Lu J, Getz G, Miska EA, Alvarez-Saavedra E, Lamb J, Peck D, Sweet-Cordero A, Ebert BL, Mak RH, Ferrando AA, Downing JR, Jacks T, Horvitz HR and Golub TR. MicroRNA expression profiles classify human cancers. ***Nature*** 2005;435:834-838.

Luan S, Sun L and Huang F. MicroRNA-34a: a novel tumor suppressor in p53-mutant glioma cell line U251. ***Arch Med Res*** 2010;41:67-74.

Lukiw WJ, Cui JG, Li YY and Culicchia F. Up-regulation of micro-RNA-221 (miRNA-221; chr Xp11.3) and caspase-3 accompanies down-regulation of the survivin-1 homolog BIRC1 (NAIP) in glioblastoma multiforme (GBM). ***J Neurooncol*** 2009;91:27-32.

Ma L, Teruya-Feldstein J and Weinberg RA. Tumour invasion and metastasis initiated by microRNA-10b in breast cancer. ***Nature*** 2007;449:682-688.

Ma L, Young J, Prabhala H, Pan E, Mestdagh P, Muth D, Teruya-Feldstein J, Reinhardt F, Onder TT, Valastyan S, Westermann F, Speleman F, Vandesompele J and Weinberg RA. miR-9, a MYC/MYCN-activated microRNA, regulates E-cadherin and cancer metastasis. ***Nat Cell Biol*** 2010;12:247-256.

Makeyev EV, Zhang J, Carrasco MA and Maniatis T. The MicroRNA miR-124 promotes neuronal differentiation by triggering brain-specific alternative pre-mRNA splicing. ***Mol Cell*** 2007;27:435-448.

Malzkorn B, Wolter M, Liesenberg F, Grzendowski M, Stuhler K, Meyer HE and Reifenberger G. Identification and functional characterization of microRNAs involved in the malignant progression of gliomas. ***Brain Pathol*** 2010;20:539-550.

Mao X, Lillington D, Child F, Russell-Jones R, Young B and Whittaker S. Comparative genomic hybridization analysis of primary cutaneous B-cell lymphomas: identification of common genomic alterations in disease pathogenesis. ***Genes Chromosomes Cancer*** 2002;35:144-155.

McDonald JM, Dunlap S, Cogdell D, Dunmire V, Wei Q, Starzinski-Powitz A, Sawaya R, Bruner J, Fuller GN, Aldape K and Zhang W. The SHREW1 gene, frequently deleted in oligodendrogliomas, functions to inhibit cell adhesion and migration. ***Cancer Biol Ther*** 2006;5:300-304.

McDonald JM, Dunmire V, Taylor E, Sawaya R, Bruner J, Fuller GN, Aldape K and Zhang W. Attenuated expression of DFFB is a hallmark of oligodendrogliomas with 1p-allelic loss. ***Mol Cancer*** 2005;4:35.

Medina R, Zaidi SK, Liu CG, Stein JL, van Wijnen AJ, Croce CM and Stein GS. MicroRNAs 221 and 222 bypass quiescence and compromise cell survival. ***Cancer Res*** 2008;68:2773-2780.

Metzger E, Wissmann M, Yin N, Muller JM, Schneider R, Peters AH, Gunther T, Buettner R and Schule R. LSD1 demethylates repressive histone marks to promote androgen-receptor-dependent transcription. ***Nature*** 2005;437:436-439.

Meyerson M and Harlow E. Identification of G1 kinase activity for cdk6, a novel cyclin D partner. ***Mol Cell Biol*** 1994;14:2077-2086.

Mohapatra G, Bollen AW, Kim DH, Lamborn K, Moore DH, Prados MD and Feuerstein BG. Genetic analysis of glioblastoma multiforme provides evidence for subgroups within the grade. ***Genes Chromosomes Cancer*** 1998;21:195-206.

Mukasa A, Ueki K, Ge X, Ishikawa S, Ide T, Fujimaki T, Nishikawa R, Asai A, Kirino T and Aburatani H. Selective expression of a subset of neuronal genes in oligodendroglioma with chromosome 1p loss. ***Brain Pathol*** 2004;14:34-42.

Nakamura M, Yang F, Fujisawa H, Yonekawa Y, Kleihues P and Ohgaki H. Loss of heterozygosity on chromosome 19 in secondary glioblastomas. ***J Neuropathol Exp Neurol*** 2000;59:539-543.

Nan Y, Han L, Zhang A, Wang G, Jia Z, Yang Y, Yue X, Pu P, Zhong Y and Kang C. MiRNA-451 plays a role as tumor suppressor in human glioma cells. ***Brain Res*** 2010;1359:14-21.

Narayan G and Murty VV. Integrative genomic approaches in cervical cancer: implications for molecular pathogenesis. ***Future Oncol*** 2010;6:1643-1652.

Nelson PT, Baldwin DA, Kloosterman WP, Kauppinen S, Plasterk RH and Mourelatos Z. RAKE and LNA-ISH reveal microRNA expression and localization in archival human brain. ***RNA*** 2006;12:187-191.

Ngo TT, Peng T, Liang XJ, Akeju O, Pastorino S, Zhang W, Kotliarov Y, Zenklusen JC, Fine HA, Maric D, Wen PY, De Girolami U, Black PM, Wu WW, Shen RF, Jeffries NO, Kang DW and Park JK. The 1p-encoded protein stathmin and resistance of malignant gliomas to nitrosoureas. ***J Natl Cancer Inst*** 2007;99:639-652.

Nishizaki T, Ozaki S, Harada K, Ito H, Arai H, Beppu T and Sasaki K. Investigation of genetic alterations associated with the grade of astrocytic tumor by comparative genomic hybridization. ***Genes Chromosomes Cancer*** 1998;21:340-346.

Nobusawa S, Watanabe T, Kleihues P and Ohgaki H. IDH1 mutations as molecular signature and predictive factor of secondary glioblastomas. ***Clin Cancer Res*** 2009;15:6002-6007.

Noushmehr H, Weisenberger DJ, Diefes K, Phillips HS, Pujara K, Berman BP, Pan F, Pelloski CE, Sulman EP, Bhat KP, Verhaak RG, Hoadley KA, Hayes DN, Perou CM, Schmidt HK, Ding L, Wilson RK, Van Den Berg D, Shen H, Bengtsson H, Neuvial P, Cope LM, Buckley J, Herman JG, Baylin SB, Laird PW and Aldape K. Identification of a CpG island methylator phenotype that defines a distinct subgroup of glioma. ***Cancer Cell*** 2010;17:510-522.

Ogryzko VV, Brinkmann E, Howard BH, Pastan I and Brinkmann U. Antisense inhibition of CAS, the human homologue of the yeast chromosome segregation gene CSE1, interferes with mitosis in HeLa cells. ***Biochemistry*** 1997;36:9493-9500.

Ohgaki H. Genetic pathways to glioblastomas. ***Neuropathology*** 2005;25:1-7.

Ohgaki H, Dessen P, Jourde B, Horstmann S, Nishikawa T, Di Patre PL, Burkhard C, Schuler D, Probst-Hensch NM, Maiorka PC, Baeza N, Pisani P, Yonekawa Y, Yasargil MG, Lutolf UM and Kleihues P. Genetic pathways to glioblastoma: a population-based study. ***Cancer Res*** 2004;64:6892-6899.

Ohgaki H and Kleihues P. Population-based studies on incidence, survival rates, and genetic alterations in astrocytic and oligodendroglial gliomas. ***J Neuropathol Exp Neurol*** 2005;64:479-489.

Ohgaki H and Kleihues P. Genetic pathways to primary and secondary glioblastoma. ***Am J Pathol*** 2007;170:1445-1453.

Ohgaki H and Kleihues P. Genetic alterations and signaling pathways in the evolution of gliomas. ***Cancer Sci*** 2009;100:2235-2241.

Okamoto Y, Di Patre PL, Burkhard C, Horstmann S, Jourde B, Fahey M, Schuler D, Probst-Hensch NM, Yasargil MG, Yonekawa Y, Lutolf UM, Kleihues P and Ohgaki H. Population-based study on incidence, survival rates, and genetic alterations of low-grade diffuse astrocytomas and oligodendrogliomas. ***Acta Neuropathol*** 2004;108:49-56.

Orom UA and Lund AH. Experimental identification of microRNA targets. ***Gene*** 2010;451:1-5.

Ossipova O, Ezan J and Sokol SY. PAR-1 phosphorylates Mind bomb to promote vertebrate neurogenesis. ***Dev Cell*** 2009;17:222-233.

Pang JC, Li KK, Lau KM, Ng YL, Wong J, Chung NY, Li HM, Chui YL, Lui VW, Chen ZP, Chan DT, Poon WS, Wang Y, Mao Y, Zhou L and Ng HK. KIAA0495/PDAM is frequently downregulated in oligodendroglial tumors and its knockdown by siRNA induces cisplatin resistance in glioma cells. ***Brain Pathol*** 2010;20:1021-1032.

Papagiannakopoulos T, Shapiro A and Kosik KS. MicroRNA-21 targets a network of key tumor-suppressive pathways in glioblastoma cells. ***Cancer Res*** 2008;68:8164-8172.

Parsons DW, Jones S, Zhang X, Lin JC, Leary RJ, Angenendt P, Mankoo P, Carter H, Siu IM, Gallia GL, Olivi A, McLendon R, Rasheed BA, Keir S, Nikolskaya T, Nikolsky Y, Busam DA, Tekleab H, Diaz LA, Jr., Hartigan J, Smith DR, Strausberg RL, Marie SK, Shinjo SM, Yan H, Riggins GJ, Bigner DD, Karchin R, Papadopoulos N, Parmigiani G, Vogelstein B, Velculescu VE and Kinzler KW. An integrated genomic analysis of human glioblastoma multiforme. ***Science*** 2008;321:1807-1812.

Pasquinelli AE, Reinhart BJ, Slack F, Martindale MQ, Kuroda MI, Maller B, Hayward DC, Ball EE, Degnan B, Muller P, Spring J, Srinivasan A, Fishman M, Finnerty J, Corbo J, Levine M, Leahy P, Davidson E and Ruvkun G. Conservation of the sequence and temporal expression of let-7 heterochronic regulatory RNA. ***Nature*** 2000;408:86-89.

Paunu N, Sallinen SL, Karhu R, Miettinen H, Sallinen P, Kononen J, Laippala P, Simola KO, Helen P and Haapasalo H. Chromosome imbalances in familial gliomas detected by comparative genomic hybridization. ***Genes Chromosomes Cancer*** 2000;29:339-346.

Paz MF, Yaya-Tur R, Rojas-Marcos I, Reynes G, Pollan M, Aguirre-Cruz L, Garcia-Lopez

JL, Piquer J, Safont MJ, Balana C, Sanchez-Cespedes M, Garcia-Villanueva M, Arribas L and Esteller M. CpG island hypermethylation of the DNA repair enzyme methyltransferase predicts response to temozolomide in primary gliomas. ***Clin Cancer Res*** 2004;10:4933-4938.

Peiro G, Diebold J, Baretton GB, Kimmig R and Lohrs U. Cellular apoptosis susceptibility gene expression in endometrial carcinoma: correlation with Bcl-2, Bax, and caspase-3 expression and outcome. ***Int J Gynecol Pathol*** 2001;20:359-367.

Peiro G, Diebold J and Lohrs U. CAS (cellular apoptosis susceptibility) gene expression in ovarian carcinoma: Correlation with 20q13.2 copy number and cyclin D1, p53, and Rb protein expression. ***Am J Clin Pathol*** 2002;118:922-929.

Pereira JD, Sansom SN, Smith J, Dobenecker MW, Tarakhovsky A and Livesey FJ. Ezh2, the histone methyltransferase of PRC2, regulates the balance between self-renewal and differentiation in the cerebral cortex. ***Proc Natl Acad Sci U S A*** 2010;107:15957-15962.

Poomsawat S, Buajeeb W, Khovidhunkit SO and Punyasingh J. Alteration in the expression of cdk4 and cdk6 proteins in oral cancer and premalignant lesions. ***J Oral Pathol Med*** 2010;39:793-799.

Rao JS. Molecular mechanisms of glioma invasiveness: the role of proteases. ***Nat Rev Cancer*** 2003;3:489-501.

Rao SA, Santosh V and Somasundaram K. Genome-wide expression profiling identifies deregulated miRNAs in malignant astrocytoma. ***Mod Pathol*** 2010;23:1404-1417.

Raveche ES, Salerno E, Scaglione BJ, Manohar V, Abbasi F, Lin YC, Fredrickson T, Landgraf P, Ramachandra S, Huppi K, Toro JR, Zenger VE, Metcalf RA and Marti GE. Abnormal microRNA-16 locus with synteny to human 13q14 linked to CLL in NZB mice. ***Blood*** 2007;109:5079-5086.

Reifenberger G, Kros JM, Louis DN and Collins VP. Oligodendroglial tumours. In: ***WHO classification of tumours of the central nervous system.***Louis DN, Ohgaki H, Wiestler OD and Cavenee WK, eds. 2007. International Agency for Research on Cancer, Lyon. pp. 53-67.

Reifenberger G and Louis DN. Oligodendroglioma: toward molecular definitions in diagnostic neuro-oncology. ***J Neuropathol Exp Neurol*** 2003;62:111-126.

Reifenberger J, Reifenberger G, Liu L, James CD, Wechsler W and Collins VP. Molecular genetic analysis of oligodendroglial tumors shows preferential allelic deletions on 19q and 1p. ***Am J Pathol*** 1994;145:1175-1190.

Reinhart BJ, Slack FJ, Basson M, Pasquinelli AE, Bettinger JC, Rougvie AE, Horvitz HR and Ruvkun G. The 21-nucleotide let-7 RNA regulates developmental timing in Caenorhabditis elegans. ***Nature*** 2000;403:901-906.

Riemenschneider MJ, Reifenberger J and Reifenberger G. Frequent biallelic inactivation and transcriptional silencing of the DIRAS3 gene at 1p31 in oligodendroglial tumors with 1p loss. ***Int J Cancer*** 2008;122:2503-2510.

Rodriguez A, Griffiths-Jones S, Ashurst JL and Bradley A. Identification of mammalian

microRNA host genes and transcription units. ***Genome Res*** 2004;14:1902-1910.

Rodriguez FJ and Giannini C. Oligodendroglial tumors: diagnostic and molecular pathology. ***Semin Diagn Pathol*** 2010;27:136-145.

Rosenberg C, Geelen E, MJ IJ, Pearson P, Tanke HJ, Dinjens WN and van Dekken H. Spectrum of genetic changes in gastro-esophageal cancer cell lines determined by an integrated molecular cytogenetic approach. ***Cancer Genet Cytogenet*** 2002;135:35-41.

Sasayama T, Nishihara M, Kondoh T, Hosoda K and Kohmura E. MicroRNA-10b is overexpressed in malignant glioma and associated with tumor invasive factors, uPAR and RhoC. ***Int J Cancer*** 2009;125:1407-1413.

Scherf U, Kalab P, Dasso M, Pastan I and Brinkmann U. The hCSE1/CAS protein is phosphorylated by HeLa extracts and MEK-1: MEK-1 phosphorylation may modulate the intracellular localization of CAS. ***Biochem Biophys Res Commun*** 1998;250:623-628.

Scherf U, Pastan I, Willingham MC and Brinkmann U. The human CAS protein which is homologous to the CSE1 yeast chromosome segregation gene product is associated with microtubules and mitotic spindle. ***Proc Natl Acad Sci U S A*** 1996;93:2670-2674.

Schulte JH, Lim S, Schramm A, Friedrichs N, Koster J, Versteeg R, Ora I, Pajtler K, Klein-Hitpass L, Kuhfittig-Kulle S, Metzger E, Schule R, Eggert A, Buettner R and Kirfel J. Lysine-specific demethylase 1 is strongly expressed in poorly differentiated neuroblastoma: implications for therapy. ***Cancer Res*** 2009;69:2065-2071.

Seiden-Long IM, Brown KR, Shih W, Wigle DA, Radulovich N, Jurisica I and Tsao MS. Transcriptional targets of hepatocyte growth factor signaling and Ki-ras oncogene activation in colorectal cancer. ***Oncogene*** 2006;25:91-102.

Sempere LF, Freemantle S, Pitha-Rowe I, Moss E, Dmitrovsky E and Ambros V. Expression profiling of mammalian microRNAs uncovers a subset of brain-expressed microRNAs with possible roles in murine and human neuronal differentiation. ***Genome Biol*** 2004;5:R13.

Sher F, Rossler R, Brouwer N, Balasubramaniyan V, Boddeke E and Copray S. Differentiation of neural stem cells into oligodendrocytes: involvement of the polycomb group protein Ezh2. ***Stem Cells*** 2008;26:2875-2883.

Shi L, Chen J, Yang J, Pan T, Zhang S and Wang Z. MiR-21 protected human glioblastoma U87MG cells from chemotherapeutic drug temozolomide induced apoptosis by decreasing Bax/Bcl-2 ratio and caspase-3 activity. ***Brain Res*** 2010;1352:255-264.

Shi L, Cheng Z, Zhang J, Li R, Zhao P, Fu Z and You Y. hsa-mir-181a and hsa-mir-181b function as tumor suppressors in human glioma cells. ***Brain Res*** 2008;1236:185-193.

Shiraki K, Fujikawa K, Sugimoto K, Ito T, Yamanaka T, Suzuki M, Yoneda K, Takase K and Nakano T. Cellular apoptosis susceptibility protein and proliferation in human hepatocellular carcinoma. ***Int J Mol Med*** 2006;18:77-81.

Silber J, Lim DA, Petritsch C, Persson AI, Maunakea AK, Yu M, Vandenberg SR,

Ginzinger DG, James CD, Costello JF, Bergers G, Weiss WA, Alvarez-Buylla A and Hodgson JG. miR-124 and miR-137 inhibit proliferation of glioblastoma multiforme cells and induce differentiation of brain tumor stem cells. ***BMC Med*** 2008;6:14.

Slaby O, Lakomy R, Fadrus P, Hrstka R, Kren L, Lzicarova E, Smrcka M, Svoboda M, Dolezalova H, Novakova J, Valik D, Vyzula R and Michalek J. MicroRNA-181 family predicts response to concomitant chemoradiotherapy with temozolomide in glioblastoma patients. ***Neoplasma*** 2010;57:264-269.

Smirnova L, Grafe A, Seiler A, Schumacher S, Nitsch R and Wulczyn FG. Regulation of miRNA expression during neural cell specification. ***Eur J Neurosci*** 2005;21:1469-1477.

Smith JS, Alderete B, Minn Y, Borell TJ, Perry A, Mohapatra G, Hosek SM, Kimmel D, O'Fallon J, Yates A, Feuerstein BG, Burger PC, Scheithauer BW and Jenkins RB. Localization of common deletion regions on 1p and 19q in human gliomas and their association with histological subtype. ***Oncogene*** 1999;18:4144-4152.

Smith JS, Tachibana I, Lee HK, Qian J, Pohl U, Mohrenweiser HW, Borell TJ, Hosek SM, Soderberg CL, von Deimling A, Perry A, Scheithauer BW, Louis DN and Jenkins RB. Mapping of the chromosome 19 q-arm glioma tumor suppressor gene using fluorescence in situ hybridization and novel microsatellite markers. ***Genes Chromosomes Cancer*** 2000;29:16-25.

Smrt RD, Szulwach KE, Pfeiffer RL, Li X, Guo W, Pathania M, Teng ZQ, Luo Y, Peng J, Bordey A, Jin P and Zhao X. MicroRNA miR-137 regulates neuronal maturation by targeting ubiquitin ligase mind bomb-1. ***Stem Cells*** 2010;28:1060-1070.

Szulwach KE, Li X, Smrt RD, Li Y, Luo Y, Lin L, Santistevan NJ, Li W, Zhao X and Jin P. Cross talk between microRNA and epigenetic regulation in adult neurogenesis. ***J Cell Biol*** 2010;189:127-141.

Tai CJ, Shen SC, Lee WR, Liao CF, Deng WP, Chiou HY, Hsieh CI, Tung JN, Chen CS, Chiou JF, Li LT, Lin CY, Hsu CH and Jiang MC. Increased cellular apoptosis susceptibility (CSE1L/CAS) protein expression promotes protrusion extension and enhances migration of MCF-7 breast cancer cells. ***Exp Cell Res*** 2010;316:2969-2981.

Tanaka T, Ohkubo S, Tatsuno I and Prives C. hCAS/CSE1L associates with chromatin and regulates expression of select p53 target genes. ***Cell*** 2007;130:638-650.

Tarantino C, Paolella G, Cozzuto L, Minopoli G, Pastore L, Parisi S and Russo T. miRNA 34a, 100, and 137 modulate differentiation of mouse embryonic stem cells. ***FASEB J*** 2010;24:3266-3273.

Tews B, Felsberg J, Hartmann C, Kunitz A, Hahn M, Toedt G, Neben K, Hummerich L, von Deimling A, Reifenberger G and Lichter P. Identification of novel oligodendroglioma-associated candidate tumor suppressor genes in 1p36 and 19q13 using microarray-based expression profiling. ***Int J Cancer*** 2006;119:792-800.

Tews B, Roerig P, Hartmann C, Hahn M, Felsberg J, Blaschke B, Sabel M, Kunitz A, Toedt G, Neben K, Benner A, von Deimling A, Reifenberger G and Lichter P. Hypermethylation and transcriptional downregulation of the CITED4 gene at 1p34.2

in oligodendroglial tumours with allelic losses on 1p and 19q. ***Oncogene*** 2007;26:5010-5016.

The Cancer Genome Altas Research Network. Comprehensive genomic characterization defines human glioblastoma genes and core pathways. ***Nature*** 2008;455:1061-1068.

Thomas M, Lieberman J and Lal A. Desperately seeking microRNA targets. ***Nat Struct Mol Biol*** 2010;17:1169-1174.

Ting AH, Jair KW, Suzuki H, Yen RW, Baylin SB and Schuebel KE. Mammalian DNA methyltransferase 1: inspiration for new directions. ***Cell Cycle*** 2004;3:1024-1026.

Tohma Y, Gratas C, Biernat W, Peraud A, Fukuda M, Yonekawa Y, Kleihues P and Ohgaki H. PTEN (MMAC1) mutations are frequent in primary glioblastomas (de novo) but not in secondary glioblastomas. ***J Neuropathol Exp Neurol*** 1998;57:684-689.

Tong CY, Hui AB, Yin XL, Pang JC, Zhu XL, Poon WS and Ng HK. Detection of oncogene amplifications in medulloblastomas by comparative genomic hybridization and array-based comparative genomic hybridization. ***J Neurosurg*** 2004;100:187-193.

Trang P, Weidhaas JB and Slack FJ. MicroRNAs as potential cancer therapeutics. ***Oncogene*** 2008;27 Suppl 2:S52-57.

Tricoli JV and Jacobson JW. MicroRNA: Potential for Cancer Detection, Diagnosis, and Prognosis. ***Cancer Res*** 2007;67:4553-4555.

Tsai CS, Chen HC, Tung JN, Tsou SS, Tsao TY, Liao CF, Chen YC, Yeh CY, Yeh KT and Jiang MC. Serum cellular apoptosis susceptibility protein is a potential prognostic marker for metastatic colorectal cancer. ***Am J Pathol*** 2010;176:1619-1628.

Tsao TY, Tsai CS, Tung JN, Chen SL, Yue CH, Liao CF, Wang CC and Jiang MC. Function of CSE1L/CAS in the secretion of HT-29 human colorectal cells and its expression in human colon. ***Mol Cell Biochem*** 2009;327:163-170.

Tung MC, Tsai CS, Tung JN, Tsao TY, Chen HC, Yeh KT, Liao CF and Jiang MC. Higher prevalence of secretory CSE1L/CAS in sera of patients with metastatic cancer. ***Cancer Epidemiol Biomarkers Prev*** 2009;18:1570-1577.

van den Bent MJ, Carpentier AF, Brandes AA, Sanson M, Taphoorn MJ, Bernsen HJ, Frenay M, Tijssen CC, Grisold W, Sipos L, Haaxma-Reiche H, Kros JM, van Kouwenhoven MC, Vecht CJ, Allgeier A, Lacombe D and Gorlia T. Adjuvant procarbazine, lomustine, and vincristine improves progression-free survival but not overall survival in newly diagnosed anaplastic oligodendrogliomas and oligoastrocytomas: a randomized European Organisation for Research and Treatment of Cancer phase III trial. ***J Clin Oncol*** 2006;24:2715-2722.

van den Bent MJ, Dubbink HJ, Marie Y, Brandes AA, Taphoorn MJ, Wesseling P, Frenay M, Tijssen CC, Lacombe D, Idbaih A, van Marion R, Kros JM, Dinjens WN, Gorlia T and Sanson M. IDH1 and IDH2 mutations are prognostic but not predictive for outcome in anaplastic oligodendroglial tumors: a report of the European Organization for Research and Treatment of Cancer Brain Tumor Group. ***Clin Cancer Res*** 2010;16:1597-1604.

van den Bent MJ, Dubbink HJ, Sanson M, van der Lee-Haarloo CR, Hegi M, Jeuken JW,

Ibdaih A, Brandes AA, Taphoorn MJ, Frenay M, Lacombe D, Gorlia T, Dinjens WN and Kros JM. MGMT promoter methylation is prognostic but not predictive for outcome to adjuvant PCV chemotherapy in anaplastic oligodendroglial tumors: a report from EORTC Brain Tumor Group Study 26951. ***J Clin Oncol*** 2009;27:5881-5886.

van den Bent MJ and Kros JM. Predictive and prognostic markers in neuro-oncology. ***J Neuropathol Exp Neurol*** 2007;66:1074-1081.

van den Bent MJ, Reni M, Gatta G and Vecht C. Oligodendroglioma. ***Crit Rev Oncol Hematol*** 2008;66:262-272.

Verhaak RG, Hoadley KA, Purdom E, Wang V, Qi Y, Wilkerson MD, Miller CR, Ding L, Golub T, Mesirov JP, Alexe G, Lawrence M, O'Kelly M, Tamayo P, Weir BA, Gabriel S, Winckler W, Gupta S, Jakkula L, Feiler HS, Hodgson JG, James CD, Sarkaria JN, Brennan C, Kahn A, Spellman PT, Wilson RK, Speed TP, Gray JW, Meyerson M, Getz G, Perou CM and Hayes DN. Integrated genomic analysis identifies clinically relevant subtypes of glioblastoma characterized by abnormalities in PDGFRA, IDH1, EGFR, and NF1. ***Cancer Cell*** 2010;17:98-110.

Visone R and Croce CM. MiRNAs and cancer. ***Am J Pathol*** 2009;174:1131-1138.

Visvanathan J, Lee S, Lee B, Lee JW and Lee SK. The microRNA miR-124 antagonizes the anti-neural REST/SCP1 pathway during embryonic CNS development. ***Genes Dev*** 2007;21:744-749.

Volinia S, Calin GA, Liu CG, Ambs S, Cimmino A, Petrocca F, Visone R, Iorio M, Roldo C, Ferracin M, Prueitt RL, Yanaihara N, Lanza G, Scarpa A, Vecchione A, Negrini M, Harris CC and Croce CM. A microRNA expression signature of human solid tumors defines cancer gene targets. ***Proc Natl Acad Sci U S A*** 2006;103:2257-2261.

Wang J, Hevi S, Kurash JK, Lei H, Gay F, Bajko J, Su H, Sun W, Chang H, Xu G, Gaudet F, Li E and Chen T. The lysine demethylase LSD1 (KDM1) is required for maintenance of global DNA methylation. ***Nat Genet*** 2009;41:125-129.

Watanabe K, Tachibana O, Sata K, Yonekawa Y, Kleihues P and Ohgaki H. Overexpression of the EGF receptor and p53 mutations are mutually exclusive in the evolution of primary and secondary glioblastomas. ***Brain Pathol*** 1996;6:217-223; discussion 223-214.

Watanabe T, Nakamura M, Yonekawa Y, Kleihues P and Ohgaki H. Promoter hypermethylation and homozygous deletion of the p14ARF and p16INK4a genes in oligodendrogliomas. ***Acta Neuropathol*** 2001;101:185-189.

Watanabe T, Nobusawa S, Kleihues P and Ohgaki H. IDH1 mutations are early events in the development of astrocytomas and oligodendrogliomas. ***Am J Pathol*** 2009;174:1149-1153.

Watanabe T, Yokoo H, Yokoo M, Yonekawa Y, Kleihues P and Ohgaki H. Concurrent inactivation of RB1 and TP53 pathways in anaplastic oligodendrogliomas. ***J Neuropathol Exp Neurol*** 2001;60:1181-1189.

Weber RG, Rieger J, Naumann U, Lichter P and Weller M. Chromosomal imbalances associated with response to chemotherapy and cytotoxic cytokines in human

malignant glioma cell lines. ***Int J Cancer*** 2001;91:213-218.

Weber RG, Sabel M, Reifenberger J, Sommer C, Oberstrass J, Reifenberger G, Kiessling M and Cremer T. Characterization of genomic alterations associated with glioma progression by comparative genomic hybridization. ***Oncogene*** 1996;13:983-994.

Weber RG, Sommer C, Albert FK, Kiessling M and Cremer T. Clinically distinct subgroups of glioblastoma multiforme studied by comparative genomic hybridization. ***Lab Invest*** 1996;74:108-119.

Webster RJ, Giles KM, Price KJ, Zhang PM, Mattick JS and Leedman PJ. Regulation of epidermal growth factor receptor signaling in human cancer cells by microRNA-7. ***J Biol Chem*** 2009;284:5731-5741.

Weller M, Felsberg J, Hartmann C, Berger H, Steinbach JP, Schramm J, Westphal M, Schackert G, Simon M, Tonn JC, Heese O, Krex D, Nikkhah G, Pietsch T, Wiestler O, Reifenberger G, von Deimling A and Loeffler M. Molecular predictors of progression-free and overall survival in patients with newly diagnosed glioblastoma: a prospective translational study of the German Glioma Network. ***J Clin Oncol*** 2009;27:5743-5750.

Wellmann A, Flemming P, Behrens P, Wuppermann K, Lang H, Oldhafer K, Pastan I and Brinkmann U. High expression of the proliferation and apoptosis associated CSE1L/CAS gene in hepatitis and liver neoplasms: correlation with tumor progression. ***Int J Mol Med*** 2001;7:489-494.

Wellmann A, Krenacs L, Fest T, Scherf U, Pastan I, Raffeld M and Brinkmann U. Localization of the cell proliferation and apoptosis-associated CAS protein in lymphoid neoplasms. ***Am J Pathol*** 1997;150:25-30.

Winter J and Diederichs S. MicroRNA biogenesis and cancer. ***Methods Mol Biol*** 2011;676:3-22.

Wong AJ, Bigner SH, Bigner DD, Kinzler KW, Hamilton SR and Vogelstein B. Increased expression of the epidermal growth factor receptor gene in malignant gliomas is invariably associated with gene amplification. ***Proc Natl Acad Sci U S A*** 1987;84:6899-6903.

Wong TS, Liu XB, Wong BY, Ng RW, Yuen AP and Wei WI. Mature miR-184 as Potential Oncogenic microRNA of Squamous Cell Carcinoma of Tongue. ***Clin Cancer Res*** 2008;14:2588-2592.

Woods K, Thomson JM and Hammond SM. Direct regulation of an oncogenic micro-RNA cluster by E2F transcription factors. ***J Biol Chem*** 2007;282:2130-2134.

Wrensch M, Jenkins RB, Chang JS, Yeh RF, Xiao Y, Decker PA, Ballman KV, Berger M, Buckner JC, Chang S, Giannini C, Halder C, Kollmeyer TM, Kosel ML, LaChance DH, McCoy L, O'Neill BP, Patoka J, Pico AR, Prados M, Quesenberry C, Rice T, Rynearson AL, Smirnov I, Tihan T, Wiemels J, Yang P and Wiencke JK. Variants in the CDKN2B and RTEL1 regions are associated with high-grade glioma susceptibility. ***Nat Genet*** 2009;41:905-908.

Xia H, Qi Y, Ng SS, Chen X, Chen S, Fang M, Li D, Zhao Y, Ge R, Li G, Chen Y, He ML, Kung HF, Lai L and Lin MC. MicroRNA-15b regulates cell cycle progression by

targeting cyclins in glioma cells. ***Biochem Biophys Res Commun*** 2009;380:205-210.

Xia H, Qi Y, Ng SS, Chen X, Li D, Chen S, Ge R, Jiang S, Li G, Chen Y, He ML, Kung HF, Lai L and Lin MC. microRNA-146b inhibits glioma cell migration and invasion by targeting MMPs. ***Brain Res*** 2009;1269:158-165.

Xia HF, He TZ, Liu CM, Cui Y, Song PP, Jin XH and Ma X. MiR-125b expression affects the proliferation and apoptosis of human glioma cells by targeting Bmf. ***Cell Physiol Biochem*** 2009;23:347-358.

Xiao Z, McGrew JT, Schroeder AJ and Fitzgerald-Hayes M. CSE1 and CSE2, two new genes required for accurate mitotic chromosome segregation in Saccharomyces cerevisiae. ***Mol Cell Biol*** 1993;13:4691-4702.

Xu J, Liao X and Wong C. Downregulations of B-cell lymphoma 2 and myeloid cell leukemia sequence 1 by microRNA 153 induce apoptosis in a glioblastoma cell line DBTRG-05MG. ***Int J Cancer*** 2010;126:1029-1035.

Yakut T, Gutenberg A, Bekar A, Egeli U, Gunawan B, Ercan I, Tolunay S, Doygun M and Schulten HJ. Correlation of chromosomal imbalances by comparative genomic hybridization and expression of EGFR, PTEN, p53, and MIB-1 in diffuse gliomas. ***Oncol Rep*** 2007;17:1037-1043.

Yan H, Parsons DW, Jin G, McLendon R, Rasheed BA, Yuan W, Kos I, Batinic-Haberle I, Jones S, Riggins GJ, Friedman H, Friedman A, Reardon D, Herndon J, Kinzler KW, Velculescu VE, Vogelstein B and Bigner DD. IDH1 and IDH2 mutations in gliomas. ***N Engl J Med*** 2009;360:765-773.

Yu L, Pena Castillo L, Mnaimneh S, Hughes TR and Brown GW. A survey of essential gene function in the yeast cell division cycle. ***Mol Biol Cell*** 2006;17:4736-4747.

Yvon AM, Wadsworth P and Jordan MA. Taxol suppresses dynamics of individual microtubules in living human tumor cells. ***Mol Biol Cell*** 1999;10:947-959.

Zawlik I, Vaccarella S, Kita D, Mittelbronn M, Franceschi S and Ohgaki H. Promoter methylation and polymorphisms of the MGMT gene in glioblastomas: a population-based study. ***Neuroepidemiology*** 2009;32:21-29.

Zhang C, Kang C, You Y, Pu P, Yang W, Zhao P, Wang G, Zhang A, Jia Z, Han L and Jiang H. Co-suppression of miR-221/222 cluster suppresses human glioma cell growth by targeting p27kip1 in vitro and in vivo. ***Int J Oncol*** 2009;34:1653-1660.

Zhang L, Huang J, Yang N, Greshock J, Megraw MS, Giannakakis A, Liang S, Naylor TL, Barchetti A, Ward MR, Yao G, Medina A, O'Brien-Jenkins A, Katsaros D, Hatzigeorgiou A, Gimotty PA, Weber BL and Coukos G. microRNAs exhibit high frequency genomic alterations in human cancer. ***Proc Natl Acad Sci U S A*** 2006;103:9136-9141.

Zhang Y, Chao T, Li R, Liu W, Chen Y, Yan X, Gong Y, Yin B, Qiang B, Zhao J, Yuan J and Peng X. MicroRNA-128 inhibits glioma cells proliferation by targeting transcription factor E2F3a. ***J Mol Med*** 2009;87:43-51.

Zhi F, Chen X, Wang S, Xia X, Shi Y, Guan W, Shao N, Qu H, Yang C, Zhang Y, Wang Q,

Wang R, Zen K, Zhang CY, Zhang J and Yang Y. The use of hsa-miR-21, hsa-miR-181b and hsa-miR-106a as prognostic indicators of astrocytoma. ***Eur J Cancer*** 2010;46:1640-1649.

Zhou J and Giannakakou P. Targeting microtubules for cancer chemotherapy. ***Curr Med Chem Anticancer Agents*** 2005;5:65-71.

Zhou X, Ren Y, Moore L, Mei M, You Y, Xu P, Wang B, Wang G, Jia Z, Pu P, Zhang W and Kang C. Downregulation of miR-21 inhibits EGFR pathway and suppresses the growth of human glioblastoma cells independent of PTEN status. ***Lab Invest*** 2010;90:144-155.

Zhu JJ, Santarius T, Wu X, Tsong J, Guha A, Wu JK, Hudson TJ and Black PM. Screening for loss of heterozygosity and microsatellite instability in oligodendrogliomas. ***Genes Chromosomes Cancer*** 1998;21:207-216.